Nº d'ordre : 40926

THESE

Présentée à

L'UNIVERSITE DE LILLE 1 SCIENCES ET TECHNOLOGIES
-UNIVERSITE LILLE NORD DE FRANCE-

Ecole Doctorale Sciences Pour l'Ingénieur
En vue de l'obtention du grade de

DOCTEUR DE L'UNIVERSITE

Spécialité : Micro et Nanotechnologie, Acoustique et télécommunication

Par
Basma EL ZEIN

GROWTH AND CHARACTERIZATION OF ZNO NANOSTRUCTURES FOR PHOTOVOLTAIC APPLICATIONS

Soutenance prévue le 7 Novembre 2012

Directeur de Thèse	M. Elhadj Dogheche	Professeur Université de Valenciennes
Rapporteur	M. Gilles Lerondel	Professeur Université de technologie de Troyes
	M. Bernard Orsal	Professeur Université de Montpellier II
Examinateur	M. Tuami Lasri	Professeur Université de Lille 1
	M. Ghassan Jabbour	Professeur Université King Abdullah de Sciences et Technologies
	M.Gilles Patriarche	Directeur de recherche Laboratoire de Photonique et de Nanostructures
	M. Didier Decoster	Professeur Université de Lille 1
	M. Dave Rogers	Directeur de Nanovation
	M. Xixiang Yang	Directeur Université King Abdullah de Sciences et Technologies

INSTITUT D'ELECTRONIQUE DE MICROELECTRONIQUE ET DE NANOTECHNOLOGIE

Nº Ordre: 40926

November 2012

Lille, Villeneuve D'ascq

Nº Ordre: 40926

GROWTH AND CHARACTERIZATION OF ZINC OXIDE (ZnO) NANOSTRUCTURES FOR PHOTOVOLTAIC DEVICES

Basma EL ZEIN

November 2012

Nº Ordre: 40926

Acknowledgments

First and foremost I want to thank my supervisor **Prof. Elhadj DOGHECHE**. It has been an honor to be under his supervision. He has taught me how good experimental physics is done. I appreciate all his contributions of time, ideas to make my Ph.D. experience productive and stimulating. The joy and enthusiasm he has for this research was contagious and motivational for me, even during tough times in the Ph.D. pursuit. Thank you so much for allowing me to stay close to my children and for his faith in me and my intellect.

Special thanks also to **Prof. Didier DECOSTER** where I very much appreciated his enthusiasm, intensity, and willingness to help and advise and always be there to encourage and motivate.

Prof. Tuami LASRI, Thank you for your encouragement, advises, help, support and for accepting to be president of my Jury.

Prof. Ghassan JABBOUR, thank you for your extended support and for being hosted at your Center.

Thank you, **Prof. Gilles LERONDEL** and **Prof. Bernard ORSAL** for being the "rapporteurs "of my thesis.

I am obliged to the examiners of my jury: Prof. Tuami Lasri, Prof. Ghassan Jabbour, Prof. Gilles Patriarche, Prof. Xixiang Zhang, Prof. Didier Decoster, Dr. Dave Rogers.

I am very grateful to **Prof. Brian MORAN**, for his precious support and help.

An extended thank you to the ***Solar and Photovoltaic Engineering research Center at King AbdulAllah University for Science and Technology*** especially **Samir BOULFRAD** for his technical advises, ideas and fruitful discussions .

I am also thankful to the ***Core Lab at King Abdullah University for Science and Technology***.

Thank you **YingBang Yao**, for your ultimate help, even during weekends, words can't convey my gratitude. I will never forget the wonderful **team of characterization** Rachid & Dalever & Kun for TEM, Lan & Dongkyu & Ali for SEM, Liang for XRD, Mohamad for XPS, and Bei for XRD, Hall effect and for answering all my inquiries. The group has been a source of friendships as well as good advice and collaboration.

The members of ***IEMN,*** specifically the opto-Group, have contributed immensely to my personal and professional time. I am especially grateful to Anisha, Floriane, Arnaud, Aurelien, Djamila, Naema, Thomas, Mathieu, Christophe, David, and Zahia.

I am also appreciative to Pascal Roussel for XRD, Bruno Capoen for Reflectivity, Ahmed Addad for TEM and Brigitte Sieber for CL, from University of Lille1.

I am very thankful to Prof. Iain Baikie from Kelvin Probe technology, for his time to conduct the SPS measurements.

Thank you to the ***Nanotechnology center at King Abdul Aziz University*** – Jeddah, Saudi Arabia presented by its Director Prof.Sami HABIB and his team mainly Noman Saleh and Zishan Khan.

Thank you to ***Dar Al Hekma*** presented by the Dean Dr.Suhair Al QURASHI, Dr.Amal Al TIJANI for bearing with me while conducting my experiments.

Nº Ordre: 40926

My hard-working ***Parents*** have sacrificed their lives for us and provided unconditional love and care. I love you so much, and I would not have made it this far without you. Thank you both for giving me strength to reach for the stars and chase my dreams. My Brothers (Ahmad & Rami) and my sister Chirine, have been my best friend all my life and I love them dearly and thank them for all their encouragement and support. Thank you, Rima for your help and kind support. I know I always have my family to count on when times are rough.

I am greatly indebted to my devoted husband Samir for sticking by my side. I feel that what we both learned a lot about life and strengthened our commitment and determination to each other and to live life to the fullest.

My angels ***Noha and Ahmad***, Thank you for your love, prayers and patience. Excuse me my dears when I was not always close to you. Your love, encouragement and prayers pushed me to continue in the hard moments of my research.

Last but not Least words can't convey my gratitude to my friends in Saudi Arabia my **sisters** (Rawan Jalal, Hala Al Attiyat, Fatima Mohammad Ali, Eman Daas), my **friends** in KAUST (Mutalifu, Racha, Issam, Ahmad, Silvano, Bilal, Gao, Silvia, Tianlei, Hana, Gehan, Maryam, Janne, Erki) my **colleagues** at Dar Al Hekma (Dr.Saleha, Aicha, Salma, Inass, Amani, Ahlam , and Yasmin). I will never forget the long hours of phone calls to solve capstone students' errors with my assistant Maha, Thank you my G.M. Special Thanks to my friends in France (Saja, Samir, and Ismail) who always supported and encouraged me even in most difficult time.

Nº Ordre: 40926

Dedication

I owe my every achievement to Allah (SWT),

My Kids (Noha, Ahmad),

My Parents (Dad, Mom),

My Husband Samir,

And my supervisor Elhadj.

And this is where I dedicate the thesis to all of them . . .

Nº Ordre: 40926

Notations

atm	Atmospheric pressure
A	Ampere
eV	Electron Volt
mJ	Mil-Joule
n	Nano 10-9
µ	Micro 10-6
Pa	Pascal
Sccm	Strandard cubic centimeter per minute
slpm	Standard Liter per minute
Torr	Pressure in Torr
V	Volt

Nº Ordre: 40926

Abbreviations:

AC	Alternative current
AFM	Atomic Force Microscope
CBD	Chemical Bath Deposition
CQDSSC	Colloidal Quantum dots Sensitized solar cell
CVD	Chemical Vapor deposition
DC	Direct current
EDS	X-ray Photoelectron Spectroscopy
EDT	Ethanedithiol
EQE	External Quantum efficiency
FWHM	Full width half maximum
FE	Field Emission
FIB	Focused Ion Beam
FTIR	Fourier transform infrared Spectroscopy
IQE	Internal Quantum Efficiency
IV	Current voltage
MPA	MercaptoPropionic acid
NW	Nanowire
NWaN	Nanowall Network
NR	Nanorod
NIR	Near infrared
PbS	Lead Sulfide
PCE	Power conversion efficiency
PL	Photoluminescence
PLD	Pulsed Laser deposition
PVD	Physical Vapor deposition
QD	Quantum Dots
SC	Solar Cell
SEM	Scan Electron microscope
SILAR	Successive Ionic Layer adsorption and reaction
SPS	Surface Photo-voltage Spectroscopy
TEM	Transmission electron microscopy
UV	Ultra violet
UHV	Ultra High Vacuum
Vzn	Zinc vacancies
Vo	Oxygen vacancies
VS	Vapor Solid
VLS	Vapor Liquid Solid
XPS	X-Ray Photoelectron Spectroscopy
XRD	X ray diffraction
XRF	X-Ray Fluorescence
Zn	Zinc
Zni	Zinc interstitials
ZnO	Zinc Oxide

Nº Ordre: 40926

Glossary

Irradiation	Is the energy per unit area on a surface.
Peak Sun Hours	Are the equivalent number of hours per day when solar irradiance averages 1,000W/m^2.
Performance Ratio **(*PR*)**	Defines the system losses such as shadowing, inverter inefficiencies and soiling effect. PR is the main index for characterizing the system performance under certain conditions.
Photovoltaic ***(PV)***	Photovoltaic describes a process which converts light to electricity by the creation of an electron/hole pair.
Photovoltaic Solar Cell	Is a semiconductor device that converts the energy from sunlight directly into electricity by the photovoltaic (PV) effect.
Quantum Dot ***(QD)***	Discovered by Louis E. Brus and termed by Mark Reed is a semiconductor whose excitons inhibit in all three spatial dimensions. Thus, QDs have properties in between semiconductors and discrete molecules.
Renewable Energy ***(RE)***	Is the energy generated from resources which are naturally replenished, such as sunlight and wind.
Sustainable	Defined by Brundtland (1987) as the development that meets the requirements of the present without compromising the capacity of future generations to meet their own requirements.
Dark Current	The dark current is a form of cell inefficiency and is the current through a device at a given bias, in the absence of light. It opposes the photocurrent.
Fill factor ***(FF)***	The fill factor is a measure of cell performance, and is the ($I \times V$) at maximum power, over the ($Isc \times Voc$).
Incident photon-to-current conversion efficiency ***(IPCE)***	The quantum efficiency of photocurrent generation from incident photons, *i.e.*, the number of electrons extracted per incident photon.
Junction	A junction is the interface shared by which two different materials.
Light path	The light path is the length, which a beam of light can travel within a cell.
Maximum power ***(mp)***	Power is defined as ($I \times V$), thus the maximum power is the maximum value of ($I \times V$) the cell is capable of.
Open-circuit voltage**, (*Voc*)**	The open-circuit voltage is the difference of electrical potential between two terminals of a device when there is no external load connected ($I = 0$).
Power conversion efficiency ***(PCE)***	The power conversion efficiency is a measure of overall cell efficiency, which compares the amount of power obtained from the cell relative to the amount of power put in.
Short-circuit current**, (*Isc*)**	The short-circuit current is measured when resistance and potential approach zero.

Nº Ordre: 40926

Keywords

Zinc Oxide,

Nanowires,

Vapor solid,

Wet oxidation,

SEM,

XRD,

PL,

CQDSSC,

Solar cell,

PbS,

Quantum dots,

One dimension – Zero Dimension nanostructure,

Nº Ordre: 40926

Peer reviewed Published work and conferences presentations

Conference & Seminars

ICMAT 2011	ZnO Nanowires for Photovoltaic Devices	B.El Zein S. Habib, A. Gokarna, E. Dogheche, D. Decoster
Hetech 2011	Growth of Zinc Oxide Nanorods in Water Vapor Environment and its promising role in Solar Cell	B.El Zein, I.Gereige, S.Boulfrad, A.Gokarna, E.Dogheche, D.Decoster, S.Habib, and G.E.Jabbour
EMRS 2012	Synthesis and Characterization of Vertically Oriented ZnO Nanowires grown on c-axis ZnO Seed Layer by Pulsed Laser Deposition	B.El Zein, Y.Yao, S.Boulfrad, E.Dogheche, D.Decoster, and G.E.Jabbour
3rd ZnO Colloquium 2012	Zinc Oxide Nanowires by Pulsed Laser Deposition	B.El Zein,Y.Yao, S.Boulfrad, E.Dogheche, D.Decoster, G.E.Jabbour

Papers:

Growth and Characterization of ZnO Nanowires on textured Seed Layer by Pulsed Laser Deposition, B.EL.Zein, Y.Yao, S.Boulfrad, E.Dogheche, G.E.Jabbour (Small 2012, in process)

Polarity of ZnO Nanowires grown by Pulsed Laser Deposition, K.Li, B.EL.Zein, Y.Yao,S.Boulfrad, E.Dogheche, G.E.Jabbour (2012 in process)

Parametric study of ZnO Nanowall network with honeycomb structure by Pulsed Laser Deposition, B.EL.Zein, S.Boulfrad, E.Dogheche, G.E.Jabbour (Small 2012, in process)

In-situ growth of PbS Nanoparticles on ZnO Nanowires by SILAR, B.El.Zein, M.Abulikum, S.Boulfrad , E.Dogheche,G.E.Jabbour (JACS 2012 , in process)

PbS Nanoparticles decorating ZnO Nanowall network with honeycomb structure for photovoltaic applications. B.EL.Zein, M.Abulikum, S.Boulfrad, E.Dogheche , G.E.Jabbour (in process)

Nº Ordre: 40926

Patents

ZnO Nanowires by Pulsed Laser Deposition, B.EL.Zein, Y.Yao, S.Boulfrad, E.Dogheche, G.E.Jabbour (in process)

ZnO Nanowall network with honeycomb structure by Pulsed Laser Deposition , B.EL.Zein, S.Boulfrad, E.Dogheche, G.E.Jabbour (in process)

Table of contents

Chapter 3: Synthesis and Characterization of ZnO Nanowires

List of Figures

List of Tables

General Introduction:

Harnessing the sun light incident on earth with inexpensive and efficient solar cells is one of the most important challenges of the 21st century. Solar cells made using nanostructured materials (nanoparticles and nanowires) are being investigated around the world to address this challenge. These new field of nanotechnology has opened up new and promising possibilities to improve environmental quality and economic prosperity.

In this thesis we show different examples of how Nano solar cell technology can help address our energy needs. We argue that nanostructured materials such as nanoparticles and nanowires present their unique advantages that can help in solar to electric energy conversion. Nanostructured materials such as nanoparticles and nanowires have unique advantages that make them useful in Photovoltaic designs. Ensembles of nanometer size materials have very large surface areas per unit volume or per unit mass. This enables one to pack very large interfacial areas into small volumes. Quantum confinement effects encountered in nanometer size materials impart them with unique optical and physical properties that are much different than the properties of the bulk material. Large surface and interfacial areas found in nanostructured materials present significant advantages both for light absorption charge generation, Charge separation and transportation, the critical steps in solar electric energy conversion. Using nanowires will improve the conduction of the electron transport and light trapping. On the other hand, using nanoparticles will provide the ability to tailor the optical properties through their size to absorb different parts of the solar spectrum with different size particles. The importance lies in synthesizing a single crystal, densely packed, long and narrow nanowire to achieve high surface areas and to tightly attach the nanoparticles on the surface of the nanowires in order to complete the solar conversion process.

Context:

The work described in this thesis was conducted at University Lille 1 Science and Technology Lille France, King Abdullah University for Science and Technology, and some at King Abdul Aziz University, Saudi Arabia.

Based on the collaboration between the University of Lille1 – KAUST and University of Lille 1- KAU, the work was divided between the three universities.

The growth by Vapor Solid Process and Vapor Liquid Solid Process in presence of water vapor with its characterization was conducted at KAU and IEMN.

The growth by Pulsed Laser Deposition (PLD) and its characterization was conducted at KAUST and IEMN. The Integration of the PbS nanoparticles and its characterization was conducted between KAUST and IEMN.

I conducted by myself all the synthesis and characterization experiments after passing by a thorough training on the different equipment's available at KAUST and KAU.

Thesis objective:

This thesis sought to advance the engineering and the science of Solar cells based on Nanowires and Sensitized Quantum dots:

It will focuses on the following Key questions:

1) Which architecture has to be selected to meet the objectives of developing an eco-green and high efficient solar cell? Different types of solar cell were reported in the literature based on nanostructure, like dye sensitized solar cells, nanowires based solar cell and quantum dots sensitized solar cells. In this research, nanowires based Colloidal Quantum dots Solar cells, is selected.
2) How can we grow vertically aligned ZnO nanowires? This was reported in the literature by using deposition techniques. In this research physical vapor phase deposition techniques (thermal evaporation, Pulsed laser deposition) were employed to grow the ZnO nanowires.
3) How can we cover the full solar spectrum? Using band gap tunable semiconductor zero dimensional (0D) Nanomaterials (CdS, PbS, CdSe, InP …) Quantum dots have demonstrated extra ordinary optical and electronic properties that open up possibilities for revolutionary advances in Photovoltaic devices . Tuning the band gap of quantum dots via the quantum size effect, enables customization of solar cells absorption to match the sun's broad visible and infra-red containing spectrum reaching the earth.
4) How can we minimize the fabrication cost? The selection of the proper materials and the synthesis of the nanostructures help in minimize the fabrication cost. The selection of Zinc oxide semiconductor and the growth technique, in addition to the use of simple techniques to grow the Nanoparticles on the ZnO Nanowires.
5) How can we design an efficient Solar cell? by combining 0D and 1D, where 1D support to anchor light harvesting and provides a convenient way to capture photo generated charges and transport them to the electrodes. While 0D provides the ability to tune the optical absorption in the solar cell through selection of semiconductor material and particle size, and the generation of electron –hole pairs per photon to achieve higher efficiencies.

Thesis Organization

The thesis is divided into the following chapters:

Chapter I presents the global energy problem and the need for an eco-green and high efficient solar cell. The different generations of solar cells will be briefly described. The focus will be on the advantages of the nanostructured solar cells and the role that one dimension and zero dimensions will play in improving the efficiency of the solar cell. The Objective of this chapter is to review the different generations, types and fundamentals of Solar cells focusing on the quantum dots sensitized solar cell. This chapter describes the chronological history and scientific advancements in research and development activities pertaining to solar cell technology from 1954 to the present.

Chapter II reviews the general properties of Zinc oxide semiconductor, and the different applications of ZnO Nanowires in different fields such as Solar cell, Light Emitting Diode, and waveguides, etc…. Different synthesis methods and techniques are illustrated and described to grow the vertically oriented ZnO nanowires. A review of past literature efforts is presented for the described synthesis methods. This chapter is aimed at providing a broad introductive background for the growth of one Dimension Nanostructure.

Chapter III presents the details of the synthesized methods and characterization properties of the ZnO Nanowires. Morphology, Structural and optical characterizations for the seed layer and the nanowires are analyzed. This chapter provides experimental details applied during my PhD research.

Chapter IV describes the attachment of the Lead Sulfide (PbS) Nanoparticles on the ZnO nanowires. Ex-situ and in-situ growth of PbS NPs are clearly described. SILAR technique is employed to decorate the ZnO Nanowires by PbS Nanoparticles with different densities and different sizes, by optimizing the process parameters. Structural , morphological and optical Characterization of the as-synthesized PbS Nanoparticles were presented and analyzed .This chapter builds on the insights of the previous chapters and describes our basic device architecture and characterization procedures.

Chapter V summarizes the major findings made during this doctoral research, and concludes with recommendations for future work in this very promising class of solution-processed photovoltaic devices.

CHAPTER 1:

SOLAR CELLS FUDAMENTALS
(From concept to device)

Contents

1-1-Introduction

Harnessing the sunlight incident on earth with inexpensive and efficient solar cells is one of the most important challenges of the 21 century. Solar cells made using nanostructures materials (Nanoparticles and Nanowires) are being investigated around the word to address this challenges. Nanowires and Nanoparticles present unique advantages that can help in solar to electric energy conversion. This chapter is divided in 4 folds. The first fold introduces the basics of energy conversion and the different generations of photovoltaic devices. It is followed by a presentation of the optical and electrical properties of a solar cell. The third fold describes the advantages of using nanostructured materials in solar cell design. Finally a description of the Quantum dots solar cells and the proposed structure of Solar cell is presented in this research.

1-2- Chapter Objectives

This chapter will meet the following objectives:

- *Highlight the importance of the solar energy as one of the sources of renewable energies*
- *Introduce the different Solar cell generations*
- *Understand basic solar cell p-n junction design and its application to the PV industry.*
- *Review the optical and electrical properties in semiconductors for solar cells*
- *Present the different Nanostructures*
- *Understand the role of one and Zero dimensional nanostructures in solar cells*
- *Describe the Colloidal Quantum Dots sensitized solar cell*

1-3- Renewable energy Technology

Photovoltaic solar energy is attractive source of energy, being abundant and indigenous sun energy resource, no or a few moving parts therefore low operating cost, capability to be assembled as modular ranging from a few watts to megawatts, low noise and low carbon dioxide emission. Provision of energy is one of the most pressing problems facing humanity in the 21st century. Without energy, it is impossible to overcome the critical issues of our time.

Energy can be obtained from different sources [1] such as chemical (fossil fuels), solar (photovoltaic cell), nuclear (uranium) and thermo-mechanical (wind, water and hot water). Each kind of energy has its own problems. The use of fossil fuels leads to the production of the greenhouse gas CO2 that warms the earth; the use of nuclear energy leads to nuclear wastes from radioactive fission products; solar and wind energy require the use of large surface areas . Currently, fossil fuel and nuclear sources are the main energy suppliers for the world. The increase of the energy need with time is expected to lead to increased atmospheric concentrations of the greenhouse gas CO2 and to the depletion of fossil fuel supplies (especially oil) in the coming decades. The continuous emission of CO2 is a serious threat to the global environment. Increasing the CO2 concentration in the atmosphere will lead to global warming [1] and as a result the climate will change. In order to meet the growing global demand for energy, while producing less CO2, the current energy sources have to be replaced by new ones. The use of fossil fuels such as oil, coal and natural gas has to be reduced. In their place we have to increase our use of renewable energy sources like solar, geothermal and wind [3].

1-4- Basics Operation of Solar Cell:

A photovoltaic or solar cell is a device that converts light energy to electrical energy by the Photovoltaic effect. In a solar cell, light (photons) is absorbed by the cell and converted to electron–hole pairs, which must be separated in order for the electrons to work on a connected load.

1-4-1- Historical overview of Photovoltaic:

Solar cell were first recognized in 1839 when a 19 year old French physicist Alexandre Edmund Becquerel, found that certain materials can produce small amount of voltage(electric current) when exposed to light. He was able to make voltage appear when he illuminated a metal electrode in a weak electrolyte solution [4], [5].
It remains a curiosity of science for the next three quarters of a century. Until In 1876, Adams and Day studied the photovoltaic effect in solids. They made solar cells of selenium that were 1 – 2% efficient. As a result, Selenium was quickly adopted in the emerging field of photography for use in light measuring devices. In 1883, Charles Fritts furthered the photovoltaic (PV) technology by coating the selenium with an

extremely thin layer of gold to form p-n junctions. Albert Einstein published a theoretical explanation of the photovoltaic effect in 1904, which won him the Nobel Prize in 1923 [4]. Around this time, a Polish scientist by the name of Jan Czochralski began to develop a method to grow perfect crystals of silicon. By the 1940s and 1950s, this process was used to grow silicon to make the first generation of single crystal silicon photovoltaic, and this technique is still currently used in the industry today [5]. Russell Ohl patented the modern junction semiconductor solar cell in 1946 (U.S. Patent 2,402,662, "Light sensitive device"), which was discovered while working on the series of advances that would lead to the transistor [6]. The modern era of photovoltaic started in 1954. In that year Chapin [8] reported a solar conversion efficiency of 6 % for a silicon single-crystal cell. In 1955 Western Electric began to sell commercial licenses for silicon PV technologies.. Already in 1958 silicon cell efficiency under terrestrial sunlight had reached 14 %. In 1954 Reynolds [9] reported 6 % solar conversion efficiency in what later came to be understood as the cuprous sulfide/cadmium sulfide hetero-junction. A summary of the history of solar cells is illustrated in Figure 1- 1.

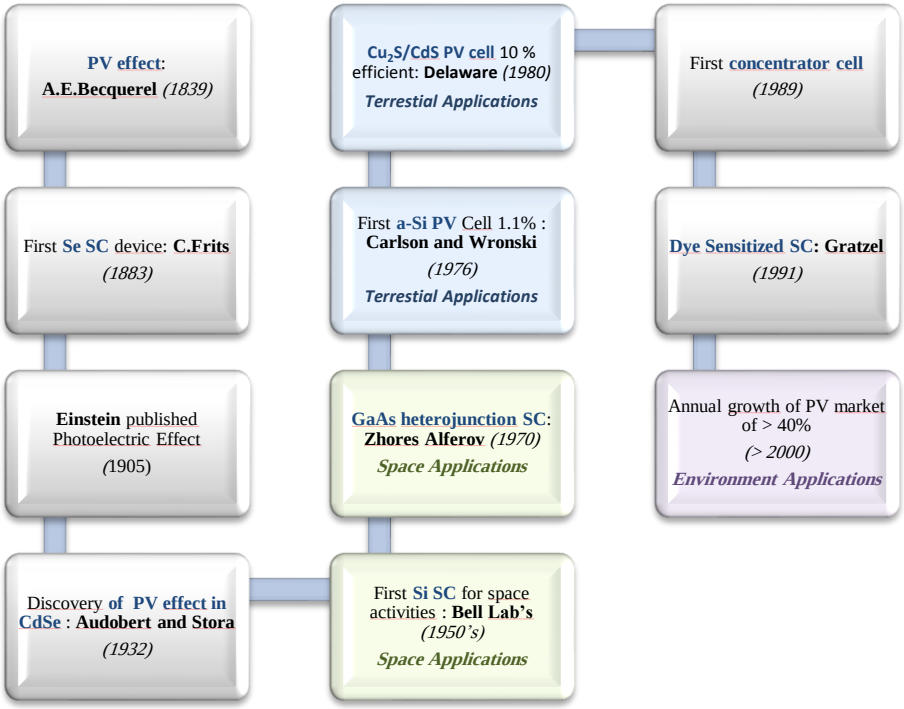

Figure 1- 1- Summary of the Photovoltaic history

1-4-2 -Generation of Solar Cells

During the Photovoltaic technology development, various materials have been investigated in order to obtain high quality photovoltaic cells, evaluated by two fundamental criteria: efficiency (ratio of the electric power output to the light power input) and production cost. According to his criteria , cells have been developed following three main ways, called 'generations' in the industry , defined by the types of semi-conductors and manufacturing techniques used . There are three major candidates for low cost, high performance photovoltaic solar modules:

I- ***First Generation solar cell*** was developed in 1970s at Bell Laboratories in New Jersey. Today they have a mature market and established production and electricity generation costs. They are based on single crystal silicon semiconductor. It exhibits a Power conversion efficiency (PCE) of 25% [10] which is approaching the theoretical Schockley –Queisser limit efficiency of 31% for single junction solar cells without light concentrating [11]. They consist of large area, high quality and single junction devices. This technology involves high energy and labor inputs which prevent any progress in reducing production cost and may take 5- 7 years to gain the payback for their purchasing and installation cost. Nevertheless, there are several inherent limitations and drawbacks to this generation. Silicon wafers are fragile, making processing difficult and limiting potential applications. The process is very laborious and energy intensive and manufacturing plant capital costs are high.

II- ***Second generation solar cell***s were developed in 1980s, based on semiconductor thin film technology. It is produced generally using chemical vapor deposition techniques like Plasma Enhanced CVD (PE_CVD). Thin film solar cells offer many advantages like the reduction of the mass of the material required, consequently a large reduction in material costs due to replacement of the high purity silicon wafer by polycrystalline or amorphous silicon, and direct band gap materials [12]. The semiconductor mass reduction allows also fitting panels on light materials or flexible materials. The most successful second generation materials have been Cadmium telluride (CdTe), Copper Indium Gallium

Selenide (CIGS), and amorphous silicon (a-Si) etc which provide an efficiency of 16.7 % [13], 20.1% [14], 9.5 % [15] respectively. The PCE is relatively lower than the first generation solar cells and not relatively low cost. But the loss of efficiency causes the necessity to enlarge the module area to obtain a suitable output current.

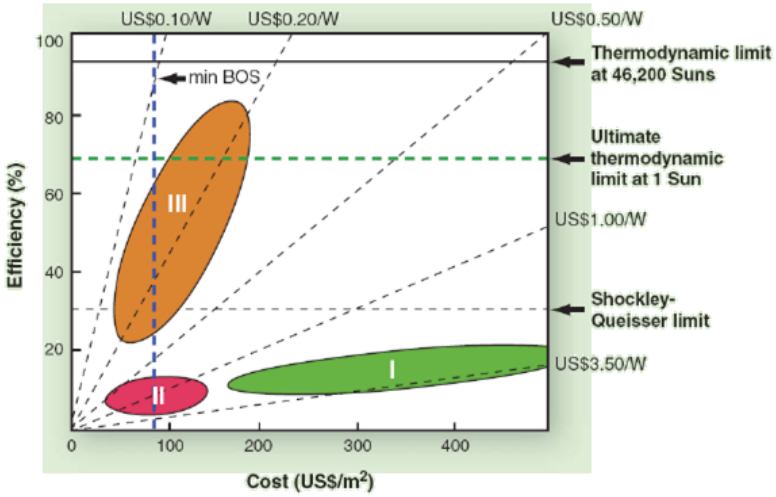

Figure 1- 2 - solar energy cost as a function of efficiency and material cost.[10]

III- ***Third generation solar cells*** are considered as the cutting edge of solar technology and still in the research phase. They are promising to achieve reasonable efficiencies at lower costs than the first and the second generation. [16] Current research are targeting conversion efficiencies of 30-60% while retaining low cost materials and manufacturing techniques. They include multifunction tandem cells [17], dye-sensitized solar cells (DSSCs) [18], Organic Solar cells (OSC) [19],[20], inorganic hybrid solar cells [21],[22], extremely thin absorber (ETA) [23], and Quantum Dots Solar cells (QDSC) .

Presently, there is concurrent research into all three generations but first generation devices (single junction, wafer based cells) still present.

1-4-3- Best Cell Efficiency:

Based on the solar cell history and the different solar cell generation, it is noticed that there is a tremendous progress in the cost effectiveness and efficiency of the solar cell. This progress is driven by the criteria of eco friendliness, sustainability and self-reliability of the energy source.

High efficiency solar cells are of interest to decrease the cost of solar energy, the chart below Figure 1- 3 illustrates the best laboratory efficiencies obtained for various materials and technologies

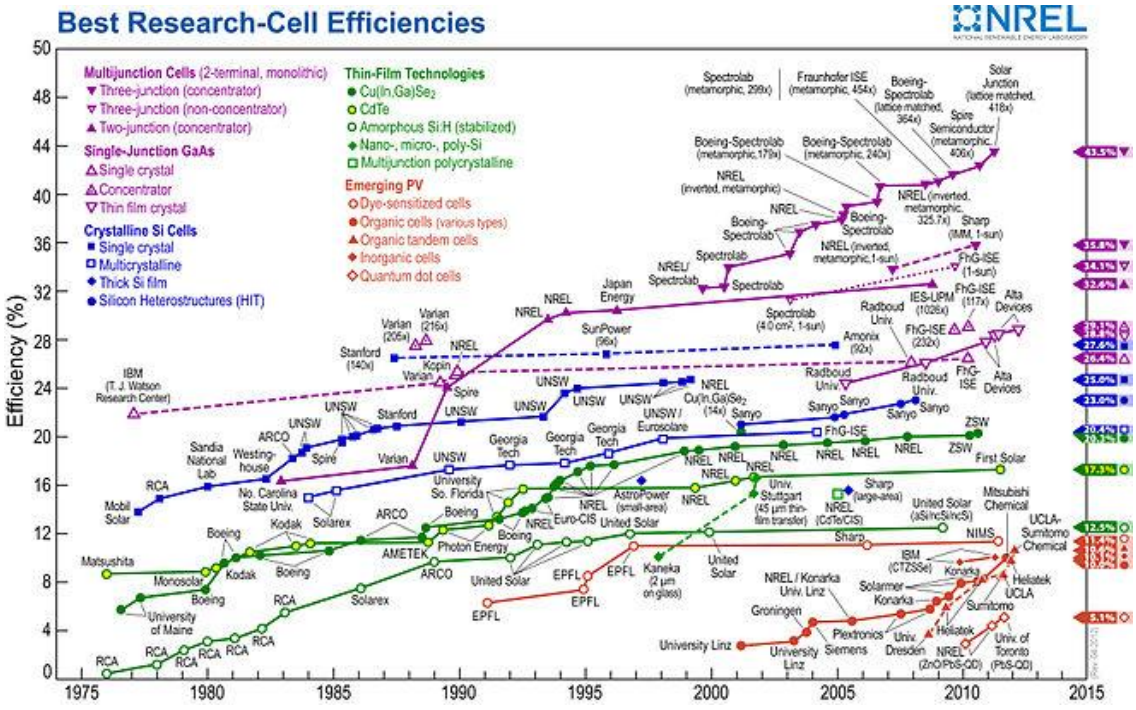

Figure 1- 3-Overview of research cell efficiencies of the different Photovoltaic technologies by the National Renewable Energy Laboratory (NREL)

Solar Spectrum:

The solar spectrum modified by the atmospheric absorption and scattering, is standardized as the AM 1.5G (air mass- 1.5 Global) with an integrated power density of 1000 w/m^2. Figure 1- 4 shows the AM 1.5 G spectrum.

The sun radiates light across a broad range of the electromagnetic spectrum. It emits continuum, a broad band of electromagnetic radiation running though the ultraviolet to the infrared (200nm → 3000nm) Figure 1- 4.

- Ultra-violet (UV) radiation (<400nm)

- Visible light (400nm -750 nm)
- Infrared radiation (>750 nm).

The wavelength of the light corresponds to its energy and so its position in the electromagnetic spectrum.

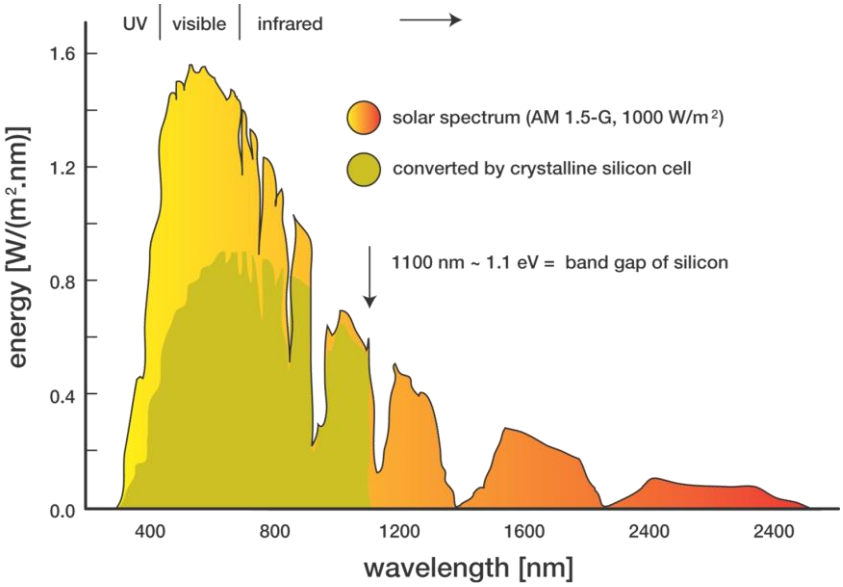

Figure 1- 4 solar Spectrum commonly used in photovoltaic

A solar cell is a large area P-N Junction .The solar cell operation is based on the Photovoltaic effect: the generation of a voltage difference at the junction of two different materials in response to visible or other radiations.

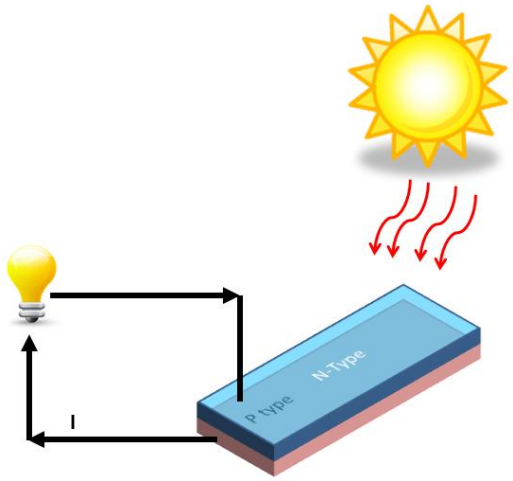

Figure 1- 5- Schematic PN junction Solar cell

The absorbed light generates carriers (electron-holes pairs or excitons), where the electron and its corresponding hole exit in a bound state due to the coulomb attraction [23]. These carriers are separated and then collected at the electrodes (Figure 1- 5).

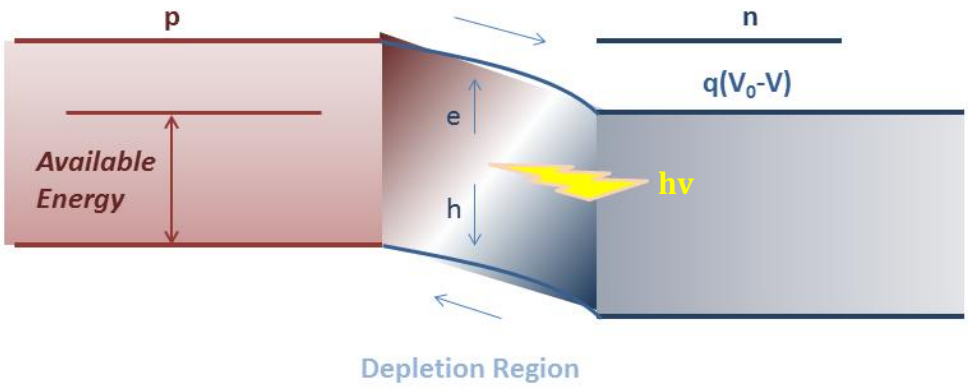

Figure 1- 6- conventional Solar cell, P-N junction showing electron and hole drift and diffusion

The electron hole pairs separate at the junction, with electrons (holes) diffusing across the depletion zone to the P-type (n-type) region, where they become thermally free and generate a current. It is crucial to minimize carrier recombination, allowing carriers to deliver the available energy to the external circuit. Recombination results in heat generation. This means that the carriers must cross the depletion region and become majority carriers on the opposite side of the junction. If they are generated and recombine on the same side of the junction they will not contribute to the flow of current. The available energy may also be optimized by minimizing the potential barrier $q(V_0 - V)$ that is required to facilitate carrier drift across the depletion region. The magnitude of $q(V_0 - V)$ is subtracted from the semiconductor bandgap, which reduces the available energy difference between electrons and holes travelling in the n-type and p-type semiconductors respectively. This causes a reduction in the operating voltage of the solar cell. If $q(V_0 - V)$ is too small, however, carriers will not be swept across the depletion region effectively enough making them more susceptible to recombination. Illustration is shown in Figure 1- 6. The generated current from light incident on a P-N junction is dependent on the mobility of the carriers in the material and the exposed surface area of the junction. Semiconductors materials with high charge mobility and low cost production are considered for developing solar cell devices.

1-4-4 – The photovoltaic effect: Photons in, Electrons Out

Solar Photovoltaic energy conversion is a one-step conversion process which generates electrical energy from light energy. Light is made up of packets of energy, called photons, whose energy depends on the frequency, and color of the light. The energy of visible photons is sufficient to excite electrons, bound into solids, up to higher energy levels where they are freer to move [Figure 1-7]. The built in asymmetry pulls the excited electrons away before they can relax and feeds them to an external circuit. The extra energy of the excited electrons generates a potential difference, or electron motive force (e.m.f). This force drives the electrons through a load in the external circuit to do electrical work. The effectiveness of a photovoltaic device depends upon the choice of light absorbing materials and the way in which they are connected to the external circuit.

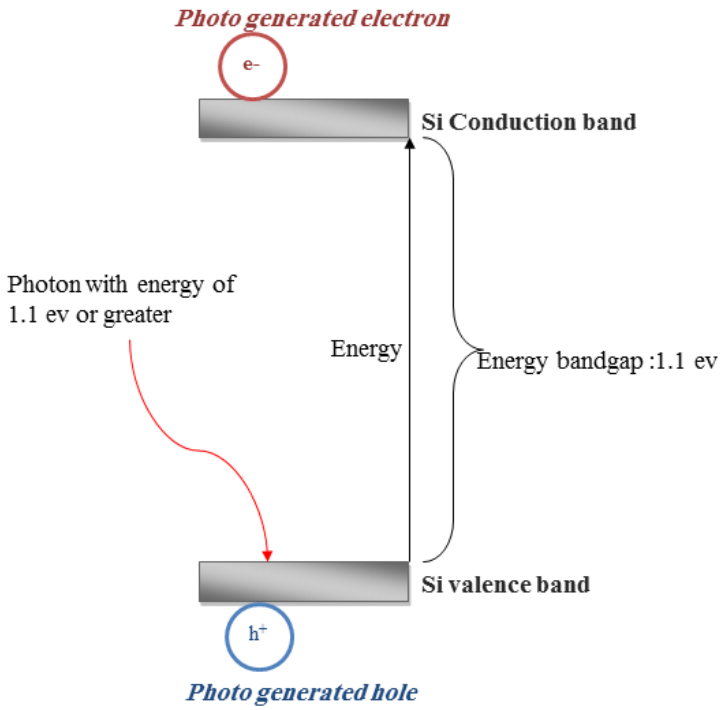

Figure 1- 7 Diagram of absorbance of a photon and the generation of an electron –hole pair in silicon

1-4-5 - Light - Optical Properties of Solar Cells:

When a light beam is impinged on a material surface, portion of the incident beam is reflected, while the other portion is either absorbed or transmitted through the material (Figure 1- 8).

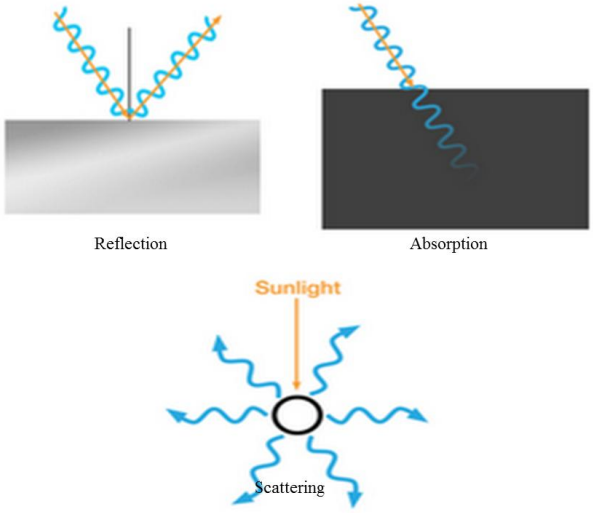

Figure 1- 8- Reflection , absorption and scattering

Light Reflection:

The reflection is the change in direction of an incident light at an interface between two different media.

Reflection of light is either specular or diffuse, depending on the nature of the interface, (mirror like, or all directions respectively).

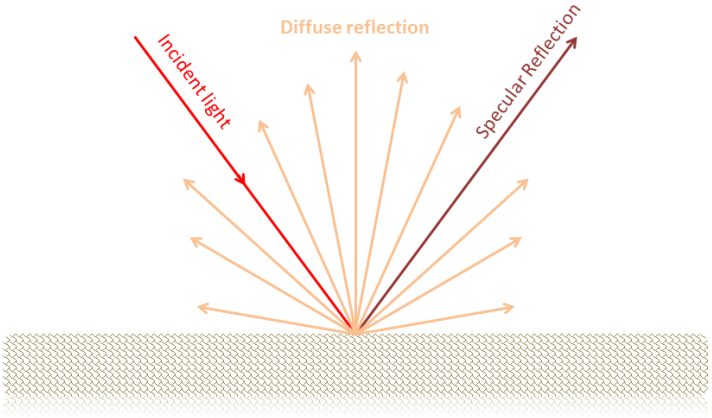

Figure 1- 9- Light reflection

Specular reflection is the mirror like reflection of light from a rough surface, in which light from a single incoming direction is reflected into a single outgoing direction. On

the other hand, the diffuse reflection is the reflection of light from a surface. When light strike the surface of a semiconductor, it bounces off in all directions due to multiple reflections by the microscopic irregularities inside the material (like grain boundaries of polycrystalline material or cell boundaries of an organic material) and by its surface if it is rough. Common model is the Lambertian reflectance, in which the light is reflected with equal luminance or radiance in all directions.

In metals, the reflectivity is typically on the order of 0.90-0.95, whereas for glasses it is close to 0.05. The high reflectivity of metals is one reason that they are opaque. High reflectivity is desired in many applications including mirrors, coatings on glasses, etc.

Light Absorption:

The absorbance of a semiconductor quantifies how much of the incident light is absorbed by it. In order to efficiently generate electron hole pairs in solar cell, light must reach the junction and be absorbed effectively. Photons have energy $E = hv$ which must be at least as large as the semiconductor band gap. It has the possibility of exciting an electron from the valence band to the conduction band.

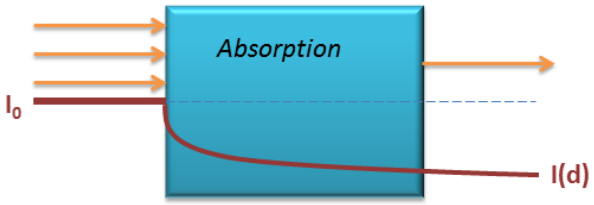

Figure 1- 10- Schematic of light absorption

A key factor in determining if a photon is absorbed or transmitted is the energy of the photon.

The photons falling onto the semiconductor can be divided into three groups (Figure 1- 11): [24]

- 1- The photons energy is equal to the band gap energy of the semiconductor (Eph=Egap) : the photon have just enough energy to create an electron – hole pair and are efficiently absorbed
- 2- The photons energy is less than the semiconductor band gap energy (Eph<Egap): the photons will interact weakly with the semiconductor passing through it as if it were transparent

- 3- The photon energy is greater than the band gap energy (Eph>Egap): the photon are strongly absorbed , however the excess of photon energy is wasted as thermalized electrons back down to the conduction band gap.

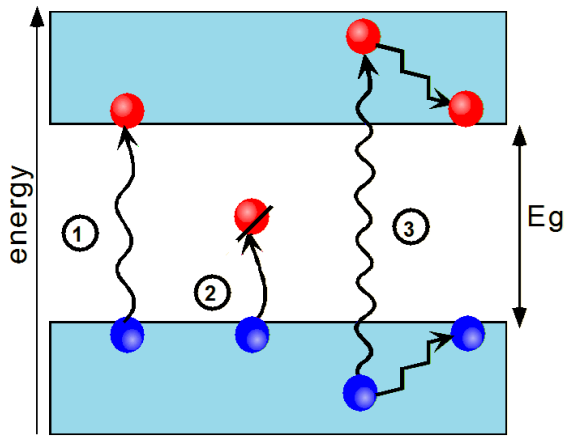

Figure 1- 11- The three groups of Photons 1)Eph=Egap,2)Eph<Egap,3) Eph>Egap

Sunlight entering the solar cell will be absorbed according to the relationship by Bouguer's law: The fraction of beam that is absorbed is related to the thickness of the materials and the manner in which the photons interact with the material's structure.

$$I = I_0 e^{(-\alpha x)}$$

where I – intensity of the beam coming out of the material,

I_0 – intensity of the incident beam,

x – path through which the photons move, and

α – linear absorption coefficient, which is characteristic of a particular material.

Light Transmission

To increase the light absorption and increase electron- hole generation, we still need to reduce the transmission loss.

The simplest method is to increase absorber thickness. Certainly, the thicker the absorber is, more light will be absorbed. Fraction of light beam that is not reflected or absorbed is transmitted through the material. $I_t = I_0(1-R)^2 e^{(-\alpha x)}$ where I_t is the intensity of the transmitted beam out of the material, and R is the reflective index R = I / I_0 .I is the reflected beam intensity and I_0 is the incident beam intensity. The process of light transmission is as presented in Figure 1- 12.

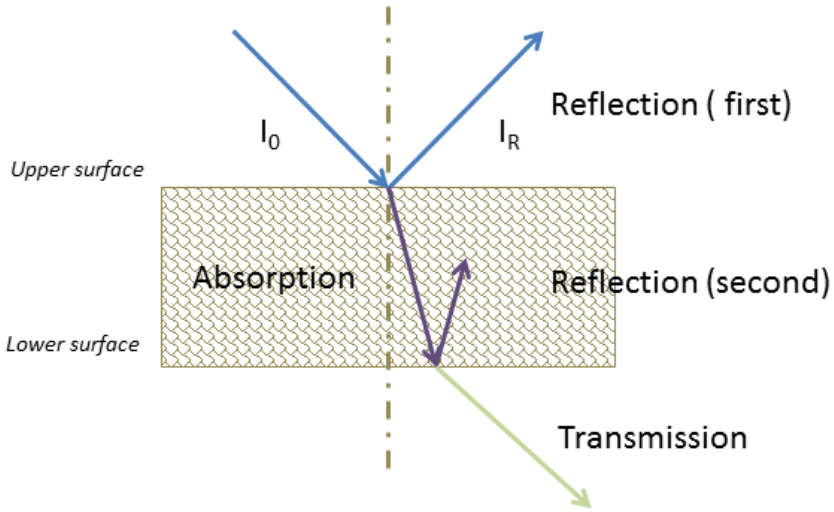

Figure 1- 12-Absorption, Reflection and Transmission

Light trapping

The optical path length is the distance that an absorbed photon may travel with in the device before it escapes out of the device (Figure 1- 13). Light trapping is achieved by changing the angle at which light travels in the solar cell by having it incident on an angled surface.

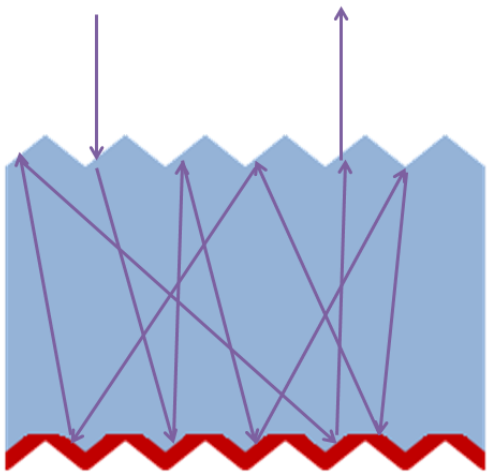

Figure 1- 13 the textured top surface reduces reflection from the solar cell and, when combined with a reflecting back surface, helps to confine or 'trap' light within the cell

1-4-6-Electrical Properties

PV cells can be modeled as a current source in parallel with a diode. When there is no light present to generate any current, the PV cell behaves like a diode. As the intensity of incident light increases, current is generated by the PV cell, as illustrated in Figure 1- 14. The source current (I_L) results from solar illumination. R_L is the load resistance and I_0 is the diode saturation current.

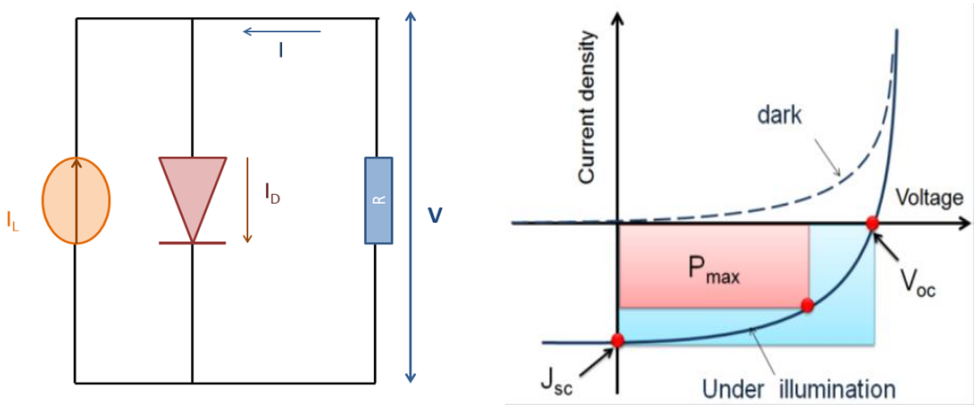

a- Equivalent circuit of a solar Cell

b- Current density voltage

Figure 1- 14- Illustration of a- Equivalent circuit of an ideal solar Cell , b- current density Voltage (J-V) characteristic of a typical solar cell.

The current –voltage (I-V) characteristics are treated as the sum of dark and short circuit photocurrent. $I = I_0 - I_L = I_0 \left[e^{\frac{qv}{KT-1}}\right] - I_L$

Figure 1- 14 shows current–voltage characteristics of a solar cell. In the dark, the current–voltage curve is strongly asymmetric and shows a diode behavior. Under illumination, the current–voltage curve exhibit vertical shift caused by light-induced current generation [25, 26, and 27]. The performance of a solar cell can be estimated from its current–voltage diagram. The basic notations of solar cell current–voltage diagrams are:

Air mass 1.5 (AM 1.5): A standard terrestrial solar spectral irradiance distribution.

Short-circuit current (J_{SC}): The current that flows in a photovoltaic device when illuminated and its electrodes are connected.

Open-circuit voltage (V_{OC}): The voltage provided by an illuminated photovoltaic device when no external load is connected. $V_{0c} = \frac{KT}{q}\ln(\frac{J_{sc}}{I_0} + I_0)$

Fill factor (FF): The ratio of the actual power a solar cell can supply to the maximum predicted by the product of its short-circuit current and its open-circuit voltage. $FF = \frac{Pm}{Jsc \times Voc}$

Power conversion efficiency (PCE) or η: The power conversion efficiency of a device is defined as the ratio between the maximum electrical power generated and the incident optical power (Pin). $PCE = \frac{Pm}{Pin} = \frac{Jsc \times Voc \times FF}{Pin}$

Quantum efficiency (QE): It is the number of electrons extracted in an external circuit divided by the number of incident photons at a certain wavelength under short circuit condition. It is the losses due to reflection at the surface.

$$QE = \frac{number\ of\ electrons}{number\ of\ photons} = \frac{Jsc(\lambda)/e}{Pin(\lambda)/(\frac{hc}{\lambda})}$$

Where λ is the wavelength, e is the elementary charge, h is the Planck constant and c is the speed of light in vacuum.

1-4-7- Solar cell Design:

As the main objective is to maximize the efficiency of an eco-green solar cell, the structure has to be designed respecting the following parameters and properties like:

- ✓ Increase the amount of light collected (absorption of light) and Decrease the reflection of light.
- ✓ Improve charge separation
- ✓ Accelerate the charge transport (Carrier collection)
- ✓ Increase light trapping.
- ✓ Minimize the Recombination of carriers

Taking in consideration:

- ✓ Use of less quantity of semiconductor material.
- ✓ Use less expensive semiconductor materials
- ✓ Increase material utilization by reducing waste in semiconductor and cell fabrication
- ✓ Simplify processing step and reducing equipment costs.

To meet the first point (increase the absorption of light) one needs a material harvesting photons from the sufficient amount of solar spectrum. Whereas the second point (improve the charge separation) requires hetero-junction interface with different work functions. On the other hand the charge transport and light trapping can be achieved by selecting the best geometry for rapid and direct charge transport. Accelerating the charge transport will minimize the recombination of carriers (electron hole). One important concept to reduce the solar cell cost and to increase the conversion efficiency is to use NANOTECHNOLOGY, i.e., to use the nanostructured material in solar cell.

1-5- Nano-structured Solar Cells

Recently, an increased motivation was noticed that employ nanostructures in solar cells in order to improve the performance of conventional solar cells, to obtain relatively high conversion efficiency from low grade (inexpensive) materials with low production cost and low-energy consumption, and to obtain a conversion efficiency higher than the theoretical limit of conventional p–n junction solar cell.

The cell designs and enhancements are categorized by the type of nanostructure utilized. These include: (a) bulk nanostructured materials [3D]; (b) quantum wells [2D]; (c) nanowires [1D]; and (d) quantum dots/nanoparticles [0D].

Nanoparticles (0D) and nanowires (1D) have their unique advantages that make them useful in photovoltaic designs. The set of nanometer size objects have very large surfaces areas per unit volume or per unit mass. The Quantum confinement effects encountered in nanometer size materials impart them with unique optical and physical properties that are much different than the properties of the bulk material. (These unique properties may allow us to surpass barriers such as the Shockley – Queisser limit). Photovoltaic (PV) devices based in nanomaterials have the potential to be inexpensive because nanoparticles and nanowires can be manufactured in bulk using solution synthesis and large area substrates can be coated from colloidal solutions using well developed coating and printing techniques .

1-5-1- One Dimensional (1D) nanostructure to enhance the Solar Cell efficiency:

Nanostructured materials are offering new opportunities to design more efficient solar cells, particularly one dimensional (1-D) nano-materials. Nanoscale inorganic materials one-dimensional (1D) structures, such as nanowires/Nanorods, nanobelts and nanotubes, have gained tremendous attention within the last decade. Among the huge variety of 1D nanostructure, semiconducting nanowires have gained particular interest due to their potential applications in optoelectronic and electronic devices.

Nanowire:

Nanowires (NW), elongated solid nanostructure, are defined as metallic or semiconducting particles having a high aspect ratio, with cross-sectional diameters. Nanowires have been extensively studied in the last decade; their roots can be traced to early work on whisker growth performed at Bell labs by Wagner and Ellis [28].

The applications of nanowires to solar cells have been attempted in several device configurations and materials systems. The earliest demonstration was from Alivisators and co-workers in 2002 [29], in which CdSe nanorods were utilized as the electronic conducting layer of a hole conducting polymer-matrix solar cell .

Morphology:

Semiconducting nanowires represent interesting solid state systems with unique geometry offering great possibility for further development of optoelectronic devices and sensors applications with numerous possibilities for studying exciting physical phenomena arising from carrier confinement and the large surface-to-volume ratio [30-35] . Recently, one dimensional (1D) nanostructures such as wires, rods/rods belts and tubes have become the focus of intensive research due to their unique geometry. Nanowires exhibit different cross section shapes (Figure 1- 13) circular, squared, triangular and hexagonal [36]. The Nanobelts exhibit the rectangular cross section shape. The nanotubes have a tubular shape that has a low mass density, a high porosity, and an extremely large surface to weight ratio.

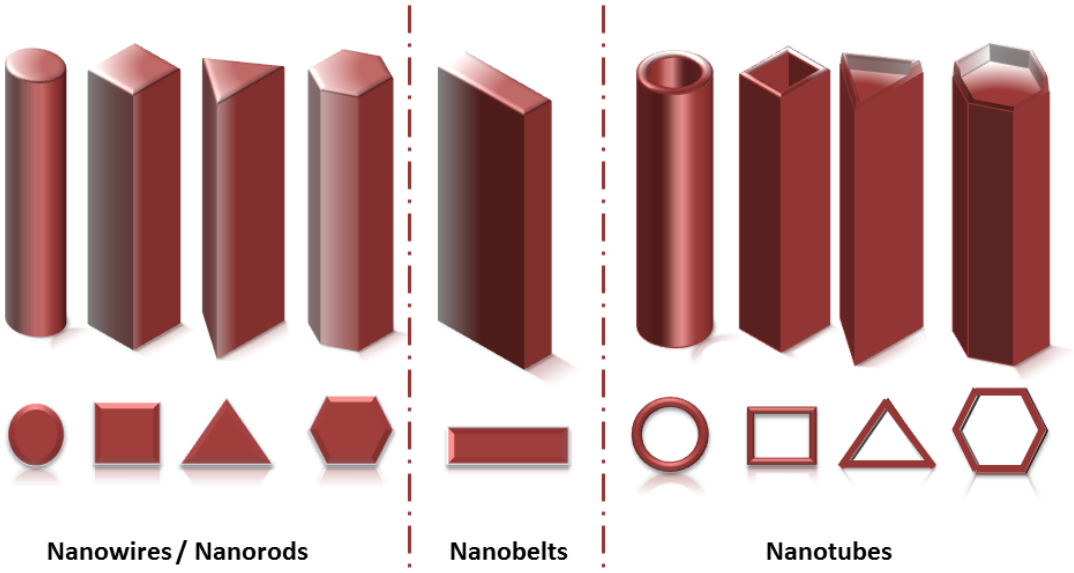

Figure 1- 15- Schematic illustration of 1 D nanostructure morphology

Applications in Photovoltaic:

In particular, 1-D nanostructures are promising for photovoltaic devices due to several advantages. One-dimensional semiconductor nanowires (NWs) offer the unique advantages such as large surface area, high optical absorption across a broad spectrum, direct path for charge transport and high charge collection efficiency [37-38]. Other benefits NWs offer are their large surface-to-volume ratio for effective chemical and catalytic reactions and a large number of surface states to minimize dark currents [39]. With respect to one-dimensional (1-D) structures, several new phenomena have been reported to date, e.g., the high surface-to-volume ratio enabling the measurement of surface optical (SO) phonon modes [40, 41, 42]. An increase in the scattered intensity is reported for nanoscale structures with respect to their bulk counterpart, describing the effect denominated as 'Raman antenna effect' [43, 44]. In addition, polarization dependent experiments on single carbon nanotubes and nanowires have shown that the physics behind Raman scattering of such 1-D nanostructures can differ significantly from the bulk [45, 46]. Well-aligned one-dimensional nanowire arrays have been widely investigated as photo electrodes for solar energy conversion because they provide direct electrical pathways ensuring the rapid collection of carriers generated throughout the device [47] , as well as affording large junction areas and low reflectance owing to light scattering and trapping [48] .

The nanowires act as a direct path for transport of charge to the anode without the presence of grain boundaries, thus leading to an enhanced performance compared to solar cells employing nanostructure (Figure 1- 16).

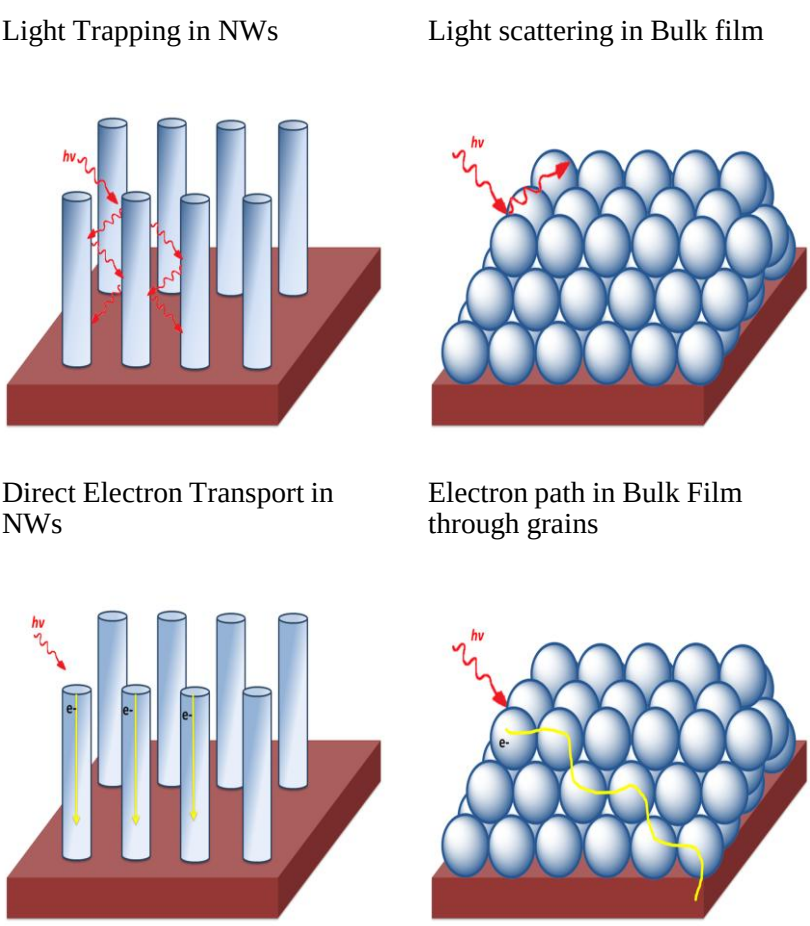

Figure 1- 16- (a) Diagrammatical Description of the Interaction of Incident Light with NWs Array; (b) Photo-generated Electron Transport in NWs Array[]

Challenges

Nanowires synthesis is very challenging in terms of preparing large areas arrays of vertically oriented nanowires and to make electrical junctions to such nanowires arrays. However, the growth of nanowires free of contaminants, controlled surface states and structural defects is still one of the key issues. On the other hand, the material used for preparing the nanowires must be sufficiently thick and pure to absorb most of the solar photons with energies above the materials' band gap. The material must have minority carrier diffusion length to effectively collect the photo-generated charge carriers.

Materials used:

The material classes of inorganic 1D nanostructures include metallic elements [49,50] , metal nitrides [51,52], oxides [53,54], carbides [55,56], and sulphides [57,58]. Oxide nanowire is one of the most important types of nanowire application. There is a high demand in recent years to advance the research of this type of nanowire. Most of the oxides are semiconductors. Among these, ZnO NWs are especially attractive due to their tunable electronic and optoelectronic properties, and the potential applications in the nanoscale electronic and micro-optoelectronic devices [59] . Nanowire-based solar cells have been reported to possess inherent advantages over traditional bilayer devices [60].

1-5-2- Zero Dimensional (0D) Nanostructure to photosensitize Solar Cell:

Integration of nanostructured materials in photovoltaic devices has been demonstrated to open the possibilities to develop a high efficient and low cost solar cell [61]. In recent years, inorganic semiconductors nanocrystals (Quantum Dots) have been found to be promising for next generation solar cell [62, 63].

Nanoparticle:

Quantum Dots (QD) are defined as semiconductors particles where the exciton Bohr radius is greater than or in the same order than the radius of the particle itself, leading to carrier confinement in all three spatial dimensions. QDs are small devices that contain a tiny droplet of free electrons. They are fabricated in semiconductor materials and have typical dimensions ranging from nanometers to a few microns. The size and shape of these structures and therefore the number of electrons they contain can be precisely controlled; a quantum dot can have anything from a single electron to a collection of several thousands.

Morphology:

Nanoparticles exhibit different morphological shapes such as spheres, platelets, squares, triangular and rectangular shapes. [64-66]

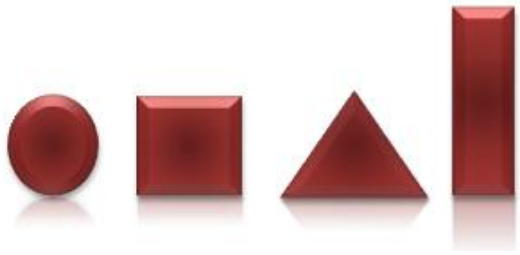

Figure 1- 17- Different morphologies of Nanocrystals

Application in photovoltaic:

Low band gap materials absorb more light and produce large current at the cost of a low voltage; in contrast, large band gap materials output high voltage but low current due to their limited absorption. As a consequence the balance between voltage and current necessitates an optimal choice of band gap in the range of 1.1 -1.4 e.V in order to yield to the best power conversion efficiency in a single junction solar cell.

Because of this very small size scale, they possess an immense surface area per unit volume, a high proportion of atoms in the surface and near surface layers, and the ability to exhibit quantum effects. [67] One way to tune the band gap of semiconductor is to manipulate its composition. According to Vegard's Law)[68], the band gap of an alloyed semiconductor is approximately equal to the compositionally weighted average of the band gap of the consistent semiconductors. Quantum confinement provides a promising alternative for band gap engineering without relying on ternary or quaternary stoichiometric tuning. Decreasing the size of particles to less than their Bohr radius, results in confinement of electron hole wave-functions and significant increase in the band gap. This strategy enable binary semiconductor compound for Photovoltaic applications [69]. The quantum dot electronic energy levels can be varied by changing their size. This allows tuning the effective band gap of the quantum dots to maximize the absorption of the solar spectrum, shift to the Quantum dot electronic levels to control charge transfer across hetero-interfaces [70] and to combine different size QDs as a possible route to inexpensive multi-junction solar cells. These effects may lead to higher photocurrents and photo-voltage. The ability to cast QD films from colloidal dispersion can lead to inexpensive solar cell manufacturing methods [71].

Challenges:

QDs following their synthesis in solution are generally capped by organic ligands that employ long chains (8-18 carbons) to ensure their solution process ability [72]. They produce insulating barriers between QDs. While poor charge transport was initially a problem in QD films, techniques have developed to exchange the long chain molecules on the QD surfaces with shorter ligands. This can reduce inter QD spacing and improve the electronic coupling between the QD [73, 74].

Materials:

It was recently reported that colloidal PbSe and PbS quantum dots can produce up to three to seven excitons per photon, when irradiated at photon energies 4 to 7.8 times the quantum dot's band gap, indicating that these materials can be more efficient in utilization of quanta in visible radiation producing multiple excitons in addition to harvesting the IR radiation of sunlight[75,76,77] .The possibility to generate multiple excitons in PbS /PbSe nanocrystals indicates the possible development of an optimized and efficient photovoltaic device in the near future.

In recent years, efficient MEG processes have been reported in PbS [78], PbSe [79], PbTe [80], CdSe [81], and Si [82]. Toward realization of this goal fundamental studies are needed to be carried out such as ultrafast exciton dynamic studies as well as better device architecture.

1-6- Nanowires Based - Colloidal Quantum Dot Sensitized Solar cell:

Driven by the unique characteristics of NWs and QDs, they are considered as potential materials for solar energy conversion. The combination of these 2 Nanostructures has been the focus of recent research. Solar energy is converted to electrical potential by a sequence of events: the absorption of light, generation of charge carriers (electrons and holes), the separation of the electrons –holes and their transport to electrodes. Figure 1- 19

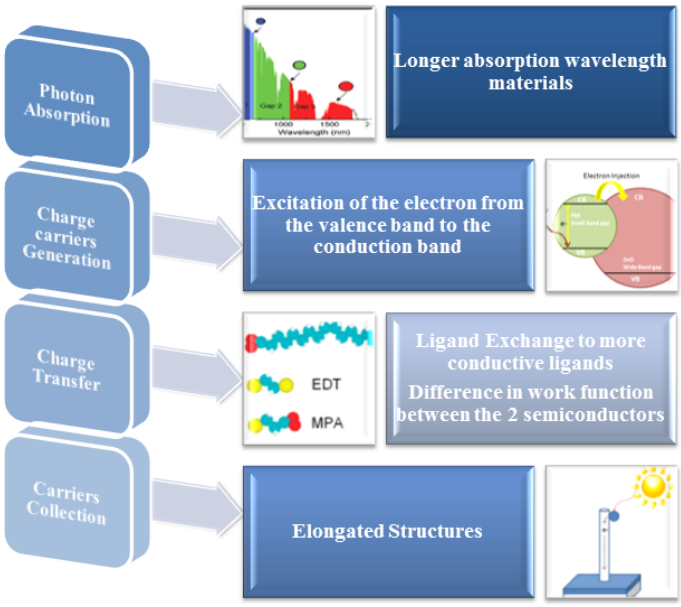

Figure 1- 18- Solar energy conversion

Photon Absorption; Narrow band gap QDs are the most suitable nanostructure to be used to maximize the absorption of the incident light upon illumination of the Photovoltaic cell. Tuning the effective band gap of the QDs, will maximize the absorption of solar spectrum. On the other hand, the periodic Array of nanowires provides excellent light trapping and improves absorption.

Generation of charge carriers: The absorption of light causes excitation of an electron from the valence band to the conduction band. The excited electron leaves behind a positive hole. QD can enhance physical processes, such as the generation of multiple excitons per absorbed photon and the extraction of hot electrons or holes.[83] In order to harvest the potential energy of this electron-hole pair through external load, the electron and hole must be separated spatially. The electron statically bound electron –hole pair called an exciton undergoes dissociation at the QDs /NWs interface.

Charge transfer: In order to harvest the energy of the generated charge, electron-hole must be separated spatially. This is achieved through electron transfer where the electron moves from the QD conduction band to the wideband band gap semiconductor conduction band. Figure 1- 20 shows the energetics of the QD

sensitizer, the wide band gap NWs semiconductor along with the electrodes. The electrons are energetically drawn to transfer to states as high as possible. In order to achieve the conversion process, the QD conduction band must be above the NW conduction band. The attachment of QD on the surface of the NWs is very critical for electrons transfer. The charge transfer occurs by diffusion assisted by the electric field generated from the difference in work functions between the two materials.[84,85] QDs can be grown directly on NWs by in-situ growth or can be attached through bi-functional linkers.

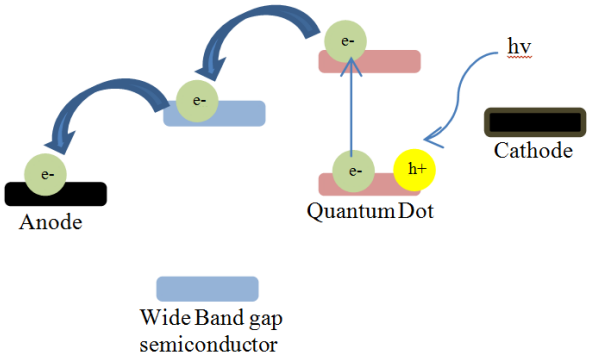

Figure 1- 19- Energetic Alignment, Wide Band gap, and Narrow Band gap Semiconductors

Carrier collections: Once electrons are transferred to the NWs, the unique geometry properties of the NWs will capture the photo-generated charges and transport them to electrodes. Furthermore the injected electrons are transported directly and very shortly to the electrode (ITO)

In this way one cycle is completed and the gained power is due to the absorbed photons by semiconductor nanocrystals. At each step, recombination of electron and hole can occur, preventing their contribution to the external current. In addition to the fundamental restrictions of the device, such as how much light can be absorbed, these recombination losses limit the overall maximum efficiency of the device and hence need to be minimized by all possible means. Furthermore the charge transfer is very important specially in the case of using a linker, where a ligand exchange process must be executed to improve the charge transfer.

1-7- Proposed Solar Cell structure

Based on the above, our research is about developing a Nanowire based Quantum Dots Sensitized Solar Cell (Figure 1- 21).

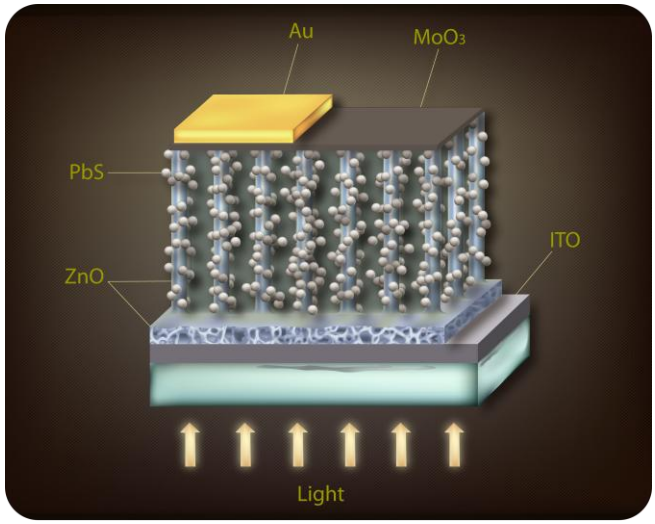

Figure 1- 20- Illustration of the Proposed Solar Cell in this research.

Glass substrates will be used for light absorption. First Electrode for electrons collection will be deposited on top of the Glass substrate with a low resistivity (50-100 Ω/cm2). ZnO Nanowires vertically oriented will be grown on the Glass substrate by use of a thin film ZnO Seed Layer. These Nanowires will improve the light absorption and trapping in addition to the rapid electrons collection and transport.

Lead sulfide (PbS) will be deposited to decorate the surface of the ZnO Nanowires which will absorb the photons and generation electron hole pairs. The link between the 2 materials and the difference in work function respecting the energetic alignment will improve the charge transport to the ZnO NWs.

An Interfacial layer of MoO3 is proposed between the PbS QDs and the top contact anode (gold – Au). Because of the architecture of the oxide/ PbS n-p hetero junction, a high work function electrode is desirable for the top contact to reduce the presence of a Schottky barrier impeding the extraction of holes from the p type PbS active layer[86]. However Gao and Luther [87] have shown that Fermi Level pinning can lead to the formation of a Schottky barrier between PbS and Gold. Molybdenum oxide has been utilized as a hole injection layer for organic films [88], as an electron blocking layer and a physical buffer layer in Solar cells [89,90,91,92].

1-8- Conclusion

The sun delivers more energy to the earth in one hour than is used in a year from all currently available sources. The Photovoltaic technology carries the built, if the world's energy needs in the near future. On the other hand, thin film shows a great promise with 24% efficiency; the silicon solar cell production remains too costly at the commercial level. Nanocrystalline hybrid array show a promising future for cheaper and more efficient solar cells, while organic polymers offer a good option in terms of cost, nanocrystalline. Quantum Dots provide a tunable absorption spectrum and promise harnessing of multiple exciton generation [93]. This chapter covered an overview of the different generations of Solar cells, and their basic working principles in addition to showing the main properties and how it will be solved using the Colloidal Quantum Dots Sensitized Solar Cell. The selection of Zinc Oxide as a wide Band gap semiconductor for the synthesis of the Nanowires will be presented showing its properties, applications and its synthesis technique in Chapter 2.

References

[1] M. S. Dresselhaus and I. L. Thomas, Nature 414, 332 (2001).
[2] B. Stambouli and E. Traversa, Renewable and Sustainable Energy Reviews 6, 297 (2002).
[3] R. M. Dell and D. A. J. Rand, J. Power Sources 100, 2 (2001).
[4] Kazmerski L.L., White F. R., and Morgan G.K. Applied Physics Letters, (29):268–270, 1976.
[5] R.L. Anderson. Solid State Electronics, 5:341, 1962.
[6] U.S. Patent 2,402,662, "Light sensitive device"
[7] D.M. Chapin, C.S. Fuller, and G.L. Pearson. Journal of Applied Physics, 1954.
[8] D.C. Reynolds, G. Leies, L.L. Antes, and R.E. Marburger. Physical Review, 96:533–534, 1954.
[9] J. H. Zhao, A. H. Wang, M. A. Green and F. Ferrazza, Appl Phys Lett 73(14), 1991-1993 (1998).
[10] M. A. Green, Physica E 14(1-2), 65-70 (2002).
[11] M. A. Green, K. Emery, Y. Hishikawa and W. Warta, Prog Photovoltaics 17(5), 320-326 (2009).
[12] X. Wu, J. C. Keane, R. G. Dhere, C. Dehart, A. Duda, T. A. Gessert, S. Asher, D. H. Levi and P. Sheldon, presented at the Conf. Proceeding, 17th European Photovoltaic Slar Energy Conference, Munich, 2001 (unpublished).
[13] Press release 05/2010, Zentrum für Sonnenenergie-und Wasserstoff-Forschung Baden-Württemberg (ZSW), Germany.
[14] J. Meier, J. Spitznagel, U. Kroll, C. Bucher, S. Fay, T. Moriarty and A. Shah, Thin Solid Films 451-52, 518-524 (2004).
[15] 4 M. A. Green, Physica E 14(1-2), 65-70 (2002).
[16] R. R. King, D. C. Law, K. M. Edmondson, C. M. Fetzer, G. S. Kinsey, H. Yoon, R. A. Sherif and N. H. Karam, Appl Phys Lett 90(18), 183516 (2007).
[17] M. Pagliaro, G. Palmisano, R. Ciriminna and V. Loddo, Energ Environ Sci 2(8), 838-844 (2009).
[18] M. Riede, T. Mueller, W. Tress, R. Schueppel and K. Leo, Nanotechnology 19(42), 424001 (2008).
[19] P. Peumans, A. Yakimov and S. R. Forrest, J Appl Phys 93(7), 3693-3723 (2003).
[20] M. Helgesen, R. Sondergaard and F. C. Krebs, J Mater Chem 20(1), 36-60 (2010).
[21] M. Skompska, Synthetic Met 160(1-2), 1-15 (2010).
[22] Konenkamp R, Hoyer P, Wahi A. Heterojunctions and devices of colloidal semiconductor films and quantum dots. J Appl Phys 1996 May 1, 1996;79(9):7029-35.
[23] John E. Ayers.Digital Integrated circuits : Analysis and Design CRC Press, 2003.
[24] DOE office of Science .Basi research needs for solar energy utilization , April 2005, http://www.sc.doe.gov/bes/reports/list.html
[25] B.A.Gregg, in organic photovoltaics, edited by S.S.Sun and N.S.Sariciftci (Marcell Dekker, Ney York , 2005) pp 139
[26] S.Gunes , K.P.Fritz,H.Neugebauer, N.S.Sariciftci, and G.D. Scholes, Sol Eng.Mater.Sol 91(5), 420-423 (2007)

[27] B.C,Thompson and J.M.J.Frechet, Angew Chen , Int Edit 47 (1), 58-77 (2008).
[28] R.S. Wagner, W.C. Ellis, Appl. Phys. Lett. 4 (1964) 89.
[29] W.U. Huynh, J.J. Dittmer, A.P. Alivisatos, Science 295 (2002) 2425.
[30] O. Hayden, R. Agarwal, W. Lu, 2008 Semiconductor Nanowire Devices, Nanotoday, 3, 12, 17480-1321
[31] P. J. Pauzauskie, P. Yang, 2006 Nanowire Photonics, Materials Today, 9, 36, 1369-7021
[32] P. Yang, R. Yan, M. Fardy, 2010 Semiconductor Nanowire: What's Next?, Nano letter, 10 152936
[33] W. Lu, C. M. Lieber, 2007 Nanoelectronics from the Bottom Up, Nat. Mater., 6 841850 1476-1122
[34] L. Cao, J. S. White, J. S. Park, J. A. Schuller, B. M. Clemens, M. L. Brongersma, 2009 Engineering Light Absorption in Semiconductor Nanowire Devices, Nat. Mat., 8 643647 , 1476-1122
[35] R. E. Algra, M. A. Verheijen, M. T. Borgstrom, L. F. Feiner, G. Immink, W. J. P. van Enckevort, E. Vlieg, E. P. A. M. Bakkers, 2008, Nature, 456 369372 , 0028-0836
[36] Kehan Yu, Junhong Chen . Nanoscale Res Lett (2009) 4:1–10 Enhancing Solar Cell Efficiencies through 1-D Nanostructures,
[37] Z. L. Wang, "ZnO nanowire and nanobelt platform for nanotechnology," Materials Science & Engineering RReports, vol. 64, pp. 33-71, Apr 3 2009.
[38] Y. G. Wei, et al., "Planar Waveguide-Nanowire Integrated Three-Dimensional Dye-Sensitized Solar Cells," Nano Letters, vol. 10, pp. 2092-2096, Jun 2010.
[39] C. Soci, A. Zhang, B. Xiang, S. A. Dayeh, D. P. R. Aplin, J. Park, X. Y. Bao, Y. H. Lo, and D. Wang, "ZnO nanowire UV photodetectors with high internal gain," Nano Lett., vol. 7, pp. 1003–9, 2007.
[40] D. Spirkoska, G. Abstreiter, i. Fontcuberta, A. Morral, 2008, Nanotechnology,19, 435704, 0957-4484
[41] S. Sahoo, S. Dhara, A. K. Arora, R. Krishnan, P. Chandramohan, M. P. Srinivasan, 2010, Appl. Phys. Lett. 96, 103113
[42] K. W. Adu, Q. Xiong, H. R. Gutierrez, G. Chen, P. C. Eklund, 2006, Appl. Phys. A 85, 287, 0947-839609478396Xiong 2006
[43] Q. Xiong, G. Chen, H. R. Gutierrex, P. C. Eklund, 2006, Appl. Phys. A, 85 299305 , 0947-8396
[44] L. Y. Cao, L. Laim, P. D. Valenzuela, B. Nabet, J. E. Spanier, (2007, (2007).,J. Raman. Spectrosc. 38 697703 697703 0377-0486
[45] J. Frechette, C. Carraro, 2006,Phys. Rev. B, 74, 2161404, 1098-012110980121
[46] L. Y. Cao, B. Nabet, J. E. Spanier, 2006, Phys. Rev. Lett., 96 1574025 , 0031-9007
[47] Y. B. Tang, Z. H. Chen, H. S. Song, C. S. Lee, H. T. Cong, H. M. Cheng, W. J. Zhang, I. Bello, S. T. Lee, 2008. Nano Lett., 8 12 (October 2008), 41914195 , 1530-6984
[48] O. L. Muskens, J. G. Rivas, R. E. Algra, E. P. A. M. Bakkers, A. Lagendijk, 2008. Nano Lett., 8 9 (August 2008), 26382642 , 1530-6984
[49] Hong BH, Bae SC, Lee CW, Jeong S, Kim KS. Science 2001;294:348–51.
[50] Nishizawa M, Menon VP, Martin CR. Science 1995;268:700–2.

[51] Liang CH, Chen LC, Hwang JS, Chen KH, Hung YT, Chen YF. Appl Phys Lett 2002;81:22–4.
[52] Ma RZ, Bando Y, Sato T. Adv Mater 2002;14:366–8.
[53] Patzke GR, Krumeich F, Nesper R. Angew Chem Int Ed 2002;41:2446–61.
[54] Mathur S, Barth S, Werner U, Hernandez-Ramirez F, Romano-Rodriguez A. Adv Mater 2008;20:1550–4.
[55] Pan ZW, Lai HL, Au FCK, Duan XF, Zhou WY, Shi WS, et al. Adv Mater 2000;12:1186–90.
[56] Ho GW, Wong ASW, Wee ATS, Welland ME. Nano Lett 2004;4:2023–6.
[57] Li QG, Penner RM. Nano Lett 2005;5:1720–5.
[58] Mao GZ, Dong WF, Kurth DG, Mohwald H. Nano Lett 2004;4:24952.
[59] Liu, C.H.; Zapien, J.A.; Yao, Y.; Meng, X.M.; Lee, C.S.; Fan, S.S.; Lifshitz, Y. & Lee, S.T. (2003). High-density, ordered ultraviolet light-emitting ZnO nanowire arrays. *Advanced Materials* 15, 838–841, ISSN: 0935–9648.
[60] Garnett, E.C., Yang, P. J. Am. Chem. Soc., **2008**, 130, 9224.
[61] Chiba.Y,Islam.A,Watanabe.Y,Koniya.R, Koide.N, Han.L , 2006 Dye sensitized solar cells with conversion efficiency of 11.1% JPN,J.App.Phys. 45,638-640
[62] Saim Emin, Surya P. Singh , Liyuan Han, Norifusa Satoh, Ashraful Islam , Solar Energy 85 (2011) 1264–1282
[63] Robel, I., Subramanian, V., Kuno, M., Kamat, P., 2006. J. Am. Chem. Soc. 128, 2385–2393
[64] N.L. Dmitruk, O.Yu. Borkovskaya, S.V. Mamykin, D.O. Naumenko, V. Meza-Laguna, E.V. Basiuk (Golovataya-Dzhymbeeva), I. Puente Lee .Thin Solid Films, Volume 518, Issue 6, 1 January 2010, Pages 1737–1743
[65] Yeong-Her Wang1 、 Chien-Jung Huang2 、 Pin-Hsiang Chiu3 Nanotechnology, 17, 5355 (October, 2006)
[66] Harekrishna Bar, Dipak K. Bhui, Gobinda P. Sahoo, Priyanka Sarkar, Santanu Pyne, Dipankar Chattopadhyay & Ajay Misra Journal of Experimental Nanoscience Volume 7, Issue 1, 2012
[67] Nanoparticles: Synthesis , stabilization passivation and functionalization by Ramanathan Nagarajan and T.Alan Hatton 2008
[68] L. Vegard: Z. Phys. 5 (1921) 17
[69] L.E.Brus, J.Chem.Phys, 1984, 80, 4403
[70] A.kingKanad,K,Tvrdy,K.Takechi, M.Kuno, P.V.Kamat, J.Am.Chem.Soc. 130 , 4007 (2008)
[71] I.Gur, N.A.Former, M.L.Geier, A.P.Alivistos, Science 310, 462 (2005)
[72] J. Tang, K. W. Kemp, S. Hoogland, K. S. Jeong, H. Liu, L. Levina, M. Furukawa, X. Wang, R. Debnath, D. Cha, Kang, W.Chou, A. Fischer, A. Amassian, J. B. Asbury& E. H. Sargent (2011) Nature Materials10, 765-771
[73] E.J.D.Klem , D.D.MacNeil, P.W.Cyr, L.Levina and E.H.Sargent , Appl.Phys.Lett 90, 183113(2007)
[74] J.H.Luther, M.Law, Q.Song,C.Perkins, M.C.Beard, A.J.Nozik ACS Nano, 2, 271 (2008).
[75] Schaller R D, Sykora M, Pietryga J M, Klimov V I (2006) Seven excitons at the cost of one: redefining the limits for conversion efficiency of photons into charge carriers. Nano Lett6: 424

[76] 49. Schaller R D, Agranovich V M, Klimov V I (2005) High efficiency carrier multiplication through direct photogeneration of multi excitons via virtual single exciton states. Nature Phys 1: 189
[77] 50. Ellinson R, Beard M, Johnson J, Yu P, Micic O, Nozik A, Shabaev A, Efros A (2005) Highly efficient multiple exciton generation in colloidal PbSe and PbS quantum dots. Nano Lett 5: 865
[78] V. Sukhovatkin, S. Hinds, L. Brzozowski, and E. H. Sargent, Science 324, 1542 (2009).
[79] J. J. H. Pijpers, R. Ulbricht, K. J. Tielrooij, A. Osherov, Y. Golan, C. Delerue, G. Allan & M. Bonn Nature Physics 5, 811 - 814 (2009))
[80] Murphy, J., Beard, M., Norman, A., Ahrenkiel, S., Johnson, J., Yu, P., Mic´ic´, O., Ellingson, R., Nozik, A., 2006.. J. Am. Chem. Soc. 128, 3241–3247.)
[81] Schaller, R., Sykora, M., Jeong, S., Klimov, V., 2006. J. Phys.Chem. B 110, 25332–25338.
[82] Beard, M., Knutsen, K., Yu, P., Luther, J., Song, Q., Metzger, W., Ellingson, R., Nozik, A., 2007. Nano Lett. 7, 2506–2512)
[83] A.J.Nozik , Physica E. 14, 115 (2002)
[84] Sariciftci N S, Heeger A J (1994). Int J Mod Phys B 8: 237
[85] Ginger D S, Greenham N S (1999). Phys
[86] Zarghami , M.H;Liu,Y.; Gibbs,M.; Gebremichael, E.; Webster, C.;Law, M. ACS Nano 2010, 2475-2485
[87] Gao,J.;Luther, J.M.; Semonin, O.E; Ellingson, R.J.;Nozik, A.J.;Bread, M.C. Nano Lett. 2011, 11, 1002-1008.
[88] Krc̈oger, M.; Hamwi, S.; Meyer, J.; Riedl, T.; Kowalsky, W.; Kahn, A. Appl. Phys. Lett. 2009, 95, 123301.
[89] Kim, D. Y.; Subbiah, J.; Sarasqueta, G.; So, F.; Ding, H.; Gao, Y. Appl. Phys. Lett. 2009, 95, 093304.
[90] Hancox, I.; Chauhan, K. V.; Sullivan, P.; Hatton, R. A.; Moshar, A.; Mulcahy, C. P. A.; Jones, T. S. Energy Environ. Sci. 2010, 3, 107.
[91] Lee, J. H.; Cho, S.; Roy, A.; Jung, H.-T.; Heeger, A. J. Appl. Phys. Lett. 2010, 96, 163303.
[92] Sun, Y.; Takacs, C. J.; Cowan, S. R.; Seo, J. H.; Gong, X.; Roy, A.; Heeger, A. J. Adv. Mater. 2011, 23, 2226–2230.
[93] DOE Office of Science. Basic Research Needs for Solar Energy Utilization , April 2005.

CHAPTER 2:

ZnO, One dimensional Nanostructure

Table of Contents

2-1- Introduction:

The growing demand of ultra-light, smart, and multifunctional devices together with faster information-processing ability has led to the discovery of many new optical materials and the miniaturization of optoelectronic devices that also feature better performance, low cost, and low power consumption. Among various nanomaterials, semiconductors NWs offer opportunities for photonics and electronics applications. As a result, they have drawn intense research interest. Obviously, the realization of nano-scale devices not only requires suitable materials with unique properties for specific applications, but also the ability to control key parameters of the nanostructures including their size, shape, spatial distribution, and doping. ZnO NWs represent one of the nanomaterial systems, where these key parameters have been best studied and controlled to date. The wide band gap II-VI semiconductors have been intensively studied for many years due to their great potentials for a variety of applications in the area of optics, electronics, piezo-electronics, sensing, etc. Particularly, as an environmental friendly material, 1D ZnO nanostructures have intensively been used in research for clean and sustainable solar energy devise.

This chapter presents the state of art in the growth of ZnO Nanowires and is divided in three folds: first to present the basic physical properties of Zinc oxide with its applications. In the second fold different ZnO Nanowires synthesis techniques are reviewed. The third fold summarizes the different characterization techniques to identify the structural, microstructural, morphological and optical properties.

2-2-Chapter Objectives:

The objectives of this chapter are to:

- Explain the reason behind selecting Zinc Oxide as material for one dimensional nanostructure for solar cell applications
- Review the properties of zinc oxide
- Describe the past, present and emerging applications of ZnO.
- Summarize the different growth techniques of ZnO Nanowires
- Describe the characterization techniques used to identify the properties of ZnO nanowires.

2-3- Properties of Zinc Oxide

2-3-1 History of Zinc oxide (ZnO) research

Photovoltaic nanowires have been invented using a wide variety of materials such as zinc oxide, copper oxide, titanium oxide, silicon, germanium, zinc sulfide, cadmium telluride, cadmium selenide, gallium nitride, indium gallium nitride, gallium arsenide, and indium arsenide [1] .Output efficiencies have steadily increased so that most material systems have now achieved efficiencies higher than 1%, with some close to 10%, but a number of unresolved questions must be answered before such materials can be used in commercial devices. ZnO is not new to the semiconductor field. The research on ZnO goes back to the first half of the last century in terms of crystal structures and properties such as: investigations on its lattice parameter in 1935 by Bunn[2], its vibrational properties with Raman scattering in 1966 by Damen et al.[3] , detailed optical studies in 1954 by Mollwo [4], and its growth by chemical-vapor transport in 1970 by Galli and Coker [5]. In terms of research on devices demonstrations, Mead in 1965 [6] studied the Au Schottky barriers, Drapak in 1968 [7] demonstrated light emitting diodes, Minami et al in 1974 [8] studied a metal insulator semiconductor structures, Tsurkan et al [9] investigated a ZnSe/ZnO p-n junction, and Brillson in 1978 [10] studied the ohmic contacts with Al/Au. The main obstacle to the development of ZnO has been the lack of reproducible and low-resistivity *p*-type ZnO, Look and Claflin[11].

Very high quality nanostructures have been prepared early on and used to deduce much of the principal properties of this material, particularly in terms of optical processes.[12] There has been a great deal of interest in zinc oxide (ZnO) semiconductor materials lately, as seen from a flow of a relevant number of publications. The interest in ZnO is fueled and waved by its prospects in optoelectronics applications owing to its unique properties (direct wide band gap *(Eg*~3.3 eV at 300 K). Some optoelectronic applications of ZnO overlap with that of GaN, another wide-gap semiconductor (*Eg* ~ 3.4 eV at 300 K) which is widely used for production of green, blue-ultraviolet, and white light-emitting devices. However, ZnO has some advantages over GaN (presented in next section) resulting in a potentially lower cost for ZnO-based devices.

2-3-2 Crystal structure and lattice parameters

Under conventional conditions, ZnO has the wurtzite structure which has a hexagonal unit cell. The oxygen anions and ZnO cations form a tetrahedral unit. The entire structure lacks of central symmetry. The structure of ZnO can be simply described as a number of alternating planes composed of tetrahedrally [13] coordinated O^{2-} and Zn^{2+} ions, stacked alternatively along the c-axis (Figure 2- 1).

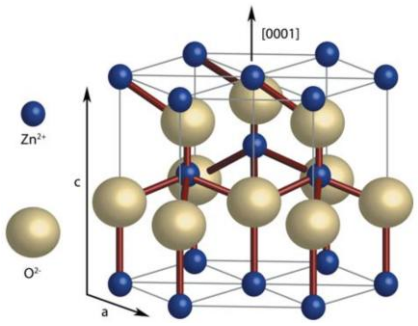

Figure 2- 1- Hexagonal wurtzite Structure of ZnO

Physical properties are summarized in **Table 2- 1**.

Table 2- 1- Physical properties of wurtzite ZnO

Properties	Value
Lattice constants(T = 300 K)	
a0	0.32469 nm
c0	0.52069 nm
Density	5.606 g/cm^3
Melting point	2248 K
Relative dielectric constant	8.66
Gap Energy	3.37eV, direct
Intrinsic carrier concentration	< 10^6 cm^{-3}
Exciton binding Energy	60 meV
Electron effective mass	0.24
Electron mobility (T = 300 K)	200 cm^2/V s
Hole effective mass	0.59
Hole mobility (T = 300 K)	5-50 cm^2/V s

2-3-3 ZnO properties and Applications

The unique properties of ZnO will provide a great opportunity for different applications that we be listed below:

a. ***Direct and wide band gap***. The band gap of ZnO is 3.44 eV at low temperatures and 3.37 eV at room temperature[14] . For comparison, the respective values for wurtzite GaN are 3.50 eV and 3.44 eV [15]. The wide band gap ZnO enables applications in optoelectronics in the blue/UV region, including light-emitting diodes, laser diodes and photodetectors[12]. Optically pumped lasing has been reported in ZnO thin films[16] , and ZnO nanowires[17]. Reports on p–n homojunctions have recently appeared in the literature[18][19][20][21], but stability and reproducibility have not been established.

b. ***Large exciton binding energy***. The free-exciton binding energy in ZnO is 60 meV [24], compared with, e.g. 25 meV in GaN [[22][16]]. This large exciton binding energy indicates that efficient excitonic emission in ZnO can persist at room temperature and higher [15]. The large exciton binding energy makes ZnO a promising material for optical devices that are based on excitonic effects.

c. ***Large piezoelectric constants***. In piezoelectric materials, an applied voltage generates a deformation in the crystal and vice versa. These materials are generally used as sensors, transducers and actuators. The low symmetry of the wurtzite crystal structure combined with a large electromechanical coupling in ZnO gives rise to strong piezoelectric and pyroelectric properties. Piezolectric ZnO films with uniform thickness and orientation have been grown on a variety of substrates using different deposition techniques, including sol–gel process, spray pyrolysis, chemical vapor deposition, molecular-beam epitaxy and sputtering[23][24][25][26][27][28][29][30].

d. ***Strong luminescence.*** Due to a strong luminescence in the green–white region of the spectrum, ZnO is also a suitable material for phosphor applications. The emission spectrum has a peak at 495 nm and a very broad half-width of 0.4 eV [31]. The n-type conductivity of ZnO makes it appropriate for applications in vacuum fluorescent displays and field emission displays.

e. ***Strong sensitivity of surface conductivity to the presence of adsorbed species***. The conductivity of ZnO thin films is very sensitive to the exposure of the surface to various gases. It can be used as a cheap smell sensor capable of detecting the

freshness of foods and drinks, due to the high sensitivity to trimethylamine present in the odor [[32].

f. ***High thermal conductivity***. This Property increases the appeal of ZnO as a substrate for homoepitaxy or heteroepitaxy (e.g. for growth of GaN, which has a very similar lattice constant) [[33][34]]. High thermal conductivity translates into high efficiency of heat removal during device operation.

g. ***Availability of large single crystals***. One of the most attractive features of ZnO as a semiconductor is that large area single crystals are available, and epitaxy substrates are now commercialized. Bulk crystals can be grown with a variety of techniques, including hydrothermal growth [35][36], vapor-phase transport [37] and pressurized melt growth [38]. Growth of thin films can be accomplished using chemical vapor deposition (MOCVD) [39], molecular-beam epitaxy [40], laser ablation [41] or sputtering[42]. The epitaxial growth of ZnO on native substrates can potentially lead to high quality thin films with reduced concentrations of extended defects. This is especially significant when compared with GaN, for which native substrates do not exist. In view of the fact that the GaN-based devices have achieved high efficiencies despite the relatively large concentration of extended defects, it is possible that a high-quality ZnO-based device could surpass the efficiencies obtained with GaN. Summary of Applications are summarized in (Figure 2- 2).

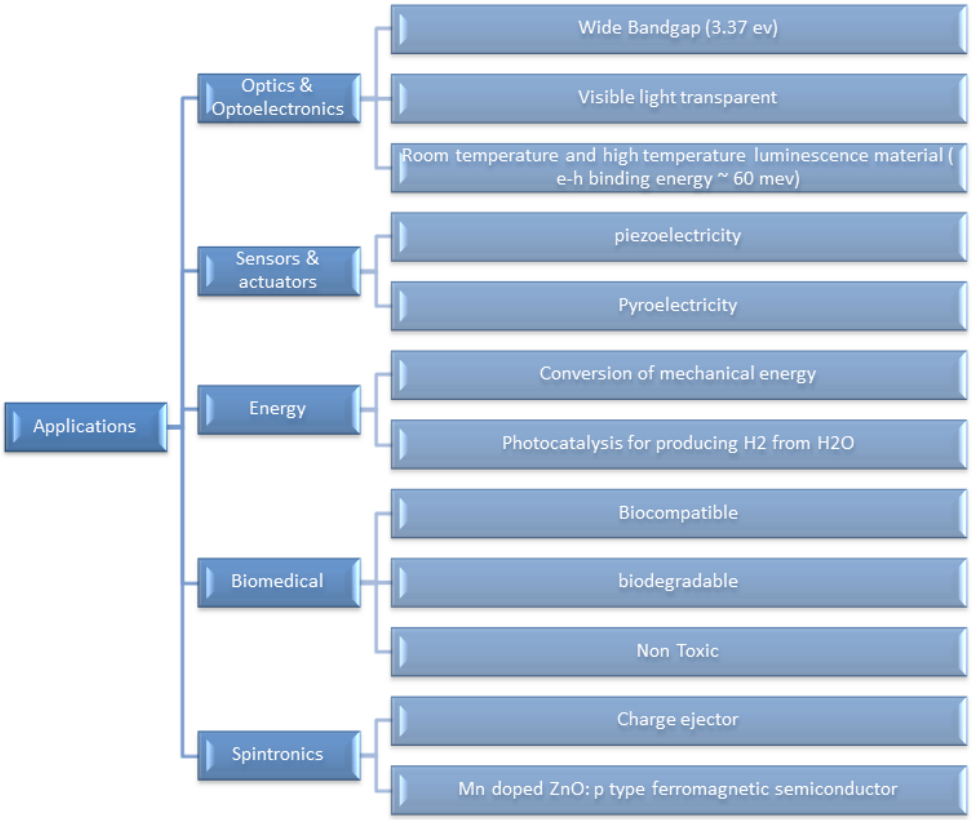

Figure 2- 2-- Chart showing the different types of Zinc oxide applications

2-3-4 Sources of Defect in ZnO

Useful information about defects in ZnO nanostructures can be obtained by examining the Photoluminescence properties at Room Temperature (RTPL). The electrons in ZnO semiconductors are photo-excited by a Xenon Lamp or laser and when they spontaneously de-excite they emit luminescence. The luminescence is analyzed with a spectrometer and the peaks in the spectra represent a direct measure of the energy levels in the semiconductor. In ZnO spectra, typically in addition to UV emission, there are also one or more emission bands in the visible spectral region which originate from defect emissions [43] .It should be noted that most of the RTPL studies of ZnO nanostructures focus on the origin of defect emission or the ratio of UV-to-visible emission. Due to small size of exciton Bohr radius in ZnO (2.34nm), quantum confinement effects can be observed only in very small nanostructures, for example Nanowire with radius 1.1nm[44] . Thus, no such effects would be expected in nanostructures in size range typically used in optoelectronic devices. However, position of the near-band-edge emission at room temperature can vary significantly due to variations in relative contributions of free exciton emission and phonon replicas, which will be different for different growth conditions[45] . Positions and proposed origin of room temperature PL peaks in ZnO summarized in Table 2- 2.

Table 2- 2- Sources of Defect in ZnO

Peak Position	Proposed Origin	Reference
373-390	Near – and edge emission	[46]
~420	O_{zn}	
~446	Shallow donor oxygen vacancy transition	[47]
~459	Zinc Interstitial	[48]
~495	Oxygen vacancy	[49]
~510	Surface defects/defect complexes	[50]
~510	Singly ionized oxygen vacancy	[51]
~520	Zinc Vacancy	[52]
~520	O_{zn}	[53]
~520	Oxygen vacancies and zinc interstitials	
~540	V_o	[54]
~560	Surface defects	[55]
~566	Shallow donor deep acceptor	[56]
~580	Oxygen interstitials,	[57]
~626	Oxygen interstitials	[58]
~750	Oxygen related defects , zinc interstitials	[59]

2-4- One Dimensional Nanostructures (1D)

2-4-1 Introduction to 1D Nanostructures

With The rapid progression of modern microelectronics, nanowires (NWs) began to draw the attention of research communities two decades ago and soon turned into a very active research field. Applications of NWs now span a broad range including diodes[60][61], field effect transistors[62], logic circuits[63][64][65][66][67], single electron transistors[68], optoelectronic devices[69][70][71][72][73][74][75], sensors[76], thermo-electrical devices[77], photo-catalysis[78][79], and piezo-electronics[80][81][82].

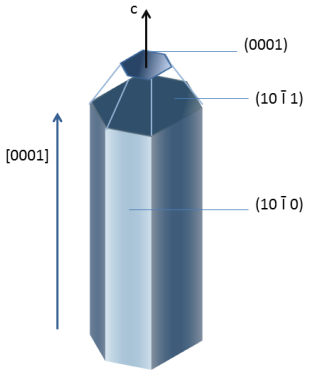

Figure 2- 3- One dimensional nanostructures, Hexagonal Nanowire.

In these realms NW structures exhibit unique and superior properties compared to their bulk counterparts, properties in which their 1 D confined transport of electrons or photons, large surface area, quantum confinement and excellent mechanical properties play major roles. For example, single-crystalline NW electrodes were introduced to batteries[83], solar cells[73], and photo electrochemical cells[79] for effective charge separation and collection. Quantum confinement in semiconductor NWs achieved by tuning the characteristic dimension allows the creation of photonic and optoelectronic devices that differ from conventional thin-film-based ones. [74] High flexibility and excellent fatigue resistance make NWs advantageous building blocks for nano-generators that search mechanical energies from the ambient environment. [80][81]In addition, the ability to integrate NWs in a large area with a controlled pattern has created a new path toward NW-based flexible electronic and optoelectronic systems that might eventually realize roll-to-roll mass production.[70] One essential aspect of the mass production of NW-based devices is the uniformity

and controllability of the NW's dimensions and properties, which require a comprehensive and intensive understanding of the 1D growth phenomena. A number of fundamental problems and issues have been addressed and solved, leading to an in-depth understanding of NW growth mechanisms as well as their precise morphology (Figure 2- 3) and property control [84].

2-4-2 Nanowires Role in Photovoltaic devices:

Over the past decade, both solar cell research and nanowire research have become hot topics within science and engineering [85][86][87][88][89]. The need for higher solar cell efficiencies at lower cost has become apparent, and at the same time synthetic control in nanoscience has improved such that high-performance electronic devices are becoming possible[90][91][92]. The unique geometry of NWs array provides low optical reflection and enhances light trapping and absorption within NWs arrays (Figure 2- 4).

a- Light trapping in NWs Array

b- Direct electron transportation in NWs Array

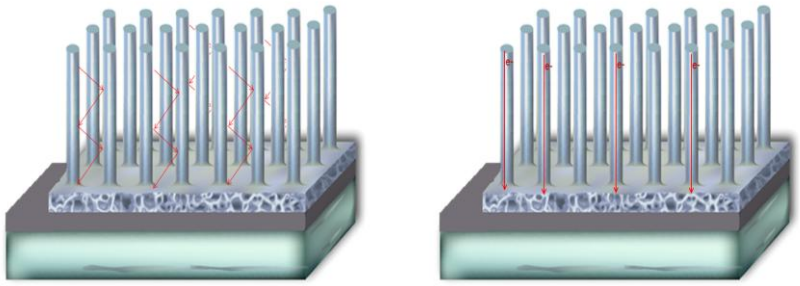

Figure 2- 4- Schematic illustratio for Nanowires in light trapping and electron transport to electrodes

As previously discussed in Chapter 1, the free standing NWs array allows the incident light to scatter within its open interiors, which is different from the easy reflection of incident light on the surface of nano-crystallines film. The scattering improves the efficiency of light absorption by increasing the photon path length and diminishing the reflection of incident light. The photo-generated electron –hole pairs in bulk thin film tend to recombine at grain boundaries before they arrive the back contact, while free standing NWs array grown on conducting substrate avoids this shortcoming because the photo-generated charges can be transported to the substrate along

individual nanowires which will enhance the photocurrent efficiency. The carrier concentration is about 10^{20} cm^{-3}, and the electron mobility reaches several tens of cm^2 V^{-1} s^{-1} in ZnO NWs material, and electronic transports occur only along the axis of the wires. These unique electronic properties mean that the photo-generated charges can be transported to the conducting substrate quickly. Nanowire solar cells have some potential benefits over traditional wafer-based or thin-film devices related to optical, electrical, and strain relaxation effects; new charge separation mechanisms; and cost. Ordered arrays of vertical nanowires with radial junctions take advantage of all these effects, although solar cells made using axial junctions (Figure 2- 5). Electron hole pairs are generated differently within semiconductor under light illumination based on the geometry of the Photovoltaic devices .Three different geometries are identified: axial, radial and substrate junctions.

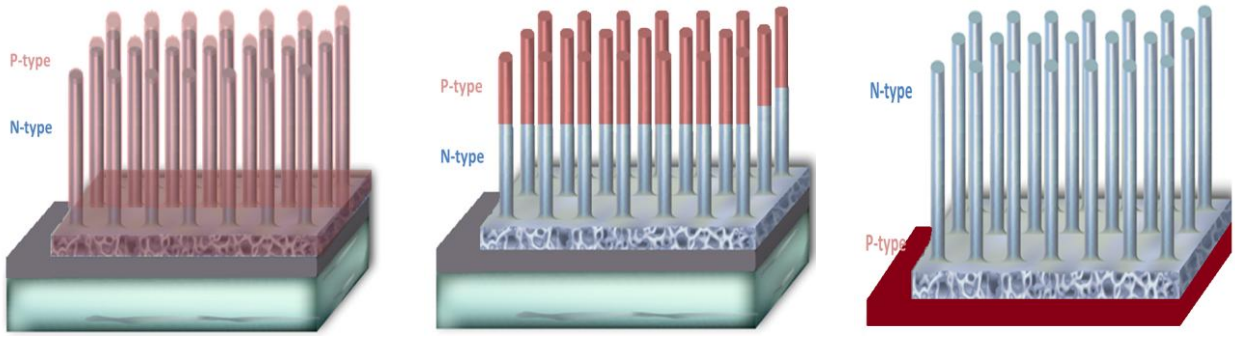

a- Radial Junction **b-Axial Junction** **c- Substrate Junction**

Figure 2- 5- Nanowire Arrays benefits for Solar Cells. a)Radial Hetero-structure , b)Axial Homo-junction , c) Substrate hetero-structure .

In axial structure, usually considered as homo-junction, the electron hole pairs are generated within the semiconductor and the carriers are separated where the electron and hole migrate in the opposite directions towards the two ends of the NWs.

The hetero-junction in a radial structure extends the interface along the surface of the Nws, resulting in a short carrier diffusion range and large interface for efficient carrier separation and transport. On the other hand, in the substrate junction, the interface is extended on the cross section of the NWs which shorten the carrier diffusion range to the diameter of the NWs. Bulk recombination in radial junction is largely suppressed due to the large junction area and short diffusion length compared to the axial and substrate junctions. Radial Junctions is selected in this research and will be presented in details in chapter 4. Excitonic Solar Cells are considered as promising inexpensive

Solar Cell type. The solar to electric energy processes are separated into different materials that comprise the solar cell. This separation allows the cell to operate as a majority carrier device where the electrons transport through electron rich materials and the holes transport through hole rich materials. The Chemical potential difference across the cell is the main driving force separation that leads to the photovoltaic effect. Nanowires of wide band gap semiconductors such as TiO_2 and ZnO find applications in variety of Excitonic Solar Cells as the electron acceptor and conductor. The Effective use of Nanowires require the ability to control and tailor their dimensions and morphology (height, diameter, spacing and planar density).

2-4-2-1 ZnO NWs Based Dye Sensitized Solar Cell (DSSC)

Among the excitonic solar cells, the dye sensitized cell (DSSC), is considered a class of low cost solar cell. In a DSSC, dye molecules are used to sensitize wide-band gap semiconductors, such as TiO_2 and ZnO, which assist in separating electrons from photo-excited dye molecules. The sensitization of wide-band gap semiconductors by adsorbed monolayers of dye molecules began in the late 1960s with the work of Gerishcer [93] and Memming [94]. 1-D wide-band gap semiconductor nanostructures were thus introduced to improve the charge collection. Upon solar irradiation, the injection of photo- generated electrons occurs from dye molecules to the conduction band of nano-crystalline films, leaving the dye in the oxidized state. The dye is restored to its original state via electron transfer in an electrolyte from an Iodide I^- ion, forming a tri-iodide I^{-3} in the redox system (Figure 2- **6**a). The limitation of the DSSC is the poor absorption of low energy photons using available dyes. The redox electrolyte's instability is one of the current challenges, where it degrades over time under UV radiation and may leak if the cell is not perfectly sealed rendering the device inefficient for long term use **Error! Reference source not found.**.

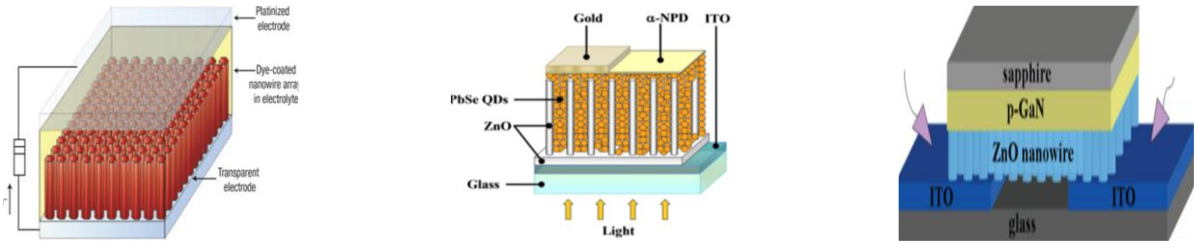

a- Dye sensitized solar cell employing ZnO nanowires [95]

b- PbSe QD/ZnO nanowire solar cell [130]

c- ZnO nanowires / p-GaN heterojunction LED [80]

Figure 2- 6-Schematic of ZnO Nanowires based a) DSSC , b) QDSSC, c) LED

2-4-2-2 ZnO Nws Based Quantum Dots Sensitized Solar Cell (QDSSC)

ZnO-based DSSCs have still lower conversion efficiencies compared withTiO2 nanoparticles, resulting from the two main obstacles:(1) instability of ZnO inacidic dyes,i.e. protons from the dyes cause the dissolution of Zn atoms at ZnO surface and thus result in the formation of excessive Zn^{2+} /dye agglomerates [96]; (2)slow electron-injection kinetics from dyes to ZnO caused by competition processes between the ultrafast electron injection and molecular relaxation [97]. To overcome these problems, semiconductor QDs have been used as photosensitizers to replace dyes, which are accordingly called QDSSCs **Error! Reference source not found.**. Theoretically, the conversion efficiency of QDSSCs can reach 44% that is considerably higher than that of DSSCs **Error! Reference source not found.**. The co-sensitization of different sized QDs will increase the adsorption coverage of solar spectrum and thus increase light harvesting efficiency, (Figure 2- 6b). Many techniques are employed using smaller band-gap materials to expand the absorbance, which in turn increase the light harvesting and overall energy-conversion efficiency of the solar cell. Many researchers reported the development of QDSSCs, which are summarized in Table 2- 3

Table 2- 3-Summary of different Nanoparticles with their deposition process

NPs	Deposition Process	PCE %	Reference
CdS	CBD	0.9	X.Yu et al (2011)[100]
CdS-CdSe	CBD	1.42	J.chen et al (2010)[102]
PbSe	Dipping in EDT Passivated solution	1.6	K.S.Leshkies et al (2009)[103]
PbS	Using Thioacetamide (ZnS)→ ZnO - PbS	--	Y.F.Zhu et al (2011)[104]
CdS-CdSe	Thioglycolic Acid	1	C.Luan et al (2011)[105]
CdS – PbS	SILAR	0.38	C.Liu et al (2011)[106]
CdTe	LbL	6.6 10^{-3}	J.Briscoe et al**Error! Reference source not found.**
CdS- CdSe	SILAR	1.72	X.Qiu et al (2011)[107]
CdSe-CdS		4.12	S.H.Im et al [108]
CdS-CdSe	CBD	--	G.Wang et al[109]
CdS	CBD	0.34	Y.Zhang et al (2009)**Error! Reference source not found.**
CdS	SILAR	3.53	Y.Tak et al (2009)[110]
CdSe	CBD	0.4	K.S.Leshkies et al (2007)**Error! Reference source not found.**
ZnS/CuInS2	CBD	0.71	K.-T.Kuo et al (2009)[112]
Cu2O	CBD	0.053	B.D.Yuhas et al (2009)[115]

CBD: Chemical Bath Deposition
SILAR: Successive Ionic Layer Adsorption and Reaction
LbL: Layer by Layer
EDT: Ethanedithiol

2-4-3 ZnO Nws LED

ZnO Nw based LED have widely studied [115][117][118][119] , owing to the unique properties of ZnO such as its low cost, ease of fabrication , large index of refraction (n~2) and large exciton binding energy (60mev). These properties make ZnO a prefereable candidate and suiTable 2- LED material, despite the lack of reliable P-doping. LED technology suffers serious challenges in terms of poor extraction efficiency and intensity dependence on the junction area. Current research focuses on dense NW arrays where the challenges can be addressed. One of the most straightforward applications of ZnO nanorods in LEDs is their growth on fabricated GaN-based LEDs to increase light extraction efficiency, and increase up to 57% has been demonstrated. Although there are few reports on ZnO-NW homojunction LEDs [69], [120] X.W.Sun et al (2009). Most of the investigations are based on hybrid structures using a polymer as the p-conducting material , [117] [121] [122][123][124][125] or p type semiconductor like GaN by E.Lai (2008) [128] , C-H.Chen et al (2010) [130] (Figure 2- 6c), S.J.An et al (2008)[126]. Summary presented in Table Table 2- 4.

Table 2- 4- Survey of Structure, Method, emission color of hetero-structure ZnO Nws LED

Junction	Emission	Growth Method	Ref
n-znO/p-GaN	456 nm	MOCVD	S.J.An et al (2008)[126]
nZnO/ Poly (3 –methylthiophene)	382nm	Electrochemical	H.Gao et al (2008)[127]
nZnO/pGaN		MOCVD	E.Lai et al (2008)[128]
n-ZnO /p-GaN	500 nm	MOCVD	C.H.Chen et al (2010)[130]
nZnO/p-ZnO	342 nm	---	X.W.Sun et al(2009)[120]
nZnO/p-Si	381 nm	Thermal evaporation	R.I.Badran et al (2010)
nZnO/PGaN	380 nm	PLD	R.Guo et al (2009)[129]
n ZnO/P-NiO	UV- Violet (500-800nm)	Solution method	Y.Y.Xi et al (2008)[131]

2-4-4 UV Photodiodes & Optical Switches

Highly sensitive nanowire switches were demonstrated [131] by exploring the photoconducting properties of individual semiconductor nanowires. The conductivity of the ZnO nanowires is extremely sensitive to ultraviolet light exposure. The light-induced conductivity increase allows us to reversibly switch the nanowires between "OFF" and "ON" states, an optical gating phenomenon analogous (Figure 2- 7).

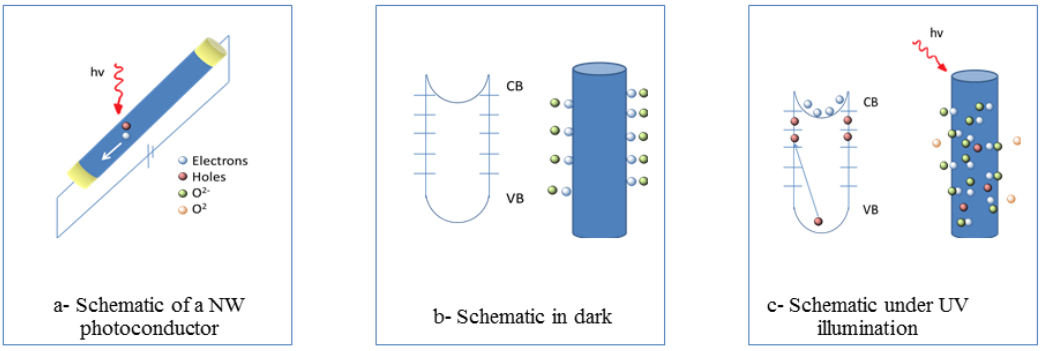

Figure 2- 7 -Photoconduction in NW **Error! Reference source not found.**

It is known that oxygen chemisorption plays a central role in regulating the photosensitivity of bulk or thin film ZnO, where a UV-sensitivity of similar magnitude has been observed. [133][135]It is believed that a similar mechanism is applicable to the nanowire system. In the dark, oxygen molecules adsorb on the nanowire surface as negatively charged ions by capturing free electrons from the n-type ZnO, thereby creating a depletion layer with low conductivity near the nanowire surface:

$$O_2(g) + e^- \rightarrow O_2^-(ad)$$

Upon exposure to UV-light, photo-generated holes migrate to the surface and discharge the adsorbed oxygen ions through surface electron - hole recombination:

$$h\upsilon \rightarrow e^- + h^+$$

$$h^+ + O_2^-(ad) \rightarrow O_2(g)$$

At the same time, the photo-generated electrons significantly increase the conductivity of the nanowire. Photoelectric gain suggests that an optical gating (analogous to the conventional electrical gating) is operating within these nanowires rather than a simple light harvesting process. It is expected that thinner nanowires may further enhance the sensitivity of the devices due to an increased surface to volume ratio, which may lead to the realization of single photon detection.

2-4-5 Horizontal ZnO Nws waveguides

Due to the large refractive index of ZnO across the visible spectrum ($n \sim 2$) [136]and large bandgap at room temperature, ZnO NWs are excellent low-loss sub-wavelength waveguides. They provide tight optical confinement for low-order modes and large acceptance angles for light coupling. Although the hexagonal cross section of the NWs influences the intensity profile of higher orders modes, the lowest order mode exhibits almost circular symmetry inside the NW [137]. The waveguiding properties of single ZnO NWs have been investigated by coupling external light into the wire, it is noticed that the light is guided to both ends of the ZnO NW from where it is emitted. While significant scattering is observed in the coupling region, no additional waveguiding losses along the ZnO NW are observed Figure 2- 8.

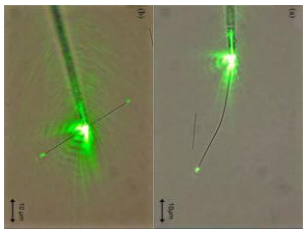

Figure 2- 8- Coupling of green laser light from a silica-tapered fiber into a ZnO NW (a) from one end and (b) at the middle. Image source: Image reproduced with permission from [138].

2-4-6 ZnO Nws Lasers

One of the most important and widely investigated applications of ZnO NWs is optically pumped ultraviolet lasing. Since the first report by Huang *et al.* [139]], many research groups have studied the mechanism of optically excited lasing in ZnO micro- and nanostructures including micropillars, NWs, and nanorods[140] [141]. High-quality single-crystalline ZnO NWs constitute ideal lasing nanocavities, which provide both a gain medium and a resonant cavity due to reflection at the planar end-facets[142]. The strong optical confinement that occurs due to the large index difference between the NW and the surrounding material provides a large modal gain by maximizing the overlap between the guided optical mode and the gain medium. Single-crystalline semiconductor nanowires have long been considered an excellent means by which to realize small and cost effective Fabry–Perot (FP) type lasers, because of the optical feedbacks provided by the naturally formed flat facets in the ends of nanowires.

2-5- Synthesis of ZnO Nanowires

It is evident that the research on 1 D ZnO nanostructures has rapidly expanded in recent years due to their special structures and novel properties. 1D ZnO has been of the few dominant nanomaterials in nanotechnology along with carbon nanotubes and silicon nanowires [143] .Many research on the fabrication of 1D ZnO nanostructures have been reported [144][145][146][147][148].Table 2- 5 presents the growth techniques of different nanostructures.

Table 2- 5- Different synthesis methods with Nanostructures grown

Nanostructures	Growth Method	T©	Ref
Nanowires/ Nanorods	Physical vapor deposition	1100	[149]
	Electrochemical deposition	70	[150]
	Thermal decomposition	90	[151]
	Metal-organic vapor –Phase epitaxial growth	400-500	[152]
	Oxidizing Zn nanowire arrays	300	[153]
	ZnO seeds assisted growth	90-900	[154]
	Vapor Phase deposition	550	[155]
	Vapor Phase transport process	900-925	[156]
Nanotubes	Microwave Plasma method	1000	[157]
	Template assisted electrochemical deposition	85	[158]
	Hydrothermal method	90	[159]
	Surfactant- assisted chemical etching process	95	[160]
	Hydrothermal decomposition	95	[161]
	Liquid phase method	65	[162]
	Electrochemical /Chemical approach	80	[163]
	Electrochemical /Chemical approach	85	[164]
Nanobelts/ Nanoribbons	Thermal evaporation	1400	[165]
	Infrared irradiation heating technique	900	[166]
	Molten salt assisted thermal evaporation	800	[167]
	Vapor phase transport and condensation deposition	1100	[168]
	Gas solid reaction process	600	[169]
	Solid vapor process	850-860	[170]

In the literature a lot of different names have been used like , Whiskers , fibers , fibrils , nanotubes , nanocables,etc. the definition of the 1 D nanostructures is not well establishes.

2-5-1 Deposition Technique and growth mechanisms:

Two standard approaches are employed in the production of 1 D structures: top down and bottom up technologies.

Top-Down is based on standard micro fabrication methods with deposition etching and ion beam milling on planar substrates in order to reduce the lateral dimensions of the films to the nanometer size. Electron beam, focused ion beam, X-ray lithography, nano-imprinting and scanning probe microscopy techniques can be used to the selective removal processes. Advantages are the use of the well developed technology of semiconductor industry and the ability to work on planar surfaces, while disadvantages are their extremely elevated costs and preparation time. The top down approach produce highly ordered nanowires, but this technology does not fulfill the industrial requirements for the production of low cost and large numbers of devices. Furthermore the 1D nanostructures produced with these techniques are not in general single crystalline.

The second approach, bottom up, is based on the assembly of molecular building blocks or chemical synthesis. Vapor phase transport, electrochemical deposition, solution based techniques or template growth are techniques that can be used. Its advantages are the high purity of the nano-crystalline materials produced, their small diameters, the low cost of the experimental set ups together with the possibility to easily vary the intentional doping and the possible formation of junctions. The main disadvantage regards their integration on planar substrates for the exploitation of their useful properties, for example transfer and contacting on transducers can be troublesome. The bottom up approach allows low cost fabrication although it could be very difficult to get them well arranged and patterned. Furthermore more control and insight onto the growth process must be achieved for their fruitful integration in functional devices. Numerous one dimensional oxide nanostructures with useful properties, compositions and morphologies have recently being fabricated using bottom up synthetic routes.

In the bottom up approach, NWs either are grown directly on the desired substrate or are first grown and then transferred to a receiver substrate. When developing 1 D nanocrystals the most important requirements are dimensions and morphology control, uniformity and crystalline properties. In order to obtain one dimensional structures a preferential growth direction with a faster growth rate must exists. In the

past years the number of synthesis techniques has grown potentially. There are different growth mechanisms depending on the presence of catalyst: vapor liquid solid (VLS), solution –liquid –solid (SLS) or vapor – solid (VS) process which is employed in this research and described in the next sections. These processes were investigated in our research.

2-5-2 Vapor phase growth:

The vapor phase approach was used in the early 60's for the preparation for micrometer-size whiskers. These whiskers were prepared either by simple physical sublimation of the source material or through reduction of a volatile metal halide. In the last years this method was used to prepare different materials in form of nanowires. The growth was performed in tubular furnace to obtain the proper temperature gradient. The source material once evaporated is transported by a carrier gas towards the growth site where it nucleates Figure 2- 9. The nucleation can start from particles or catalyst, following the VS, VLS mechanisms.

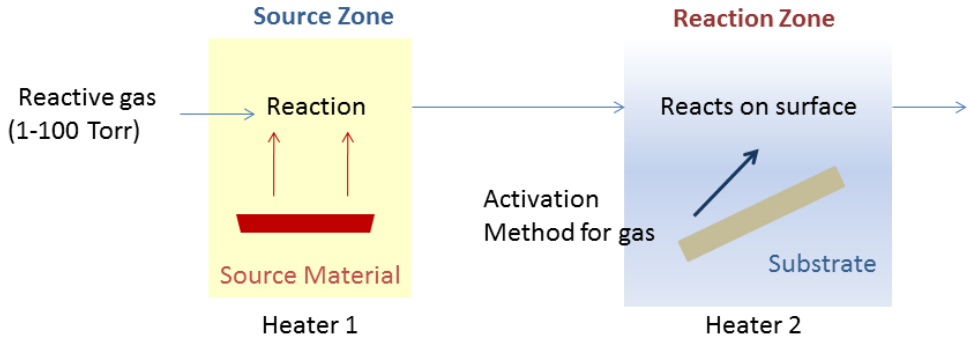

Figure 2- 9-Illustration of the vapor deposition mechanism

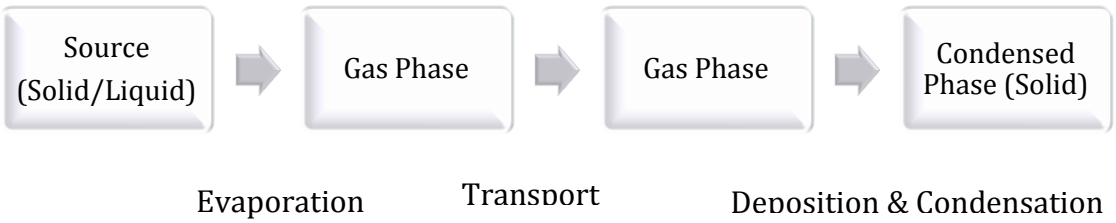

Figure 2- 10-Schematic of the Physical vapor deposition

Vapor deposition is presented in two techniques which are:

Physical Vapor Deposition (PVD) is based on evaporating a source material and reassembling it into a nanowire without changing the basic chemical components of

the starting material. Variants of PVD include thermal evaporation, pulsed laser deposition and sputter deposition. Comparison is summarized in (Table 2- 6). Chemical Vapor Deposition (CVD) involves a chemical change occurring in the vapor phase, whether through re-arrangements of the source material's elements, made possible by excess energy provided to the system or through reactions of the source vapor with gasses introduced separately in the system.

The factors that distinguish PVD from CVD are the following: reliance on solid or molten sources, as opposed to generally gaseous precursors in CVD; the physical mechanisms (evaporation or by means of impact) by which source atoms enter the gas phase; a reduced background pressure through which the gaseous species are transported; the general absence of chemical reactions in the gas phase and at the substrate surface (only reactive PVD processes are exceptions).

Table 2- 6- PVD and CVD comparison

	techniques	Pros	Cons
PVD	Thermal evaporation	High quality Nanostructures variety No chemical waste	High temperature Vacuum Small scale Bad adhesion to substrate
	Sputtering	Doping Good adhesion to substrate Low temperature capability	High vacuum Nanostructures Difficulty
	PLD	High quality Variety of Products Precise control of composition Doping profile	High vacuum Expensive equipment Small scale up
CVD	Thermal CVD / LPCVD	Industrial used technique Nanostructures capable	High temperature vacuum
	PECVD	Lower operation temperature Film deposition	Nanostructure difficulty Vacuum condition
	LCVD	Precise control of nanostructure Dimension Doping	Vacuum Facility requirement
	MOCVD	High quality Products variety Nanostructures capability	Toxic Chemical High vacuum High temperature Expensive facility
	MBE	Ultra high crystal quality Nanostructure capable Control of doping	Ultra high vacuum Expensive instrument Critical operation requirement Small scale

The process started with evaporation that is based on the concept that there exists a finite “vapor pressure” above any material. The material either sublimes (direct solid to vapor transition) or evaporates (liquid to vapor transition).(see Figure 2- 10)

Second the transportation where the evaporated species will be carried by the carrier gas introduced in the furnace to the substrate. The transportation is followed by the condensation, where the carried species will be deposited /condensate on the substrate that is placed at different temperature.

There are several ways to generate Zn and Oxygen vapor:

- Decomposition of ZnO is a direct and simple method; however it is limited to very high temperatures (~ 1400 °C)
- Another Direct method is to heat up Zn powder under oxygen flow (which facilitates relative low growth temperature (500-700 °C) but the ratio between the Zn Vapor pressure and oxygen pressure needs to be carefully controlled in order to obtain desired ZnO nanostructures. $2Zn + O_2 \rightarrow 2ZnO$
- Also another method is the carbo-thermal method, ZnO powder is mixed with graphite powder as a source material. At about 800- 1100 °C graphite reduces ZnO to form Zn and CO/CO2 vapors. $2ZnO \rightarrow 2Zn + O_2$
- Zn and CO/CO2 react and result in ZnO crystals. The advantage of this method lies in that the existence of graphite significantly lowers the decomposition temperature of ZnO. $ZnO(s) + C(s) \rightarrow Zn(g) + CO(g)$
- Another direct method is to heat up Zn Powder under argon where oxygen will be generated from the water vapor from the distilled water installed inside the furnace. At high temperature ~ 600 °C the water vapor will decompose in oxygen and hydrogen (Figure 2- 11). $2H_2O \rightarrow 2H_2 + O_2$

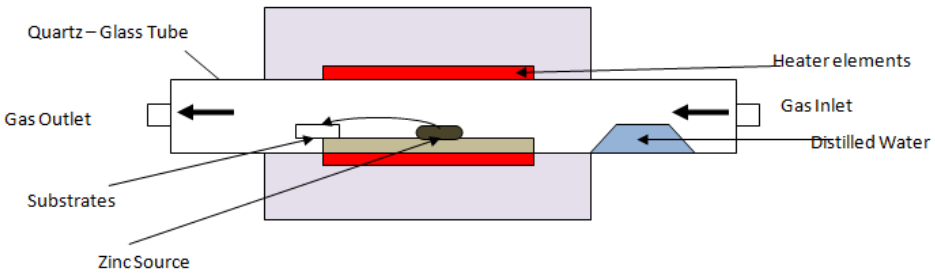

Figure 2- 11- Schematic illustration of the experimental setup of the Vapor deposition technique

The Condensation can be controlled by controlling the substrate temperature *Ts*. At Higher substrate temperatures, the thermal energy and the surface diffusivity of adsorbed molecules increase, and the deposited film will be annealed. On the other hand, too much heat will desorb the deposited film, evaporating it away. During CVD

the growth rate of the film is limited by either surface reaction kinetics, mass transport (diffusion) of precursors to the substrate, or the feed rate of the precursors.

2-5-2-1 Vapor Liquid Solid:

The VLS mechanism was first reported in 1964 by Wagneret al [172], but it was popularized by Lieber et al in 1990 [173] to control the composition and structure of Nanowire for various applications. VLS is a mechanism of growth from CVD and based on introducing a catalyst liquid alloy phase on the substrates which adsorb vapor to super-saturation levels and from which crystal growth can subsequently occur from nucleated seeds at the liquid solid interface. One of the main characteristics of the VLS growth mechanism is the use of catalyst to lower the growth temperature and to control the morphology of ZnO NWs.

Mechanism of VLS:

Generally, source powders loaded in an alumina boat are located in the middle of the furnace, the highest temperature region. The desired nano-materials are deposited on substrates placed certain distance away from the source in the down-stream direction of the carrier gas. Several parameters are influencing the morphology of the final products. The temperature must be measured by a thermal couple placed at the center of the furnace chamber but outside and on the top of the tube. As a single zone furnace, the temperature readout is the only feedback available to control the temperature inside the furnace. It is essential to know the temperature gradient along the horizontal direction because the local deposition temperature is coupled for the distance from the substrate to tube center where the highest temperature is.

The growth mechanism of ZnO nanowires in high temperature furnace is still not fully understood. In VLS growth mode of ZnO nanowire by Au catalyst, Au particles form Au-ZnO eutectic alloy phase at 800°Cand adsorb ZnO gas atoms to nucleate crystalline Nanowire growth at a temperature just higher than the eutectic temperature. The use of optimal growth temperature and process parameters is critical to ensure catalytic growth. At a specific temperature the catalyst melts into liquids spheres, which absorb the ZnO vapor and form a liquid alloy. The liquid spheres become supersaturated with more ZnO vapor absorbed and ZnO can separates out underneath the liquid spheres (Figure 2- 12).

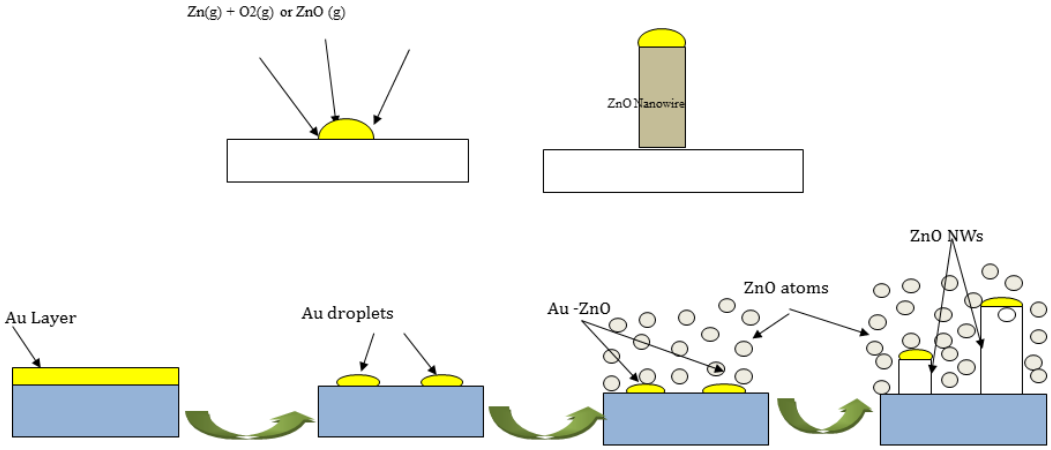

Figure 2- 12-VLS Schematic Illustration

Catalyst acts as the preferential sites for the growth of nanowires. The thickness of the catalyst layer somehow determines the size and the density of the liquid spheres in turn determines the diameter and density of the nanowires. See Figure 2- 13.

So with further control of the catalyst as a pattern by electron lithography or ink jet printing, the accurate control of dimensions, location and density is possible and this is an essential step for the actual applications.

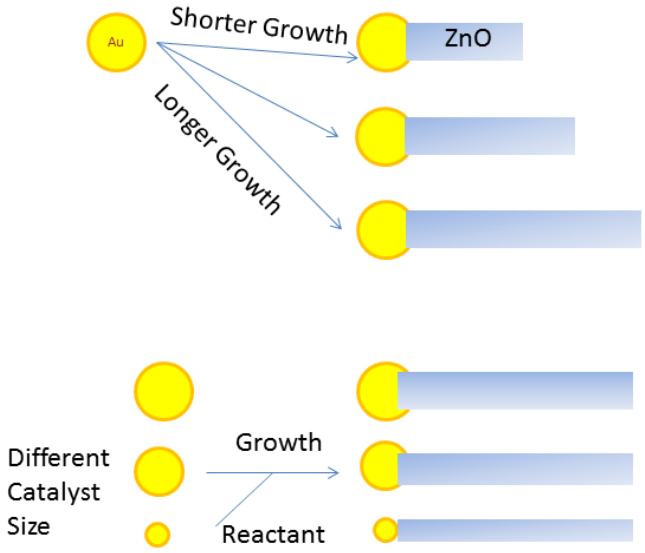

Figure 2- 13- Schematic illustration showing the VLS Process with catalyst

2-5-2-2 Vapor solid Mechanism

Nanowires can be grown without extra metal catalysts by thermally evaporating a suitable source material near its melting point and then depositing at cooler temperature. Such a self-organization process, which does not involve droplets as the catalyst is referred to as a vapor solid (VS) mechanism. The vapor solid process is often called self-catalytic growth since the nanostructures grow directly from the vapor phases. Plausible growth mechanisms such as the anisotropic growth, defect-induced growth and self-catalytic growth have been suggested based on electron microscopy studies. According to the classical theories of crystal growth from liquid or vapor phases, the growth fronts play a crucial role for the deposition of atoms.

There are two kinds of microscopic surfaces:

1- Rough surfaces on which atoms of about several layers are not well arranged. Deposition of atoms is easy compared to a flat surface and crystal growth can continue if enough source atoms are continuously provided.

2- Atomically flat surfaces on which atoms are well arranged. Atoms from the source have a weak bonding with flat surfaces and can easily return to the liquid /vapor phase. Atoms deposition occurs only on the atomic steps.

Mechanism of Growth

The VS growth takes place when the nanowire crystallization originated form the direct condensation from the vapor phase without the use of a catalyzer. Two peculiar effects were registered: - lattice defects at the beginning of the growth, and the nanowire growth rate that was higher than the calculated condensation rate from the vapor phase which was explained by that all the faces of the nanowire adsorb the molecules that afterwards diffuse on the principal growth surface of the wire (Figure 2- 14). The VS process occurs in many catalysts free growth processes. Under high temperature condition, source materials are vaporized and then directly condensed on the surface placed in the low temperature region. Once the condensation process occurs the initially condensed molecules from seed crystals serving as the nucleation sites. As a result they facilitate directional growth to minimize the surface energy.

The vapor solid VS growth was attributed also for a two-step high temperature, catalyst free physical evaporation.

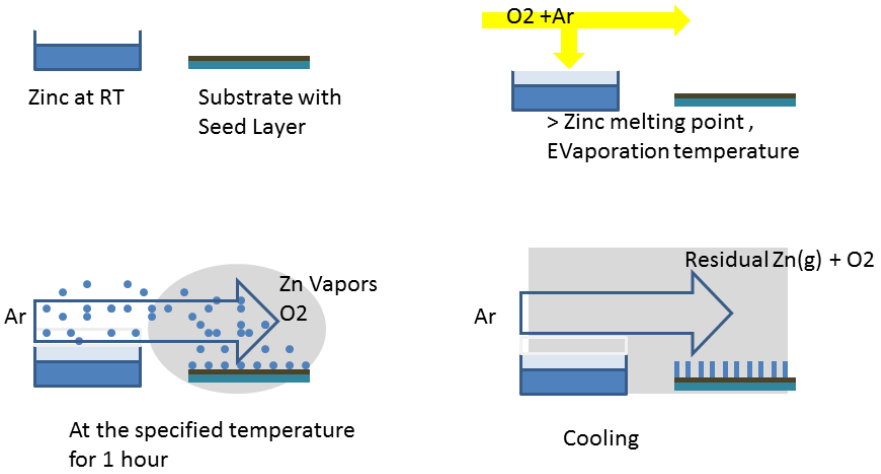

Figure 2- 14-Schematic illustration of the VS Process

VS process is capable of producing a variety of nanostructures including Nanowires, Nano rods, nanobelts, and other complex nanostructures such as nanohelixed and nanobelts by Kong et al **Error! Reference source not found.**. When oxygen is added to the reaction chamber the liquid droplets solidify quickly by oxidation and the formation of ZnO nanowires can eventually be observed. The control of NWs diameter is accomplished mainly by changing the evaporation and collection temperature such as vapor pressure. But no tight control of the spatial arrangement has been achieved so far. Literature reports the growth of ZnO NWs by vapor deposition such as:

Z.W.Li et al (2005) [174] carried out the at 600°Cin open air for 1 h in a horizontal tube furnace on glass substrate with Zinc (Zn) seed layer . The nanowires were randomly oriented.

C.H.Xu et al (2011)[176] , deposited Zn on glass and by wet oxidation have grown ZnO Nws at 390°Cin Oxygen and Nitrogen environment at 1 atm pressure with a flow if gas of 400ml/min. in dry oxygen , feather like nanostrcutre was observed , while nothing in wet oxygen . On the other hand, Nws of 10 um of length were grown in dry nitrogen, and 2um length Nws in wet nitrogen environment.

Z.W.Li, et al (2007)**Error! Reference source not found.**, used glass substrate with zinc seed layer . Wet oxidation technique was employed at 300 to 600 °C, in an Ar , N_2 and O_2 atmospheric environment for 10 hours .It was noticed that particles of ZO aggregated together shaped in short chains of 50 and 30 nm in oxygen environment .

At 350 °C, short blade like nanowishers, of 2 µm long with some of 6 um long were observed with a diameter 150-480 nm. At 420°C, thin NWs were observed of 20-50 µm Length.

[177] R.Chen et al (2011) used Zn precursor oxidized on oxygen environment at 380-450 °C, at different thickness deposition of seed layer NWs were observed (randomly oriented), using Wet oxidation .

2-5-2-3 Thermal Evaporation:

This technique can be carried out in a relative simple setup composed of a vertical furnace. The solid material will be placed at the bottom of the furnace. It will be heated up to a specific temperature. The evaporated material will be transported by the means of a carrier gas and can be deposited on substrates placed on top of the vertical furnace at lower temperature (Figure 2- 15). Where they will be absorbed, nucleated and grow on the desired substrate. The material vapor finally condenses in form of thin film on the substrate surface and on the vacuum chamber walls that causes a great waste of evaporated.

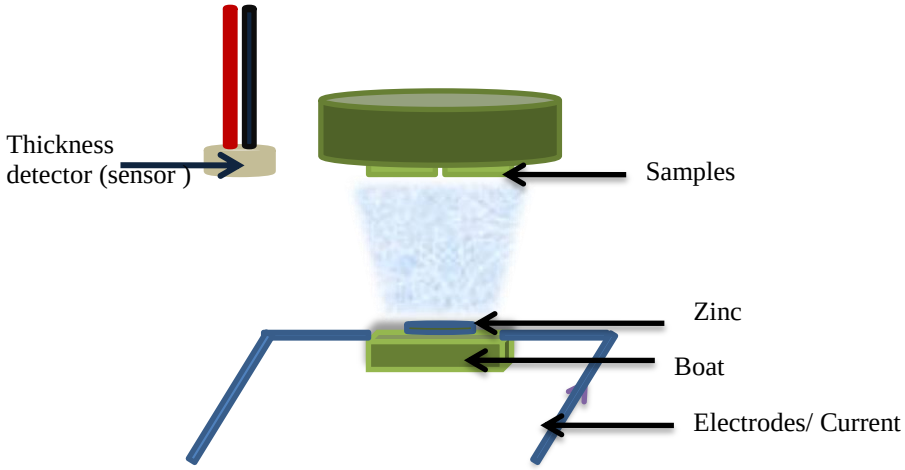

Figure 2- 15- Schematic illustration showing the thermal evaporation process in vaccum

Error! Reference source not found. H.W.Kim (2010) used Vertical furnace, where a silicon substrate coated with Zinc were used the heating time of the zinc powder was for 1 h with a gas flow of 2 slm (N2) and pressure from 10^{-5} to 1 Torr. By varying the

temperature different sized of Nanowires were observed: At 900°C→ 200 – 550 nm; 950 °C → 90-190 nm ;1000 °C → 50-150 nm ; 1050°C→ 30-90 nm

2-5-2-4 Pulsed Laser Deposition:

In 1965 Smith and Turner, after the publications of some works about the use of ruby laser to vaporize and excite atoms from a solid surface, used laser to deposit thin films marking the start of the development of the pulsed laser deposition (PLD) technique(Figure 2- 16). PLD is a thin film deposition technique where a high power pulsed laser beam is focused inside a vacuum chamber to strike a target of the desired compound. Material is then ablated from the target to form a plasma plume direct to the substrate where the compounds condenses as a thin film [180]

Pulsed laser deposition as a film growth technique has attained its reputed fame and has attracted wide spread interest after it has been used successfully to grow high-temperature T_c superconducting films in 1987. During the last decade, pulsed laser deposition has been employed to fabricate crystalline thin films with epitaxy quality. Ceramic oxide, nitride films, metallic multilayers, and various super-lattices grown by PLD have been demonstrated. Recently, using PLD to synthesis nanotubes [181], nano-powders [182]and quantum dots [183] have also been reported. Production-related issues concerning reproducibility[184], large-area scale-up [185] and multiple-level have begun to be addressed. It may start up another era of thin film fabrication in industry. Pulsed laser deposition (PLD) is recognized as an important method for synthesizing ZnO films with excellent electronic and optical properties.

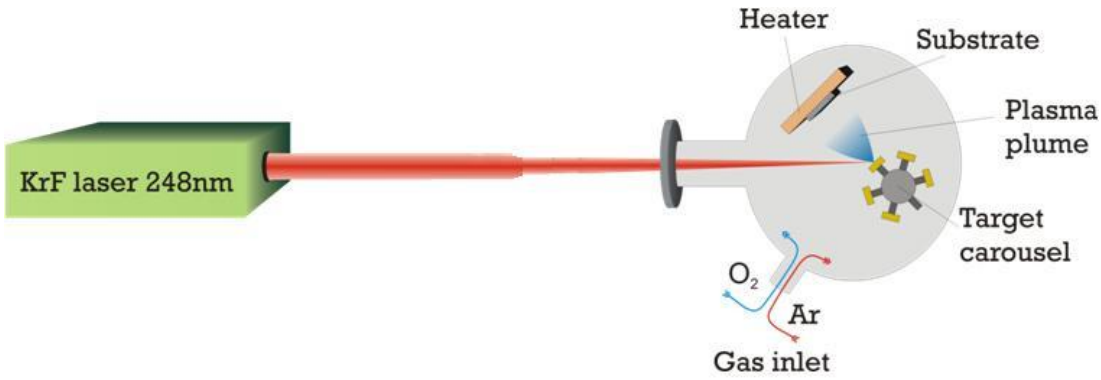

Figure 2- 16- Schematic of the Pulsed Laser Deposition (PLD)

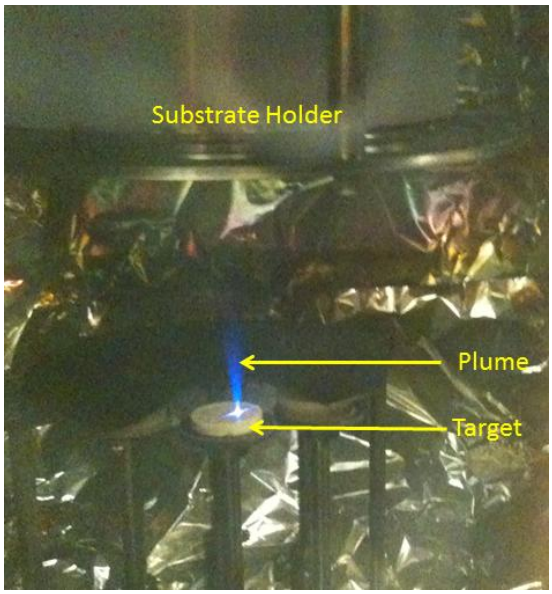

Figure 2- 17- Example of Plume in PLD chamber

Mechanisms of PLD

The principle of pulsed laser deposition, in contrast to the simplicity of the system set-up, is a very complex physical phenomenon. It involves all the physical processes of laser-material interaction during the impact of the high-power pulsed radiation on a solid target Figure 2- 17. It also includes the formation of the plasma plume[1] with high energetic species, the subsequent transfer of the ablated material through the plasma plume onto the heated substrate surface and the final film growth process. Thus PLD generally can be divided into the following four stages:

1. Laser radiation interaction with the target
2. Dynamic of the ablation materials
3. Decomposition of the ablation materials onto the substrate
4. Nucleation and growth of a thin film on the substrate surface (Figure 2- 18)

[1] Plume is referred to the plasma created by ablated target in contact with the laser

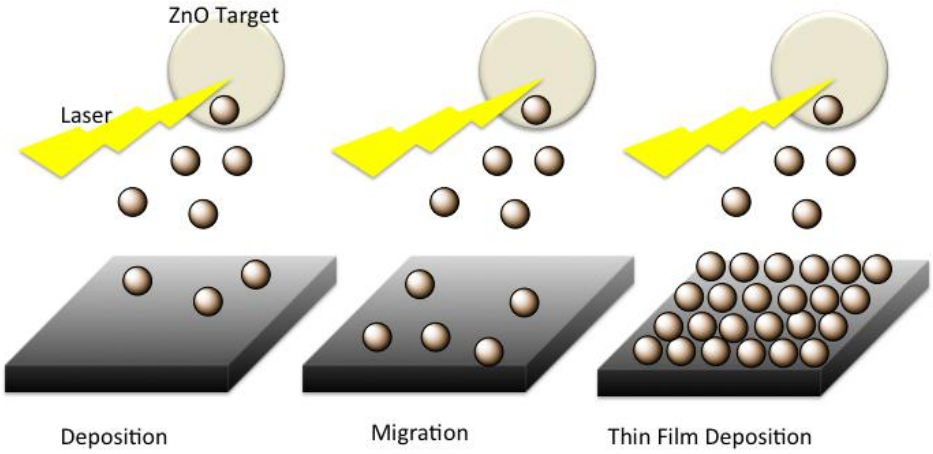

Figure 2- 18-Schematic illustration of the thin film growth by PLD

In the first stage, the laser beam is focused onto the surface of the target. At sufficiently high energy density and short pulse duration, all elements in the target surface are rapidly heated up to their evaporation temperature. Materials are dissociated from the target and ablated out with stoichiometry as in the target.

During the second stage the emitted materials tend to move towards the substrate according to the laws of gas-dynamic and show the forward peaking phenomenon[186]. The laser spot size and the plasma temperature have significant effects on the deposited film uniformity. The target-to-substrate distance is another parameter that governs the angular spread of the ablated materials.

The third stage is important to determine the quality of thin film. The ejected high-energy species impinge onto the substrate surface and may induce various type of damage to the substrate. These energetic species sputter some of the surface atoms and a collision region is established between the incident flow and the sputtered atoms. Film grows immediately after this thermalized region (collision region) is formed. The region serves as a source for condensation of particles. When the condensation rate is higher than the rate of particles supplied by the sputtering, thermal equilibrium condition can be reached quickly and film grows on the substrate surface at the expense of the direct flow of the ablation particle.

Growth of crystalline films depends on many factors such as the density, energy, degree of ionization and the type of the condensing material, as well as the temperature and the physical-chemical properties of the substrate.

The crystalline film growth depends on the surface mobility of the adatom (vapor atoms). Normally, the adatom will diffuse through several atomic distances before sticking to a stable position within the newly formed film. The surface temperature of the substrate determines the adatom's surface diffusion ability. High temperature favors rapid and defect free crystal growth, whereas low temperature or large super-saturation crystal growth may be overwhelmed by energetic particle impingement, resulting in disordered or even amorphous structures.

The literature is rich with successful growth of ZnO Nanowires/Nanorods by PLD. They differ by the parameter used like Gas, Pressure inside the chamber, distance between the target and the substrate, Temperature and Laser energy and Frequency.

Few reports of ZnO nanorod synthesis by PLD methods have appeared thus far. Yan et al. [187]demonstrated growth of oriented Ga-doped ZnO nanorod arrays on GaN/sapphire substrates, but only at certain specific Ga-doping levels. Nobis et al. [188]have reported growth of ZnO micropillars on sapphire, at a substrate temperature T_{sub} ~ 915°C and in the presence of an Au catalyst.

[189]S.H.Dala et al (2006) controlled the growth of vertically aligned ZnO NWs , in function of the thickness of the Au catalyst , deposition temperature and oxygen pressure . The most aligned nanowires were found at 5 mbar in a temperature range of 860-800°Cwith a flow ratio of 27 sccm of a N_2 /O_2 mixture.

[190]L.C.Tien et al (2008) synthesized ZnO Nws on a ZnO thin film template. The Nws were grown at 500 mTorr , with a distance of 2.5 cm , and laser energy (~ 3 J/cm2) freq 5 hz , temp (500-800°C). Parametric study at different pressure (150-500mTorr) and Temperature (500-800C) were applied to understand the growth process of the ZnO NWS.

[191]R.Guo et al.(2009) successfully have grown vertically and horizontally aligned Nws on sapphire substrate c-cut and a-cut sapphire substrates at 1000°C, Argon pressure 260 Torr and the distance between target and substrate was arounf 1.5 cm with laser energy of (4J/cm2) and frequency of 20 hz.

[192]A.Marcu et al (2009) , also have grown ZnO Nws using gold catalyst under 1Pa oxygen Pressure and 750°Csubstrate temperature. Distance target substrate was 5 cm, laser energy (100mJ/Pulse) with a frequency of 10 Hz. Substrate used (0001) single crystal alumina.

Error! Reference source not found.T.Premkumar et al (2010) deposited on Al2O3 (0001) and Si(100) substrates , vertically aligned hexagonal pyramidal ZnO Nanorods . Laser energy (3j/cm2) 10hz)

D=2.5 cm, oxygen pressure 7 Torr,

[193]H.Kumrakuru et al, successfully grown on (0001) sapphire substrate, oxygen pressure at 10 mTorr, d= 5 cm , temp = 600C (30mj/cm2) 5 and 10 hz.

Error! Reference source not found. W.Z.Liu et al (2011) , controlled the growth size of the ZnO Nanowires by catalyst free high pressure PLD. Ar pressure 4- 6 Torr , Tsubstrate = 600-850°C , d= 2.5 cm, 10 hz and 5 hz ,

2-6- Experimental and Characterization equipment

The advancement of material science, nanotechnology, depends on the effective use of advanced characterization and modeling techniques. During the last 30 years, there has been a tremendous improvement in the field of materials, with the development of increasing numbers of novel materials. During the same period there have been large numbers of significant breakthroughs in the development of advanced characterization techniques.

The fundamental of nanotechnology lies in the fact that properties of material change dramatically when their size is reduced to the nanometer range. Characterizing the synthesized nano-sized materials is an emerging field posing lot of challenges to scientists and technologists. The important characterization techniques used for nanotechnology research in solar materials widely covers such as structural /microstructural properties and optical properties.

Wet oxidation and Pulsed Laser Deposition synthesis:

Vapor phase deposition in humid environment and pulsed laser deposition are the techniques selected in this research due to their unique properties previously described.

Vapor phase deposition wet oxidation experiments were conducted in horizontal furnace Syskey LPCVD and in in KMT OTF-1200X Furnace (Figure 2- 19). Thermal evaporation experiments were conducted used a custom made vertical furnace (Figure 2- 20). On the other hand pulsed laser deposition was conducted using Neocerra Pioneer 180 (Figure 2- 21).

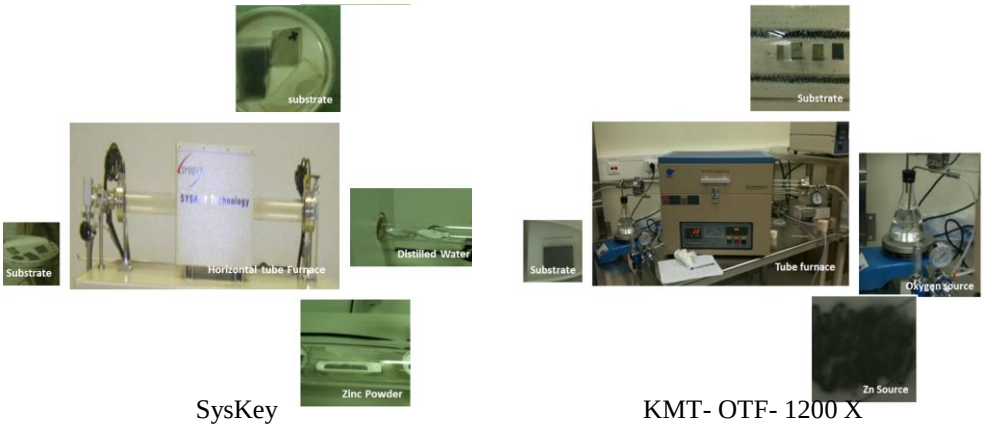

SysKey KMT- OTF- 1200 X

Figure 2- 19- Experimental setup VS_ VLS , Tube furnace

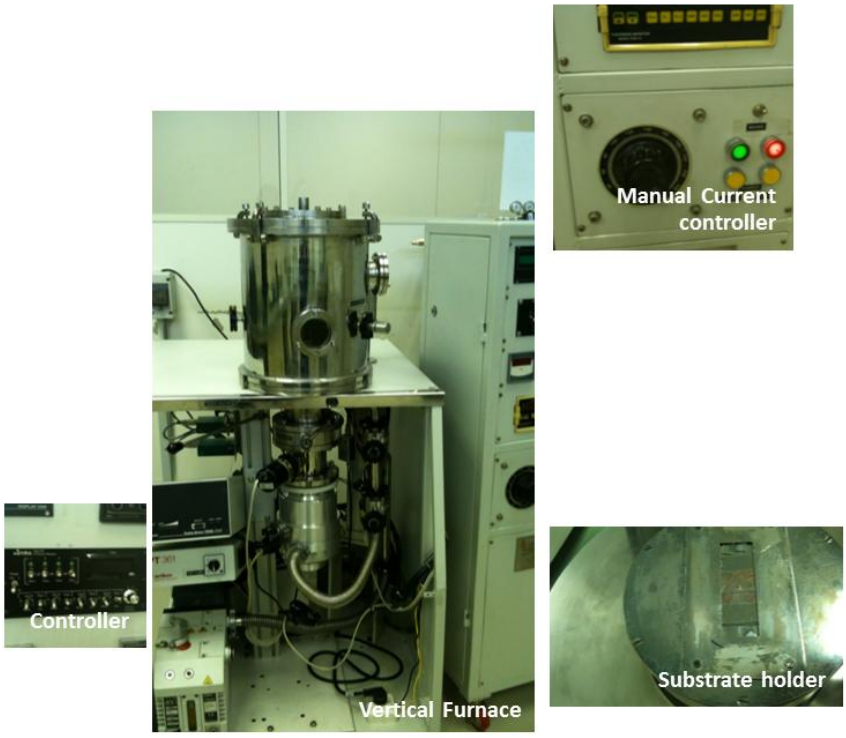

Figure 2- 20-Thermal evaporation equipment in Vaccum

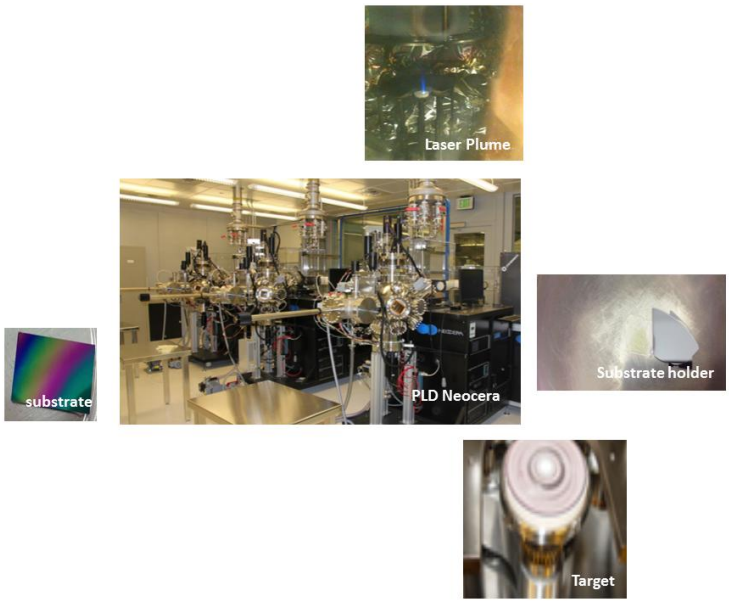

Figure 2- 21- PLD Used in the experimental work- NEOCERA

Structural and Microstructural characterization

The properties of materials are determined by their structure, which depends on composition and growth conditions. The formation and development of defects of the crystal structure and their influence on the materials properties is also essential to be studied. Thus, it is necessary to characterize both composition and microstructure at the highest levels of resolution possible in order to understand materials behavior and to facilitate the design of new improved materials. Such a characterization requires advanced methods of analysis using microscopic, diffraction, and spectroscopic techniques. In order to characterize the polycrystalline bulk and thin films of manganites, such as X-ray diffraction (XRD), and electron diffraction (ED) for structure, scanning electron microscopy (SEM), atomic force microscopy (AFM), transmission electron microscopy (TEM) for microstructure.

The structural properties of the as-grown NWs were characterized using Bruker D8 Discover high resolution XRD with CuKα and λ=1.5406A° (Figure 2-22d). The morphological properties were examined with FEI Nova Nano SEM 630(Figure 2- 22e).Topography of the Nanostructures deposited is checked by AFM ICON (Figure 2- 22b). The photoluminescence properties were studied using a Fluoromax-4 spectro-fluorometer Horiba Scientific having a 150W ozone free Xenon arc lamp (Figure 2- 22c). The samples were excited at 325 nm. LabRAM Aramis - Raman Spectrometer was also employed for PL measurements excited at RT using

HeCd Laser 325 nm. X-Ray Photoelectron Spectroscopy (XPS) measurements were carried out using a monochromatic Al Kα X-ray source operating at 150 W. The survey and high-resolution spectra were collected at fixed analyzer pass energies of 160 and 20 eV, respectively. Binding energies were referenced to the C 1s binding energy of adventitious carbon contamination, which was set at 284.8 eV. The atomic concentration of each element present on the surface is determined. Values given are normalized to 100% using the elements detected. Detection limits are approximately 0.05 to 1.0 atomic %. Major factors affecting detection limits are the element itself (heavier elements generally have lower detection limits), interferences (can include photoelectron peaks and Auger electron peaks from other elements) and background (mainly caused by signal from electrons that have lost energy to the matrix). The accuracy of measurement of the binding energy is ± 0.1 eV and uncertainty ≤ 0.2 eV.

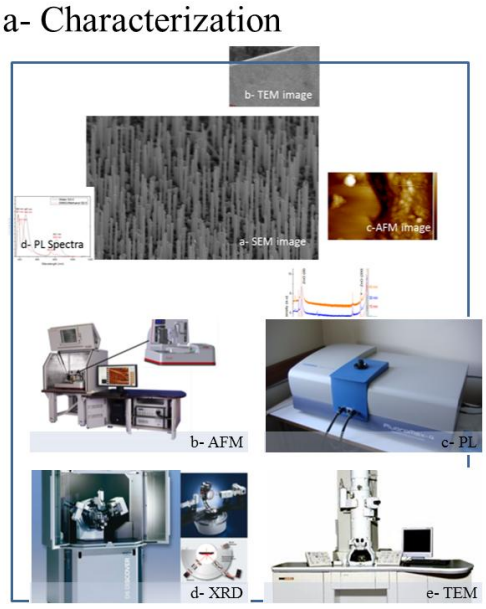

Figure 2- 22- Characterization Equipments

2-7- Conclusion

Nanowires Materials in Photovoltaic devices provide a large interface which is important for an effective charge separation, band transport of carriers (charge transfer) and non-flat morphology that reduces reflection of an incident radiation. 1 D ZnO NWs are very promising class of Nano-scale building blocks for environment friendly and cost effective solar cells. Radial synthesis is fundamental of their technological applications; therefore many synthesis methods have been developed. Via these methods, various nanostructures can be synthesized. ZnO NWs provide important functions for solar cells benefiting from their large surface area, carrier transport and improved light scattering. ZnO is one of the first materials employed in DSSC with a best efficiency of 6.58 %. To improve efficiency of Solar cells, the efforts regarding ZnO Solar cell focus on main aspects:

- Develop method to synthesize high quality 1 D ZnO nanostructures
- Find new QD sensitizers for electron generation and light absorption.

The literature is rich of successful growth of ZnO Nanowires by different synthesis techniques. In this research we selected the vapor phase approach such as Pulsed Laser Deposition, and thermal evaporation in wet and dry environment due to its unique properties and its availability in the lab.

The employed synthesis techniques, their mechanism and properties were presented in details in this chapter. The Experimental process, characterization of the synthesized ZnO NWs and discussion the obtained results will be elaborated in details in chapter3.

References:

[1] E. C. Garnett, M. L. Brongersma, Y. Cui, and M. D. McGehee (2011) , Annual Review of Materials Research Vol. 41: 269-295
[2] Bunn [Proc. Phys. Soc. London **47**, 836 (1935)],
[3] Damen et al. [Phys. Rev. **142**, 570 (1966)],
[4] Mollwo [Z. Angew. Phys. **6**, 257 (1954)],
[5] Galli and Coker [Appl. Phys. Lett. **16**, 439 (1970)].
[6] Mead [Phys. Lett. **18**, 218 (1965)],
[7] Drapak [Semiconductors **2**, 624 (1968)],
[8] Minami et al. [Jpn. J. Appl. Phys. **13**, 1475 (1974)],
[9] Tsurkan et al. [Semiconductors **6**, 1183 (1975)],
[10] Brillson [J. Vac. Sci. Technol. **15**, 1378 (1978)].
[11] Look and Claflin [Phys. Status Solidi B **241**, 624(2004)].
[12] Ü. Özgür,a_ Ya. I. Alivov, C. Liu, A. Teke,b_ M. A. Reshchikov, S. Doğan,c_ V. Avrutin, S.-J. Cho, and H. Morkoçd_ JOURNAL OF APPLIED PHYSICS 98, 041301 (2005)
[13] Z.L.Wang,Materials Science and Engineering R 64 (2009) 33-71
[14] Mang A, Reimann K and R¨ubenacke St 1995 Solid State Commun. 94 251
[15] Madelung O (ed) 1996 Semiconductors—Basic Data 2nd Revised Edn (Berlin: Springer)
[16] Bagnall D M, Chen Y F, Zhu Z, Yao T, Koyama S, Shen M Y and Goto T 1997 Appl. Phys. Lett. 70 2230
[17] Huang M H, Mao S, Feick H, Yan H, Wu Y, Kind H, Weber E, Russo R and Yang P 2001 Science 292 1897
[18] Tsukazaki A et al 2005 Nature Mater. 4 42
[19] Ryu Y R, Kim W J and White H W 2000 J. Cryst. Growth 219 419
[20] Mandalapu L J, Yang Z, Xiu F X, Zhao D T and Liu J L 2006 Appl. Phys. Lett. 88 092103
[21] Chu S, Olmedo M, Yang Z, Kong J and Liu J L 2008 Appl. Phys. Lett. 93 181106
[22] Reynolds D C, Look D C and Jogai B 1996 Solid State Commun. 99 873
[23] Kamalasanan M N and Chandra S 1996 Thin Solid Films 288 112
[24] Paraguay F D, Estrada W L, Acosta D R N, Andrade E and Miki-Yoshida M 1999 Thin Solid Films 350 192
[25] Funakubo H, Mizutani N, Yonetsu M, Saiki A and Shinozaki K 1999 J. Electroceram. 4:S1 25
[26] Sakurai K, Kanehiro M, Nakahara K, Tanabe T, Fujita S and Fujita S 2000 J. Cryst. Growth 209 522
[27] Yamamoto T, Shiosaki T and Kawabata A 1980 J. Appl. Phys. 51 3113
[28] Molarius J, Kaitila J, Pensala T and Ylimlammi M 2003 J. Mater. Sci.: Mater. Electron. 14 431
[29] Ondo-Ndong R, Ferblantier G, Pascal-Delannoy F, Boyer A and Foucaran A 2003 Microelectron. J. 34 1087
[30] Gardeniers J G E, Rittersma Z M and Burger G J 1998 J. Appl. Phys. 83 7844
[31] Shionoya S and Yen W H (ed) 1997 Phosphor Handbook By Phosphor Research Society (Boca Raton, FL: CRC Press)
[32] Nanto H, Sokooshi H and Usuda T 1991 Solid-State Sensors and Actuators 24–27 596
[33] Florescu D I, Mourokh L G, Pollak F H, Look D C, Cantwell G and Li X 2002 J. Appl. Phys. 91 890
[34] ¨ Ozg¨ur ¨U, Gu X, Chevtchenko S, Spradlin J, Cho S-J, Morkoc¸ H, Pollak F H, Everitt H O, Nemeth B and Nause J E 2006 J. Electr. Mater. 35 550
[35] Maeda K, Sato M, Niikura I and Fukuda T 2005 Semicond. Sci. Technol. 20 S49
[36] Ohshima E, Ogino H, Niikura I, Maeda K, Sato M, Ito M and Fukuda T 2004 J. Cryst.Growth 260 166
[37] Look D C, Reynolds D C, Sizelove J R, Jones R L, Litton C W, Cantwell G and Harsch W C 1998 Solid State Commun. 105 399
[38] Nause J and Nemeth B 2005 Semicond. Sci. Technol. 20 S45
[39] Ive T, Ben-Yaacov T, Van de Walle C G, Mishra U K, DenBaars S P and Speck J S 2008 J. Cryst. Growth 310 3407
[40] Heinze S, Krtschil A, Blasing J, Hempel T, Veit P, Dadgar A, Christen J and Krost A 2007 J. Cryst. Growth 308 170
[41] Ardakani H K 1996 Thin Sol. Films 287 280
[42] Quaranta F, Valentini A, Rizzi F R and Casamassima G 1993 J. Appl. Phys. 74 244

[43] A.B.Djuriˇ si´ c, Y.H.Leung,Small2(8–9)(2006)944–961.
[44] Y. Gu, L. Kuskovsky, M. Yin, S. O'Brien, G.F. Naumark, Appl. Phys. Lett. 85 (17) (2004) 3833–3835.
[45] T. Voss, C. Bekeny, L. Wischmeier, H. Gafsi, S. B ¨ orner, W. Schade, A.C. Mofor, A. Bakin, A. Waag, Appl. Phys. Lett. 89 (18) (2006) 182107 (1–3).
[46] Q.X. Zhao, P. Klason, M. Willander, H.M. Zhong, W. Lu, J.H. Yang, Appl. Phys. Lett. 87 (21) (2005) 211912 (1–3). First peak 373 – 5
[47] D.H. Zhang, Z.Y. Xue, Q.P. Wang, J. Phys. D: Appl. Phys. 35 (21) (2002) 2837–2840.
[48] M.K. Patra, K. Manzoor, M. Manoth, S.P. Vadera, N. Kumar, J. Lumin. 128 (2) (2008) 267–272.
[49] N.Y. Garces, L. Wang, L. Bai, N.C. Giles, L.E. Halliburton, G. Cantwell, Appl. Phys. Lett. 81 (4) (2002) 622–624.
[50] A.B.Djurisic,W.C.H.Choy, V.A.L.Roy, Y.H.Leung, C.Y.Kwong, K.W.Cheah, T.K.GunduRao, W.K. Chan, H.F.Lui, C.Surya, Adv.Funct.Mater.14 (9) (2004) 856–864.
[51] K. Vanheusden, C.H. Seager, W.L. Warren, D.R. Tallant, J.A. Voigt, Appl. Phys. Lett. 68 (3) (1996) 403–405.
[52] B. Lin, Z. Fu, Y. Jia, Appl. Phys. Lett. 79 (7) (2001) 943–945.
[53] X. Liu, X. Wu, H. Cao, R.P.H. Chang, J. Appl. Phys. 95 (6) (2004) 3141–3147.
[54] A. van Dijken, E.A. Meulenkamp, D. Vanmaekelbergh, A. Meijerink, J. Phys. Chem. B 104 (8) (2000) 1715–1723.
[55] I. Shalish, H. Temkin, V. Narayanamurti, Phys. Rev. B 69 (24) (2004) 245401 (1–4).
[56] M.A. Reshchikov, J.Q. Xie, B. Hertog, A. Osinsky, J. Appl. Phys. 103 (10) (2008) 103514 (1–8)
[57] D.Li, Y.H.Leung, A.B.Djuri ˇ si´ c, Z.T.Liu, M.H.Xie, S.L.Shi, S.J.Xu, W.K.Chan, Appl. Phys. Lett. 85 (9) (2004)1601–1603.
[58] J. Qiu, X. Li, W. He, S.-J. Park, H.-K. Kim, Y.-H. Hwang, J.-H. Lee, Y.-D. Kim, Nanotechnology 20 (15) (2009) 155603 (1–9).
[59] R.B.M. Cross, M.M. De Souza, E. Sankara Narayanan, Nanotechnology 16 (10) (2005) 2188–2192
[60] K. Tomioka, J. Motohisa, S. Hara, K. Hiruma, and T. Fukui, Nano Lett. 10, 1639 (2010).
[61] S. Xu, C. Xu, Y. Liu, Y. F. Hu, R. S. Yang, Q. Yang, J. H. Ryou, H. J. Kim, Z. Lochner, S. Choi, R. Dupuis, and Z. L. Wang, Adv. Mater. 22, 4749 (2010).
[62] S. Vandenbrouck, K. Madjour, D. Theron, Y. J. Dong, Y. Li, C. M. Lieber, and C. Gaquiere, IEEE Electron Device Lett. 30, 322 (2009).
[63] G. H. Yu and C. M. Lieber, Pure Appl. Chem. 82, 2295 (2010).
[64] N. A. Kotov, J. O. Winter, I. P. Clements, E. Jan, B. P. Timko, S. Campidelli, S. Pathak, A. Mazzatenta, C. M. Lieber, M. Prato, R. V. Bellamkonda, G. A. Silva, N. W. S. Kam, F. Patolsky, and L. Ballerini, Adv. Mater. 21, 3970 (2009).
[65] X. C. Jiang, J. S. Hu, L. A. Fitzgerald, J. C. Biffinger, P. Xie, B. R. Ringeisen, and C. M. Lieber, Proc. Natl. Acad. Sci. U.S.A. 107, 16806 (2010).
[66] H. Yan, H. S. Choe, S. W. Nam, Y. J. Hu, S. Das, J. F. Klemic, J. C. Ellenbogen, and C. M. Lieber, Nature 470, 240 (2011).
[67] B. Z. Tian, T. Cohen-Karni, Q. A. Qing, X. J. Duan, P. Xie, and C. M. Lieber, Science 329, 830 (2010).
[68] S. Nam, X. C. Jiang, Q. H. Xiong, D. Ham, and C. M. Lieber, Proc. Natl. Acad. Sci. U.S.A. 106, 21035 (2009).
[69] D. J. Gargas, M. E. Toimil-Molares, and P. D. Yang, J. Am. Chem. Soc. 131, 2125 (2009).
[70] X. D. Wang, C. J. Summers, and Z. L. Wang, Nano Lett. 4, 423 (2004).
[71] E. Garnett and P. D. Yang, Nano Lett. 10, 1082 (2010).
[72] F. Qian, Y. Li, S. Gradecak, H. G. Park, Y. J. Dong, Y. Ding, Z. L.Wang, and C. M. Lieber, Nature Mater. 7, 701 (2008).
[73] M. Law, L. E. Greene, J. C. Johnson, R. Saykally, and P. D. Yang, Nature Mater. 4, 455 (2005).
[74] R. X. Yan, D. Gargas, and P. D. Yang, Nat. Photonics 3, 569 (2009).
[75] B. Tian, T. J. Kempa, and C. M. Lieber, Chem. Soc. Rev. 38, 16 (2009).
[76] A. Ponzoni, E. Comini, G. Sberveglieri, J. Zhou, S. Z. Deng, N. S. Xu, Y. Ding, and Z. L. Wang, Appl. Phys. Lett. 88, 203101 (2006).
[77] A. I. Hochbaum and P. D. Yang, Chem. Rev. 110, 527 (2010).
[78] J. Shi, Y. Hara, C. L. Sun, M. Anderson, and X. D. Wang, Nano Lett. 11, 3413 (2011).

[79] S. W. Boettcher, J. M. Spurgeon, M. C. Putnam, E. L. Warren, D. B. Turner-Evans, M. D. Kelzenberg, J. R. Maiolo, H. A. Atwater, and N. S. Lewis, Science 327, 185 (2010).
[80] C. T. Huang, J. H. Song, W. F. Lee, Y. Ding, Z. Y. Gao, Y. Hao, L. J. Chen, and Z. L. Wang, J. Am. Chem. Soc. 132, 4766 (2010).
[81] Z. L. Wang, Nano Today 5, 540 (2010).
[82] Z. L. Wang, J. Phys. Chem. Lett. 1, 1388 (2010).
[83] C. K. Chan, H. L. Peng, G. Liu, K. McIlwrath, X. F. Zhang, R. A. Huggins, and Y. Cui, Nat. Nanotechnol. 3, 31 (2008).
[84] S. A. Morin, M. J. Bierman, J. Tong, and S. Jin, Science 328, 476 (2010).
[85] Ginley D, Green M, Collins R. 2008. MRS Bull. 33:355–73
[86] Hochbaum AI, Yang P. 2010. Chem. Rev. 110(1):527–46
[87] Tian B, Kempa TJ, Lieber CM. 2009. Chem. Soc. Rev. 38(1):16–24
[88] Fan Z, Ruebusch DJ, Rathore AA, Kapadia R, Ergen O, et al. 2009. Nano Res. 2(11):829–43
[89] Yu K, Chen J. 2008. Nanoscale Res. Lett. 4(1):1–10
[90] Cao L, Park J, Fan P, Clemens B, Brongersma ML. 2010.. Nano Lett. 10(4):1229–33
[91] Gunawan O, Sekaric L, Majumdar A, Rooks M, Appenzeller J, et al. 2008. Nano Lett. 8(6):1566–71
[92] Ford AC, Ho JC, Chueh Y, Tseng Y, Fan Z, et al. 2009. Nano Lett. 9(1):360–65
[93] H. Gerischer, Photochem. Photobiol. 16, 243 (1972)
[94] R. Memming, Photochem. Photobiol. 16, 325 (1972)
[95] M. Law, L.E. Greene, J.C. Johnson, R. Saykally, P.D. Yang, Nature Materials 4 (2005) 455–459.
[96] Grätzel M. Journal of Photochemistry and Photobiology C: Photochemistry Reviews 2003 10/31;4(2):145-53.
[97] Q. F. Zhang, C. S. Dandeneau, X. Zhou and G. Cao, Adv. Mater. 21, 4087 (2009).
[98] Q. F. Zhang, C. S. Dandeneau, X. Zhou and G. Cao, Adv. Mater. 21, 4087 (2009).
[99] Chen et al, "An oleic acid-capped CdSe quantum-dot sensitized solar cell", Appl. Phys. Lett. 94, 153115 (2009).
[100] Gao, F; Wang, Y; Zhang, J; Shi, D; Wang, M; Humphry-Baker, R; Wang, P; Zakeeruddin, Sm; Grätzel, M (2008). Chemical communications (23): 2635–7
[101] Xuelian Yu , Xin Song, Jing Sun, Xiwen Du* Power and Energy Engineering Conference (APPEEC), 2010 Asia-Pacific
[102] J. Chen, J. Wua, W. Leia, J.L. Songb, W.Q. Dengb, X.W. Sunc, Applied Surface Science 256 (2010) 7438–7441
[103] Kurtis S. Leschkies, Alan G. Jacobs, David J. Norris,a_ and Eray S. Aydila_ APPLIED PHYSICS LETTERS 95, 193103 _2009_
[104] Y.F. Zhu ⇑, G.H. Zhou, H.Y. Ding, A.H. Liu, Y.B. Lin, Y.W. Dong , Superlattices and Microstructures 50 (2011) 549–556
[105] Chunyan Luan, Aleksandar Vaneski, Andrei S Susha, Xueqing Xu, Hong-En Wang, Xue Chen, Jun Xu, Wenjun Zhang, Chun-Sing Lee, Andrey L Rogach and Juan Antonio Zapien Luan et al. Nanoscale Research Letters 2011, 6:340
[106] Chengcheng Liu, Zhifeng Liu, Yabin Li, Jing Ya, Lei E, Li An , Applied Surface Science 257 (2011) 7041–7046
[107] J. Briscoe, D. E. Gallardo, S. Hatch,a V. Lesnyak, N.i Gaponik and S. Dunn J. Mater. Chem., 2011, 21, 2517
[108] Xinku Qiu, Wenxiu Que, Xingtian Yin, Jin Zhang and Jin Chen, Semicond. Sci. Technol. 26 (2011) 095028 (7pp)
[109] S H. Im, H.-J Kim and S. Il Seok , Nanotechnology 22 (2011) 395502 (5pp)
[110] G. Wang, X. Yang, F. Qian, J. Z. Zhang, and Y. Li , Nano Lett. 2010, 10, 1088–1092
[111] Y. Zhang, T. Xie, T. Jiang, X. Wei, S. Pang, X. and DejunWang., Nanotechnology 20 (2009) 155707
[112] Y.Tak, S. J. Hong, J. S. Lee, and K. Yong, CRYSTAL GROWTH & DESIGN 2009 VOL. 9, NO. 6 2627–2632
[113] K. S. Leschkies, R. Divakar, J. Basu, E. Enache-Pommer, J. E. Boercker, C. Barry Carter, U. R. Kortshagen, D. J. Norris, and E. S. Aydil 2007 American Chemical Society, Vol. 7, No. 61793-1798
[114] Chih-Yin Kuo, Ming-Shin Su, Ching-Shun Ku, Shu-Min Wang, Hsin-Yi Leeb and Kung-Hwa Wei, J. Mater. Chem., 2011, 21, 11605
[115] B. D. Yuhas and P. Yang , J. AM. CHEM. SOC. 2009, *131*, 3756–3761
[116] C. Chen et al., Appl. Phys. Lett., vol. 95, no. 22, pp. 223101-1–223101-3, 2009.

[117] X. Zhang, M. Lu, Y. Zhang, L. Chen, and Z. L. Wang,Adv. Mater., vol. 21, no. 27, pp. 2767– 2770, 2009.
[118] M. A. Zimmler et al. Nano Lett., vol. 8, no. 6, pp. 1695–1699, Jun. 2008.
[119] X. Fang, J. Li, D. Zhao, D. Shen, B. Li, and X. Wang, J. Phys. Chem. C, vol. 113, no. 50, pp. 21208–21212, Dec. 2009.
[120] X. W. Sun et al., "Appl. Phys. Lett., vol. 95, no. 13, pp. 133124-1– 133124-3, 2009.
[121] J. Bao, M. A. Zimmler, F. Capasso, X. Wang, and Z. F. Ren, Nano Lett., vol. 6, no. 8, pp. 1719–1722, 2006.
[122] M. A. Zimmler, T. Voss, C. Ronning, and F. Capasso, Appl. Phys. Lett., vol. 94, no. 24, pp. 241120-1–241120-3, 2009.
[123] R.K¨onenkamp, R.C.Word, andM.Godinez, Nano Lett., vol. 5, no. 10, pp. 2005–2008, Oct. 2005.
[124] A. El-Shaer et al., Phys.Stat. Sol. (b), vol. 247, no. 6, pp. 1564–1567, 2010.
[125] A. Nadarajah, R. C. Word, J. Meiss, and R. Konenkamp, Nano Lett., vol. 8, no. 2, pp. 534–537, Feb. 2008.
[126] S. J An, J H Chae, G-C Yi, and G H. Park APP. PHY. LETT. 92, 121108 (2008)
[127] H. Gao, J. Zhou, Z. Lin . Electrochemistry Communications 10 (2008) 146–150
[128] E Lai, W Kim, and P. Yang Nano Res (2008) 1: 123 128
[129] Y-S Choi, J-W Kang, D-K Hwang, and S-J Park, IEEE TRANSACTIONS ON ELECTRON DEVICES, VOL. 57, NO. 1, JANUARY 2010
[130] C-H Chen, S-J Chang,S-P Chang, M-J Li, I-C Chen, T-J Hsueh, A-D Hsu, and C-L Hsu J. Phys. Chem. C 2010, 114, 12422–12426
[131] Y. Y. Xi, Y. F. Hsu, A. B. Djurišić, A. M. C. Ng, W. K. Chan, H. L. Tam, and K. W. Cheah, Appl. Phys. Lett. 92, 113505 (2008).
[132] H.Kind,H.Yan,B.Messer,M.Law,P.Yang,Adv.Mater 2002,14, No2.
[133] C. Soci *et al.*, *Nano Lett.*, vol. 7, no. 4, pp. 1003–1009, Apr. 2007.
[134] J.B.K.Law and J.T.L.Thong, Apll.Phys.Lett.,Vol. 88, no 13 , pp.133114-1 – 133114-3 , 2006
[135] C.Soci et al , Nano let.,Vol7, no 4 , pp 1003-1009 (2007)
[136] H. Yoshikawa and S. Adachi, Jpn. J. Appl. Phys., vol. 36, no. 1, pp. 6237–6243, 1997.
[137] R. Hauschild and H. Kalt, Appl. Phys. Lett., vol. 89, no. 12, pp. 123107-1–123107-3, 2006.
[138] T. Voss, Advances in Solid State Physics, vol. 48. Berlin, Heidelberg: Springer Berlin Heidelberg, p. 57, 2009.
[139] M. H. Huang et al., Science, vol. 292, no. 5523, pp. 1897–1899, Jun. 2001.
[140] J. Fallert et al., Opt. Express, vol. 16, no. 2, pp. 1125–1131, Jan. 2008.
[141] M. A. Zimmler, J. Bao, F. Capasso, S. M¨uller, and C. Ronning, Appl. Phys. Lett., vol. 93, no. 5, pp. 051101-1–051101-3, 2008.
[142] L. K. van Vugt, S. R¨uhle, and D. Vanmaekelbergh, Nano Lett., vol. 6, no. 12, pp. 2707–2711, Dec. 2006.
[143] Z.L. Wang, ACS Nano 2 (2008) 1987–1992.
[144] L.Li, S.Pan, X.Dou, Y.Zhu, X.Huang, Y.Yang, G.Li, L.Zhang, Journal of Physical Chemistry C 111(2007)7288–7291.
[145] H.Zeng, X.Xu, Y.Bando, U.K.Gautam, T.Zhai, X.Fang, B. Liu, D.Golberg, Advanced Functional Materials 19 (2009) 3165–3172.
[146] L.Li, T.Zhai, H.Zeng, X.Fang, Y.Bando, D.Golberg, J. of Mate Chem 21 (2011)40–56.
[147] J.Yan, X.Fang, L.Zhang, Y.Bando, U.K.Gautam, B.Dierre, T.Sekiguchi, D.Golberg, Nano Letters 8 (2008) 2794–2799.
[148] X.Fang, Y.Bando, U.K.Gautam, T.Zhai, S.Gradecak, D.Golberg, Journal of Materials Chemistry 19 (2009)5683–5689.
[149] Y.C.Kong, D.P.Yu,B.Zhang, W.Fang, S.Q.Feng, App Physics Letters 78 (2001) 407–409.
[150] H.Zeng, Y.Bando, X.Xu, L.Li, T.Zhai, X.Fang, D.Golberg, European Journal of Inorganic Chemistry 27 (2010) 4339–4343.
[151] L.Vayssieres, Advanced Materials 15 (2003) 464–466.
[152] W.I.Park, D.H.Kim, S.W.Jung, G.C.Yi, Applied Physics Letters 80(2002)4232–4234.
[153] Y.Li, G.W.Meng, L.D.Zhang, F.Phillipp, Applied Physics Letters 76(2000)2011–2013.
[154] L.E.Greene,M.Law,D.H.Tan,M.Montano,J.Goldberger, G. Somorjai, P.D.Yang, Nano Letters 5 (2005) 1231–1236.
[155] L.E.Greene,M.Law,J.Goldberger,F.Kim,J.C.Johnson, Y.F.Zhang ,R.J.Saykally, P.D.Yang, Angewandte Chemie International Edition42(2003)3031–3034.
[156] Y.K.Tseng,C.J.Huang,H.M.Cheng,I.N.Lin,K.S.Liu, I.C. Chen, Advanced Functional Materials 13 (2003) 811–814.

[157] M.H.Huang,Y.Wu,H.Feick,N.Tran,E.Weber,P.Yang, Adv Materials 13 (2001) 113–116.
[158] X.H.Zhang, S.Y.Xie, Z.Y.Jiang, X.Zhang, Z.Q.Tian, Z.X.Xie, R.B. Huang, L.S.Zheng, Journal of Physical Chemistry B 107 (2003)10114–10118.
[159] Y.Sun, G.M.Fuge, N.A.Fox, D.J.Riley, M.N.R.Ashfold, Adv Mater 17 (2005) 2477–2481.
[160] H.Q.Wang, M.Li, L.C.Jia, L.Li, G.Z.Wang, Y.X.Zhang, G.H. Li, Nanoscale Research Letters 5 (2010)1102–1106.
[161] A.Wei, X.W.Sun, C.X.Xu, Z.L.Dong, M.B.Yu, W.Huang, App Phy Lett 88 (2006) 231102.
[162] H.Yu, Z.Zhang, M.Han, X.Hao, F.Zhu, Journal of the American Chemical Society 127 (2005)2378–2379.
[163] J.Elias,R.Tena-Zaera,G.Y.Wang,C.L_evy-Cl_ement, Chemistry of Materials 20 (2008) 6633–6637.
[164] G.W.She,X.H.Zhang,W.S.Shi,X.Fan,J.C.Chang,C.S.Lee, S.T.Lee, C.H.Liu, Applied Physics Letters 92 (2008) 053111–053113.
[165] Z.W.Pan,Z.R.Dai,Z.L.Wang,Science291(2001)1947–1949.
[166] P.X. Gao, Y. Ding, W. Mai, W.L Hughes, C.Lao, Z.L.Wang, Science 309 (2005) 1700–1704.
[167] Y. Li, Y. Bando, T. Sato, K. Kurashima, Applied Physics Letters 81 (2002) 144–146.
[168] W. Wang, B. Zeng, J. Yang, B. Poudel, J. Huang, M.J. Naughton, Z. Ren, Advanced Materials 18 (2006) 3275–3278.
[169] J.H. He, Y.H. Lin, M.E. McConney, V.V. Tsukruk, Z.L. Wang, G. Bao, Journal of Applied Physics 102 (2007) 084303–084304.
[170] X. Wen, Y. Fang, Q. Pang, C. Yang, J. Wang, W. Ge, K.S. Wong, S. Yang, Journal of Physical Chemistry B 109 (2005) 15303–15308.
[171] X. Wang, Y. Ding, C.J. Summers, Z.L. Wang, J. of Phy Chem B 108 (2004) 8773–8777.
[172] wagneret : R.S.Wagner, W.C.Ellis, App.Phys.Lett, 1964,4 , 89-90.
[173] C.M.Lieber, MRS,Bull 2003,28,486-491.
[174] X. Y. Kong, Z. L. Wang, *Nano. Lett.* 3, 1625 **(2003).**
[175] Z.W. Li, W. Gao , Roger J. Reeves, Surface & Coatings Technology 198 (2005) 319– 323
[176] C. H. Xu, H. F. Lui and C. Surya, (2011) Materials Letters V:65 Issue 1, PP(27-30)
[177] Li, Z.W. and W. Gao. Thin Solid Films, 2007. 515(7-8): p. 3323-3329.
[178] R. Chen ,C Zou, X.Yan, A.Alyamani, W.Gao, thin Solid Film 519 (2011) 1837-1844
[179] H.W.Kim,M.A.Kebe,H.S.Kim,B.Srinivasa,D.Y.Kim,J.Y.Park , S.S.Kim, Curr. App.Phys 10 (2010) 52-56
[180] R. K. Singh and D. Kumar, "Advances in Pulsed Laser Deposition of Thin Films" Kluwer publishers, (1998)
[181] Y. Zhang, H. Gu, and S. Iijima, Appl. Phys. Lett. 73, 3827 (1998)
[182] D.B. Geohegan, A.A. Puretzky, and D.L. Rader, Appl. Phys. Lett. 74, 3788 (1999)
[183] T.J. Goodwin, V.L. Leppert, S.H. Risbud, I.M. Kennedy, and H.W.H. Lee, Appl. Phys. Lett. 10, 3122 (1997)
[184] J.T. Cheung, I.M. Gergis, J. James and R.E. DeWames, Appl. Phys. Lett. 60, 3180 (1992)
[185] J.A. Greer and H.J. Van Hook, Mater. Res. Soc. Symp. Proc. 191, 171 (1990)
[186] A.Namiki,T.Kawai,K.Ichige,Surf.Sci 166 ,129 (1986).
[187] M. Yan, H.T. Zhang, E.J. Widjaja, R.P.H. Chang, J. Appl. Phys. 94 (2003) 5240.
[188] T. Nobis, E.M. Kaidashev, A. Rahm, M. Lorenz, J. Lenzner, M. Grundmann, Nano Lett. 4 (2004) 797.
[189] S H Dalal, D L Baptista, K BKTeo, R G Lacerda, D A Jefferson andW I Milne Nanotechnology 17 (2006) 4811–4818
[190] L. C. Tien, S. J. Pearton, D. P. Norton , F. Ren J Mater Sci (2008) 43:6925–6932
[191] R. Guo, M. Matsumoto, T. Matsumoto, M. Higashihata, D. Nakamura, T. Okada , Applied Surface Science 255 (2009) 9671–9675
[192] A.Marcus (2009)
[193] T. Premkumar, Y. S. Zhou, Y. F. Lu, and K. Baskar, App. Materials & Interfaces VOL. 2 • NO. 10 • 2863–2869 • 2010
[194] H. Kumarakuru ,D. Cherns , G. M. Fuge , Surface & Coatings Technology 205 (2011) 5083–5087
[195] W.Z. Liu, H. Y. Xu, L. Wang, X. H. Li, and Y. C. Liu AIP ADVANCES 1, 022145 (2011)

CHAPTER 3:
Synthesis and Characterization of Zinc Oxide (ZnO) Nanowires (NWs)

Contents

3-1 Introduction

Controlling the growth of ZnO Nws is necessary to optimize the performance of NW based photovoltaic solar cells. This chapter reports the investigation of the nucleation and growth mechanism of ZnO Nws by vapor deposition and pulsed laser deposition. The efficiency and performance of any optical and electrical nano-devices are directly determined by the properties of underlying nanostructures, which are in turn greatly dependent on the crystallographic orientation size shape and morphology. The deposition techniques and their corresponding deposition parameters play an important role in controlling the morphology and physical properties of the nanostructures. The physical deposition techniques have been successfully employed to prepare a wide variety of ZnO Nanostructures. The high quality materials produced by physical deposition dependence on the catalyst used and the seed layer is also investigated. The chapter is divided in 3 sections; the first presents the substrate preparation, selection, cleaning and attachment to the substrate holder. The second section illustrates the deposition of the seed layer/catalyst by different deposition techniques. While the third section describes the parametric study of the synthesis of the ZnO NWs (randomly and vertically oriented).

Chapter Main Sections

3-2 Objectives

The objectives of chapter 3 are the following:

- Illustrate the experimental work
- Identify the morphological, structural and optical properties of the deposited Seed Layer by different techniques
- Identify the morphological, structural and optical properties of the Synthesized ZnO NWs
- Present and discuss the obtained results

3-3 Substrate Preparation

3- 3-1-Substrate selection

Although the vertical alignment of ZnO nanostructures can be assisted by an electric field, [1] in most cases, the alignment is realized by lattice matching between ZnO and the substrate. Several types of epitaxy substrates have been utilized, including sapphire [2],GaN [2], ZnO film coated substrate, [3]SiC [4] and Si substrate[5].

Table 3- 1- Lattice matching with ZnO

Material	**ZnO**	**GaN**	**Sapphire**	**SiC**	**Si**
Crystal structure	Wurtzite	Wurtzite	Hexagonal	Wurtzite	Diamond
Lattice constant (nm)	a=0.325 c=0.521	a=0.319 c=0.519	a=0.475 c=1.299	a=0.309 c=1.512	a=b=c=0.543
Epitaxial plane	(0001)	(0001)	(1120)	(0001)	(100)
Lattice Mismatch	0	1.9% [6]	0.08%[5]	5.5%[4]	18.6% [7]

Table 3- 1 summarized the lattice matching between ZnO and other Materials. Different types of substrates (Figure 3-1) were employed in this research like Si (100) p type, Glass and sapphire to study the effect of substrate on the growth of the ZnO Nanostructures.

Different types of Substrates

a

Prediced Si

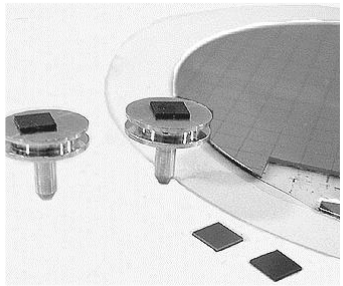

b

Figure 3- 1- Different Types of Substrates, Glass, Si , Sapphire

3-3-2 Substrate Cleaning

Proper cleaning and preparation of substrates prior to deposition is critical to the deposition of the ZnO thin films. Substrates were successively sonicated in Ethanol, Acetone and isopropanol for 10 minutes each. Substrates were rinsed with Di-ionized water before each sonication. Finally they were purged with Nitrogen (N_2) for drying. Cycle presented in Figure 3- 2.

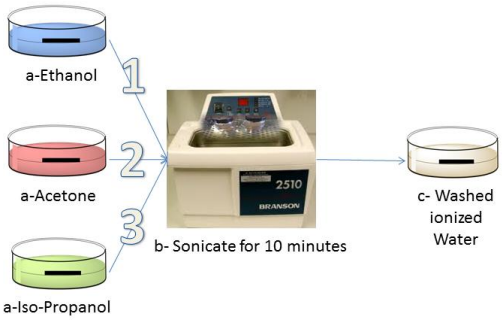

Figure 3- 2- Schematic illustration of the Cleaning Process of the substrates

3-3-3 Substrate attaching to holders

Substrates were introduced in the used equipment in different ways based on its position, and temperature. If the substrates were placed on top of the targets (top down), Figure 3- 3a, they can be either attached by silver paste, or fixed by metallic frame on the inner edges of the frame in high temp environment and attached by copper tape in low temp environment . If the substrates were placed same plane of the targets (top up), Figure 3- 3-b, they can be directly placed on ceramic or quartz boats.

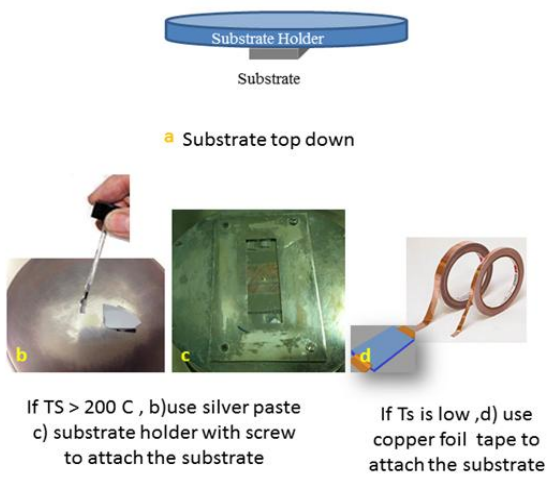

a-Different way of attaching the substrate to the substrate holder a)by Silver Paste, b)by copper

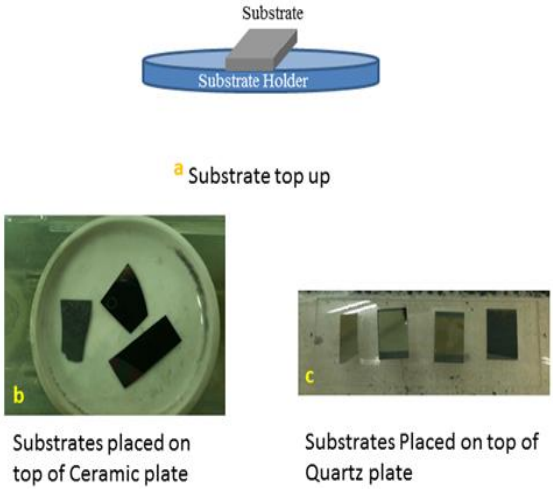

b- Schematic illustrating the placement of the Substrates in case of substrates top up

Figure 3- 3- Attaching means of the substrate to the substrate holder a) substrate top down b) substrate top up

3-4 Seed Layer Deposition

The ZnO nanostructures morphology and crystallization is strongly dependent on the substrate / seed layer. Various buffer layer materials were deposited on different substrates (Figure 3- 4) to investigate their effect on the growth of the ZnO nanostructures such as Zn, ZnO and as catalyst (Gold (Au), and Platinum (Pt)). Sputtering was used to deposit a thin layer of Au and Pt catalyst, while thermal evaporation, RF magnetron sputtering and Pulsed laser deposition method were used to deposit Zn and ZnO. The objective of varying the deposition technique is to study the effect of the morphology and quality of the buffer layer on the growth of the ZnO nanostructures. Substrates used are presented in Table 3- 2.

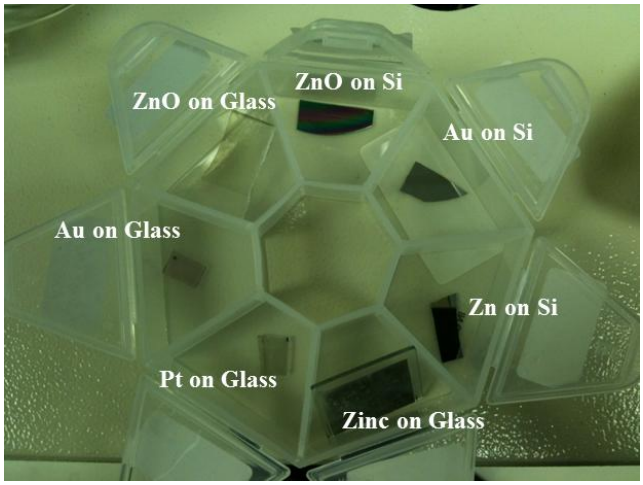

Figure 3- 4 - Different types of Substrates with different Seed Layer

Table 3- 2 Substrates used in this research with their properties and deposited material

Substrates	Properties	Deposited material
Si	P (100)	Zn by thermal evaporation , ZnO by PLD*, RF Sputtering
Glass – ITO	Thickness 1 mm	ZnO by PLD
Glass	Thickness 0.45 mm	ITO by RF Sputtering + ZnO by PLD
Glass	Thickness 1 mm	Au, Pt by Sputtering Zn by thermal evaporation

*PLD: Pulsed Laser Deposition

3-4-1 Zn Seed Layer Deposition by thermal evaporation

Zn is a very active element and inclines to react with oxygen and forms oxide when exposed to oxygen or air. It is well known that the oxidation of metals could be divided into two groups according to the ratio of the molar volume of the metal oxide to that of the corresponding metal [8]. If the volume of an oxide is smaller than that of the metal, the oxide is likely to contain voids and may fail to isolate effectively the

metal from the air, and the oxidation will proceed at a uniform rate owing to the non-protective character of the oxide film. However, when the volume of an oxide is larger than that of the metal, a compact oxide film will form, which tends to shield the metal from the air, and the oxidation rate falls off as the oxide film thickens. Observations show that the very light metals, such as Na, K, Mg, and Ca, belong to the first class, and the heavier metals, such as Fe, Ni, Cu, Zn etc., are grouped into the second class. Many researchers reported the use of Zn seed layer for the growth of ZnO Nws deposited by different techniques: S.Ren et al (2006) [9] used Zn substrate, O.Martinez et al (2011) [10] deposited Zn thin layer by thermal evaporation, while C-Fu Lin et al (2010) [12] deposited Zn layer by ion beam sputtering and A.Sekar et al (2005) [13] sprayed Zn on Si wafers. In this work, metallic Zn (>>99.99% purity) was thermally evaporated in standard vacuum equipment onto unheated glass and Si (100) substrates. The experimental setup consists of a vertical cylinder, where Zn powder was placed in a co boat, the distance between the Zn powder source and the substrates was ap. around 8 cm (Figure 3-7) Parameters are summarized in Table 3- 3.

Table 3- 3-Zn Seed layer deposition Parameters

Pressure	Ar (50 sccm)
Distance target - Substrate	8 cm
Temp target	400 °C
Temp substrate	RT
Duration	15 minutes for a thickness of 200 nm

Argon gas was flowed into the vacuumed chamber. The Boat containing the Zn Powder was heated manually until it reached 400 °C with an average rate of 10 °C /minute plasma has been seen inside the chamber during the deposition. The thickness of the Zn film was around 200 nm identified by thickness sensor attached to the substrate holder at the same level of the substrate. After deposition the glass and Si substrate were covered with black powder (Figure 3- 5).

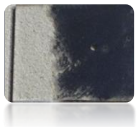

Figure 3- 5- Glass Substrate with Zn Seed Layer by thermal evaporation in vertical furnace: the black zone presented the zone with the deposited Zinc film.

3-4-2 ITO Electrode By RF- sputtering:

As mentioned in chapter 1, the proposed Solar cell, is based on Glass Substrate coated with ITO as bottom electrode. During the research , it is been noticed that The commercialized Glass ITO substrates which have a 1 mm thickness present a problem of heat transfer on the surface of the Glass substrates . Thus, a thinner Glass substrate was used and thin layer of ITO should be deposited. Transparent and conductive oxide (TCO) layers are widely used for many microelectronics applications, such as transparent electrical contacts electrodes in displays, touch screens, thin film solar cells, etc. [14][15][16][17]. Tin doped indium oxide (or indium tin oxide, ITO) is one of the most investigated and used transparent conductive oxides due to the high electrical conductivity and high transparency in the visible light wavelength range [18].

Among several different methods used for ITO deposition (sputtering, evaporation, chemical vapor deposition, sol–gel method, spray pyrolysis, etc.), DC and RF magnetron sputtering are the most attractive techniques for industrial development because of high deposition rate, good reproducibility and possibility of using commercially available large area sputtering systems [19][20][21][22][23].RF sputtering of ITO layers was performed in a commercial inline sputtering system (MRC-603) equipped with a load-lock. A 5 x 15 $in.^2$

ITO target (10 wt% SnO_2) was used for the deposition. The base pressure of the vacuum system was 1.3 x 10^{-6} mbar. ITO sputtering was done in an Ar gas at pressure of 5 mTorr with a RF power of 80 W. The sputtering time for the optimized process was about 30 min to 75 min for 75 nm to 200 nm thick ITO layers deposition. Parameters summarized in Table 3- 4.

The substrates were annealed in air at 350 °C for 1 hour, following the diagram of Figure 3- 6a.The resistivity of the deposited ITO thin film was measured before annealing and after annealing and summarized in Figure 3- 6b. In order to decrease the resistivity of the ITO thin film deposition, we need to increase the thickness of the deposited film. Liu et al[24] have reported that the crystalline structure is observed for ITO film grown on glass prepared by Ion beam assisted deposition technique at Room Temperature (RT).

Table 3- 4- Parameters of ITO Deposition

	ITO1	ITO2	ITO3
Time (s)	1800	3600	4500
Pressure (mTorr)	5	5	5
Height (mm)	180	180	180
Argon Gas (sccm)	25	25	25
Mode	RF 80 W	RF 80 W	RF 80 W
Thickness (nm)	73	155	200
R before Annealing (Ω)	3 000	530	320
R after Annealing (Ω)	700	270	160

a- Annealing diagram of the ITO thin film deposited by Sputtering

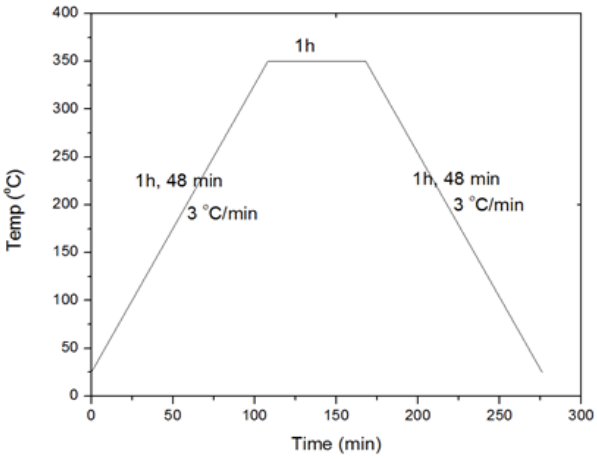

b- Resistivity chart in function of thickness of the ITO thin film deposited by Sputtering before and after annealing

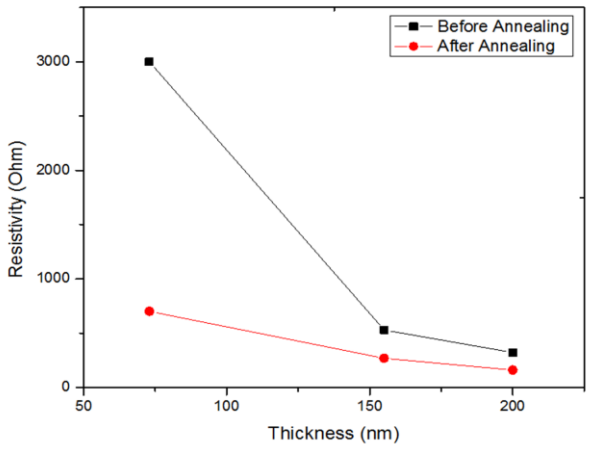

Figure 3- 6- Diagrams presenting a-the annealing process in function of time and b- resistivity before and after annealing, of the ITO thin film deposited by sputtering.

It is known that the electrical conductivity is proportional to the product of carrier concentration and the mobility. Therefore the decrease of film resistivity is due to either the increases of carrier concentration / Hall mobility in ITO films. Gan and Zhang reported the Hall mobility of the film increases with the thickness of the film. The increase of Hal mobility with the thickness occurs because the surface of a thin film affects the conduction of charge carriers by interrupting carrier transit along their mean free path. The rapid increase of resistivity with decreasing film thickness can be attributed to the increasing importance of carrier scattering from the outer surface, the discontinuity and the big amount of deficiencies in the initial growing period of the film[25].

3-4-3 Catalyst Deposition:

For VLS process, thin layer of catalyst (Au) should be coated on the surface of the substrate .Substrates were placed in the center of an auto fine coaters JFC 1200 (Figure 3- 11). Once the pressure in the chamber reached 2.5 Pa and a current of 30mA was employed in the coater for a deposition time of 25s. A thin layer of Gold (Au) of 15 nm thickness was deposited on Glass and Si substrates. The deposited catalyst was annealed at 500 °C in air for 30 min based on the diagram in Figure 3- 7. The annealing will allow Au nanoparticles to be formed on the surface of the substrates.

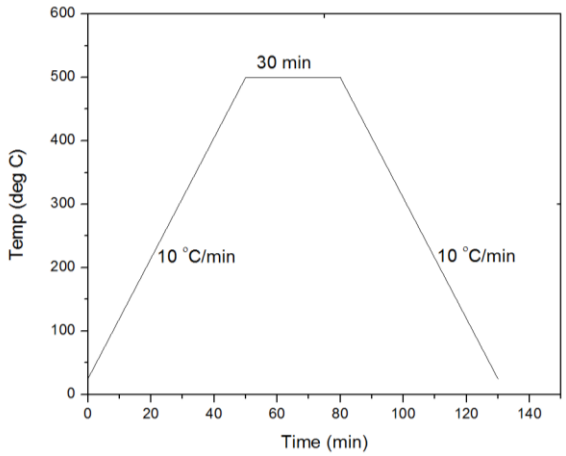

Figure 3- 7- Diagram of Annealing process in function of time of the Au catalyst by coating

3-4-4 ZnO Seed layer deposition:

ZnO thin film was deposited by different means like RF sputtering (done in France) and by Pulsed Laser Deposition. The deposition process is elaborated in details in this section.

3-4-4-1 Seed Layer Deposition by Sputtering

ZnO thin film buffer layers were deposited on the Si substrates using radio frequency (RF) sputtering technique. The sputtering was carried out at room temperature using ZnO (99.99 % purity) target in a pure argon gas atmosphere at a RF of 13.56 MHz. The thicknesses of the sputter deposited ZnO films were approximately 200 nm. Our Colleague “Floriane Leroy” carried out this process in IEMN (Figure 3- 8). (It was only used in the Wet oxidation process).

a- SEM image of the ZnO SL deposited by RF sputtering

b- XRD Spectra of ZnO SL deposited by RF sputtering

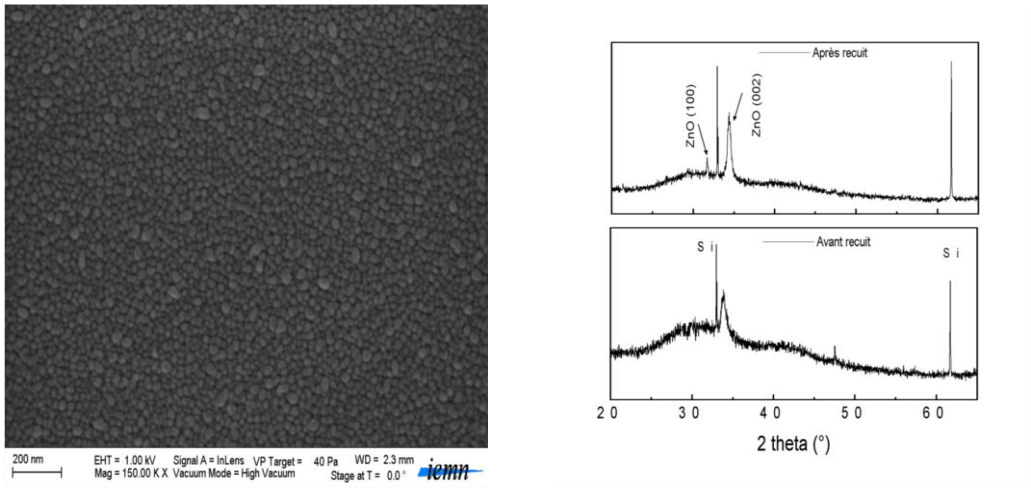

Figure 3- 8- SEM and XRD of the ZnO SL deposited by RF Sputtering in IEMN

3-4-4-2 ZnO Seed **Layer** Deposition by PLD**:**

High quality ZnO Seed layer was deposited by Pulsed laser deposition. The deposited film exhibits a Nanowall Network (NWaN) with honeycomb structure. It is known that reflection loss of solar cells can be reduced by texturizing the surface of the substrates. Honeycomb textured structures were proposed by research group using acid based etching [26] and reactive ion etching (RIE) techniques[27] and by using metal catalyst [28].

It has been suggested that ZnO NWaN with honeycomb structure can be used as energy-storage devices, chemical and biological sensors and dye-sensitized solar cells, as well as memory devices, because they have a large surface-to-volume ratio. [29][30]ZnO NWaNs can potentially be used for optoelectronics and sensors due to their large surface area, diverse shape, and ease of manipulation for device application [31][32][33][34][35]Figure 3- 9 reveals clearly the morphology of the deposited ZnO film, which shows a NWaN with a Honeycomb structure. To understand the growth process, the deposition was studied at different deposition time. Other parametric studies were also conducted: deposition at different temperature and at different oxygen pressure.

Experimental:

A kryton fluoride (Krf) laser system (λ= 248 nm, 15 ns, 10 Hz and 500mJ per pulse) was used in this experiment. The laser beam was focused by focal lens on to a ZnO target for around 8J.mm^{-2}.The purity of the pressed powder ZnO target used is 99.9%. ZnO films were produced in vacuum chamber pumped down to a base pressure of 10^{-6} Torr. The substrates were (100) Si P-Type wafers, and Glass substrates coated with ITO pre-diced into 1.5 cm^2 pieces and positioned around 9 cm from the target surface. The substrate surface was oriented almost normal to the target surface. Before starting deposition, the target surface was ablated with the substrate-masked flag to clean the target surface of possible environment contaminants. To be more accurate about the substrate temperature, it was noticed that the temperature of the substrate is 20% less than the set temperature (provided by the manufacturer). The substrate with deposited ZnO film exhibits a multi-color surface, reflecting the optical properties caused by different thickness (Figure 3- 9).

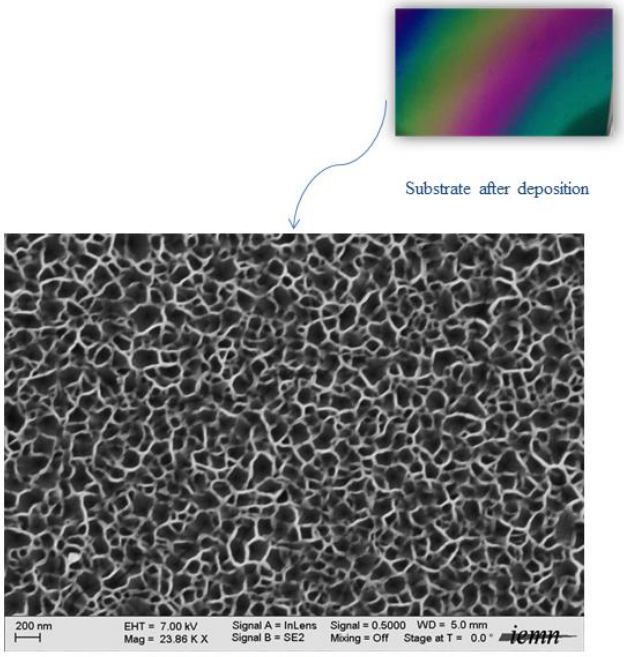

Figure 3- 9- Colorful Substrate after ZnO NWaN with honeycomb structure deposition.

Many parameters influence on the nanostructures deposited by PLD and their quality such as substrate to target distance, background oxygen pressure and the substrate temperature.

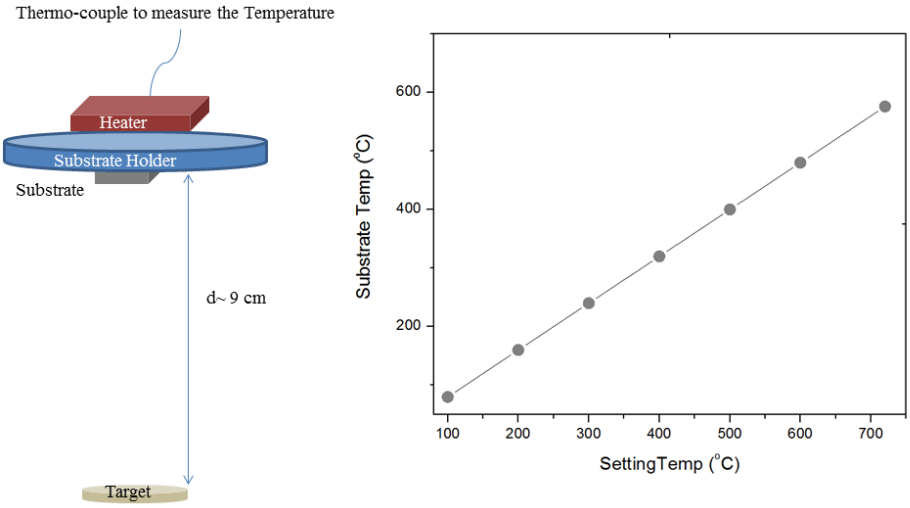

Figure 3- 10 - Diagram showing the relationship between the set temperature (Heater) and the actual temperature (Substrate)

3-4-4-2-1 Effect of Deposition Time

ZnO NWaN with honeycomb structure were successfully grown by catalyst free PLD. In order to understand the growth process, deposition at different period of time was employed. Parameters used are summarized in Table 3- 5.

Table 3- 5- Deposition parameters

Oxygen Pressure	10 mTorr
Setting Temperature	600°C
Laser Energy	500 mJ
Deposition Time	5min, 7 min, 10 min, 15 min, 30 min, 45 min

The PLD growth for ZnO NWaNs was carried out on Si (100) substrate at a pressure of 10mTorr for different duration of time ranging from 5 min to 45 min. The PLD growth temperature used was 500 °C. Figure 3- 11 shows the Scanning electron microscope (SEM) images of ZnO NWaNs at different deposition duration of time 5min, 10 min, 15 min, 30 min and 45 min. These images show that the two dimensional ZnO NWaNs were grown vertically on the substrates. The pores size ranges from 50 nm to 140nm and the walls between the walls exhibit a thickness of ~ 50 nm. The size of the nanowalls is remarkably uniform over the whole substrate. The density of the nanowalls increased with the deposition time. To understand the growth evolution of the ZnO NWaNs, SEM images of the ZnO NWaNs grown at different time intervals are shown in Figure 3- 11 (a)-(e). It is known that crystals exhibit different growth rates for various crystal facets[36] .

a-5 min

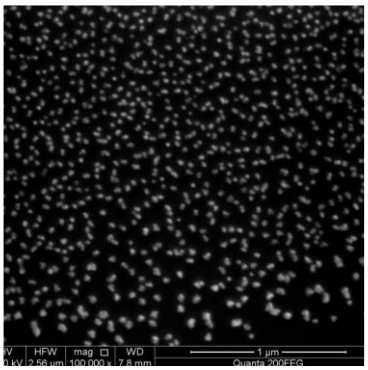

b- 7min

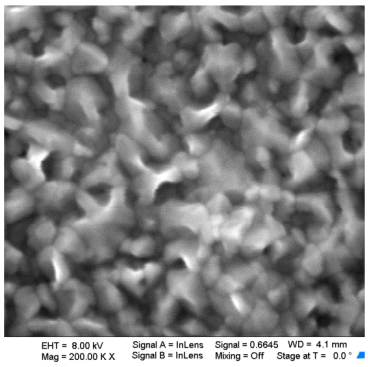

c- 10 min

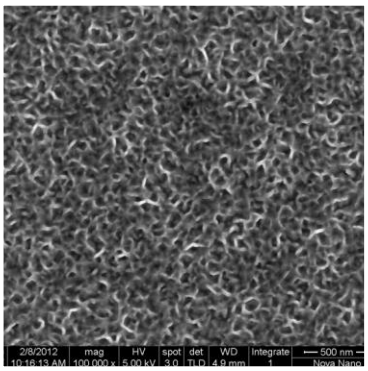

d-15 min

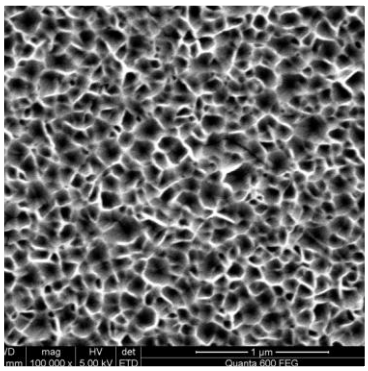

Figure 3- 11- SEM Images of ZnO Seed Layer deposited on Si (100) P(O_2) = 10 mTorr, Ts=600°C at different deposition time

The XRD Spectra of the deposited ZnO NWaNs at different deposition time are shown in Figure 3- 12. The diffraction peak of the ZnO NWaNs occurs at 34.5°, which is related to the ZnO [0002] Bragg Reflection in addition to the (200) plane. This suggests the fully c-axis preferred orientation of the NWaNs. It is clear that as long as we increase the duration of deposition, the film crystallinity improves and quality increases. With the increase in film thickness the deposited layer provides the nucleation centers and allows the highly crystalline layer due to the reduction in the formation energy and highly c-axis oriented film can be obtained at higher thickness and crystallinity is found to depend strongly on film thickness , deposition rate and substrate temperature.

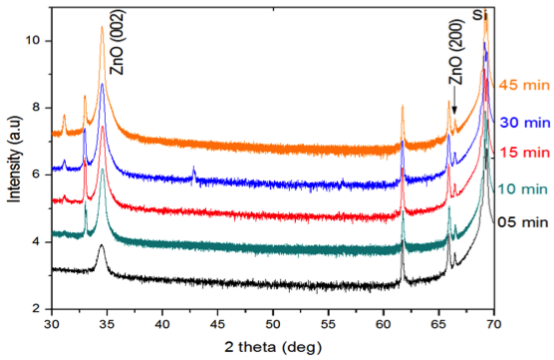

Figure 3- 12- XRD Spectra of ZnO Seed layer deposited on Si, P(O2)= 10 m Torr, TS= 600 °C, at different deposition time

Figure 3- 13a depicts the PL measurements at Room Temperature using HeCd Laser (325 nm, 8mW) for all the samples. It present different peak positions of the band edge emission in the UV region as well as defect induced emissions in the visible region. It is clear that the deposition at different duration of the ZnO NWaNs showed very similar PL spectra, dominated by a strong, narrow ultraviolet (UV) emission centered between 475 and 382 nm. This UV emission is attributed to free exciton recombination a near band transition of wide band gap ZnO which is considered as the Near Band Energy (NBE). It is noticed from figure 3-13b that NBE peaks at different deposition time present a blue shift in function of the deposition time, reflecting that by increasing the deposition time (thickness of the film) less quantum confinement can be identified.

a- Pl Spectra of the ZnO NWsN at different deposition time

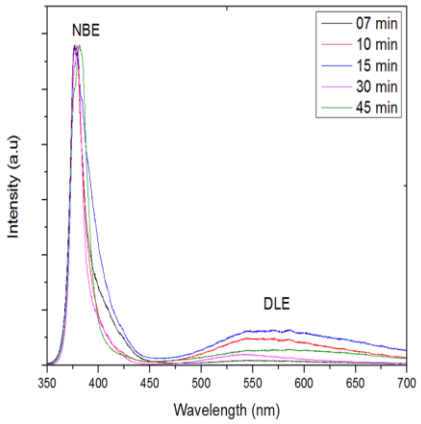

b- The NBE presented in function of the time deposition

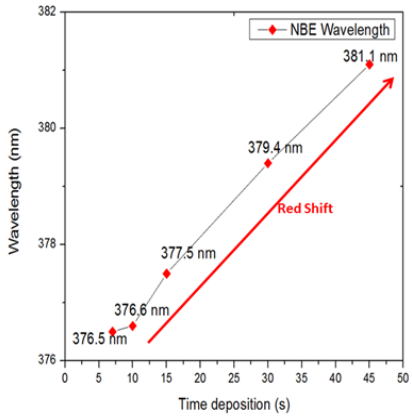

Figure 3- 13 a)RT- PL Spectra of ZnO Seed layer deposited on Si, P(O2)= 10 m Torr, TS= 600 °C, at different deposition time. b) NBE variation in function of deposition time

Defect level emission (DLE) band is broad and intense. It is composed of an emission peak centered in the green and yellow band. The peak in the green zone is assigned to shallow donor effects (doubly occupied vacancies / zinc interstitials) and the one in the yellow zone is assigned to deep effects (oxygen interstitials). Defects traditionally associated with the green emission include oxygen vacancies and interstitial Zn atoms, whereas interstitial O atoms have been suggested as carriers of the orange red emission [37]. We conclude that the importance of Oxygen vacancies increase with the deposition time. The oxygen vacancies emission at ~ 541.363 nm, 546.772 nm, 547.7634 nm, 542,895 nm and 548.57 nm of the samples S07,S10,S15,S30, and S45 min respectively . On the other hand the oxygen interstitials emission at 584.746 nm, 584.1803 nm and 586.25 nm of the samples S10, S15, S45 respectively. The peaks are very weak compared with the near band energy emission. To evaluate the defect level of ZnO Nanowall Network with honeycomb structure at different deposition time, we calculate the intensity ratio of the NBE to that of DLE ($r = \frac{I_{NBE}}{I_{DLE}}$). The larger the ratio is the better quality of deposited film we have. The ratio that corresponds to the green emission is respectively to the deposition time (61,11.5,9,28.7 and 20.36), and the ratio corresponding to the yellow emission is 12.12 ,8.86 and 19.9 respectively to the deposition time 10min, 15 min and 45 min.

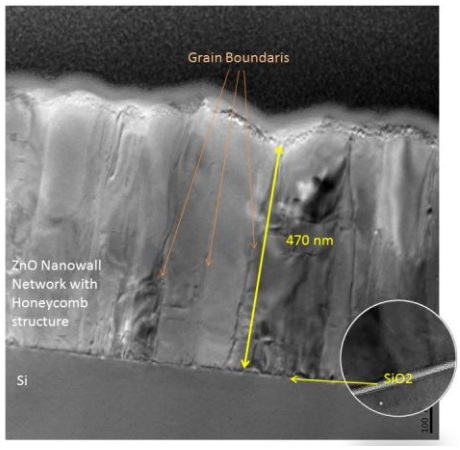

Figure 3- 14 - TEM Images of ZnO NWaN with Honeycomb structure

The crystallography of ZnO NWaN, was further investigated using TEM. Figure 3-14, is a cross section image of the ZnO film. The orientation can be revealed by the image. TEM results suggest single crystal ZnO NWaN was grown with c-axis Orientation with a thickness of 470 nm. Only few crystal defects such as dislocations and stacking faults were observed. A HRTEM image shows the ZnO crystal lattice is

continuous across the film. The Grains were grown perpendicular to the substrates even though they were deposited on Si (100) substrates. Grain size forming the columnar structure seems to be similar to each other in the range of 90-120 nm.

Figure 3- 15a presents the XPS Spectra of the ZnO NWaN with honeycomb structure. It illustrates the XPS Spectra from the ZnO Nws indicating the presence of the following elements Zn, O, C and Si. No contaminations were detected on the sample surface. The XPS Spectra of the Zn-2p is presented in Figure 3- 15b and O-1s is presented in Figure 3- 15c. The ZnO NWs display a peak at 1021.4 eV and 1046.1 Ev which are in agreement with the binding energies of Zn $2p_{3/2}$ and Zn $2p_{1/2}$ respectively. The ZnO NWaN with honeycomb structure exhibit an asymmetric peak at 530.1 eV observed in O1-s core level spectrum of Figure 3- 15c. Figure 3- 15d reveals an intense peak at 102.3 eV which corresponds to Si_{2p}. It is noticed that Si element can be identified in the ZnO NWaN, which might be caused by the porosity of the nanowall. The ratio of Zn2p, O1s is around 1.14 which reflects the high quality of ZnO NWaN, deposited in Oxygen environment (Table 3- 6).

a-XPS Spectrum

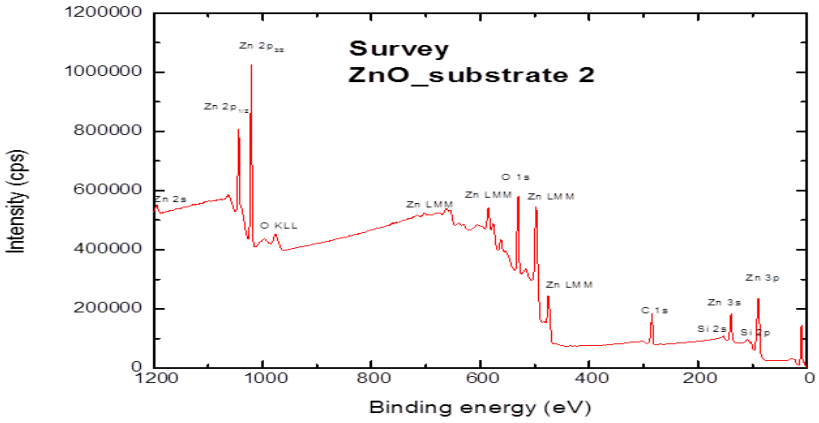

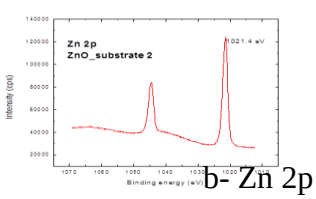

b- Zn 2p

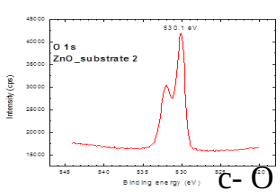

c- O 1s

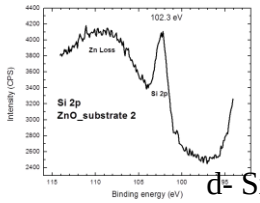

d- Si 2p

Figure 3- 15- XPS Measurements for ZnO Nanowall Netowork with honeycomb structure.

Table 3- 6- Atomic Concentration of Zn, O, C, and Si elements in ZnO Nanowall

Elements	Zn	O	C	Si
Atomic concentration (%)	35.7	31.3	30.0	3.0

Discussion

The film growth process occurs in three different stages in a typical Pulsed Laser deposition (PLD). It started when the laser strikes the solid target of ZnO and produces a highly forward directed plume of gas phase material. The plume then interacts chemically and physically with the background gas, and finally the ablated material condenses onto the Si substrates where the thin film nucleates and grows.

In order to interpret the evolution growth of ZnO NWaN , the deposition was done for different duration. As presented in TEM images (Figure 3- 14), a thin layer of SiO_2 was formed on the surface of the Si Substrate, which might have improved the lattice mismatch between the Si and the ZnO deposited nanostructures. Working at high temperature of (600 °C) and relatively low Oxygen pressure (10mTorr) affected the growth of the ZnO NWaN . The effect of oxygen pressure and substrate temperature on the morphological, structural and optical properties of the ZnO NWaN will be presented and interpreted in details in the coming sections. Small islands were formed on the Si substrate surface after 5 minutes of deposition Figure 3-11 (a). By a continuous supply the ablated species, these islands tend to combine with each other Figure 3- 11(b).

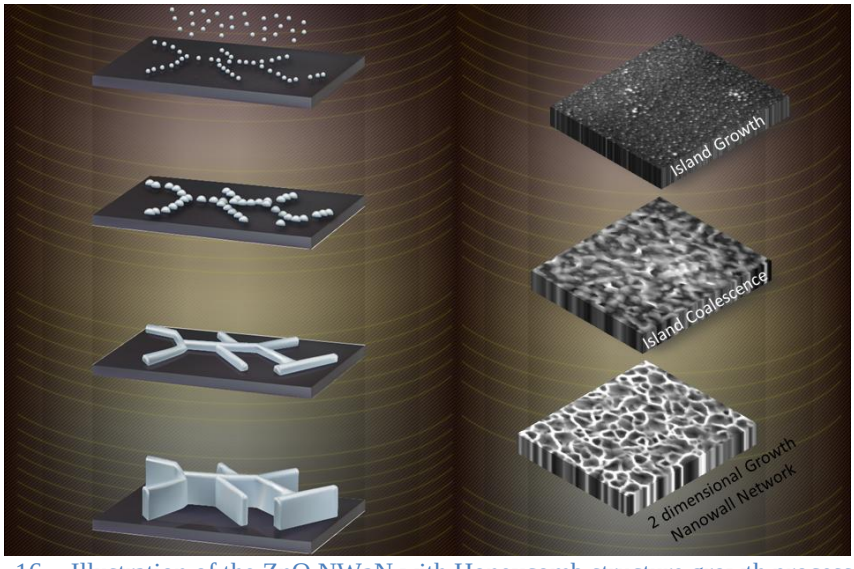

Figure 3- 16–– Illustration of the ZnO NWaN with Honeycomb structure growth process by PLD

By increasing the growth time, two dimensional growth modes is grown that lead to the generation of ZnO NWaN with honeycomb structure. While The Vapor Liquid Solid (VLS) mechanism is the most common process that explains the growth evolution of the NWaNs where a metal catalyst plays an important role in the formation of the ZnO nanostructures, no catalyst was used in our case, which indicates that our growth process does not follow the VLS mechanism. Illustration of the growth process is presented in Figure 3- 16.

3-4-4-2-2 Effect of Oxygen Pressure

The effect of oxygen pressure on ZnO Properties has been investigated by many researchers [37]. It is been found that it is possible to obtain relatively high quality ZnO thin film by controlling oxygen pressure. The objective of this parametric study is to check the growth of the ZnO NWaN with honeycomb structure can at higher pressure. Parameters used are presented in Table 3- 7.

Table 3- 7 – Parameters of Deposition

Oxygen Pressure	**10 mTorr , 50 mTorr, 150 mTorr, 500 mTorr**
Setting Temperature	600 °C
Laser Energy	500 mJ
Deposition Time	45 min

ZnO thin film were deposited at different Oxygen pressure maintained during the deposition ranging from 10 mTorr to 500 mTorr and substrate temperature of 500 °C for 45 minutes. Figure 3- 17 shows SEM images of ZnO films deposited at varied oxygen pressure (10 mTorr, 50 mTorr, 150 mTorr and 500 mTorr). It is noticed that the morphology of films obtained at low oxygen pressure is quite different from that obtained at high oxygen pressure Figure 3- 17 a-d. At low pressure 10 mTorr, the film is composed of ZnO NWaN with honeycomb structure with non-uniform cell size. While at higher pressure, a macroporous film is grown on the Si substrate, and composed of nanopost with pencil shape morphology.

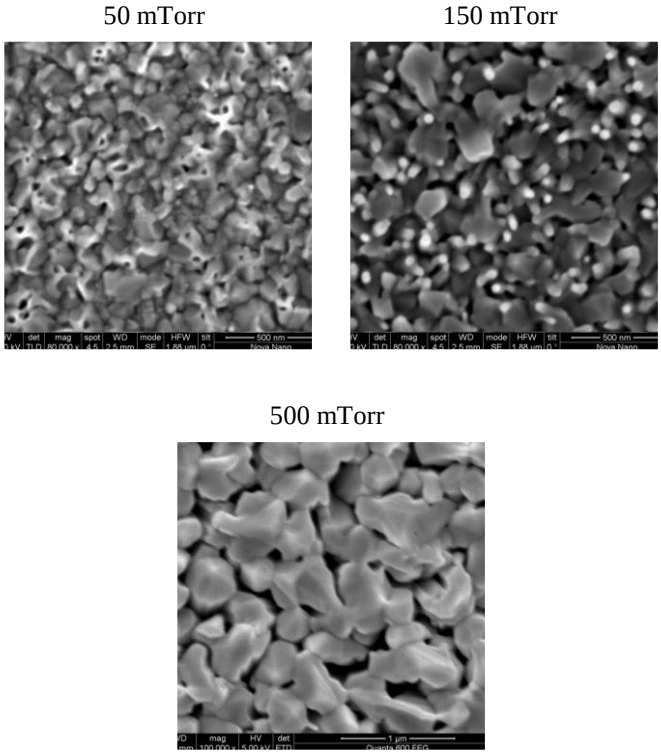

Figure 3- 17- SEM Images of ZnO Seed Layer deposited on Si(100) t=45 min , Ts=600 °C at different Oxygen Pressure

It is clear that the crystallinity of the thin film deposited depends on the oxygen pressure. The films deposited at higher oxygen pressure 500mTorr show random orientation and more peaks (002), (101), (102), (103), (200) plane are present on the spectrum Figure 3- 18, hence the crystalline quality has degraded. However some peaks vanish or become weaker when oxygen pressure decreases, the film quality is improved and crystallites become more aligned, only (002) and (200) planes are shown suggesting the fully c-axis preferred orientation of the film.

Figure 3- 19a presents different peak positions of the band edge emission in the UV region (NBE) as well as defect induced emissions in the visible region (DLE). It is seen that the PL spectra of the different thin film deposited at different pressure are very similar, dominated by a strong, narrow ultraviolet (UV) emission centered at 381.1 nm (3.253 eV) , 378.75 nm(3.27 eV), 376.12 nm(3.297eV) and 375.857 nm(3.3 eV) corresponding to the deposition at 10 mTorr, 50 mTorr, 150 mTorr and 500 mTorr Oxygen pressure respectively.

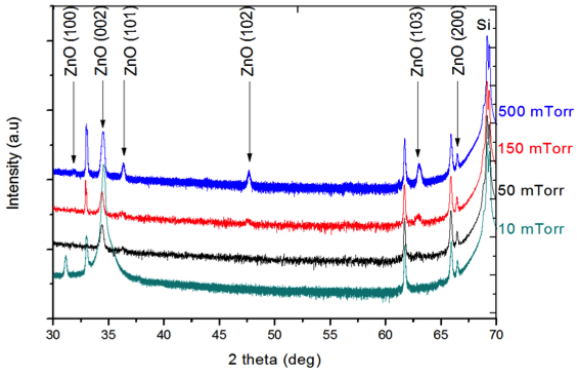

Figure 3- 18- XRD Spectra of ZnO Seed Layer deposited on Si(100) t=45 min , Ts=600 °C at different Oxygen Pressure

It is noticed that by increasing the pressure, the band edge emission in the UV is blue-shifted (figure 3-19b) of 20 meV, 27 meV and 3meV respectively similar to the results observed in semiconductor quantum dots and quantum well. On the other hand by decreasing the Oxygen pressure, more peaks in the visible region are identified due to several factors such as oxygen deficiency, impurities centers, and presence of particles onto the surface [38]. This is reflected by the intensity ratio of NBE to DLE that can be identified in the green and yellow region of the visible area. The ratio for the green emission is 20,226.7, and 226.7 while for the yellow emission, the ratio is 19.7, 266.7 and 266.7 corresponding to samples at 10 , 50 and 150 mTorr. No DLE can be identified for the ZnO NWaN deposited at 500 mTorr.

a- Pl Spectra of the ZnO NWsN at different deposition time

b- The NBE presented in function of the time deposition

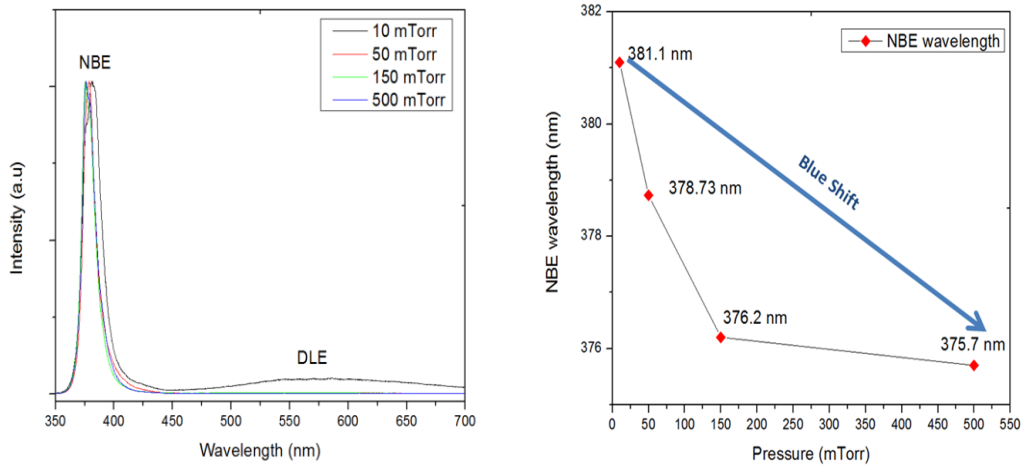

Figure 3- 19- a) RT- PL Spectra of ZnO Seed Layer deposited on Si(100) t=45 min , Ts=600 °C at different Oxygen Pressure. . b) NBE variation in function of oxygen background pressure.

Discussion:

PLD makes the composition of a stoichiometric ZnO target surface, besides substantial loss of target surface material under successive laser ablation at low oxygen pressure [40]. At low pressure the emitted atoms and ions from the target surface, after laser interaction, condense on the substrate surface to form a continuous film. The mean free path of the ablated species depends upon the processing pressure and increases with decreasing pressure[41]. When films are processed under high surface pressures the ablated species undergo a large number of collisions with background gas molecules and the condensation of species in the gas phase results in the formation of nanosize particles reflected in the blue shift of the UV emission wavelength(Figure 3-19). The settlement of these nanoparticles, on the surface of the substrates, promotes the formation of a dense and smooth film (Figure 3- 20). The nucleation of nanoparticles on the substrate is controlled either by the processing conditions or by using a catalytic layer and lead to the fabrication of interesting nanostructures. The deposition at (10 mTorr) leads to reduction in the strain with minimal surface roughness. Oxygen pressure influences both the deposition rate and the kinetic energy of ejected species. The kinetic energy of the ablated species reduces with the increase in pressure due to the large number of collisions with background gas molecules and it is commonly observed that the size of the ablated plume decreases with increase in oxygen pressure. (Its effect will be described in details in next section)

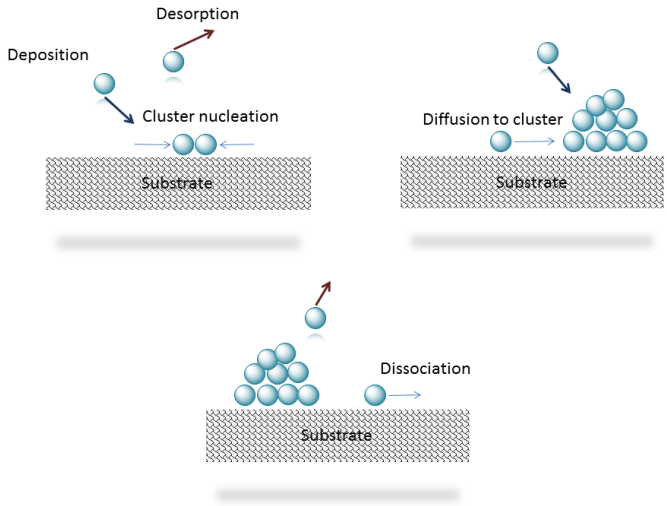

Figure 3- 20- Deposition Process of ZnO Nanoparticles

3-4-4-2-3 Effect of Substrate temperature

The temperature of the substrate aids in surface diffusion S.L.King et al [42] suggested that higher temperature can provide sufficient energy for deposited species and allows them to migrate to low energy sites on the substrate. The objective of this study is to identify the temperature effect on the growth of the ZnO nanowall with honeycomb structure. The ZnO films were deposited at different substrate temperatures (600°C to RT). The chamber was maintained at an oxygen pressure of 10mTorr during the deposition at a growth period of 45 min. Parameters of deposition summarized in Table 3- 8.

Table 3- 8 - Parameters of deposition

Oxygen Pressure	**10 mTorr**
Setting Temperature	RT, 200 °C, 400 °C, 600 °C (20 % loss on the substrate)
Laser Energy	500 mJ
Deposition Time	45 min

Figure 3- 21 shows the SEM of the ZnO nanowalls and network with honeycomb structure grown on Si Substrates. The interlinked ZnO nanowalls were obtained at 600 °C, 400 °C, while at 200 °C and RT, it didn't show any nanowall structure. The width and height of the nanowalls were 120$\pm$ 50nm and 800 nm respectively. Figure 3- 22 shows the X Ray Diffraction pattern of the ZnO nanowalls grown at different temperature on Si substrates without using catalyst. In addition to the substrate and substrate holder peaks, ZnO nanostructures show strong peaks corresponding to ZnO (002) and (200) planes. The Strong (002) Peak shows that the ZnO nanostructures were preferentially oriented along the c-axis [0002] which indicates that the as grown nanostructures have good epitaxial orientation with the Si Substrates at different temperatures.

Figure 3- 23a compares the photoluminescence spectra of the ZnO nanowalls networks grown at 600°C, 400°C, 200°C and RT on Si Substrates. The spectra show a strong near band edge (NBE) emission of ZnO around 379.831 nm (3.264eV) , 374.7831 nm (3.3 eV) , 379.831 nm (3.264 eV) and 381.1 nm (3.253 eV) corresponding to the samples deposited at RT, 200 °C , 400 °C and 600 °C respectively.

a- SEM Image ZnO thin film deposited at 400°C

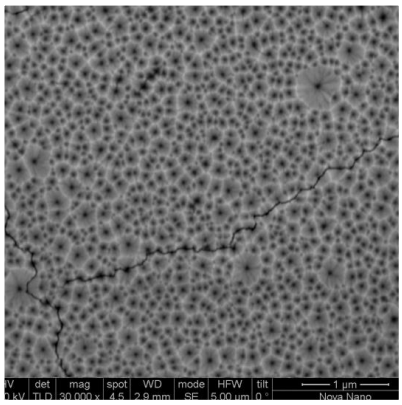

b- SEM Image of ZnO thin film deposited at 200°C

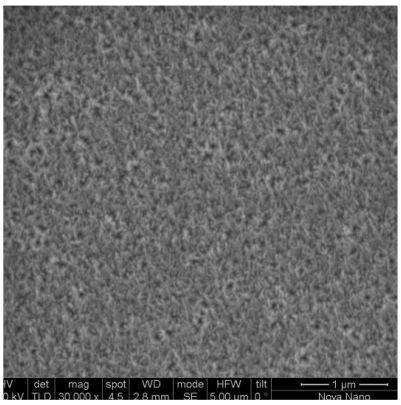

c-SEM image of ZnO thin film deposited at RT

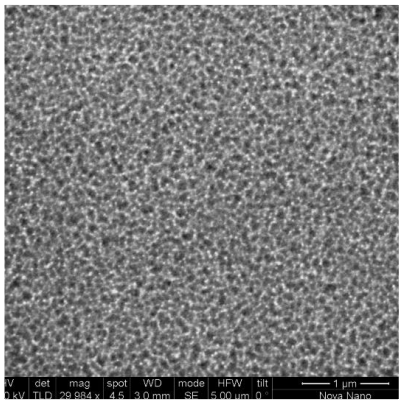

d- AFM image of ZnO thin film deposited at RT

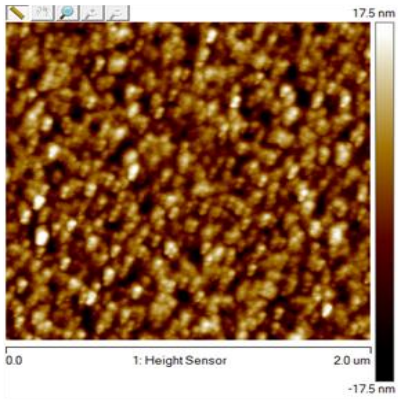

Figure 3- 21- SEM Images of ZnO films deposited on Si(100) t=45 min , $P(O_2)$ = 10 mTorr at a- 400°C b- 200°C c-RT and AFM Image of ZnO thin Film deposited on Si(100), t =45 min , $P(O_2)$ =10mTorr at RT.

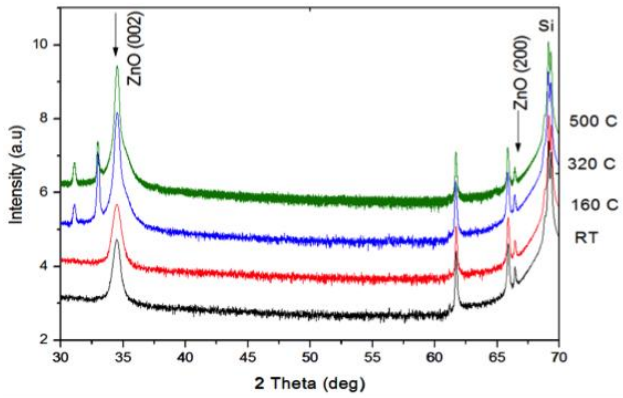

Figure 3- 22-XRD Spectra of ZnO Seed Layer deposited on Si(100) t=45 min , $P(O_2)$ = 10 mTorr at different Substrate temperature

a- Pl Spectra of the ZnO NWsN at different deposition temperature

b- The NBE presented in function of the temperature deposition

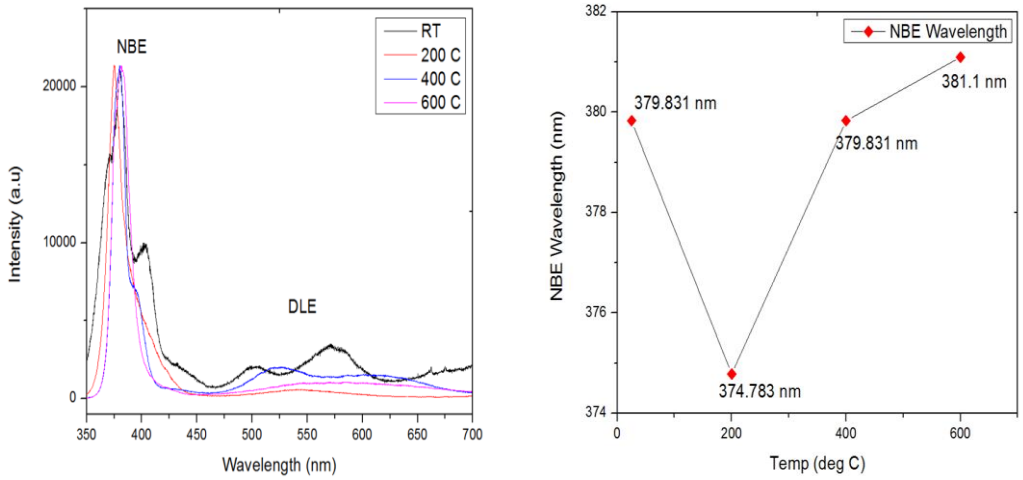

Figure 3- 23- a) RT- PL spectra of ZnO Seed Layer deposited on Si(100) t=45 min , $P(O_2)$ = 10 mTorr at different Substrate temperature. . b) NBE variation in function of substrate temperature.

It is noticed from figure 3-23b that the NBE is red-shifted starting from 200 °C. The RTPL spectrum of the thin film deposited at RT reveals more peaks in the UV-blue region at 370.486 nm (3.347 eV), 379.831 nm (3.264 eV) and 403 nm (3.07 eV) . Usually, at low temperatures excitons are bound to donors or acceptors in ZnO lattice and PL emission comes predominantly by their recombination. This luminescence is called *bound exciton* (*BX*) emission and it is placed at energies (~ 3.36-3.38 eV, ~ 366-369 nm, at low temperature) slightly lower than ZnO energy gap. The emission at 403.3 nm (3.07 eV) is attributed to transitions from conduction band to Zinc vacancy levels by X.L.Wu et al (2001). In all these cases, this band has been attributed to zinc-related defects.

Discussion:

The substrate Temperature in PLD process is critical due to the activation of the surface mobility of the species deposited onto the surface of the substrate. At low temperature a crystalline ZnO film with low surface roughness is obtained 5.83 nm [Figure 3- 21c, d]. The c-axis orientation of ZnO thin film degrades at substrate temperature (Figure 3- 22) due to the reduced surface mobility and migration of species on the substrate surface and the low quality of surface texture. The nucleation process depends on the interfacial energies between the substrate surface and the condensing species, and highly dependent on the substrate temperature. The

crystallinity of the film dependent on the surface mobility of the condensing species .Figure 3- 20 illustrates that the species will diffuse for few atomic distances before sticking to a stable position within the deposited film. At high substrate temperature, a rapid and defect free crystallites have been formed, whereas at low substrate temperature a disordered and poorly crystallized structures are developed.

3-4-4-2-4 Effect of Substrate:

Glass and Si substrates were used to check the effect of substrate on the growth of ZnO NWaN with honeycomb structure. Because of residual stress effect on film growth, the nature of the substrate plays an important role in film properties [43]. It affects both film morphology and preferential orientation. Optical transmittance is affected by film thickness, surface roughness, oxygen deficiency and impurity centers. The granular structures grain shape and grain boundaries losses by simple or multiple wave scattering. All these parameters aver very important to get high quality optical films. Figure 3- 24 illustrates the ZnO NWaN synthesized on Glass-ITO substrates.

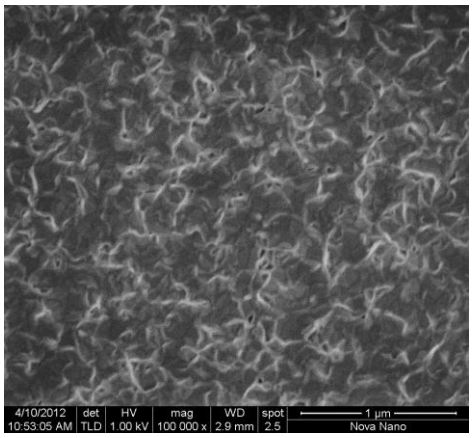

Figure 3- 24-SEM Image of ZnO NWaN deposited on Glass substrates coated with thin layer of ITO at 600 °C for 45 min at 10mTorr Oxygen background

4-4-2-5 Conclusion of the ZnO Seed Layer Deposition by PLD:

High quality ZnO NWaN with honeycomb structure have been successfully grown on Si and Glass-ITO, at high temperature (600°C) and low oxygen pressure (10 mTorr). This textured surface will be used as seed layer for the growth of the ZnO NWs by PLD. Details of the process are presented in next section.

3-5 Growth of ZnO NWs

Based on the above the Zn and ZnO buffer layers were deposited on Si and Glass substrates. Different techniques were employed to see the effect on the growth of the ZnO NWs. Table 3- 8 summarizes the results obtained using different ZnO NWs Growth techniques(wet oxidation , thermal evaporation and PLD) on different types of Seed layer materials (Zn, ZnO) – catalyst (Au). Details of Growth process is elaborated in the next sections.

Table 3- 9- Survey of the results obtained by different techniques using different seed layer

Growth technique	Types of Substrates	Seed layer & Deposition technique	Nanostructures
Wet Oxidation	Glass Si(100)	Zn – Thermal evaporation ZnO by sputtering Au by coating	NWs No results NWs
Thermal Evaporation	Glass Si(100)	---	Tetrapods
PLD	Si (100) Glass- ITO	ZnO by PLD	ZnO NWs

3-5-1 ZnO NWs by Wet Oxidation

Wet Oxidation [44] showed to produce nanostructures that have high plasticity and good adhesion to substrates. Wet oxidation is selected due to its advantage in reducing the oxidation temperature (< 800°C instead of 1400°C explained in chapter 2), which results in reducing the instrument requirement and cost. Thermal evaporation in the presence of water is based on a solid state thermal sublimation process , in which the source materials (powder form Zn (>>99.99% purity) is placed at the center of the furnace, and this material is sublimated by increasing the temperature; The resulted vapor phase in the presence of water vapor will give nanostructures under certain conditions. By controlling the type of Gas, the growth temperature, the seed layer material and the position of the substrates, various structures will be produced. Zn powders like other powders have some weakness like free standing and poor adhesion with the supporting substrates. However, few reports showed the effects of introducing water vapor to the oxidation atmosphere to form ZnO nanostructure and produce ZnO nanostructures from oxidation of Zn films Table 3- 10. [45] Reported the working temperature to be between 380°C and 450°C with a flow of oxygen 0.3 l/min, by bubbling oxygen in a water flask so that the oxygen carries with it the water vapor inside the furnace to conduct wet oxidation. The growth duration was for 4 hours and the results were very long NWs (> 300nm

length). Pure Zn (>> 99.99%) was placed at the hot spot of the horizontal tube furnace. The substrates are placed at the downstream side of the furnace and the distilled water at the upper stream of the furnace (presented in chapter 2). The Zn source is evaporated then transported by the humid carrier gas, oxidized and deposited onto the surface of the substrate coated with Zn seed layer. It is expected that by changing the gas introduced in the chamber (Ar, N_2, O_2), and the temperature (650°C …950°C), the morphology and quality of the ZnO nanostructures will change. The placement of the Substrates, Zn source and the distilled water is very critical for the proper growth of the ZnO nanostructures.

Table 3- 10- Survey of ZnO NWs synthesis by vapor transport in wet environment

Precursor used	Substrate	Carrier gas	Time	Nanostructure	Ref
ZnO + Graphite (950° C)	Si+ SiO2+ Zn SL	Ar+ O2	1 h	NWs	[46]
Zn (600°C)	Si+Au (20 nm)	Ar+O2	--	NWs randomly oriented	[47]
ZnO + graphite (975 °C)	Ti, Mo foil + Au	Ar+O2	45 min	NWs randomly oriented	[48]
Zn (620-630 °C)	Si(100),Si(111),Glass	Ar+O2	40 min	NWs	[49]
ZnO + graphite (930 °C)	SiO2,Au,ZnO,Au/ZnO	Ar	30 min	Nws randomly Oriented	[50]
ZnO + graphite (950 °C)	c-Al2-O3 +Au	Ar	1h	Nws	[51]
Zn (900 °C)	Si	Ar+ O2	30 min	Tetrapods	[52]
Zn (900°C – 1050 °C)	Si+Au	N2	1 h	NWs randomly oriented	[53]
Zn (650 °C)	Alumina + Zn	Ar+O2	30 min	NWs	[54]

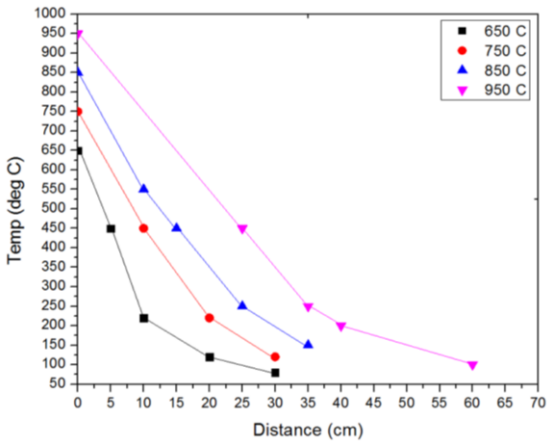

Figure 3- 25- Illustration of the horizontal tube furnace and the degradation of temperature in function of the distance from the hot spot of the furnace.

Having a one zone furnace, it is necessary to identify the degradation of the temperature in function of the distance from the center of the furnace (hot Spot). Taking in consideration the size of the furnace, the temperature at different zone was

measured by thermo-couple. The Zn powder source is placed at the hot spot of the furnace (point 0), the substrate at the zone of a lower temperature around 450 °C and the distilled water at the zone of Temp 200°C and 100°C. Figure 3- 25 reveals the temperature drop from the center to side of the furnace for different temperatures at the center (960 °C… 650 °C). The Zn powder was heated up to 450°C, close to the melting point of the Zn (420°C) with a dwell time of 5 min which is enough to introduce the gas inside the chamber. The temperature was then increased up to the desired temperature. Once the desired temperature was reached the system was shut down for cooling to RT Figure 3- 26.

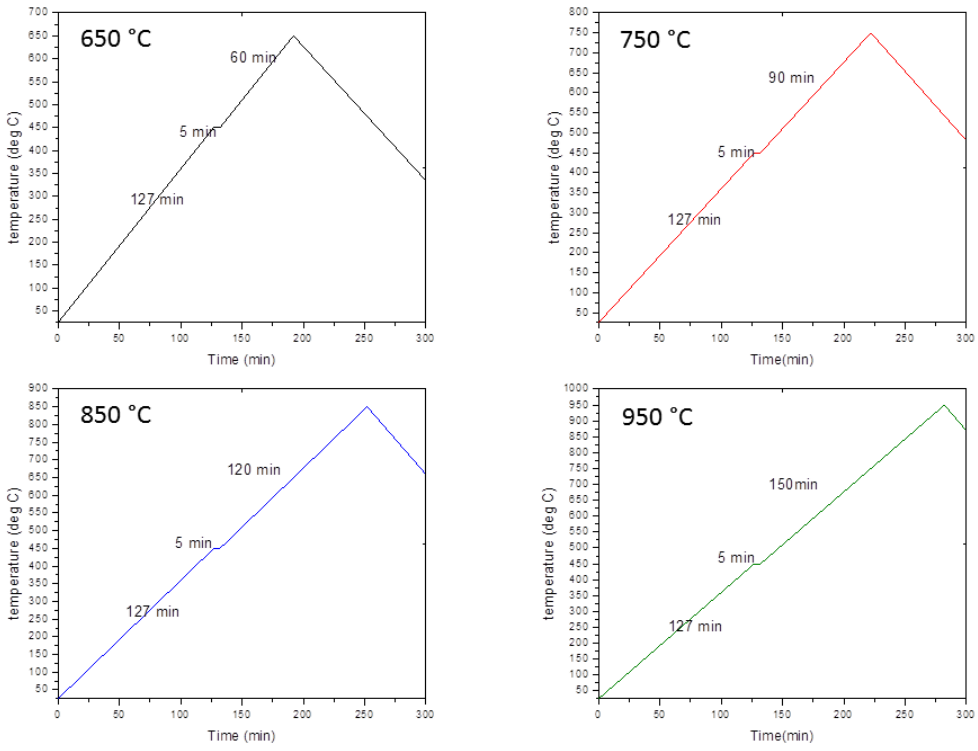

Figure 3- 26- Diagram of the deposition process. The temperature is set in function of time. Dwell time at 450 °C for 5 min , to present an enough time to introduce the gas in the chamber

3-5-1-1 Growth of ZnO NWs in Wet Oxygen Environment at 750 °C

Different types of substrates with different seed layer were introduced inside the furnace. The Oxygen gas was introduced inside the chamber at 450°C. The temperature was then increased with a rate of 3°C/10 minutes up to 750°C. Parameters summarized in Table 3- 11.

Table 3- 11- conditions for the growth of ZnO NWs

Parameter	NW Growth
Substrate	Si (100), Glass
Nucleation mater	Au , Zn , ZnO
Source Precursor	Zn
Gas flow	Oxygen
Growth temperature	400-750 °C
Growth Time	1h 30 minutes
Growth Pressure	atmospheric

Figure 3- 27 illustrate the morphology of ZnO synthesized over glass and Si substrates. ZnO nanoparticles were clearly aggregating on the Glass substrate with Zn seed layer and Si with ZnO seed layer. No NWs were identified Figure 3- 27 b,c. On the other hand the substrates with Au catalyst, cubical shape nanoparticles of 80 to 273 nm of size were distributed on the surface of the Glass substrate (Figure 3- 27 a). While in Figure 3- 27-d, hexagonal shape nanostructures were noticed with a spacing of 50 to 150 nm, and diameter of 50-70 nm. Tilted view and cross section confirm the growth of ZnO Nanorods on Si (100) substrates with Zn seed layer Figure 3- 37.

Deposited ZnO nanostructures were polycrystalline confirmed in Figure 3- 38. Figure 3- 28 and Figure 3- 29 illustrate the RTPL Spectra of ZnO films deposited on Glass and Si substrates with different seed layer respectively. Only Glass substrates coated with Annealed gold (at 500 °C) showed a peak value at 383 nm, followed by the Glass substrate coated with Zn with a UV emission at 382.16nm. And it was noticed that all samples showed another peak value between 410 nm - 472 nm in the range of the blue visible emission. Low defect is reflected in Sample S1 and S3, having an intensity ratio UV to visible > 1. Samples S5 and S6, showed a peak value at 382 nm and it was noticed that all samples showed another peak value at 470.6 nm. It is noticed that the intensity ratio UV/Defect in substrate is higher than the other substrates which reflects less defect. (Table 3- 12)

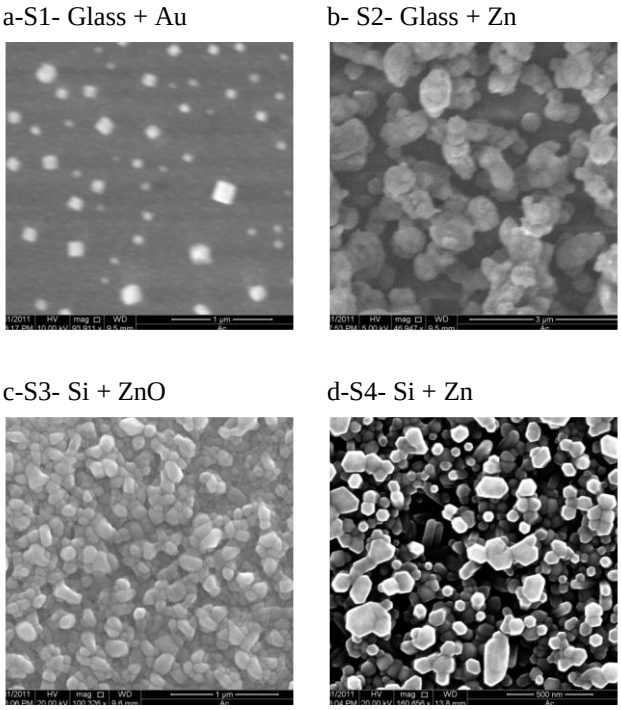

Figure 3- 27- SEM images of ZnO Nanostructures deposited in wet oxygen environment at 750 °C on different substrates and Seed layer.

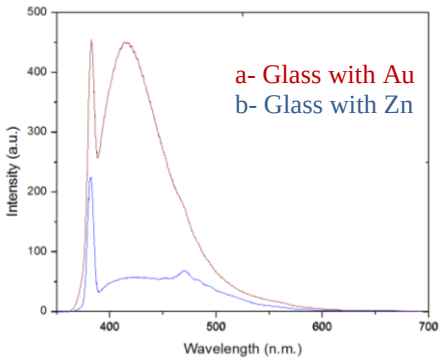

Figure 3- 28: The PL Spectrum of ZnO deposited on different Glass substrates seeded with (a) Annealed Au , (b) Zn

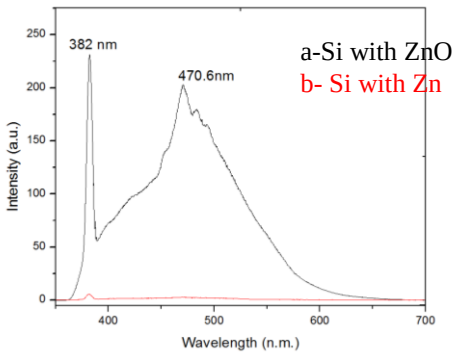

Figure 3- 29: The PL Spectrum of ZnO deposited on different Si substrates seeded with (a) ZnO, (b) Zn

Table 3- 12- intensity ratio UV/Defect on Glass substrate with different seeding layer

	S1- Glass + Au	S2- Glass +Zn	S3- Si + ZnO	S4- Si+Zn
Peak	@383nm	@382.16nm	@382nm	@382 nm
UV / Visible	1.01	3.264	1.15	2.93

Discussion :

ZnO NWs were successfully grown on Si substrate with Zn SL at 750 °C. The environment rich of oxygen (Gas flowed in the chamber and the oxygen generated from the water vapor inside the chamber). On the other hand Glass substrate with Zinc SL didn't reveal any NWs structure; it might be caused from the heat transfer problem in Glass substrates.

3-5-1-2 Growth of ZnO NWs in Wet Argon Environment at 750 °C

The oxygen gas was replaced with Argon and the temperature was maintained the same. Parameters presented in Table 3- 13.

Table 3- 13- conditions for the growth of ZnO NWs

Parameter	NW Growth
Substrate	Si (100), Glass
Nucleation mater	Au , Zn , ZnO
Source Precursor	Zn
Gas flow	Ar
Growth temperature	400-750 °C
Growth Time	1h 30 minutes
Growth Pressure	atmospheric

ZnO nanoparticles were aggregated on the surface of the Glass and Si substrates coated with Zn seed layer Figure 3- 30 b,d. The films are relatively porous. Figure 3-30 b shows a film composed of a hexahedron like particles of 380 nm , which is considered as a stack of many flat facets.

Figure3- 30-c shows fine particles aggregated to form clusters of 140-26 nm shaped in short chains. Figure3-30 a, shows the start of ZnO NWs more oriented that needs to be grown for a longer period of time, Au nanoparticles are shown on the top of the NWs. Agglomeration of ZnO Nanoparticles characterization of melting is identified in Figure 3- 30 c. On the other hand, ZnO nanoparticles are distributed on top of the surface of the substrate of 44-76 nm diameters (Figure 3- 30e). Optical properties were reflected in Figure 3- 31 and 32 that illustrate the RTPL Spectra of ZnO films deposited on Glass and Si substrates with different seeding materials.

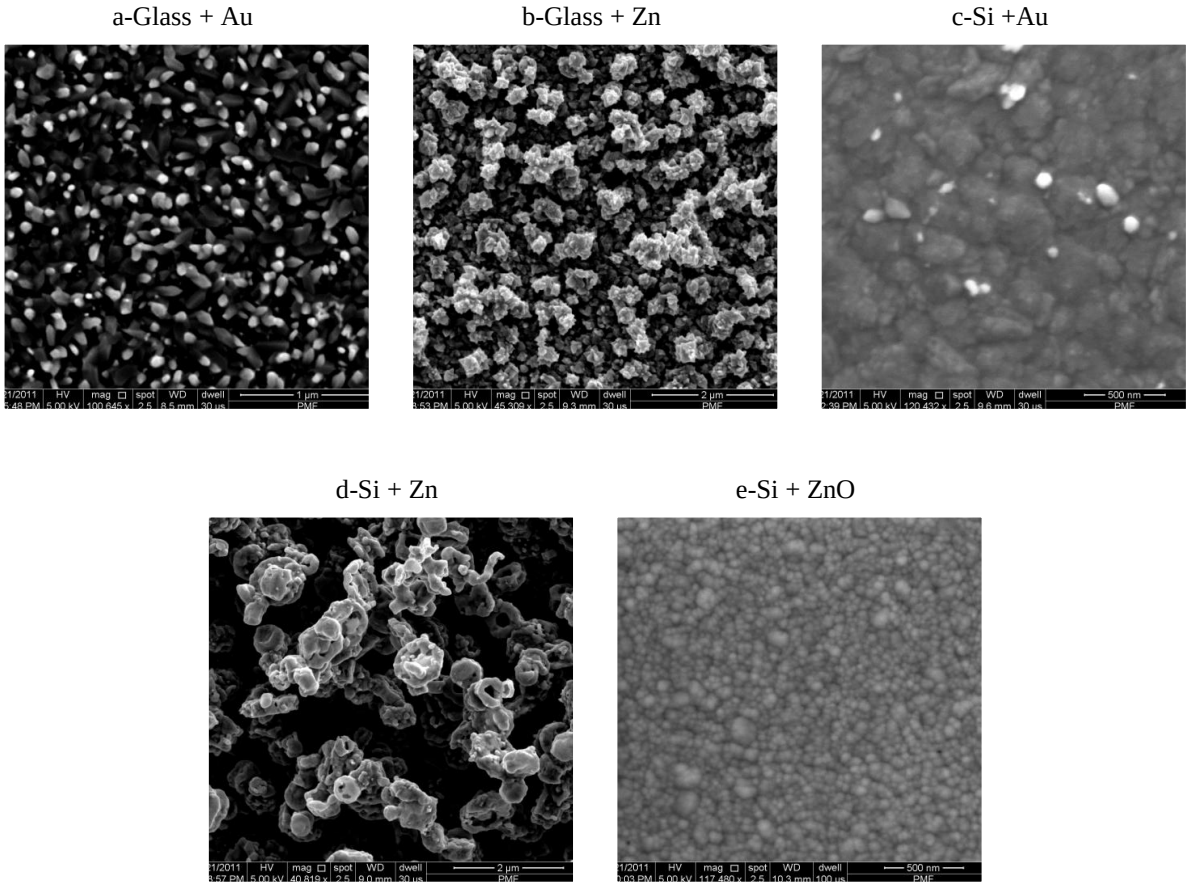

Figure 3- 30- SEM images of ZnO Nanostructures deposited in Wet Argon Environment at 750 °C on different substrates and seed layer.

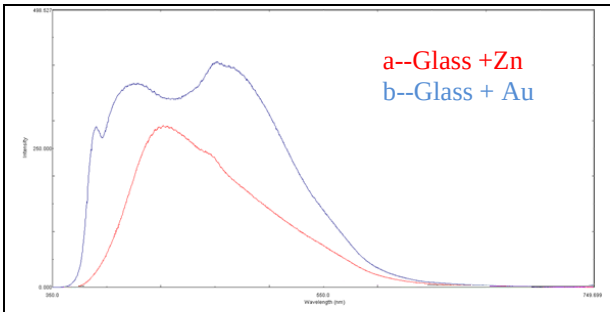

Figure 3- 31 The PL Spectrum of ZnO deposited on different Glass substrates seeded with (a) Zn, (b) Au.

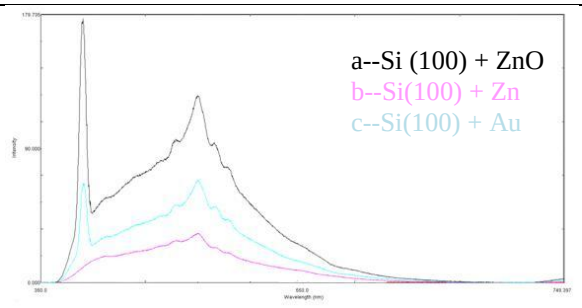

Figure 3- 32: The PL Spectrum of ZnO deposited on different Glass substrates seeded with (a) ZnO, (b) Zn, (d) Au

Glass substrates coated with Au for 50s depositions and Annealed at 500 °C showed a peak value at 382.4nm and it was noticed that all samples showed another peak value between 400nm - 500 nm. Si substrates coated with Au (25s) and with ZnO showed a peak value at 382.4nm and it was noticed that all samples showed another peak value at 470.4 nm. Fewer defects were identified from the Si substrate with ZnO as seed

layer. The intensity ratio UV/visible is presented in Table 3- 13. By comapring the different types subtrates (Si and Glass) coated with the same seed layer (ZnO , Zn and Au) it is been observed that on Si substrate the Peak value at 382 nm was clearly shown , with higher intensity.

Table 3- 14- intensity ratio UV/Defect

Substrates	Si (100) +ZnO	Si (100) + Zn	Si (100) + Au
UV/visible ratio	1.416	0.9729	0.325

Discussion:

Short ZnO Whiskers were grown by VLS on Glass+ Au substrates. On the other hand ZnO particles aggregate in clusters to form chains on Si substrates with Zn SL.

3-5-1-3 Growth of ZnO NWs in Wet Nitrogen Environment at 950 °C

The gas was again replaced with Nitrogen at higher temperature of 950 °C. Parameters summarized in Table 3- 15.

Table 3- 15- conditions for the growth of ZnO NWs

Parameter	NW Growth
Substrate	Si (100), Glass
Nucleation mater	Au , Zn , ZnO
Source Precursor	Zn
Gas flow	N_2
Growth temperature	400- 950 °C (100 °C in 30 minutes)
Growth Time	2h 30 minutes
Growth Pressure	atmospheric

Figure 3- 33 illustrates the morphology of ZnO Nanostructures synthesized over glass and Si substrates with different seed layer. Fig 33-a shows short ZnO NWs of 85 nm diameters and 150 nm lengths, while longer NWs were clearly seen in Figure 3- 33-b for the Si substrate with Zn Seed layer. NWs randomly oriented with length of 5 um, and diameter ranging from 70 nm to 150 nm. Aggregating ZnO Nanoparticles on Glass substrate with Zn SL, were shown in Figure 3- 33-c. The Si substrate with ZnO Seed layer exhibits a platelets shape of 80-200 nm size (Figure 3- 33 d). On the other hand, ZnO Nanoparticles were distributed on the surface of the Glass substrates coated with Au catalyst. Figure 3- 34 and Figure 3- 35 reveals the RT PL Spectra of

ZnO Nanostructures deposited in wet Nitrogen Environment at 950 °C on glass and Si substrates with different seed layers.

a- S1: Si + Au

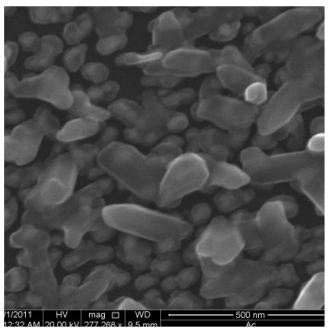

b- S2: Si + Zn

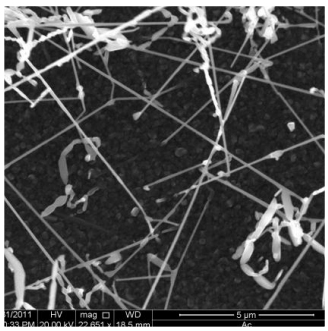

c-S3: Glass + Zn

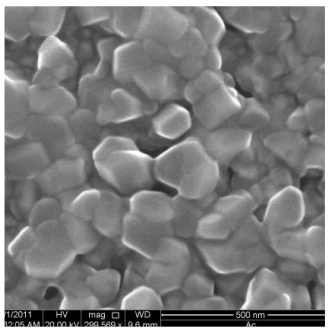

d-S4: Si ZnO

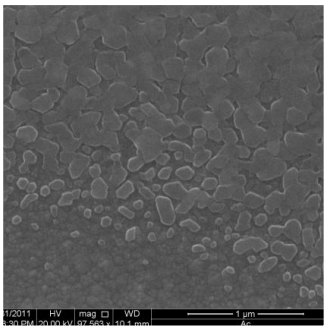

e-S5: Glass Au

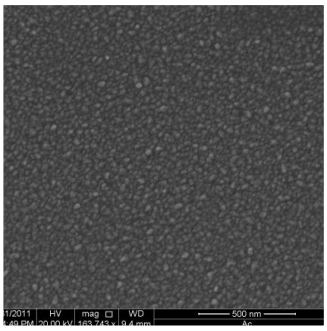

Figure 3- 33- SEM images of ZnO Nanostructures deposited in Wet Nitrogen Environment at 950 °C on different substrates and seed layer

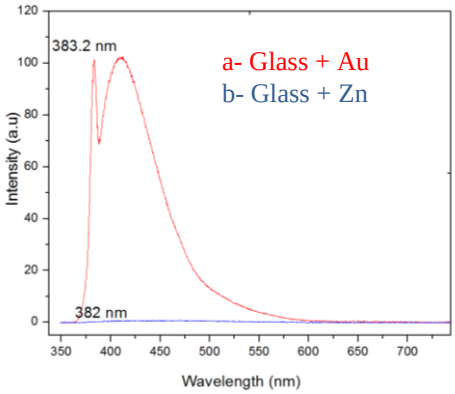

Figure 3- 34: The PL Spectrum of ZnO deposited on different Glass substrates seeded with (a) Au , (b) Zn

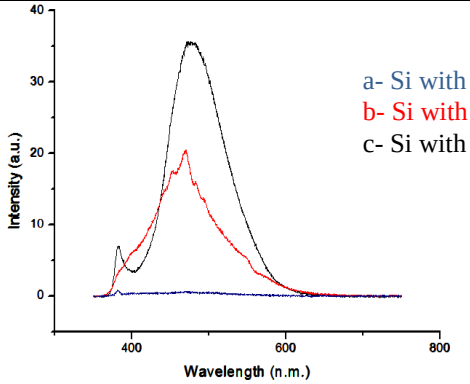

Figure 3- 35: The PL Spectrum of ZnO deposited on different Si substrates seeded with (a) ZnO, (b)Au, (c) Zn

Glass substrates with Zn and ZnO seed layer showed a UV emission at 382nm while glass coated with Au catalyst presents a UV emission at 383 nm respectively with a blue emission between 410nm - 500 nm. . (Table 3- 16)

Table 3- 16- intensity ratio UV/Defect on Glass substrate with different seeding layer

	Glass + Au	Glass + Zn
Ratio UV/ visible	0.9888	0.38

Only Si substrates coated with ZnO showed a peak value at 382.3nm and it was noticed that all samples showed another peak value at 471 nm. Fewer defects are observed in ZnO Nanostructures grown on Si substrates with ZnO Seed layer. The intensity ratio is presented in Table 3- 17.

Table 3- 17- intensity ratio UV/Defect on Si substrate with different seeding layer

Substrates	Si (100) +ZnO	Si (100) + Au	Si (100) +Zn
ratio UV/Visible	1.26	0.157	0.197

Discussion:

ZnO NWs randomly oriented were grown on Si substrates with Zn SL, at very high temperature (950 °C) which is higher than the boiling point of the Zn (907 °C). While the ZnO over-layer on Si substrates agglomerated in platelets might be caused by the melting characteristic of the ZnO.

3-5-1-4 Growth of ZnO NWs in Wet Oxygen Environment at different temperatures.

Different nanostructures were synthesized at different temperatures and different carrier gas. The Objective of this study is to identify the effect of temperature on the ZnO NWs grown in Wet oxygen environment. The growth conditions of ZnO NWs are presented in Table 3- 18.

Table 3- 18- Conditions for the Growth of ZnO NWs

Parameter	NW Growth
Substrate	Si (100)
Nucleation mater	Zn
Source precursor	Zn
Gas flow	Oxygen
Growth temperature	650 °C, 750 °C, 850°C
Heating rate	3°C /min
Growth Pressure	atmospheric

NWs / nanorods were grown on Si (100) substrate at different temperatures 650°C, 750°C and 850°C. Figure 3- 36 illustrates the side view of the ZnO Nanowhishkers grown at 650°C. The NWs grown have an average length of 363 nm and a diameter

of 20 nm and are randomly oriented. It is clear from the top view that the deposited nanostructure reveals high porosity.

a-Top view b- Cross section

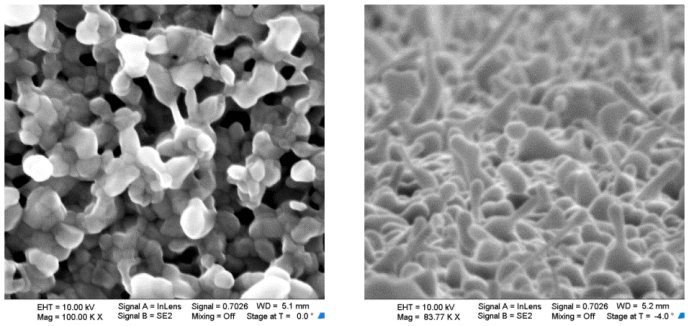

Figure 3- 36- SEM of ZnO Nanorods Grown at 650 ° C

a- Top View b-Cross section

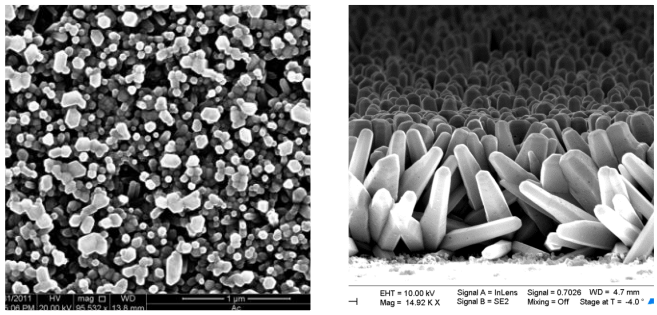

c- Top view d- Tilted view

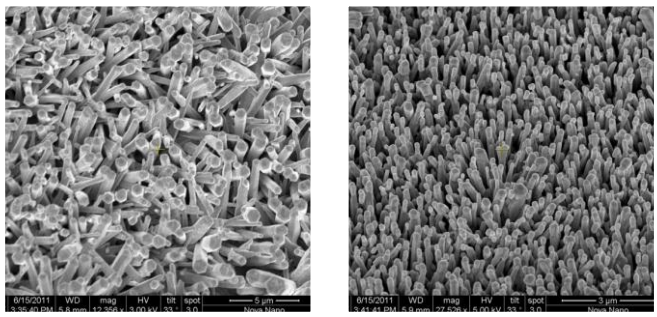

Figure 3- 37- SEM of ZnO Nanorods Grown at 750 °C

Figure 3- 37 a,c illustrate the top view while 37b , d show the side and the tilted view of ZnO nanorods grown at 750°C. A grass form was shown and the average length of nanorods 1.5 μm and diameter ranges from 50 nm to 130 nm. While Figure 3- 38 illustrates the top and side view of ZnO NWs grown at 850°C, a feather like

morphology is shown; NWs were grown randomly on the surface with a length of 1 μm and a diameter of ~ 50 nm.

a- Top view b- Corss section

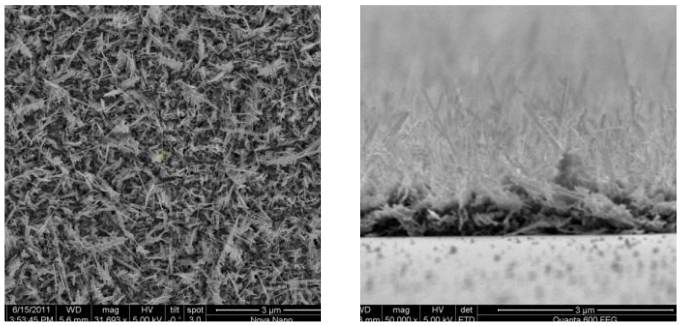

Figure 3- 38- SEM of ZnO NWs Grown with Wet oxidation at 850 °C

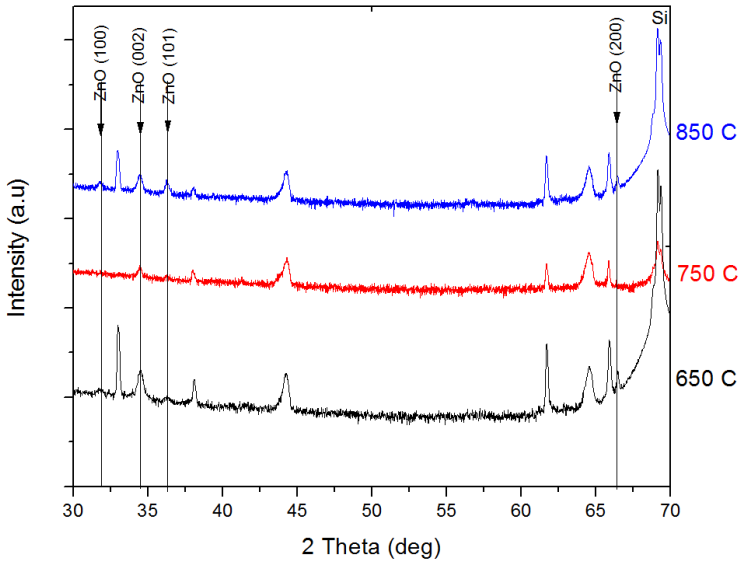

Figure 3- 39- XRD Spectrum of as-synthesized ZnO NWs at a) 650°C, b) 750°C and c) 850 °C

XRD pattern Figure 3- 39 of ZnO nanorods grown at 650°C, 750°C and 850°C reflects that the nanostructures are polycrystalline, with a high intensity at the plane (002) and other planes like (100), (002), (101), (102), (110), (103),(200) and (112) based on Table 3- 19 . The average crystal size was calculated with the Scherrer formula (1) and it was found that it ranges from 9 nm to 24 nm.

$D = \frac{0.9\lambda}{\beta \cos\theta}$ (1) Where λ= 0.154060 nm, β is the full width at half maximum (FWHM) in rad, and θ is the diffraction angle.

Table 3- 19- 2 theta Shown on the XRD Spectra at a) 650°C, b) 750 °C and c) 850 °C

2 θ at 650°C	**31.6°**	**34.5°**	**36.33°**	**66.42°**
2 θ at 750°C	31.76°	34.44°	36.25°	x
2 θ at 850°C	31.8°	34.45°	36.275°	66.35°
Plane	(100)	(002)	(101)	(200)

Optical properties were identified by RT –PL measurements (Figure 3- 40). PL spectra of ZnO may consist of the peaks of UV (~ 382 nm), Blue (~471nm), and green (~ 510 nm) , where in our work strong emissions of UV and blue could be realized at room temperature through processing control. It has been noticed based on Table 3- 17 that the UV emission peak value was at 382 nm, 382 nm and 384 nm for the ZnO nanorods grown at 650°C, 750°C and 850°C respectively while the highest intensity ratio was noticed to be for the one grown at 750°C. It is observed that the variation of growth temperature has affected the PL spectra of the ZnO nanorods, showing an enhancement in the relative intensity ratio of UV emission to blue with the increase of temperature, but was not reflected at 850°C. The ZnO NWs synthesized by wet oxidation did not give any obvious visible light emission in the range of 510- 700 nm which is related to the deeper level defects such as oxygen vacancies and Zn interstitials[55]. The Absence of visible light emission is caused by the use of water vapor that was reported in [56]reporting that the water-assisted oxidation improves the crystalline of the oxide product.

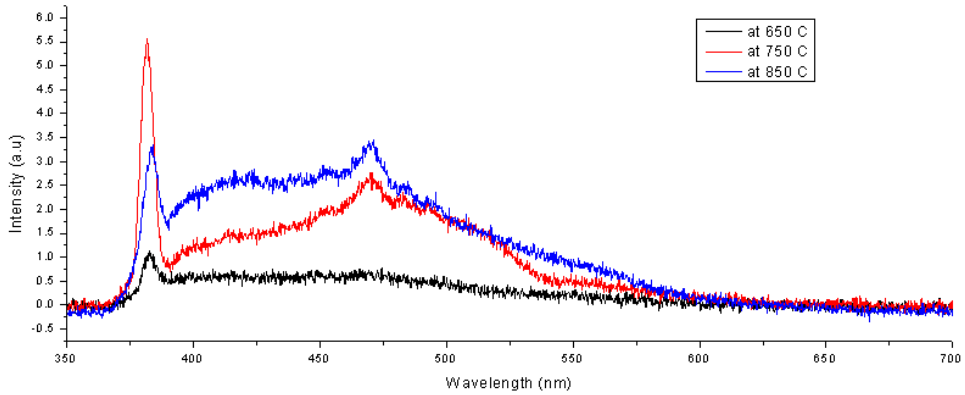

Figure 3- 40- PL spectra of ZnO nanorods at different temperatures 650°C, 750°C, and 850°C

Table 3- 20- UV/Visible intensity ratio at 650° C, 750 °C and 850° C

	At 650 °C @ 382 nm	**At 750 °C @ 382 nm**	**At 850 °C @ 384 nm**
UV/ Visible (@ 471 nm	2.176	2.22	0.955

Discussion:

ZnO NWs were successfully grown on Si substrate coated with Zn SL at different temperatures 650 °C, 750 °C and 850 °C. The optimized results were obtained at 750°C. The startup and nucleation of the ZnO NWs randomly oriented was observed for a growth at 650°C. On the other, at 850°C, ZnO feather like shape were obtained . The Thickness of the seed layer must be properly adjusted in order to achieve better results. Zn/O_2 concentration in vapor phase and liquid Zn condensed on substrate favor the NW growth. The Liquid Zn condensed on the zone where the Temperature is close to the melting point of Zn. Well shaped ZnO NWs were found close to the metallic Zn source. But it is irreproducible since it was linked to the condensation of Zn droplets that cannot be controlled.

3-5-1-5 Conclusion for wet oxidation process:

Parametric studies were applied in this research using the wet oxidation process using Zn as source material. The parameters that have been varied are the Temperature, the inert gas and the Seed layer material or the catalyst used. It is noticed that ZnO NWs were grown successfully on Si substrate coated with Zn thin film as seed layer. Summary of results presented in Table 3- 21.

Table 3- 21- Survey of ZnO Nanostructures obtained in different environments.

Gas	Temp	Substrate	Nanostructures
Oxygen	650 °C	Si + Zn	Whiskers (~100 nm length)
Oxygen	750 °C	Si+Zn	Vertically oriented ZnO NWs of 1.3 µm
		Glass + Zn	Aggregation of ZnO particles
		Si + ZnO	ZnO Nanoparticles
		Glass + Au	Cubical Au particles
Oxygen	850 °C	Si+ Zn	Very long ZnO NWs Feather like morphology
Argon	750 °C	Si + Zn	Aggregation of ZnO Particles in form of clusters shaped in short chains
		Glass + Zn	Aggregation of ZnO Particles in form of clusters shaped in short chains
		Si + Au	Agglomeration ZnO nanoparticles – melted
		Glass + Au	ZnO NWs with Au drops on the top
		Si + ZnO	ZnO Nanoparticles
Nitrogen	950 °C	Si + Zn	ZnO Nws of 4 µm
		Glass + Zn	ZnO Nanopillars
		Si + ZnO	ZnO Platelets
		Si + Au	ZnO Nws randomly oriented of 100 nm
		Glass + Au	ZnO nanoparticles

In wet oxidation process, the faster absorption and easier breakup of water vapor can accelerate the kinetics of oxidation, which enables some of the Zn surface structure to transform to nucleation sites for ZnO NWs/ nanorods. If the heating temperature is low the energy for Zn vapor is not sufficient, and the atoms are deposited exactly where they land creating a roughness uneven film with nuclei clusters, the nuclei clusters will lead to several ZnO NWs assembly in a growth process. At higher temperature (medial temperature) the growth process of the number of nuclei assembled in each nuclei cluster is fewer; the closing nuclei devoured each other to become a larger grain in the initial growth stage. The NWs growing from large diameter NWs will lead to larger diameters. After nucleation sites were formed on the surface, the Zn atoms surface diffused and reacted with absorbed water vapor will dominating the growth of ZnO NWs. The growth process will stop when the NW becomes too long for the Zn atoms to diffuse to the tips or the process was stopped at a specific temperature. Using Temperature between 650°C and 950°C which is considered as higher than the melting point of Zn (420°C) which suggests that Zn Liquid phase is involved in the NWs nucleation(lower temperature do not lead to NWs formation). We expect that oxidation has taken place in a rich Zn atmosphere. VS mechanism takes place in which the liquid phase is involved only in the nucleation and vapor feeds the growth[57]. Inner Zn metal partially melts and vaporizes forming a Zn atmosphere in addition to the one evaporated from the source. However Zn can be oxidized before the evaporation process, which may result in different morphology of ZnO formed at different temperatures. VS and VLS mechanism takes place with the substrates with Zn and Au respectively (Figure 3-41), already explained in chapter 2. It should be highlighted that the working parameters cannot be used and applied on a different setup , where the length , diameter of the tube furnace influence the selection of the placement of the substrate , the temperature used and the growth time. We need to create the most suitable local conditions for NW growth, high Zn vapor pressure and large Zn/O_2 ratio at the applied temperature. The thickness of the Zn overlayer is very critical if it is too thin; zinc evaporation prevents the growth or gives low density and in-homogenous deposition of NWs. While it is very thick an undesired layer remains on the substrate after the growth. A thicker Zn SL is needed to feed the ZnO NW growth to compensate the Zn Losses due to evaporation effects.

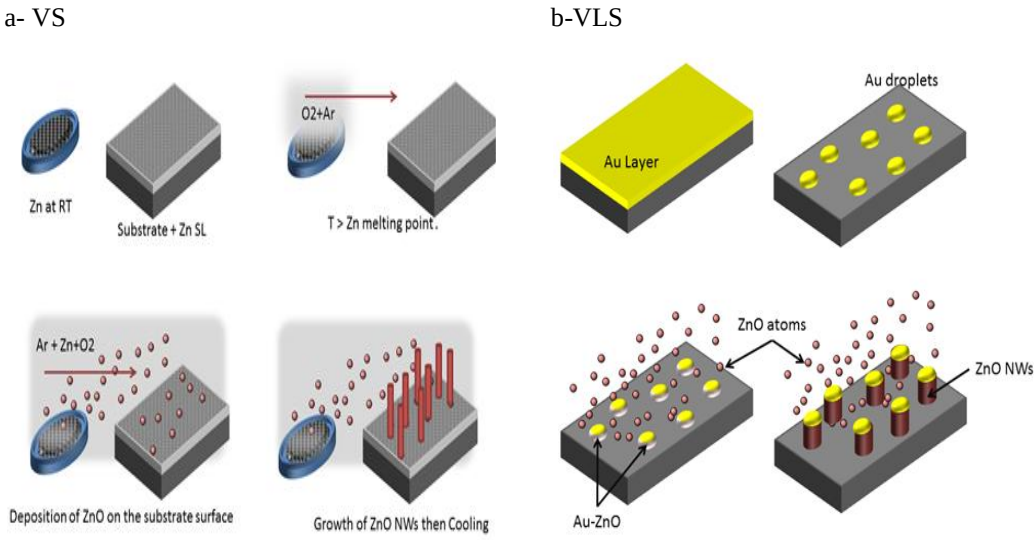

Figure 3- 41- Schematic Illustration of VS and VLS process

3-5-2 Growth of ZnO Polypod by thermal Evaporation

It was expected that by placing the substrates on top of the source, ZnO NWs will be grown. Metallic Zn (99.99% purity) was evaporated in standard vacuum equipment onto unheated Glass and Si (100) substrates. The experimental setup presented in chapter 2 , where Zn powder was placed in a Molybdenum boat , the distance between the Zn powder and the substrate was short around 5 -7 cm. Zn Powder was heated manually until 400 °C with a heat rate of 10°C /minute. 50 sccm oxygen gas was flowed in the vacuumed chamber while deposition. Then the Temperature was increased gradually to 1000 °C, plasma has been seen inside the chamber. The oxidation of the evaporated Zn was oxidized for 15 minutes. While taking the samples out of the chamber, a white powder on the surface of the substrates (Figure 3- 42) was clearly observed.

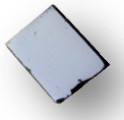

Figure 3- 42- Si Substrate after ZnO polypod Deposition , white powder on the surface of the silicon substrate

Figure 3- 43 illustrates the morphology of ZnO polypod nanostrucutres grown on Glass and Si substrates. These ZnO Nanostructures were grown uniformly with a length of hundreds of nanometers. The tetrapod-like ZnO nanostructures consist of

four needles shaped tetrahedrally arranged legs connected at the center junction which can be regarded as a central nucleus, forming a tetrapod-like structure. The legs of the tetrapod-like ZnO nanostructures are up to several hundred nm in length, and each leg is tapered off from the center to its end. The root diameters of the tetrapod-like ZnO nanostructures are in the range of 30- 70 nm, while the tips have an average diameter of about 16 nm. All samples show typical luminescence behavior with 2 emissions of a narrow UV at 384.85 nm (50 sccm), 381.5 nm (at 75 and 100 sccm) and a broad blue-green band at 469.16 nm. In Figure 3- 43b, the intensity ratio between the UV emission and the visible emission of the film is presented in Table 3- 22. Highlighting fewer defect at 50 sccm Oxygen flow.

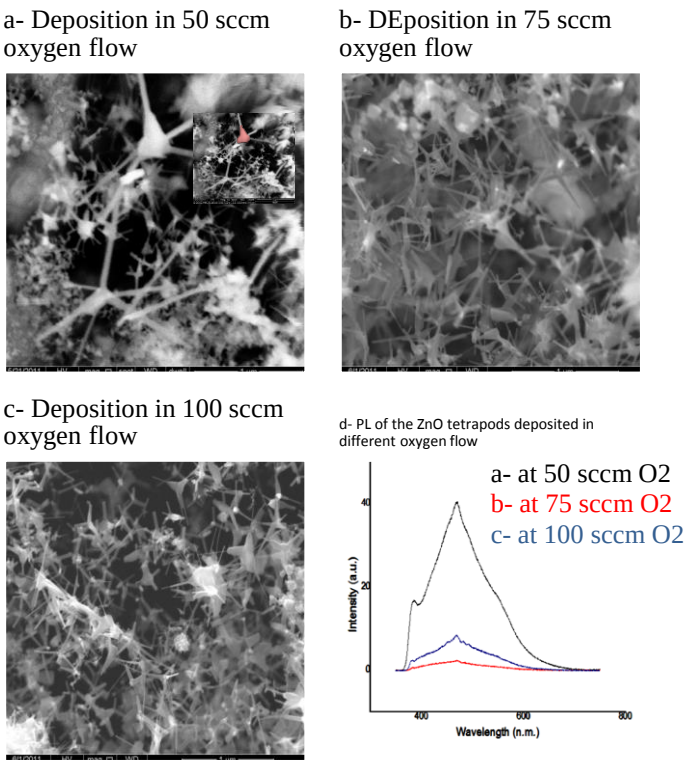

Figure 3- 43- ZnO oxidized over Glass substrate in Vacuum, at 1000 °C , with Oxygen flow of a)50 sccm b) 75 sccm c) 100 sccm d) Room Temperature PL Spectrum on glass Substrates synthesis with oxygen flow rate of (a) 50 sccm (b) 75sccm (c) 100 sccm

Table 3- 22- Intensity ratio UV emission/ visible emission on Glass substrate

Substrate	50 sccm	75 sccm	100 sccm
ratio UV/visible	0.415	0.261	0.28

Conclusion for Thermal evaporation:

Among the various morphologies of ZnO nanostructures, tetrapod and multipod nanostructures have attracted extensive attentions [58][59]. The tetrapod-like and multipod-like nanostructures of ZnO have unique applications in both functional and structural materials due to their semi-conductivity, single-crystalline character, and excellent mechanical properties [60]. The evaporation of Zn is violent breakout process at high temperature 900°C (boiling point of Zn is 907 °C). Due to the oxygen circulation in the chamber, ZnO and suboxides ZnO_x ($x<1$ in case of low flow of oxygen) are transported and deposited on the substrates which are at low temperature. ZnO vapors condense on the surface of the substrates. ZnO are octahedral nuclei which lead to the formation of the tetrapod like ZnO nanostructures. Mechanism explained below , Zn powder evaporates (Zn(s)→ Zn(g)) , the Zn vapor oxidize in presence of oxygen $Zn(g) + O_2(g) \rightarrow ZnO(g)$ / $Zn(g) + O_2(g) \rightarrow ZnO_x(g)$. Zn (g) and ZnO (g) condense on the surface of the substrates.

Zn (g)→ Zn (l) and ZnO(g)→ ZnO(l).

$Zn(l) + O_2(g) \rightarrow ZnO(s)$ / $ZnO_x(l) + O_2(g) \rightarrow ZnO(s)$

The octahedral nuclei [61][62]has the lowest surface energy, where the needles like ZnO form and grow along the [0001].Flower like ZnO nanostructures are observed due to the high temperature and high super-saturation during crystal growth process.

3-5-3 ZnO Nws by Pulsed Laser Deposition

Very high quality, vertically oriented ZnO NWs were successfully grown on ZnO Seed layer by Pulsed Laser Deposition. ZnO Seed layer deposited by PLD was used in this experiment. It was noticed that by increasing the oxygen pressure in the chamber to 500 mTorr, Nanopillars with hundreds of nm diameter (nanopost with Pencil shape morphology) were obtained. On the other hand the distance between target and substrate was almost 9 cm, which is long distance for ablated species to reach Figure 3- 44. Thus we suggested increasing the pressure (> 500 mTorr) to decrease the diameter of the nanopillars and decreasing the distance between the target and the substrate.

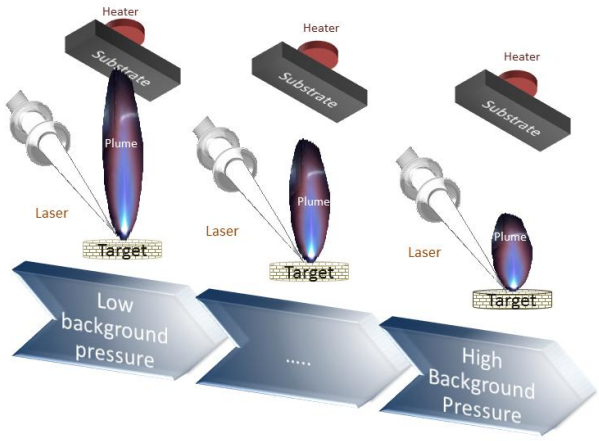

Figure 3- 44- Plume Size decrease with the increase of background pressure

An extension of 1 cm diameter, and 2.5 cm length was attached to the substrate holder. The distance between target and substrate was shortened to 6.5 cm, considered as the limit; otherwise it will affect the path of the laser. The short distance between target and substrate was also reported in the literature summarized in Table 3- 23. Substrate temperature was measured in air in order to identify the relationship between the set temperature and the substrate temperature Figure 3- 45.

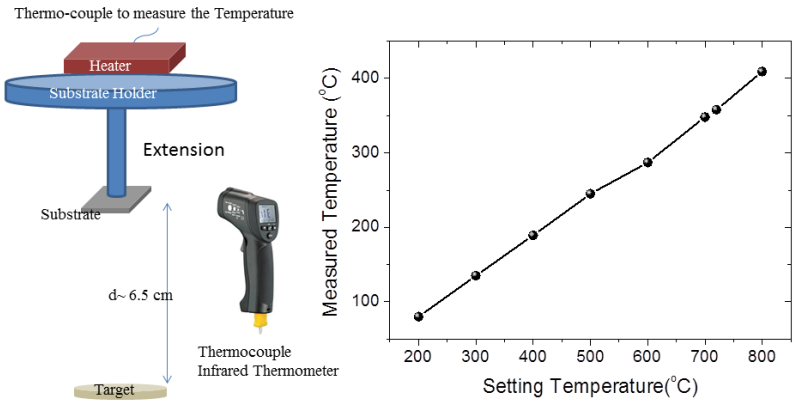

Figure 3- 45 –Illustration of the substrate Temp in fucntion of the Heater substrate

Parametric study was applied in this experiment by varying some parameters such as Substrate type, gas pressure, growth time and energy.

Table 3- 23- Survey of ZnO nanostructures prepared by PLD

Material	Substrate	Temp (°C)	Pressure (Torr)	Distance* (cm)	Structure	Diameter (nm)	Length (µm)	Ref
ZnO	Sapphire (0001)	600-700	1-5	2	Nanorods	300	6	[63]
ZnO	Si(100)	450-500	5	2.5	Nanorods	120-200	12	[64]
ZnO	SiO2/Si/Au	900	400	-	NW	20	10	[65]
ZnO	Sapphire (0001)	600	5	2	Nanorods	300	6	[66]
ZnO	Si(100)	600-850	4.8-6.3	2.5	NW	20-50	0.5-2	[67]
ZnO	a-sapphire c-sapphire	1000	260	1.5	NW	200	0.5- 3	[68]
ZnO	c-Sapphire ZnO SL	500-800	150-500x10^{-3}	2.5	NW	50-90	Few µm	[69]
ZnO	Sapphire (0001)	-	260	1.2-2.5	Nanorods	130-200	1.5-4	[70]
ZnO	c-sapphire	600	100-200x10^{-3}	5	Nanorod	150-200	0.9	[71]
ZnO:Al	Sapphire	650	10-2	5	Nanorod	-	-	[72]
ZnO:Mg	a-sapphire c-sapphire +Au	870- 950	18-150	0.5-3.5	NW	150	1.5-20	[73]

*Distance present the distance between target and substrate

3-5-3-1 Effect of Substrate on the growth of ZnO Nws.

ZnO NWs were synthesized by PLD on Si (100) and Sapphire (0001) substrates. Parameters are summarized in Table 3- 24. The objective of this study is to check the lattice matching effect on the ZnO Nws synthesis.

Table 3- 24- Parameters used for the growth of ZnO NWs on different substrates

Temperature	< 500° C
Gas Pressure	5 Torr
Deposition time	30 minutes
Dtarget –sub	6.5 cm

Figure 3- 46a, b reveals the morphology of ZnO NWs deposited on different substrates. In Figure 3- 46 a,b the NWs are randomly oriented because of lattice mismatching. On the other hand Figure 3- 46 c and d confirm the vertically oriented ZnO NWs grown on ZnO Seed layer deposited on Si and Glass + ITO substrates respectively.

a- ZnO NWs grown on Si Substrate

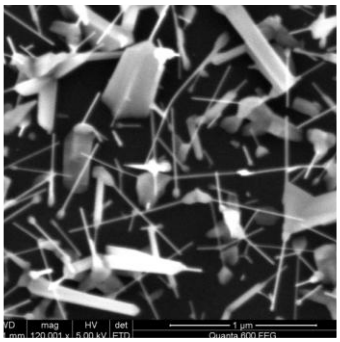

b-ZnO NWs grown on Sapphire substrate

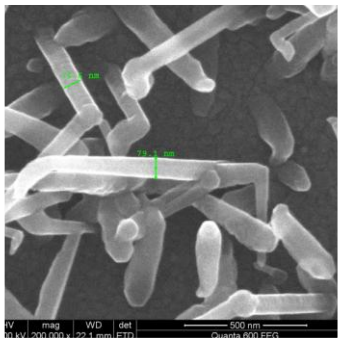

c- ZnO NWs deposited on Si substrate + ZnO SL

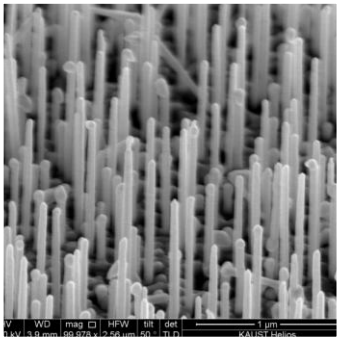

d-ZnO NWs deposited on Glass+ITO+ZnO SL

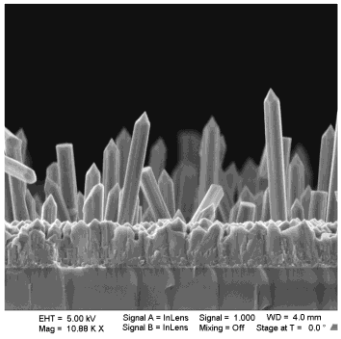

Figure 3- 46- SEM Images of ZnO NWs gorwn on different substrates /Seed layer

ZnO NWaN with honeycomb structure was formed at 10 mTorr background pressure. By increasing the Pressure in the chamber ZnO nanopillars were formed. Thus we suggested by increasing the gas pressure, the nanopilars will decrease of their diameter. The deposition was carried in Argon environment of 5 Torr Pressure. ZnO NWs randomly oriented were grown on the surface of the Si (100) substrate (Figure 3- 46a). Thus to test substrate that have better lattice matching, Si substrate was replaced with Sapphire (0001). As the temperature was lower than 500°C, randomly oriented ZnO NWs were observed Figure 3- 46b.

In this experiment, the seed layer (SL) is the ZnO NWaN with honeycomb structure grown by PLD. Figure 3- 46 c,d show the vertically oriented ZnO NWs grown on Si substrates with ZnO SL , and Glass + ITO substrates with ZnO SL .

The ZnO Nws were grown perpendicularly to the surface of the substrate in the direction [0002]. The ZnO NWs grown on Glass ITO exhibit a Pencil shape.

a- XRD spectrum

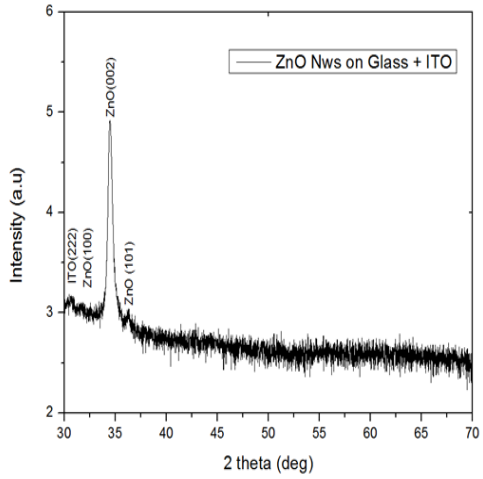

b- PL spectrum

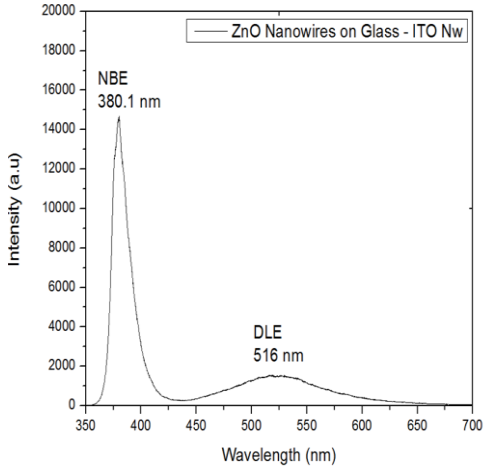

Figure 3- 47- XRD and PL Spectra of ZnO NWs grown on Glass – ITO with ZnO SL deposited by PLD at 5 Torr , Tsub<500 °C , $d_{target-substrate}$ = 6.5 cm.

Figure 3- 47a illustrates the XRD spectrum of the ZnO NWs deposited on Glass + ITO substrates with ZnO SL deposited by PLD. The Figure 3- 47a reveals a very intense peak at 34.4 which correspond to (002) plane. Nevertheless ZnO (100) and ZnO (101) peaks indicate that some fraction of the deposited material is not c-axis oriented, the patterned can be indexed to the ZnO hexagonal wurtzite structure with lattice constants of a= 0.325 nm and c= 0.512 nm. Compared with standard diffraction patterns, no characteristic peaks from impurities (Zn) are detected which indicates

that the ZnO NWs possess a high crystalline quality. The RTPL measurement excited by Laser HeCd laser (325 nm, 8mW) is depicted in Figure 3- 47b. It presents different peak positions of the band edge emission in the UV region at 380.1 nm (2.4 eV) as well as defect induced emissions in the visible green region at 516 nm(2.4 eV).

3-5-3-2 Effect of Pressure on the growth of ZnO NWs

After checking the effect of substrate and SL, ZnO NWs were grown at different Pressure. The objective of this study is to study the influence of pressure on the density and the thickness of the NWs. Parameters summarized in Table 3- 25. ZnO NanoPillars or Nanopost grown at 2.5 Torr has smaller diameter (100-170 nm) than the one grown at 500 mTorr (290-400 nm). By increasing the Pressure to 5 Torr, ZnO NWs vertically oriented are clearly observed in Figure 3- 48b.

Table 3- 25- Parameters of the ZnO Nws synthesis

Pressure (Argon)	2.5 Torr , 5 Torr, 7.5 Torr and 10 Torr
Temperature	< 500 °C
D target-sub	6.5 cm

The NWs are grown perpendicular to the substrate surface. Moreover, they are characterized by hexagonal edge geometry. Since no catalyst was used, it is suggested that the seed layer plays an important role in the nucleation of the NW directional growth.

A typical XRD pattern of the ZnO NW array at 2.5, 5, 7.5 and 10 Torr is shown in Figure 3- 49. Only main diffraction lines from the (002) and (004) planes can be observed having the highest peak shown at 34.58° and 34.47°for the NWs at 5 and 10 Torr, respectively. It is constructive to note that the NWs array has a c-axis orientation. The other diffraction peaks shown in the Figure 3- are due to the substrate holder. The slight shift seen between the 2 peak of the (002) plane direction of the ZnO SL and the ZnO NWs maybe caused by the low oxidation of the ZnO NW due to the background Argon environment.

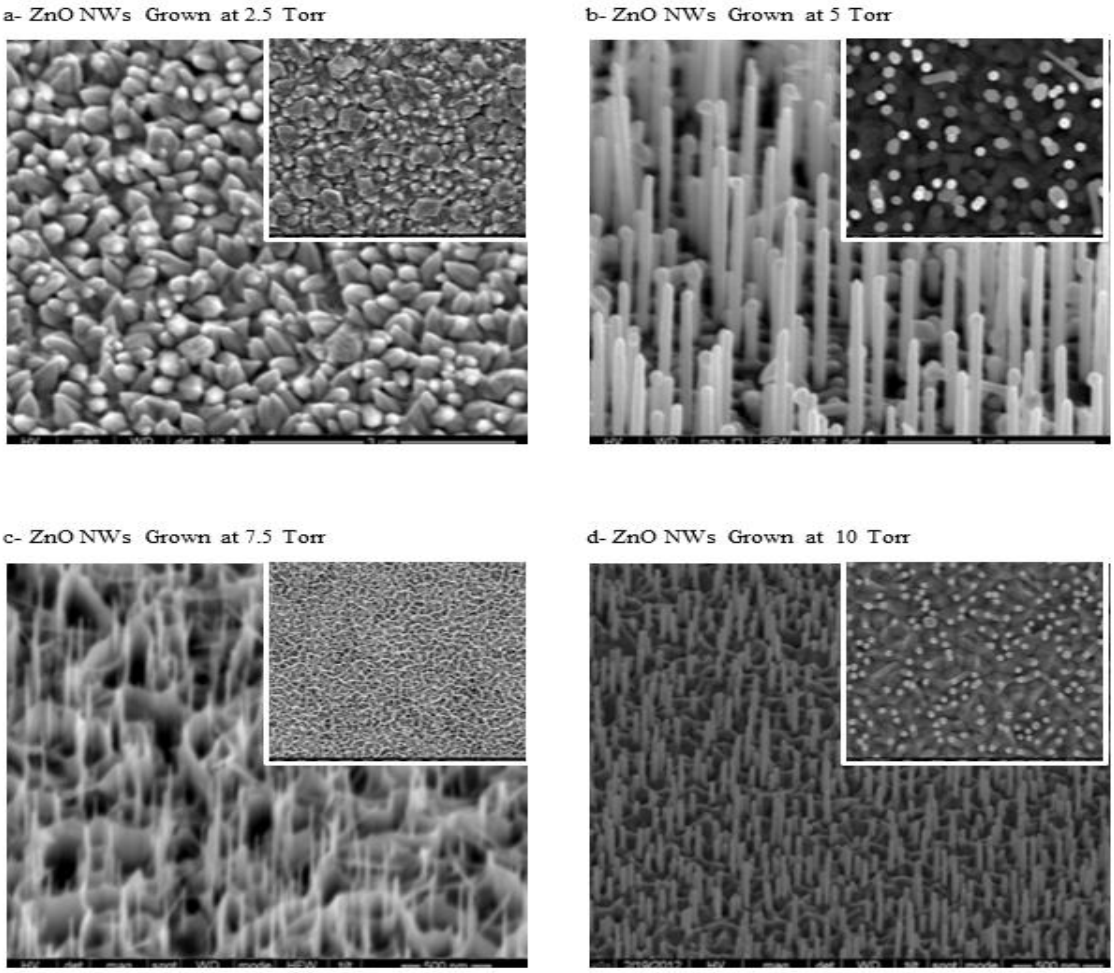

Figure 3- 48- SEM images tilted view (inset – top view) of ZnO NWs grown on ZnO SL, Ts<500°C , Laser Energy 350 mJ at a- 2.5 Torr, b- 5 Torr, c- 7.5 Torr, d- 10 Torr

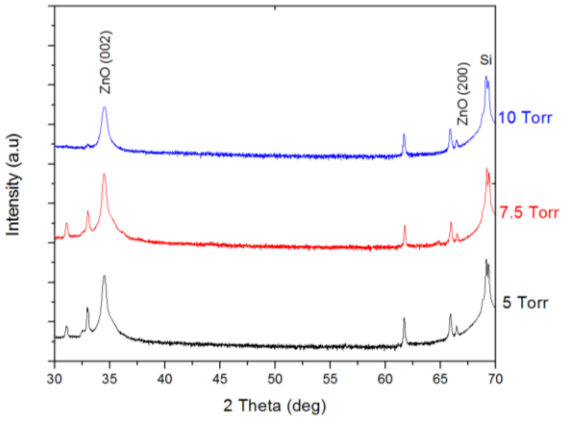

Figure 3- 49- XRD Spectra of ZnO NWs grown at different Argon Pressure

Figure 3- 50 depicts PL measurements of the ZnO Nws grown by PLD at different argon pressure 5, 7.5 and 10 Torr. Different peak positions of the band edge emission in the UV region as well as defect-induced emissions in the visible region

can be seen in the Figure 3-. The NWs at different pressure spectra exhibit normal band-gap emission in the UV region at ca. 379.4 nm (3.268 eV), 378.57 nm (3.275 eV) and 379.2 nm (3.27 eV) of the 3 samples at 5, 7.5 and 10 Torr respectively. The emission in the visible region namely green (541 nm (2.29 eV), 530.2 nm (2.33 eV) and 539 nm (2.3 eV) of the 3 samples respectively) and yellow (585 nm). Defect induced emission in the visible region results from several types of defects in ZnO. [74]

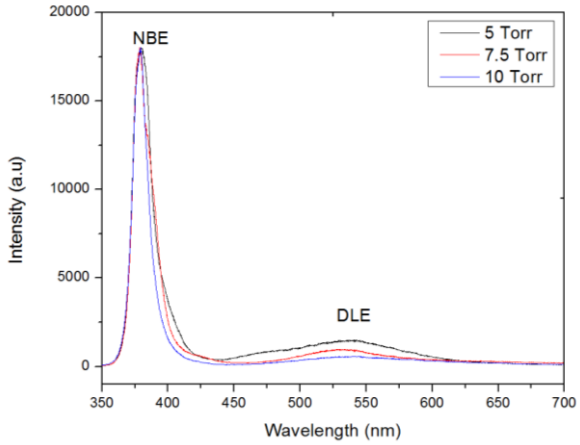

Figure 3- 50- RT – PL Spectra of ZnO NWs **deposited at different Argon pressure**

Table 3- 26 presents the intensity ratio of UV/ visible emission. It shows that the UV to green emission and UV to yellow emission for ZnO NWs are high. By increasing the pressure fewer defects in the NWs, are reflects. Other research [75]and other experiment related to ZnO prepared by PLD, showed different morphologies of ZnO thin film prepared by PLD, caused by the effect of oxygen pressure on plume dynamics.

Table 3- 26- Intensity Ratio UV/Visible of ZnO NWs deposited at different pressure

	UV/Green	UV/yellow
NWs at 5 Torr	11.868	22
NWs at 7.5 Torr	17.88	37
NWs at 10 Torr	30.6	45.4

More detailed structure of the ZnO NWs on ZnO SL was further investigated by TEM. Figure 3- 51 shows a low resolution image, HRTEM image and selected area electron diffraction (SAED) pattern of a single ZnO NW. It is clear that the ZnO NWs are very straight with an extremely uniform diameter of about 54 nm. SAED pattern

and HRTEM strongly suggest that the NWs have single domain Wurtzite structure with high crystal quality. HRTEM image shows the lattice distance about 0.52 nm consistent along the c-axis of Wurtzite ZnO crystal .SAED pattern revealed the exact grow of NWs along the ZnO [0002] Direction, consistent with XRD result (Figure 3- 48). Figure 3- 51b reveals the growth of ZnO NWs that nucleate from the concave tip near the grain boundaries between two ZnO thin grains.

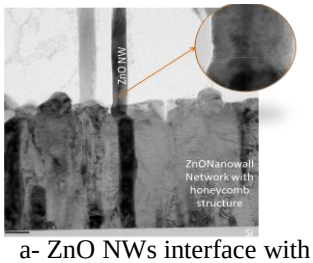

a- ZnO NWs interface with Seed layer

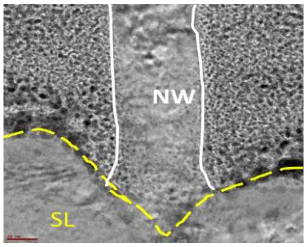

b- Single ZnO NW

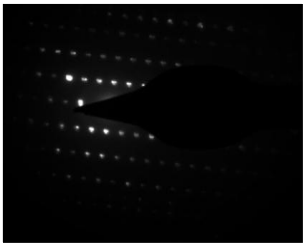

c -FFT

Figure 3- 51- TEM Images of ZnO NWs grown on ZnO Seed Layer by PLD

Figure 3- 52 illustrates the XPS Spectra from the ZnO Nws indicating the presence of the following elements Zn, O, and C. No contaminations were detected on the sample surface. The XPS Spectra of the Zn-2p is presented in Figure 3- 52b and O-1s is presented in Figure 3- 52d. The ZnO NWs display a peak at 1021.4 eV and 1046.1 Ev which are in agreement with the binding energies of Zn $2p_{3/2}$ and Zn $2p_{1/2}$ respectively. The ZnO Nws exhibit an asymmetric peak at 530.1 eV observed in O1-s core level spectrum of Figure 3- 52c. On the other hand no peaks of Si2p can be identified in Figure 3- 52d. The ratio of Zn2p, O1s is around 1.24 which is higher than its corresponding ratio calculated for the ZnO NWaN , which might be caused by the growth of ZnO Nws in Argon Environment (Table 3- 28). The Zn $2p_{3/2}$ spectrum of ZnO suffers from an overlap with the metal peak binding energy. Chemical state determination can be made using the modified Auger Parameter. The modified Auger Parameter (calculated by adding the binding energy of the most intense photoelectron

peak with the kinetic energy of the sharpest Auger peak) is equal to 2010.1 eV, which corresponds to ZnO NWs.[76]

Table 3- 27- Auger Parameters

	Modified Auger Parameter
Zn	2013.8 eV
ZnO	2010.4 eV

a- XPS Spectrum

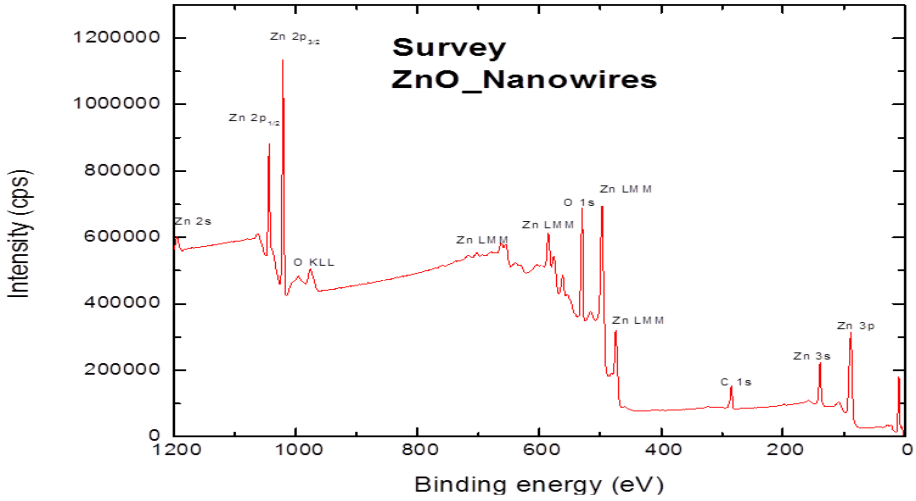

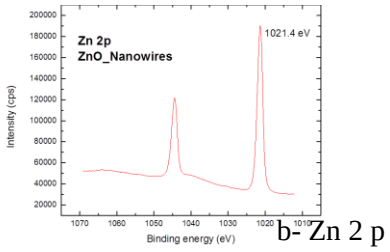

b- Zn 2 p

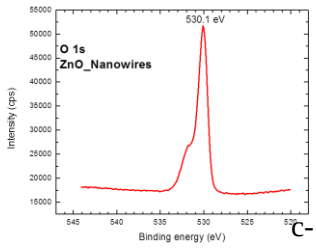

c- O 1s

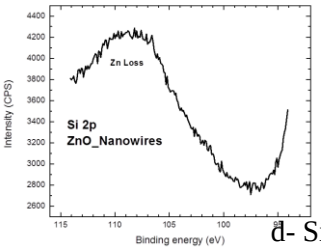

d- Si 2p

Figure 3- 52- XPS Spectra of ZnO NWs grown at P(Ar)= 10 Torr ; Temp < 500 °C by PLD on ZnO Seed layer

Table 3- 28- Atomic concentration of Zn,O, and C Elements

Elements	Zn	O	C	Si
Atomic concentration (%)	44.3	35.1	20.6	0.0

Discussion:

In PLD, the introduction of gas within the deposition chamber causes a decrease in the kinetic energy of the ejected particles due to plasma confinement by surrounding gas. At the so–called stopping distance where the plasma has lost most of its kinetic energy, the particles move into the background gas by diffusion till the substrate. The grown NWs have a high density and are distributed over the entire substrate and perpendicular to the substrate. Thus the crystal structure of the seed layer has a considerable effect on the crystallographic orientation of the ZnO NWs. They exhibit UV band gap luminescence that is due to the wide band gap of ZnO [77] and the tensile strain that turns to be more intensive as the diameter of the ZnO nanostructure increases [78]. Many parameters affected the growth of the ZnO Nws in comparison with the literature such as substrate temperature, gas pressure and the substrate –target spacing. The temperature used in this research was less than 500°C, which is lower than 700°C used in [79] .The temperature effect is related to the surface diffusion; Tien et al [80] have suggested that a high temperature can provide sufficient energy for deposited species and make them migrate to low energy sites for growth. The high temperature provide sufficient energy for deposited species, from the ablation target to migrate to low energy sites for growth at higher energy sites. [81]In order to achieve the one-dimensional growth it is important to provide sufficient surface mobility to reach low energy nucleation sites. The pressure used in this research was 5Torr-10Torr, recommended by [82][83]but lower than [84][85] which were around 200 Torr. It is noticed that the length of the NWs is ~ half around 600nm with a diameter ~ 30 nm. The spacing between the NWs ranges from 46nm to 138 nm, which is larger than the one at 5 Torr that might be caused by the high pressure. When the deposition is processed under high pressure, the ablated particles undergo a large number of collisions with background gas molecules and the condensation of species in the gas phase results in the formation of nanosize particles. The gas pressure influences both the deposition rate and the kinetic energy of ejected particles. The kinetic energy of the ablated particles reduces and the size of the ablated plume decreases when increasing the gas pressure. That's why it is recommended to reduce the distance between the target and substrate while working at higher pressure in order to maintain the optimum energy of the ablated species. The limitation of the PLD equipment used is in the target-substrate distance that will affect the growth of

ZnO NWs. At pressure higher than 1 Torr, the gas phase collisions yield ZnO nanoparticle formation in the ablation plume. It is suggested that the NW growth is affected by the condensation of ablated particles in the laser ablation plume. The distance between the target and substrate was ~ 6.5 cm in comparison with [86][87] where the distance was between 2.5 and 5cm. Due to nanoparticles that determine the growth of NWs, the kinetic energy also has played an important role, as it is in our case low which leads to thinner NWs.

3-5-3-3 Effect of Deposition time on the growth of ZnO NWs (growth rate)

To understand the growth Process of the ZnO Nws by PLD on ZnO SL, deposition duration varied between 5 min to 30 minutes.

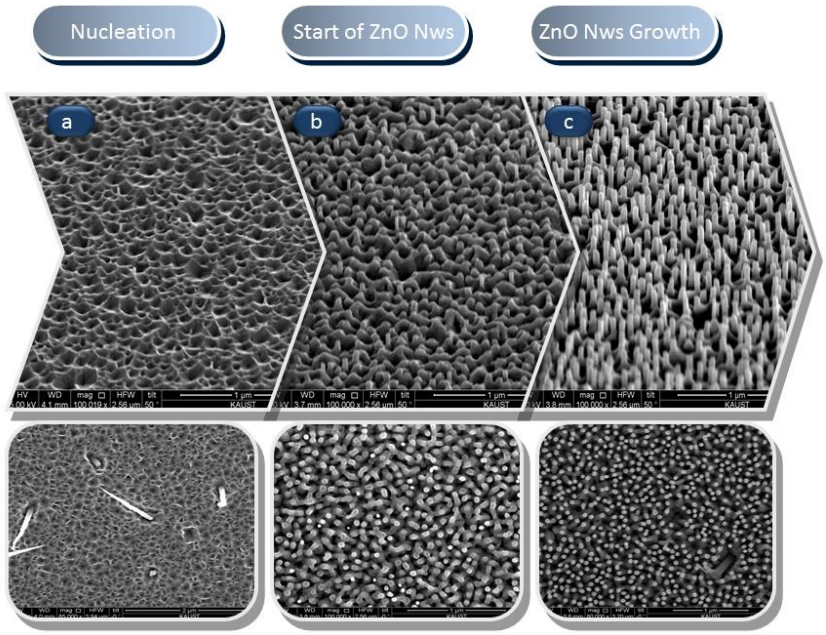

Figure 3- 53- SEM images tilted/top view of ZnO NWs grown on ZnO Seed layer at 10 Torr, Ts<500 °C, Laser Energy 350 mJ , by PLD for a- 10 min, b- 20 min, c- 30 min.

Figure 3- 53, 54 reveal the Morphology of the ZnO NWs grown on Si substrates with ZnO Seed layer by PLD. It is observed that the growth start at 20 minutes NWs with a diameter of 48 nm and length of ~ 100 nm , while at 30 min of deposition the diameter increases to 58 nm and the length to 200 nm. The suggested ZnO NWs growth process illustrates in Figure 3- 51. ZnO species are adsorbed onto the ZnO Nanoparticles on the SL surface. ZnO droplets migrate to the nuclei points that act as energetically favorable sites for ZnO nanostructure growth. This is due to the higher

sticking coefficient of ZnO on the nuclei sites. For the ZnO crystal, the growth rates V along the normal direction of different index planes are described as follows:

$$V(0001) > V(10\bar{1}0) > V(10\bar{1}\bar{1}) > V(10\bar{1}1) > V(000\bar{1}) \ .$$

The NWs type morphologies are frequently obtained. The presence of ZNO SL can efficiently lower the nucleation energy barrier and heterogenous nucleation easily occurs on the SL due to the matching lattice structure and the polar nature of the PLD ZNO SL, having the benefit of increasing the nucleation sites of ZnO NWs.

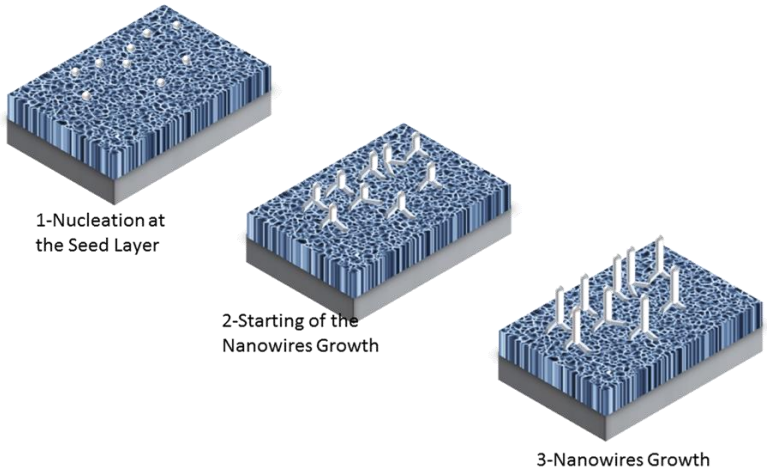

Figure 3- 54- Illustration of the growth process of ZnO NWs on ZnO Seed layer by PLD.

Based on the above and Because of the large quantity of ZnO that has migrated from the surface, and the continuous supply of ZnO the ZnO NWs has grown in the favorable direction [0002]. NWs grow from the outer layers through the self-catalytic vapor deposition process. The NWs length increases with growth time, and the density of the NWs varies with the nucleation sites on the surface of the SL and the Argon pressure in the PLD chamber.

3-5-3-4 ZnO NWs Bending and Bundling under SEM

Glass slides coated with thin film of both ITO (75 nm) and ZnO SL of 400 nm thickness, were used as substrates for subsequent growth of ZnO NW array.

ITO thin film was sputtered by RF-Sputtering discussed previously, and ZnO thin film was deposited by PLD discussed in paragraph. ZnO NWs were grown at 10 Torr Argon environments; temperature was less than 500 °C with laser pulse energy of 400mJ and target-substrate distance of 6.5 cm.

Figure 3- 56a presents the XRD spectrum of the ZnO NWs grown on Glass ITO substrate. IT is clearly seen the high peak of ZnO (002) revealing the c-axis orientation. Different peak positions of the band edge emission in the UV region (379.5 nm) as well as defect induced emission in the visible region: Green (531nm), and yellow (584.2 nm) that were clearly depicted in the PL spectrum of Figure 3- 56b.

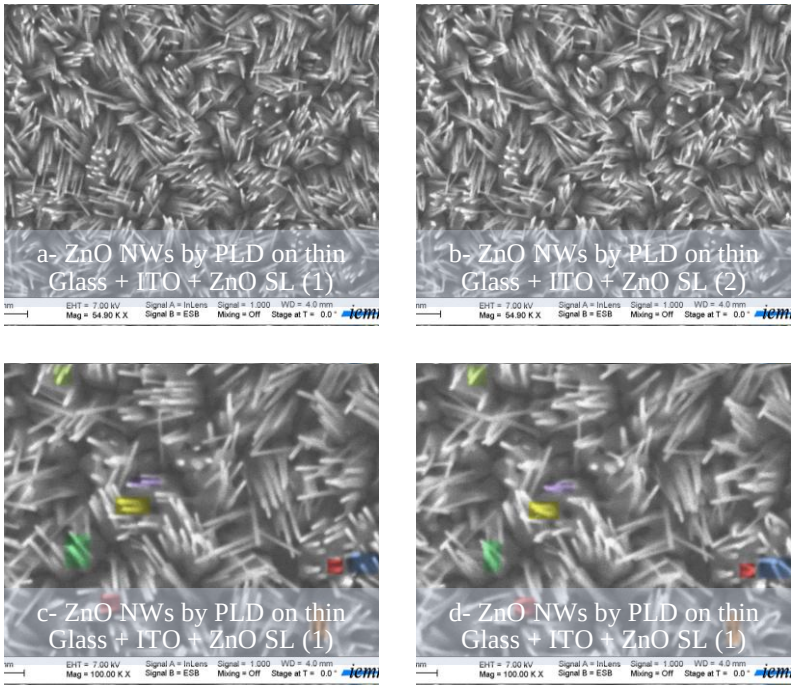

Figure 3- 55- SEM Imgaes top view of ZnO NWs gorwn at 10 Torr in Argon environment , 400mJ for 15 minutes.

a- XRD Spectrum of ZnO Nws grown on Glass- ITO + ZnO SL at 10 Torr, T_{sub}<500°C

b- PL Spectrum of ZnO Nws grown on Glass- ITO + ZnO SL at 10 Torr , T_{sub}<500°C

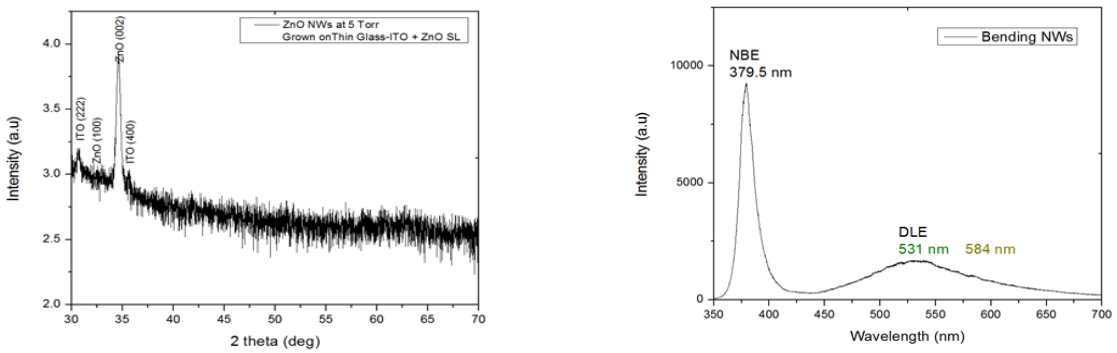

Figure 3- 56- XRD and PL Spectra of ZnO NWs grown on Glass – ITO with ZnO SL deposited by PLD at 10 Torr , Tsub<500 °C , $d_{target-substrate}$ = 6.5 cm

Discussion:

We speculate in Figure 3- 55 b,c,d , that some of the ZnO NWs tend to incline due to geometric instability .Since ZnO NWs have piezoelectric properties, this cause the side surface to be either positively or negatively charged. Bundling was noticed from vertically aligned ZnO NWs. The reason might be from the electron beam bombardment during SEM, or to electrostatic interactions due to charged (0001) polar surfaces. ZnO NWs grown along the *c* axis of a wurtzite structure can be described schematically as the alternative stacking of planes of fourfold coordinated O^{2-} and Zn^{2+} ions, and thus flat top surfaces of ZnO 1D nanostructures are either Zn^{+} or O^{-} terminated (0001) surfaces. Schematic illustrated in Figure 3- 57.

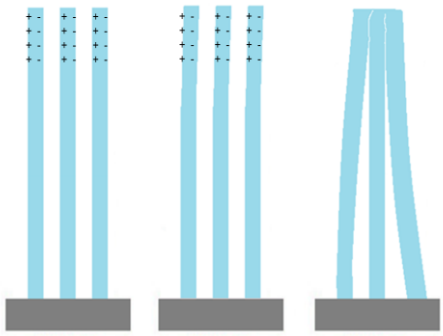

Figure 3- 57- Illustration of ZnO NWs bending and bundling under SEM

The uncompensated Zn^+ and O^- terminated surfaces result in net positive and negative charges, respectively. The bending and bundling of NWs were more clearly observed from the SEM images. Many NWs were bent and attracted to each other at or near their tips to form bundles of various numbers of NWs. Considering the NW separation over a few hundred nanometers, it was unlikely that the van der Waals interaction was responsible for the observed self-attraction. Moreover, it was found that some of the NWs in close proximity did not contact each other, but bent further in such a way to make contact with ones farther apart to form a crossed configuration. This indicates that repulsive interaction was occurring in addition to attractive interaction. Presumably, the opposite charges of Zn^+ and O^- terminated hexagonal facets of NWs were the origin of these interactions[88].

Field emission[89] (FE) is one of the most important applications since the emitting efficiency can be highly improved by the alignment. Comprehensive theoretical and experimental research on FE has been mainly conducted on carbon nanotubes (CNTs) owing to their good conductivity, chemical stability, and easy as well as cost-effective fabrication. Oxide semiconducting NWs, which are more stable at high temperatures in an oxygen environment and have a more controllable electronic property, have been considered more and more as alternative FE sources instead of CNTs. With a large exciton binding energy and high melting temperature, ZnO NWs have recently been studied as an effective FE source. However, very little research has been performed on optimizing their FE property by controlling the density of the aligned ZnO NWs. On the other hand the bending and bundling of the ZnO NWs might adversely affect the transport of electrons in a photovoltaic device.

3-6 Conclusion

ZnO NWs were successfully grown by vapor transport in wet environment, on Si (100) substrates with Zn SL and ZnO SL deposited by thermal evaporation and by Sputtering and PLD respectively. The high Quality ZnO NWs were synthesized on Si (100) and Glass ITO substrates with textured ZnO SL deposited by PLD. Benefited from the perfect lattice match, the ZnO nuclei were formed epitaxially on the c-oriented ZnO thin film/Si substrate. Combined with the fact that [0001] is the preferential growth direction for ZnO nanowires, ZnO nanowire arrays are expected to synthesize vertically to the substrate surface in our experiment. Different techniques were employed to grow vertically oriented ZnO NWs on different types of substrates, different Seed layer materials and different catalysts. The growth of ZnO NWs can be controlled by controlling the parameters. The vapor transport in horizontal tube furnace is based on a try and error or semi systematic system which is often used for finding the optimum conditions for the growth. The growth depends on diameter of the tube, used pressure, flow and a number of other parameters. Each system has its specific growth conditions, which cannot be transferred to other systems. On the other hand the pulsed assisted vapor deposition, PLD, is a simple and effective technique. It has a major advantage of transferring the target composition leading to stoichiometric deposition. It was found to be beneficial for improving the quality of the deposited film. The growth of NWs by PLD is optimized. The spacing and the density is affected by the Argon pressure inside the chamber. The length of the NWs is influenced by the deposition time. ZnO NWs were synthesized for the Solar Cell applications Figure 3- 58. Based on the proposed Solar Cell structure (chapter 1), these ZnO NWs will be sensitized with Lead Sulfide (PbS) QDs to form the PN Radial Junction that will be investigated in chapter 4.

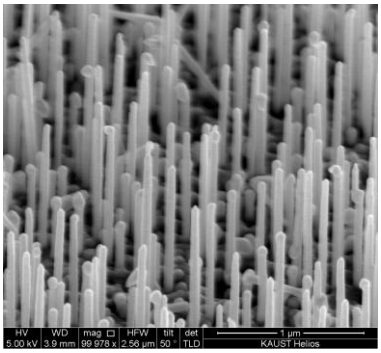

Figure 3- 58-vertically oriented ZnO NWs grown on Si Substrates and Glass- ITO Substrates.

References

[1] M. Yan, H. T. Zhang, E. J. Widjaja, and R. P. H. Chang, *J. Appl. Phys.* 94, 5240 **(2003).**
[2] H. J. Fan, F. Fleischer, W. Lee, K. Nielsch, R. Scholz, M. Zacharias, U. Gösele, A. Dadgar, and A. Krost, *Supperlattice Microst.* 36, 95 **(2004).**
[3] S. Y. Li, P. Lin, C. Y. Lee, M. S. Ho, T. Y. Tseng, *J. Nanosci. Nanotech.* 4, 968 **(2004).**
[4] H. T. Ng, J. Han, T. Yamada, P. Nguyen, Y. P. Chen, M. Meyyappan, *Nano. Lett.* 4, 1247 **(2004)**.
[5] C. Geng, Y. Jiang, Y. Yao, X. Meng, J. A. Zapien, C. S. Lee, Y. Lifshitz, and S. T. Lee, *Adv. Funct. Mater.* 14, 589 **(2004).**
[6] C. J. Lee, T. J. Lee, S. C. Lyu, Y. Zhang, H. Ruh, H. J. Lee, *Appl. Phys. Lett.* 81, 3648 **(2002).**
[7] X.-H. Zhang, S.-Y. Xie, Z.-Y. Jing, Z.-X. Xie, R.-B. Huang, L.-S. Zheng, J.-Y. Kang, T. Sekiguchi, *J. Solid State Chem. 173*, 109 (**2003)**.
[8] Ulick R. Evans, An Introduction to Metallic Corrosion, 3rd ed., Edward Arnold, 1981.
[9] S. Ren ,Y.F. Bai, Jun Chen ,S.Z. Deng, N.S. Xu, Q.B. Wu , Shihe Yang, Materials Letters 61 (2007) 666–670
[10] O. Martinez,, V. Hortelanoa, J. Jiménez, J.L. Plaza, S. de Dios, J. Olvera, E. Diéguez, R. Fath, J.G. Lozano, T. Ben, D. Gonzelez, J. Mass Journal of Alloys and Compounds 509 (2011) 5400–5407
[11] C.-F. Lin and L.-C.Chao, 2010 IEEE
[12] A. Sekar, S.H. Kim, A. Umar, Y.B. Hahn, Journal of Crystal Growth 277 (2005) 471–478
[13] F. Kurdesau, G. Khripunov, A.F. da Cunha, M. Kaelin, A.N. Tiwari Journal of Non-Crystalline Solids, Volume 352, Issues 9–20, 15 June 2006, Pages 1466–1470
[14] Y. Leterrier, L. Me´dico, F. Demarco, J.-A.E. Ma˚nson, U. Betz, M.F. Escola`, M. Kharrazi Olsson, F. Atamny, Thin Solid Films 460 (2004) 156.
[15] N. Kikuchi, E. Kusano, E. Kishio, A. Kinbara, Vacuum 66 (2002) 365.
[16] T. Nakada, Y. Hirabayashi, T. Tokado, D. Ohmori, T. Mise, Solar Energy 77 (2004) 739.
[17] A.N. Tiwari, G. Khrypunov, F. Kurdzesau, D.L. Batzner, A. Romeo, H. Zogg, Progress in Photovoltaics: Research and Application 12 (2004) 33.
[18] I. Hamberg, C.G. Granqvist, J. Appl. Phys. 60 (1986) R123.
[19] Kerkache L., Layadi A., Dogheche E., Remiens D. Eur. Phys. J.-Appl. Phys., 39, 1 (2007) 1-5 Doi: 10.1051/Epjap:2007113
[20] Kerkache L., Layadi A., Dogheche E., Remiens D. J. Phys. D-Appl. Phys., 39, 1 (2006) 184-189 Doi: 10.1088/0022-3727/39/1/027
[21] Kerkache L., Layadi A., Dogheche E., Remiens D. J. Alloy. Compd., 509, 20 (2011) 6072-6076 (Available Online March 10, 2011 ; Published May 19, 2011) Doi: 10.1016/J.Jallcom.2011.03.022
[22] H.-C. Lee, J.-Y. Seo, Y.-W. Choi, D.-W. Lee, Vacuum 72 (2004) 269
[23] J.-O. Park, J.-H. Lee, J.-J. Kim, S.-H. Cho, Y.K. Cho, Thin Solid Films 474 (2005) 127
[24] C.Liu, T.Matsutani,T.Asanuma,K.Murai, M.Kiuchi, E.Alves, M.Reis 2003 J.App.Phys. 93 2262
[25] M.Z.Gao, R.Job,D-S.Xue, W.R. Fahrner (2008) Chin.Phys.lett 25, No4 , 1380.
[26] O. Shultz, G. Emanuel, S.W. Glunz, G.P. Willeke, in: Proceedings of the Third World Conference on Photovoltaic Solar Energy Conversion, 2003, pp. 1360–1363.
[27] P. Manshanden, A.R. Burgers, W.A. Nositschuka, O. Voigt, A.W. Weeber, in: Conference Record of 29th IEEE Photovoltaic Specialists Conference, 2002, pp. 324–327.
[28] YMa1, C P Wong1, X T Zeng2, T Yu1, Y Zhu1 and Z X Shen1 Appl. Phys. 42 (2009) 065417
[29] Y.Zhang, K.Y u, D.Jiang, Z.Zhu, H.Geng, and L.Luo, Appl. Surf. Sci. 242, 212 (2005).
[30] M.La w, L.E.Greene, J.C.Johnson, R.Saykally , and P.Y ang, Nat. Mater. 4, 455 (2005).
[31] Y.J. Hong, J. Yoo, Y.-J. Kim, C.-H. Lee, M. Kim, G.-C. Yi, Adv. Mater. 20 (2008) 1.
[32]] H.T. Ng, J. Li, M.K. Smith, P. Nguyen, A. Cassell, J. Han, M. Meyyappan, Science. 300 (2003) 1249.
[33] S.-W. Kim, H.-K. Park, M.-S. Yi, N.-M. Park, J.-H. Park, S.-H. Kim, S.-L. Maeng, C.-J. Choi, S.-E. Moon, Appl. Phys. Lett. 90 (2007) 033107.
[34] C.-C.Wu, D.-S.Wuu, T.-N. Chen, T.-E. Yu, P.-R. Lin, R.-H. Horng, H.-Y. Lai, Jpn. J. Appl. Phys. 47 (2008) 746.
[35] S.-W. Kim, S. Fujita, M.S. Yi, D.H. Yoon, Appl. Phys. Lett. 88 (2006) 253114.

[36] J.S.Jeong,J.Y.Lee,J.H.Cho,C.J.Lee,S.J.An,G.C.Yi, and R.Gronsky: Nanotechnology 16(2005) 2455
[37] X.Liu,X.Wu, H.Cao,R.P.H.Chang,J.Appl.Phys 95 (2004) 3141
[38] P. Singh, A. Kumar, A. Kaushal, D. Kaur, A. Pandey, R.N. Goyal, Bull. Mater. Sci. 31 (2008) 573–577.
[39] S.Lemlikchi, S.Abdelli-Messaci, S.Lafane, T.Kerdja, A.Guittoum,M.Saad Appl. Surf.Scien 256(2010) 5650-5655
[40] H.Koinuma, MRS Bull. 19 (1994) 21. *X.L. Wu et al., Appl. Phys. Lett.* ***78****, 2285 (2001).*
[41] S.L.King,J.G.E.Gardeniers and I.W.Boyd, App.Surf.Sci. 96-98 (1996) 811
[42] S. Zhang, D. Sun, X.L. Bui, , Imperial College Press, 2007, pp. 1–104.
[43] R. Chen ,C Zou, X.Yan, A.Alyamani, W.Gao, thin Solid Film 519 (2011) 1837-1844
[44] D.Vogel, P.Kruger, J.Pollman, Phys.Rev.B 52(1995) R14316
[45] R. Chen ,C Zou, X.Yan, A.Alyamani, W.Gao, thin Solid Film 519 (2011) 1837-1844
[46] S.N.Cha, B.G.Song,J.E.Jang,J.E.Jung,I.T>Han,J.H.Ha,J.P.Hong,D.J.Kang,and J.M.Kim, Nanotechnology 19(2008) 235601
[47] W.Water,T.H.Fang,L-W.Ji, C-C.Lee Materials Science and Engineering B 158 (2009) 75-78
[48] E.W.Petersen,E.M.Likovich,K.J.Russell and V.Narayanamurti Nanotechnology 20 (2009) 405603
[49] A.N.Red'Kin,A.N.Gruzintsev,E.E.Yakimov,O.V.Kononenko, and D.V.Roshchupkin Inorganic materials 2011,vol 47,No 7,pp.740-745
[50] Y-H.Kang,C-G.Choi,Y-S.Kim,J-K.Kim , Materoals letters 63 (2009) 679-682
[51] W.Y.Song,J.H.Yang, D.V. Dinh,T.I. Shin,S.M.Kang, S-W.Kim, D.H.Yoon J.Phys and Chem of Solids 69 (2008) 1486-1490
[52] S.N.F.Hasim,M.A.Abdul Hamid, R.Shamsudin,A.Jalar J.Phys and Chem of solids 70 (2009) 1501-1504
[53] H.W.Kim,M.A.Kebede,H.S.Kim,B.Srinivasa,D.Y.Kim,J.Y.Park,S.S.Kim Current applied physics 10 (2010) 52-56
[54] M.Zha,D.Calestani,A.Zappettini,R.Mosca,M.Mazzera,L.Lazzarini and L.Zanotti , Nanotechnology 19 (2008) 325603
[55] S. Fujihara, Y. Ogawa, A. Kasai, Chem. Mater. 16 (2004) 2965
[56] D.munoz-Rojas,J.Fraxedas, P.Gomez-Romero, N.Casan-Pastor, J.Solid state Chem 178 (2005) 295
[57] L.Zanotti, M.Zha, D.Calestani, E.Comini, G.Sberveglieri, Cryst.Res.Technol 40 (2005) 932.
[58] Djurišić AB, Leung YH, Choy WCH, Cheah KW, Chan WK. Appl Phys Lett 2004;84:2635–7
[59] Xu CX, Sun XW. J Cryst Growth 2005;277:330–4.
[60] Wang JM, Gao L. J Cryst Growth 2004;262:290–4.
[61] L.Feng, A.Liu, M.Liu, Y.Ma, J.Wei, B.Man, Materils characterization 61(2010) 128-133
[62] Y.Dai,Y.Zhang,Z.L.Wang Solid State communications 126(2003) 629-633
[63] M.Kawakami,A.B.Hartano,Y.Nkata and T.Okada,Jpn.J.Appl.Phys.42 (2003) L33.
[64] V.Gupta,P.Bhattacharya,Y.I.Yuzuk and R.S.Katiyar , Mat.Res.Soc.Symp.Proc.Vol.818(2004) M8.26.1
[65] Z.Liu,D.Zhang,C.Li and C.Zhou Proc.3rd IEEE conf. on Nanotechnology , 2003,Vol2 pp.59, DOI: 10.1109/NANO.2003.1230980
[66] B.H.Agung,M.Kawakami,Y.Nakata,X.Ning,and T.Okada, the 5th Pacific Rim conference on Laser and Electro-optics 2003,vol2 pp.667,DOI: 10.1109/CLEOPR.2003.1277210
[67] W.Z.Liu,H.Y.Xu,L.Wang,X.H.Li and Y.C.Liu AIP Advances 1,022145 (2011)
[68] R.Guo,M.Matsumoto,T.Matsumoto,M.Higashihata,D.Nakamura,T.Okada App.Surf.Scien 255 (2009) 9671-9675
[69] L.C.Tien,S.J.Pearton,D.P.Norton,F.Ren, J.Mater Sci (2008) 43: 6925-6932
[70] R.Guo,J.Nishimura,M.Matsumoto,M.Higashihata,D.Nakamura,T.Okada Jap.J.App.Phys 47,1,(2008),pp. 741-745
[71] R.J.Mendelsberg,M.Kerler,S.M.Durbin,R.J.Reeves Superlattices and Micorstructures 43 (2008) 594-599
[72] H.Kumarakuru,D.Cherns,G.M.Fuge, Surface &Coatings Technology 205 (2011) 5083-5087
[73] M.Lorentz,E.M.Kaidashev,A.Rahm, T.Nobis, J.Lenzner, G.Wagner,D.Specmann,H.Hochmuth and M.Grundmann, Appl.Phys.Lett. 86 (2005) 143113
[74] S.Lemlikchi,S.Abdelli-Messaci, S.Lafane, T.Kerdja, A.Guittoum, M.Saad, Appl.Surf.Scien 256 (2010) 5650-5655
[75] Y.Tak,D.Park,K.Yong, J.Vac.Sci.Technol.B 24,2047 (2006)

[76] O. Lupan , G.A. Emelchenko, V.V. Ursaki, G. Chai, A.N. Redkin, A.N. Gruzintsev, I.M. Tiginyanu, L. Chow, L.K. Ono, B. Roldan Cuenya, H. Heinrich, E.E. Yakimov , Materials Research Bulletin 45 (2010) 1026–1032
[77] J.S. Lee, K. Park, M.I. Kang, I.W. Park, S.W. Kim, W.K. Cho, H.S. Han, S.S. Kim, J. Crystal Growth 254 (2003) 423
[78] Daisuke NAKAMURA, Takafumi MATSUMOTO, Akio KUMEDA, Kazuyuki TOYA, Kota OKAZAKI, Mitsuhiro HIGASHIHATA and Tatsuo OKADA , JLMN-Journal of Laser Micro/Nanoengineering Vol. 6, No. 1, 2011
[79] Y.SunG.M.Fuge, M.N.R. Ashfold , Superlattices and Microstructures 39 (2006) 33-40
[80] L.C.Tien, S.J.Pearton, D.P.Norton and F.Ren, J.Mater.Sci 43, 6925 (2008)
[81] W.Z.Liu, H.Y.Xu, L.Wang, X.H.Li, and Y.C.Liu AIP Advances 1, 002145 (2011)
[82] S.Lemlikchi,S.Abdelli-Messaci, S.Lafane, T.Kerdja, A.Guittoum, M.Saad, Appl.Surf.Scien 256 (2010) 5650-5655
[83] R.S.Ajimsha, R.Manoj, P.M.Aneesh, M.K.Jayaraj current applied physics 10 (2010) 693- 697
[84] Mitsuhiro HIGASHIHATA and Tatsuo OKADA , JLMN-Journal of Laser Micro/Nanoengineering Vol. 6, No. 1, 2011
[85] R.Guo, M.Matsumoto, T.Matsumoto, M.Higashihata, D.Nakamura,T.Okada , Applied Surface – Science 255 (2009) 9671-9675
[86] R.S.Ajimsha, R.Manoj, P.M.Aneesh, M.K.Jayaraj current applied physics 10 (2010) 693- 697
[87] R.Guo, M.Matsumoto, T.Matsumoto, M.Higashihata, D.Nakamura,T.Okada , Applied Surface – Science 255 (2009) 9671-9675
[88] Jinzhang Liu, Soonil Lee, Kyungmoon Lee, Y H Ahn, Ji-Yong Park and Ken Ha Koh (2008)
[89] Xudong Wang, Jun Zhou, Changshi Lao, Jinhui Song, Ningsheng Xu, and Zhong L. Wang. (2007)

CHAPTER 4:
Integration of QDs with NWs for QDSSC

Contents

4-1 Introduction

To date, a broad range of nanostructured materials have been investigated as potential building blocks for constructing the future generation of Photovoltaic devices. 0D nanostructures, Nanoparticles (NPs) with tunable band gaps can allow for efficient optical absorption, charge generation and can be active in a number of different regions of the spectrum ranging from visible to Near Infra-red (NIR). A significant effort has been given on the hybrid structures obtained by combining Nanowires (NWs) with NPs. Lead chalcogenide NPs are an important set of nanosized materials. Lead sulfide (PbS) as II-VI compound has unique properties among chalcogenide semiconductors, is selected in this research. This chapter is divided in 4 folds. The first fold presents the role of NPs in PV devices, followed by a description of the PbS properties and its different synthesis techniques. The third fold describes the ligand exchange process presenting the morphology of the obtained NPs. The Last fold is about the attachment of PbS NPs with and without ligand on ZnO NWs by different techniques with their characterization results and discussions.

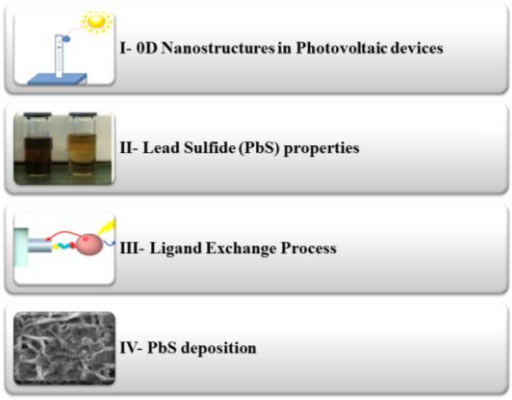

Sections of Chapter 4

4-2 Objectives

The objectives of Chapter 4 are the following:

- Present radial hetero-junction
- Integrate 0D with 1D nanostructure.
- Select the proper p-type semiconductor for radial junction.
- Synthesize the PbS Nanoparticles
- Prove the attachment of PbS on ZnO Nanowires
- Characterize the PbS/ZnO Radial Junction , for Solar cell applications

4-3 Zero Dimensional (0D) and one Dimensional (1D) Nanostructures for Hetero-junctions Nanowires based solar cells.

Size and morphology dependent properties such as quantum confinement effects sin semiconductor nanostructures provide a rational approach toward a highly efficient solar energy conversion process [1]. It has been demonstrated that the optical absorption properties and band gap of QDs can be tuned for efficient harvest of the entire solar spectrum. Significant efforts have been placed on the application of QDs in PV devices in which the photo-generated electrons and holes are transported to external circuits[2][3][4][5].

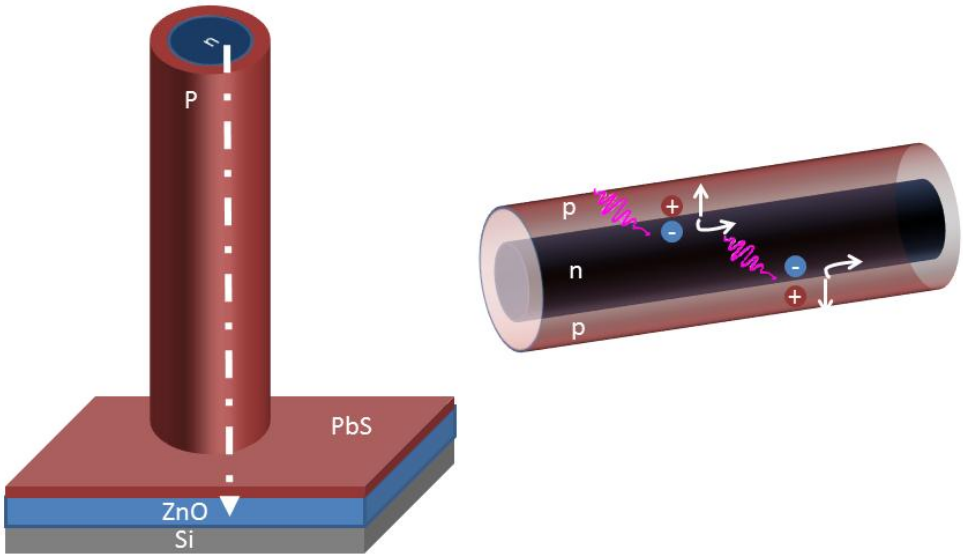

Figure 4- 1-Illustration of Radial Junction based on ZnO NWs with PbS NPs

Zero dimensional (0D) and one dimensional (1D) nanostructures have attracted good attention owing to their unique physical and chemical properties in solar energy harvesting, conversion and storage[6]. Quantum Dots, (0D) nanostructures, with their tunable band gap and optical properties to harvest the entire solar spectrum, can improve the optical absorption, charge generation[7], but limited by the lack of mechanism for effective charge separation and transportation. On the other hand Nanowires (NWs), 1D nanostructure, provide the charge separation and transportation[8]. Driven by these unique properties, ZnO NWs and PbS QDs are combined together to form the hybrid radial junction solar cell (Figure 4- 1). The

radial structure extends the hetero-junction interface along the surface of the NWs resulting in a short carrier diffusion range and a large interface for efficient carrier separation and transport. Due to the large junction area and short diffusion length, the recombination of charge carriers is suspended.

4-4- Lead Sulfide (PbS) Nanoparticles

The primary photochemical event leading to photocurrent generation in QDSCs is the charge separation at the metal chalcogenide-metal oxide interface. It's been demonstrated that the charge separation in CdS-ZnO and CdS-TiO_2 coupled semiconductor has been improved [9].

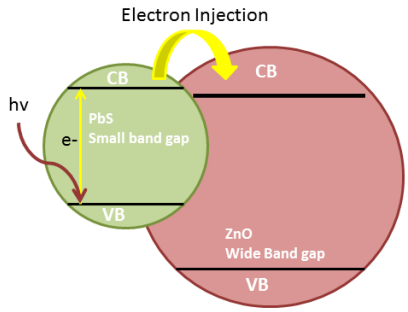

Figure 4- 2- Charge injectionfrom excited semiconductor nanocrystal PbS into ZnO NPs in the operation of QD sensitized solar cell

Efforts have been made to design this type of semiconductors assembly (Figure 4-2). The matching of the band energies of two semiconductors facilitates the desired function to induce electron-hole recombination for a LED or improve charge separation by driving electrons and holes in two different nanoparticles for a Solar Cell. The QD must first absorb a photon, placing it in an electronically excited state $QD + h\upsilon \rightarrow QD^{*}$ **(1).**

Shortly after the absorption, the electron and hole relax to their most energetically favorable states, namely the conduction and valence band edges, respectively, creating an electron–hole pair $QD^{*} \rightarrow QD(e^{-} + h^{+})$ **(2)**. In order to harvest the potential energy of this electron–hole pair through an external load, the electron and hole must be separated spatially. This is achieved through the electron transfer depicted in $QD(e^{-} + h^{+}) + ZnO \rightarrow QD(h^{+}) + ZnO(e^{-})$**(3)** whereby an electron moves from the QD conduction band to the ZnO conduction band.

Note that there are two other potential fates of the electron–hole pair: non-radiative $QD(e^{-} + h^{+}) \rightarrow QD + Heat$ (3') and radiative $QD(e^{-} + h^{+}) \rightarrow QD + h\upsilon$ (3")

recombination. Once spatially separated from the photo-generated hole, the electron must then navigate the ZnO scaffold (4) $\boldsymbol{ZnO(e^-) \rightarrow ZnO(e^-)_{nearest\ neighbor}}$**(4)**. Once at the working electrode surface, the electron must transfer to the circuit at the working electrode $\boldsymbol{ZnO(e^-) + electrode \rightarrow ZnO + electrode\ (e^-)}$ **(5)**. Meanwhile, the photo-generated hole remaining in the QD valence band is scavenged by the electrolyte species $\boldsymbol{QD(h^+) + electrode \rightarrow QD + electrode\ (h^+)}$ **(6)**, which then needs to diffuse spatially away from the QD layer and to the counter electrode[10].

4-4-1 Lead Sulfide (PbS) nanoparticles Properties

The choice of semiconductor materials is critical for the performance of the solar cell since the intrinsic properties of the semiconductors determine the light absorption, charge generation, separation and transportation as well as the photo/chemical stability. The wide use of QDs (CdS[11],CdSe [12],PbS [13],InO[14],InAs[15]) as sensitizer of solar cells has been spurred in the past years in order to achieve high efficiency(expected 44%). In this regard, Wang et al [16], have fabricated a new structure with CdS NPs on ZnO NWs heterostructure arrays. On the basis of mesoporous TiO_2 films Lee et al[17] has successfully prepared a PbS sensitized solar cell with a relative ideal energy conversion efficiency.

PbS and PbSe are considered as important class of high quality nanosized materials. PbSe QDs have practical disadvantages where several studies have already reported on their poor stability in air [18][19][20]. In this respect, PbS QDs may offer a suitable alternative to PbSe QDs and a synthesis which produces a large size range of bright and stable PbS QDs is highly desirable.

Lead Sulphide (PbS) is a II-VI compound and has unique properties among semiconductors. PbS has a large excitonic Bohr radius of around 18 nm and hence the band gap of PbS particles can be easily tuned to anywhere between 0.41 eV to 2 eV covering the entire visible spectrum[21][22][23].

4-4-2 PbS synthesis

Different PbS QDs Synthesis techniques were reported in the literature. It is quite important to develop techniques to control the dispersion / aggregation phenomena of nanoparticles to apply them into functional materials and products. Two broad techniques, the in-situ and ex-situ growth are presented and employed in this research.

In-situ Growth

In-situ growth depends on the nucleation mechanism inside the nanostructure followed by QD growth which usually leads to a polydisperse QD size distribution. The absence of a linker molecule at the QD-Wide band gap semiconductor interface leads to efficient charge injection from the QD into the wide band gap material. High surface coverage can be achieved with in-situ methods. Two methods can be employed the Chemical Bath Deposition (CBD) [24] and the Successive Ionic Layer Adsorption and Reaction (SILAR) [25]. CBD [26]is a direct growth process done by immersing wide band gap nanostructure into a solution that contains the cationic and anionic precursors which react slowly in one bath. The size of the PbS NPs deposited on a substrate can be controlled by the reaction time. The deposition of metal chalcogenide semiconducting thin films occurs due to substrate maintained in contact with dilute chemical bath containing metal and chalcogen ions. The film formation on substrate takes place when ionic product exceeds solubility product. However, this results into precipitate formation in the bulk of solution, which cannot be eliminated. This results in unnecessary formation of precipitation and loss of material. On the other hand, SILAR [27]is based on two vessels separating the cationic and anionic precursors. It is more convenient for precisely controlling the size of the produced PbS NPs as only the number of repeated cycles has to be controlled. SILAR method can be employed in order to avoid such unnecessary precipitation. Thin films are obtained by immersing substrate into separately placed cationic (Pb^{2+}) and anionic (S^{2-}) precursors and rinsing between every immersion with ion-exchanged water. The rinsing time in ion exchange water is critical for ionic layer formation. Thus, precipitation formation i.e. wastage of material, is avoided in SILAR method.

Ex-situ Growth

Ex-situ growth [28][29]or monodisperse QDs with molecular linker is based on three components which are precursors, organic surfactants and solvents. This technique involve the use of capping agents such as Oleic Acid (OA) to stop the growth at the

desired size and size distribution, to improve the solubility of the NPs and stabilization by passivizing the surface and to prevent agglomeration of the NPs (Figure 4-3).

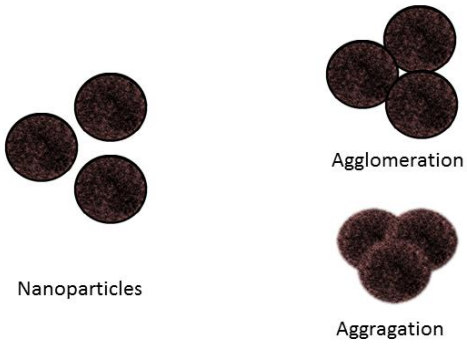

Figure 4- 3- Nanoparticles dispersed, Aggreagated and aggloerated

PbS CQD passivated by the original OA ligands used during synthesis exhibit extremely low mobility as a result of the insulating nature of the long alkyl chains [30]. To make high mobility solids, it is necessary to replace the original ligands with shorter molecules that increase the electronic coupling between neighboring nanocrystals .

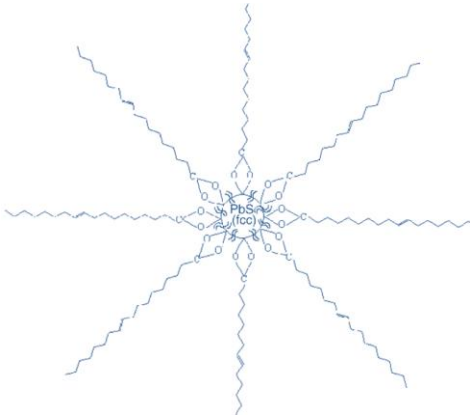

Figure 4- 4 Model of Oleic acid capped PbS nanoparticles [30]

The model of Oleic Acide (OA) capped PbS nanoparticles is shown in Figure 4- 4. Since PbS nanocore was embedded in the monolayer of OA, the dispersion capacity in the organic solvent and stability in the air. The repulsion between the surface capping layers enables the PbS nanocore away from agglomeration. The capping layer of OA stabilized the PbS NPs and made the OA-capped NPs to be a potential oil additive.

4-5- Ex- situ Growth of PbS QDs & Ligand Exchange

PbS QDs were purchased from Mk nano Canada[1], synthesized by the ex-situ growth with different nanoparticles sizes of 6.4 nm, 7.2nm and 9.4 nm where the crystalline core size is of 2.4nm, 3.2nm, and 5.4 nm. These Nanoparticles will be used after ligand exchange processed and will be attached to the ZnO Nanowires. Properties provided by the vendor summarized in Table 4-1.

Table 4- 1- Properties of PbS CQDs purchased from MK-Nano

Criteria	T850	T1100	T1500
Emission Peak	882 nm	1030 nm	1508 nm
Absorption Peak	763 nm	1007 nm	1461 nm
Emission Peak FWHM	118 nm	-	146 nm
Nano-crystal diameter	2.4 nm	3.2 nm	5.4 nm
Total particle diameter (crystalline core + Ligands)	6.4 nm	7.2 nm	9.4 nm
Molar extinction coeff. (based on core data)	2.8 E+04	6.2 E+04	1.3 E+05
Nano--crystal MW (µg/nmol) (crystalline core)	1.1 E+04	2.1 E+04	5.8E+04
Particle MW (µg/nmol) (crystalline core+ligands)	5.4 E+04	8.3 E+04	4.5E+05

4-5-1 PbS NPs characterization results and discussion

Nanoparticles Characterization:

By controlling the size of PbS CQDs in synthesis, the absorption onset can be tuned from 3000 nm to 600 nm [31][32]. The objective of combining three different sizes of PbS NPs is to have a triple junction solar cell based on ZnO Nws. The first layer will be composed of the smallest PbS CQDs with 2.4 nm diameter and absorption of 763 nm. The second layer is composed of PbS CQDs of 3.2 nm with absorption of 1007 nm. The third layer is composed of PbS CQDs with a diameter of 5.4 nm and absorption of 1461 nm. The resultant distribution of spectral absorbance is illustrated in Figure 4- 5.

[1] www.MKnano.com

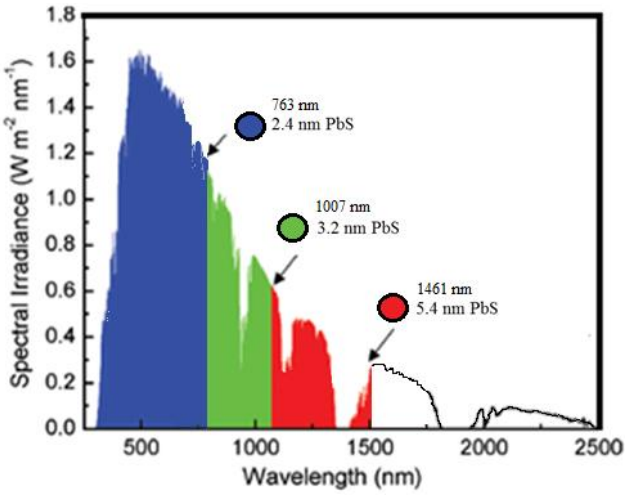

Figure 4- 5 Concept of using the three different sizes if PbS nanoparticles to build the solar cell

a- Absorption

b- Photoluminescence

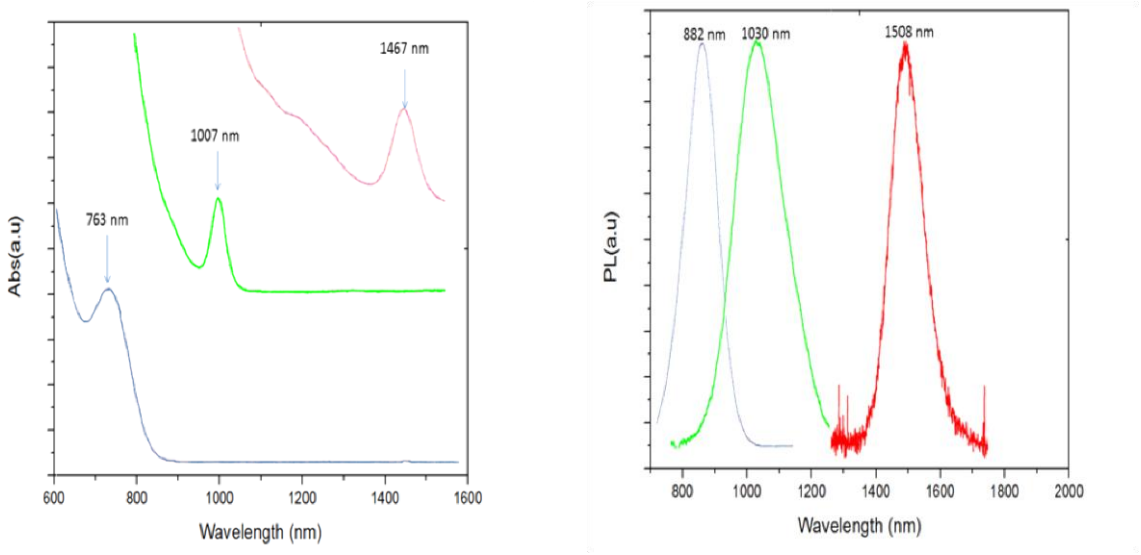

Figure 4- 6- Absorption and Emission spectra of the PbS QDs bought from MK-Nano.

Figure 4- 6-shows the solution absorption spectra of the OA capped PbS NPs dissolved in toluene. These OA capped PbS NPs have different diameter of 2.4 nm, 3.2nm and 5.4 nm, with a high peak in the range of ~ 763 nm, ~ 1007 nm and ~ 1461 nm respectively. Figure 4- 6-b shows the emission spectra of the three OA Capped PbS NPs , which present a very high peak at 882 nm ~ 1.4 eV , 1030 ~ 1.2 eV and 1508 nm ~0.822 eV respectively.

a- PbS QDs of 2.4 nm

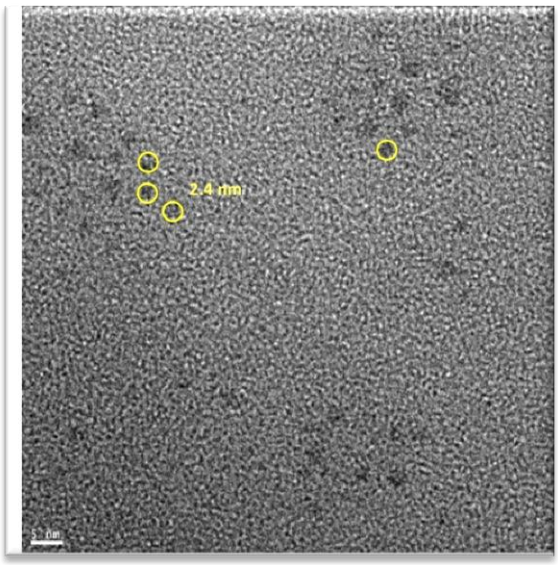

b-PbS QDs of 3.2 nm

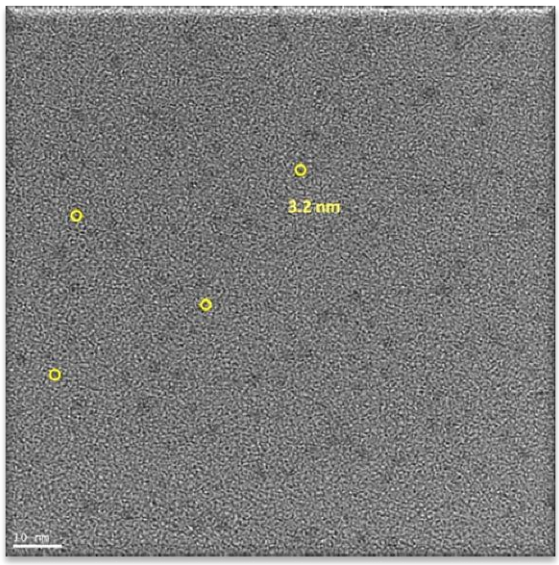

c- PbS QDs of 5.4 nm

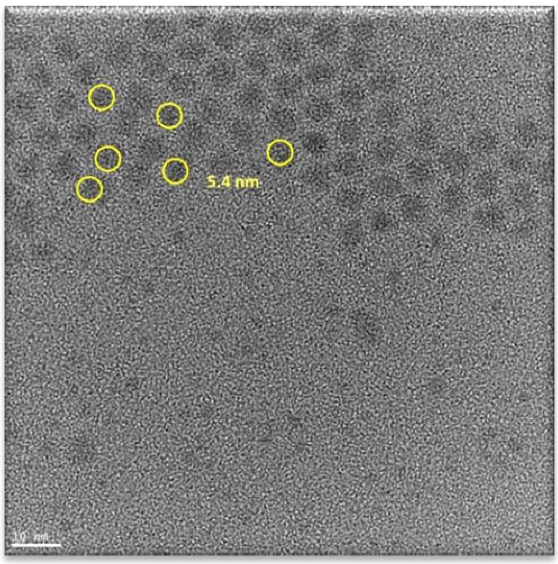

Figure 4- 7- TEM images of the PbS Nanoparticles bought from MK-Nano

Figure 4- 7 a-c illustrates the TEM images of the three different sizes OA capped PbS NPs, it was found that the nanoparticles didn't agglomerate and they are well Dispersed. The TEM images confirm the size of the NPs of 2.5 nm, 3.4nm and 5.4 nm diameters.

Figure 4- 8 shows the FTIR absorbance spectra of the three sizes Oleic acid capped PbS nanoparticles. The characteristics can be clearly seen that some peaks around

3000 , 2900, 2850, 1465 and 722 cm^{-1} exist in the IR spectra which indicated the existence of =C-H group and long alkyl chain in the OA capped PbS NPs. This reveals that the OA is capping the surface of the PbS nanoparticles.

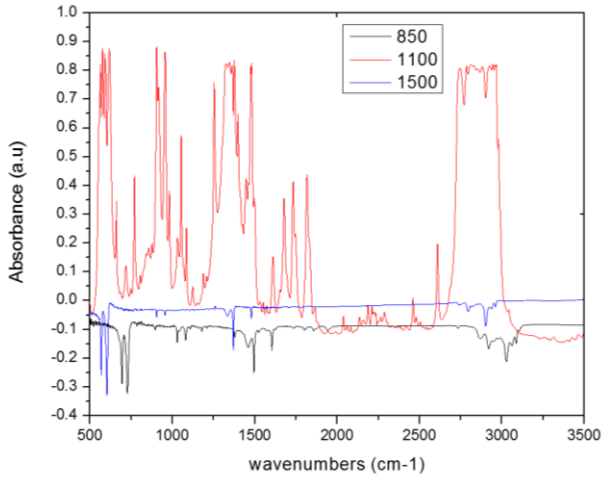

Figure 4- 8-FTIR Spectra of Oleic Acid capped PbS T-850, T1100 and T 1500 nanoparticles

4-5-2 PbS Ligand Exchange

To facilitate the use of PbS Nps in devices, these NPS should be packed tightly on the surface of the device substrates. PbS CQDs synthesized by hot solution chemistry have dielectric capping layers such as OA, and consequently a de-capping process is required to inspire the contact between the PbS CQDs, and neighboring nanostructures[33].

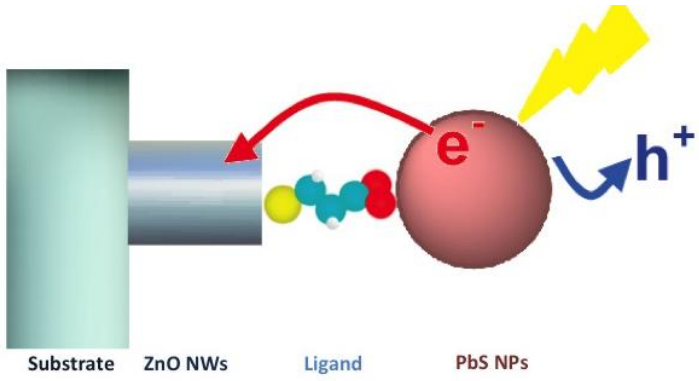

Figure 4- 14- concept of attaching the PbS nanoparticles on the ZnO nanowires

Much attention has been devoted to the development of new ligand strategies that minimize the inter-particle spacing to promote carrier transport and lower the defect density to reduce recombination loss (best reported efficiency of 5.1%) [34] Short alkylthiols [35], aromatic thiols[36], alkulamines [37] and mercaptocarboxylic

acids(MPA)(21) (Figure 4- 15) have all shown promise in achieving effective passivation while reducing inter-particle spacing [38][39][40] .

Thiols[41][42] have been shown to affect significantly the electrical properties of nanocrystal films. Ethanedithiol (EDT) is a short organic that has~0.5 nm size and has recently been reported to enhance 10 fold the power conversion efficiency (PCE) of CQD PV devices. In [43] the external Quantum Efficiency (EQE) increased from 5 to 22% and PCE to 2.6 %. In the course of study, treatment using Ethanethiol leads to an improvement in carrier collection for greater than that expected from transport considerations alone.

The passivation strategy based on 3 mercaptopropionic acid (MPA) enables significantly enhancement of the mobility lifetime products of PbS CQDs films leading to increase in both the diffusion lengths of charge carriers and the power conversion efficiencies of PbS CQDs PV test structures [44].

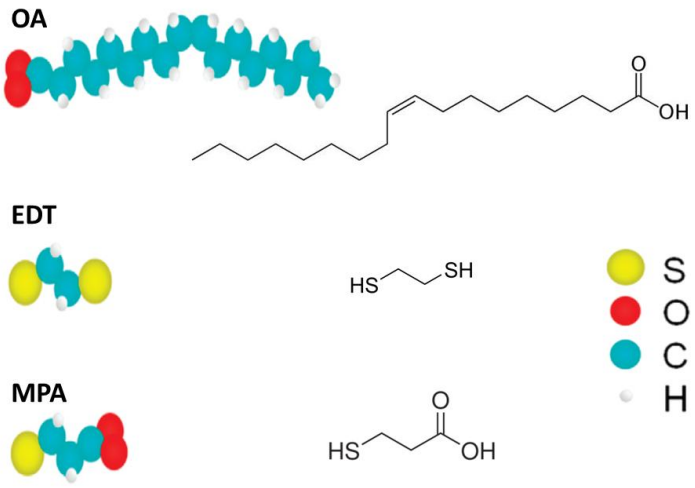

Figure 4- 9- Graphic Illustration of different Ligands used.

4-5-2-1 Ligand Exchange Process

In our Research, EDT and MPA were used for ligand exchange Figure 4- 9. The Ligand exchange was carried out in air , a 0.5 ml of OA capped PbS QDs (5.4 nm) from MK-Nano were mixed with 1 ml of toluene, the mixture was placed on hot plate of 70 °C after adding 1 ml of new ligand (EDT/MPA). The mixture was left at 70 C for 1 hour. The PbS-QDs were precipitated by addition of 10 ml of Ethanol separated

by centrifugation at 7000 rpm for 15 min and dried, then re-dispersed in 1 ml toluene. No additional polymers were used for aggregation studies (Figure 4- 10-11).

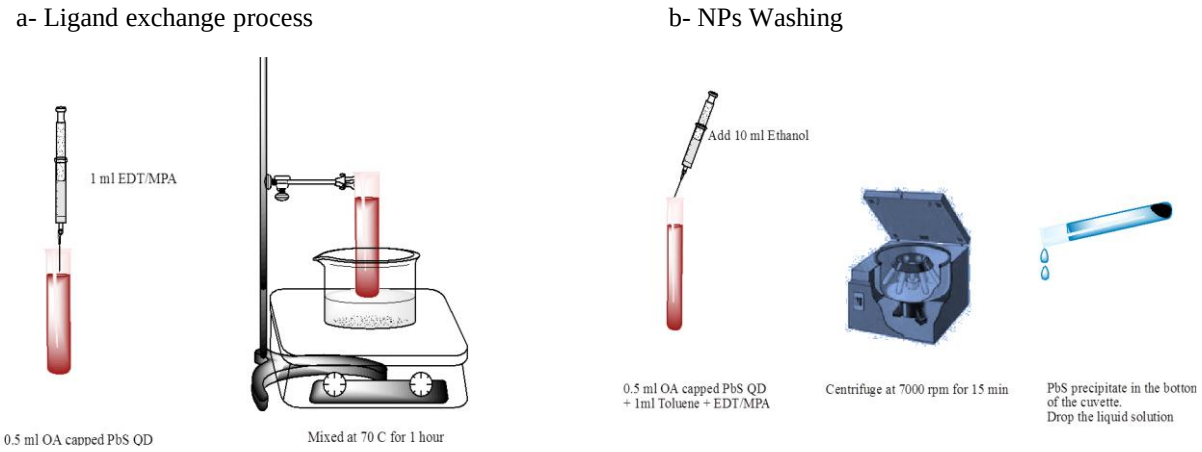

Figure 4- 10 – illustration of Ligand exchange Process

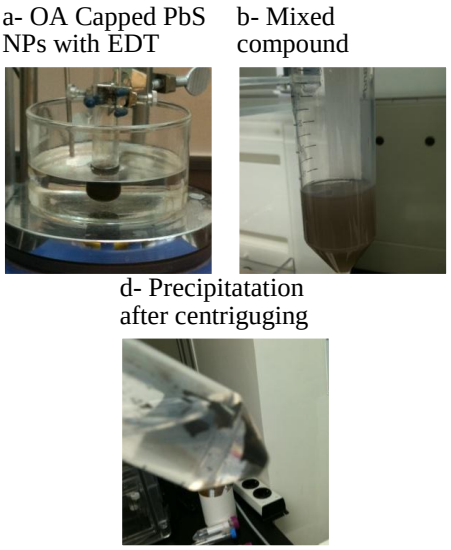

Figure 4- 11- Ligand exchange process

4-5-2-2 PbS Nanoparticles Characterization after ligand exchange

Ligand Exchange with EDT

PbS nanobelts were observed by TEM images Figure 4- 12. The nanobelt size was from 1.2 µm to 14 µm in length and 150 nm to 525 nm in width. A number of recent reports [45][46] have investigated the effect of added EDT on the morphology of PbS QDs. They studied the triggered aggregation of nanocrystals PbS that can be used to assemble the nanocrystals into relatively ordered larger scale structures. They

mentioned that the use of High EDT concentration and longtime reaction will lead to the formation of the PbS nano-belts. EDT is a strongly interacting molecule and has been considered to increase solar cell efficiencies for polymer solar cell [47]. However they do not appear to be any studies concerning the effect of EDT added on PbS QDs dispersion stability or self-assembly. The effect of high EDT Values on QD morphologies can be further studied. As our objective was to exchange the OA with EDT ligand, we stopped at this level. CdTe is known for QDs Spontaneous organization into crystallites via aggregation recrystallization [48].It was caused by the ligand removal by colloid dissolution using solvent mixing. In our case simply adding EDT caused this self-assembly, it must likely that ligand displacement by EDT is the responsible of the change in morphology. By minimizing the EDT concentration to 0.3 ml, the nanobelt morphology was still observed but in less quantity.

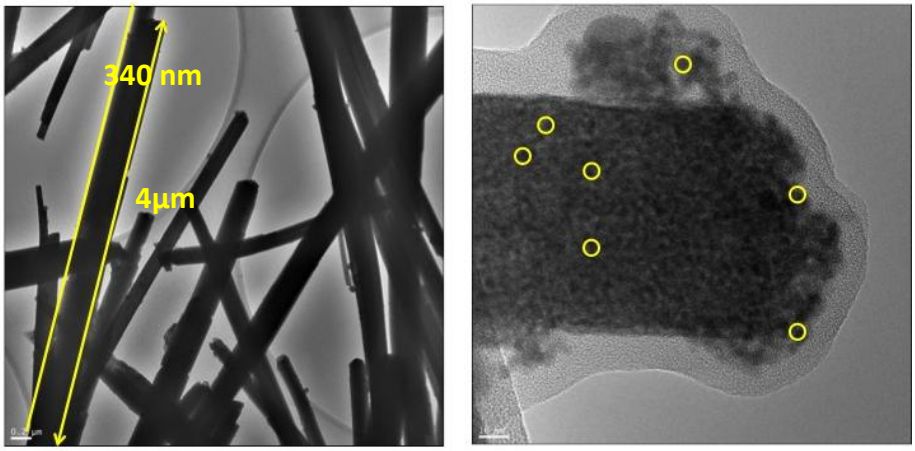

Figure 4- 12- TEM image of PbS Nanobelts after Ligand Exchange with EDT

Figure 4- 13 , reveals the linear absorption spectra of the PbS nanobelts exhibit blue shift from 1467 nm to 1380 nm in the absorption edges compared to that of the PbS NPs before ligand exchange. Figure 4- 14 shows the FT-IR transmission spectra of PbS NPs before and after ligand exchange with EDT. , OA capped PbS nanoparticles, and non-capped PbS respectively. The identified peaks in the OA spectrum corresponds to the long alkyl chain, the double bond between carbon atoms and the carboxylic acid group[49]. It shows the antisymmetric C H stretching vibration of the CH_2 group around 2920 and the CH_2 deformation vibration at 1465 cm^{-1}.

Namely, the surface-capping agent capped on the surface of PbS nanoparticles not by physically adsorption, but undergoes chemical reaction process. The broad band near

3447 cm^{-1} in Figure 4- 14 indicates that there are large amounts of adsorbed water in the capped and non-capped PbS nanoparticles due to the high surface energy of nanoparticles. On the other hand these peaks disappear after ligand exchange with EDT.

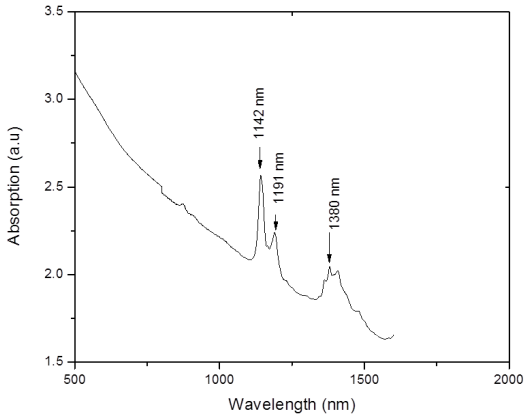

Figure 4- 13- Absorption spectrum – PbS nanoparticles after Ligand Exchange with EDT

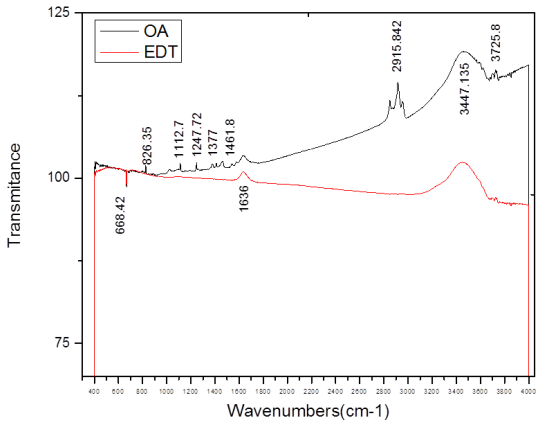

Figure 4- 14- FTIR Spectra of PbS nanoparticles

Ligand Exchange with MPA:

The same process was applied for MPA ligand exchange, and the PbS NPs were dispersed in Toluene.

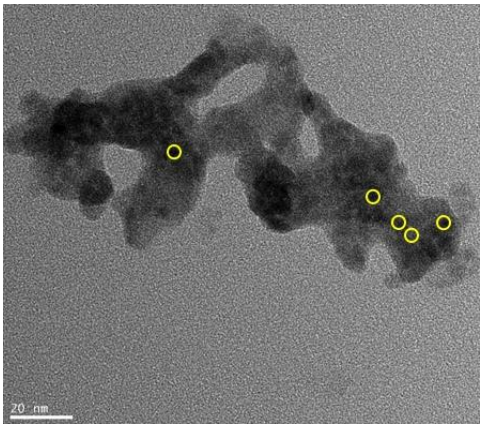

Figure 4- 15- TEM images of PbS NPS of 5.4 nm after Ligand Exchange with MPA

TEM images Figure 4- 15 illustrates the aggregation of the PbS NPs after ligand exchange with MPA spaced by ~ 1 nm.

Conclusion:

The ligand exchange process needs to be optimized, further investigations can be done on the nanobelt aggregated PbS NPs. Organic ligands is still present.

4-6- Attachment of PbS NPs by ex-situ growth

The PbS nanoparticles bought from MKNano were used in this experiment. Different techniques were employed, manual deposition with a drop on the surface of the substrate with and without Nanowires treatment.

4-6-1 Dropping of PbS Nanoparticles dispersed in toluene solution

PbS NPs were dropped on the surface of the substrate manually using a pipette Figure 4- 16. To facilitate the attachment of the NPs on the surface of the ZnO NWs, The ZnO Nws were pretreated by a surfactant. Different surfactants were used like Olamine(OLA) , Dioctyl sodium sulfosuccinate (AOT).

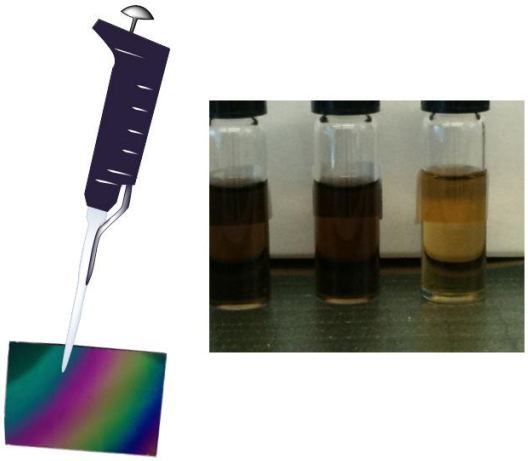

Figure 4- 16- Manual impregnation

OA capped PbS NPs deposited manually on ZnO NWs

The PbS deposition is confirmed by TEM that shows in Figure 4- 17 that the PbS NPs of 5.4 nm of diameter, are deposited randomly on the ZnO NWs . The PbS NPs are capped with an organic material, some are deposited on top of the top of the NWs and they are distributed randomly on the lateral surface of the ZnO Nws.

SEM top View

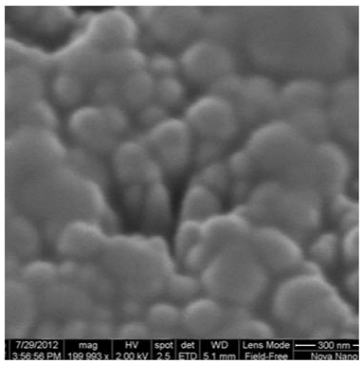

TEM images

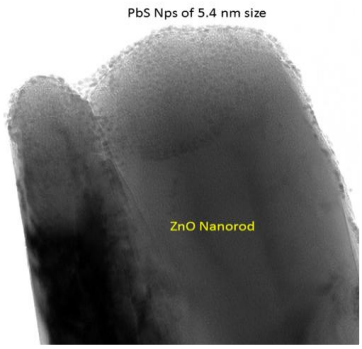

TEM images

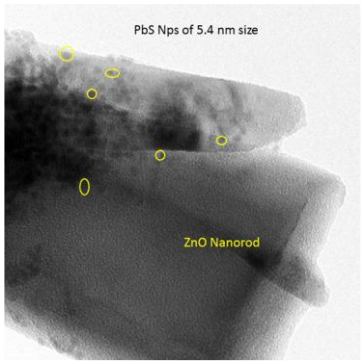

Figure 4- 17- SEM and TEM Images of OA capped PbS NPS deposited on ZnO Nanorods

On the other hand, PbS NPs with MPA ligand were deposited manually on top of the ZnO NWs. Figure 4- 18 illustrates the SEM Images of PbS NPs with MPA ligand deposited manually on ZnO NWs.

SEM images

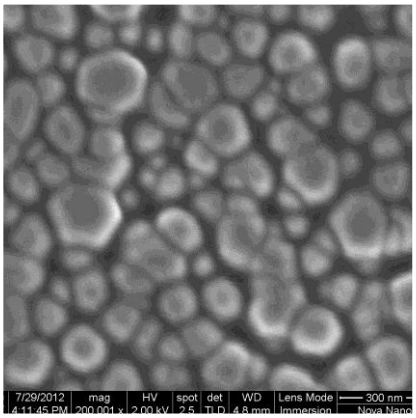

Figure 4- 18- SEM image of PbS NPS with MPA Ligand deposited on ZnO NWs

4-6-2 Dip Coating of Substrate in three different solutions of OA capped PbS Nanoparticles of different sizes:

In order to have a triple junction and to cover the solar spectrum different sizes of PbS NPs have to be deposited on the surface of the ZnO NWs.

Experimental process:

Three solutions of different sizes were prepared:

S1 is composed of 0.5 ml of OA capped PbS NPs of 2.4 nm + 1 ml toluene.

S2 is composed of 0.5 ml of OA capped PbS NPs of 3.2 nm + 1 ml toluene.

S3 is composed of 0.5 ml of OA capped PbS NPs of 5.4 nm + 1 ml toluene.

The Sample was deposited three times for 60 s in S1 after being dried by Nitrogen. The process is repeated with the other two solutions S2 and S3. TEM images confirm the deposition of the PbS NPs of different sizes (Figure 4- 19).

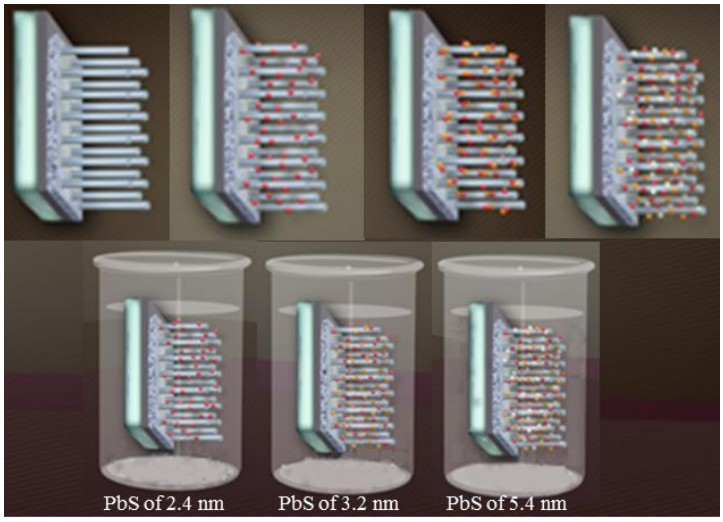

Figure 4- 19: illustration of Deposition process of 3 different sizes of PbS NPs.

It is noticed from TEM images figure 4-20, that some NPs were attached on the lateral surface of the NWs, while the majority was deposited on the Seed Layer (bottom of the ZnO NWs). PbS NPs of the different sizes were identified in the TEM images. The TEM image of PbS NPs–ZnO NWs was observed after scratching the top surface of the substrate and putting it on the TEM Grid during the sample preparation.

Figure 4-21 illustrates the PL spectra of the deposited PbS NPs of different sizes. It present different peak positions of the band edge emission in the UV region as well as defect induced emissions in the visible region.

It is dominated by a strong, narrow ultraviolet (UV) emission centered at 380.1 nm (3.2623 eV). Other broad peaks were identified in the visible region (3.2623eV).

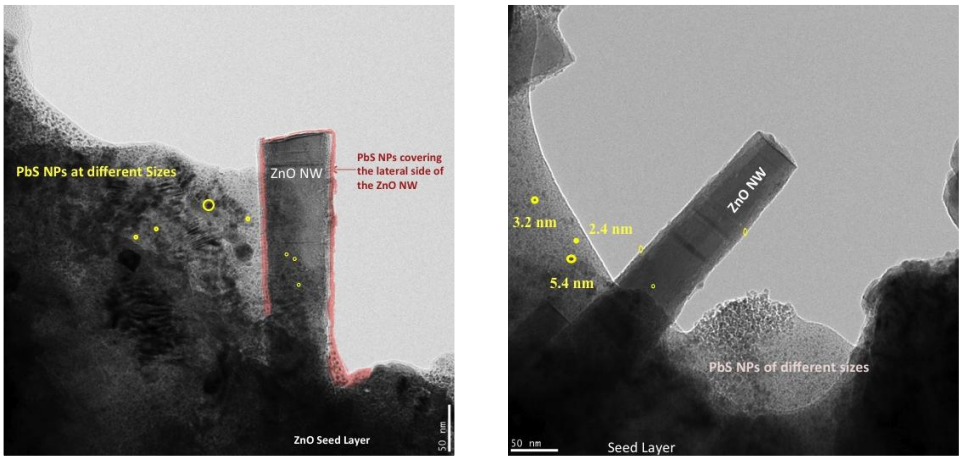

Figure 4- 20- TEM images of the PbS NPs of different sizes deposited by dipping for 60 s on ZnO NWs grown by PLD

This UV emission is attributed to free exciton recombination a near band transition of wide band gap ZnO. As seen from Figure 4- 21a, the green and yellow emission of the visible region is shown. Figure 4-21-b presents the PL spectrum excited with Xenon lamp at 650 nm. More peaks at 882 nm and 1003 nm were identified, showing the presence of the 2 different sizes of the PbS NPs of 2.4 and 3.2 nm.

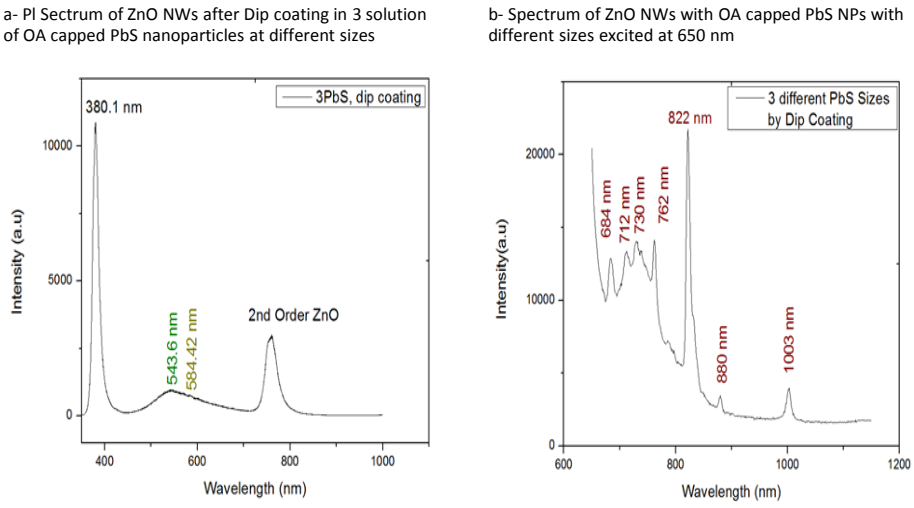

Figure 4- 21- Spectrum of ZnO NWs / PbS NPs of 2.4, 3.2 and 5.4 nm of diameter, a- excitation by HeCd laser at 325 nm, b- excitation by xenon Lamp excitation at 650 nm

Conclusion:

The PbS NPs were attached on the surface of the ZnO NWs by the mean of organic ligand. Still the Process of Ligand exchange should be optimized.

4-6-3 In-situ growth of PbS NPs by SILAR Technique

SILAR method is relatively a new method, first reported in 1985 by Ristov *et al*.[50] The name SILAR was ascribed to this method by Nicolau (1985) [51]and discussed in subsequent papers of Nicolau and coworkers (Nicolau and Minnard 1988 [52]; Nicolau *et al* 1988[53]), which deals with ZnS, CdZnS and CdS thin films.

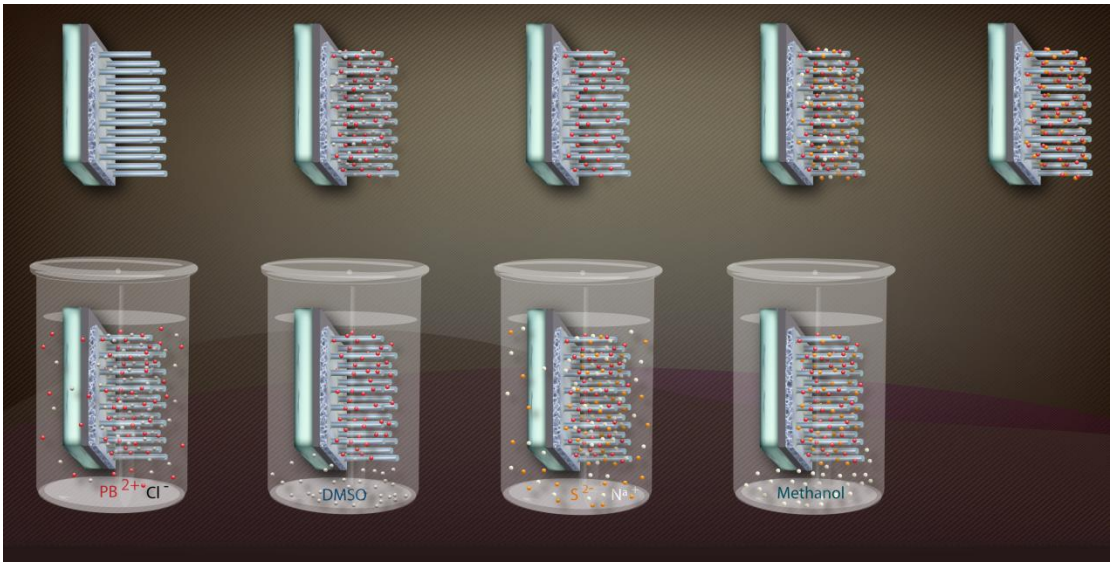

Figure 4- 22- The scheme of SILAR method for the deposition of PbS thin films (○Pb^{2+}; ● S^{2-}): (a) Pb^{2+}cationic precursor, (b) ion exchange water, (c) S^{2-}anionic precursor and (d) ion exchange water

SILAR method has many advantages like:

- It does not require high quality target and/or substrates nor does it require vacuum at any stage, which is of a great advantage for industrial application,
- The deposition rate and the thickness of the film can be easily controlled by changing the deposition cycles,
- The processing is done at room temperature can produce films on less robust materials,
- There are no restrictions on substrate material, dimensions or its surface profile.
- It is relatively inexpensive, simple and convenient for large area deposition.
- The starting materials are commonly available and cheap materials.

In our research, he SILAR technique will be employed for the attachment of the PbS NPs on the ZnO NWs.

4-6-3-1 Substrate pre-treatment

The cleanness and hydrophilicity of substrates play an important role in the deposition of films. Contaminated substrates result in nonuniform film formation. The surface of the free standing ZnO NWs is hydrophobic , therefore oxygen plasma ashing (Figure 4- 23) was performed for 3 minutes to make ZnO Nws hydrophilic to get better wettability. It also removes organic matter; the products being carbon oxides and water vapor, which are volatile and pumped away by the vacuum system.

The oxygen plasma may modify the ZnO Nanowire surface in many ways to enhance the QD adsorption. The oxygen plasma charges the Nanowire surface, create dangling bonds through ion bombardments, and or remove surface contaminations. The surface hydroxyl and hydrocarbon species may prevent the QDs from attaching to the nanowire surface through the carboxyl group and adversely affect the surface coverage of the nanowires.

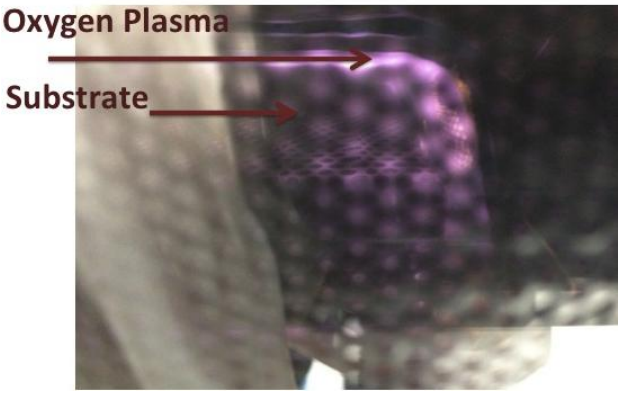

Figure 4- 23- Plasma Ashing

4-6-3-2 Experimental Process

Different trials were performed presented here as scenarios. The first one presents the process of dipping the ZnO NWs in Anionic and cationic solutions without rinsing or drying. The second scenario is to mix the two solutions (anionic and cationic) together and leave the ZnO NWs dipped for 24 hours in the compound solution. The third scenario is the regular SILAR process, which include the 3 phases of dipping in cationic and anionic solution, then rinsing and finishing by drying. Different substrates were selected for these experiments such as ZnO NWs grown by hydrothermal by our colleague “Anisha Gokarna, IEMN, France), ZnO NWs grown by PLD, ZnO Nanowall Network with honeycomb structure deposited by PLD too.

Scenario 1: SILAR without Rinsing

ZnO NWs were dipped successively into $PbCl_2$ dissolved in 10 ml of Dimethyl sulfoxide (DMSO) solution for different period of times(40 s and 60 s) dried in Nitrogen and then dipped again for 40s /60 s into Na_2S dissolved in Methanol and DMSO. Illustration of Process presented in Figure 4- 24.

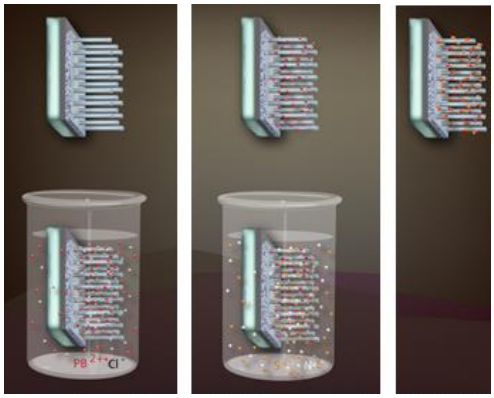

Figure 4- 24-Illustration of the SILAR Process without Rinsing

Different parameters were changed summarized in Table 4- 2.

Table 4- 2- Parameters set in Scenario 1

	$PbCl_2$ (mg)	Na_2S (mg)	Na_2S Solvent	Dip time	# of Cycles	
S1-1	16.8	4.8	DMSO	40 s	7 cycles	
S2-1	16.8	4.8	Methanol	60 s	6 cycles	
S3-1	16.8	4.8	Methanol	60 s	6 cycles	No drying
S1-2	18.4	5.21	Methanol	60 s	10 cycles	

5 solutions with different concentration and different solvents were prepared:

The cationic Solutions A1, and A2 are composed of 16.8 mg of $PbCl_2$ dissolved in 10ml DMSO, and 18.4 mg of $PbCl_2$ also dissolved in 10 ml DMSO respectively.

The anionic Solution B1, B2 and B3 are composed of 4.8 mg of Na_2S dissolved in 10 ml of Methanol and 5.21 mg of Na_2S in 10 ml of Methanol and 4.8 mg of Na_2S in 10 ml of DMSO respectively. Substrate A, ZnO NWs were dipped successively into Solution A1 for 40 s dried in Nitrogen and then dipped again in solution B3 for 40s. This cycle was repeated 7 times. By changing the Solvent of the anionic solution, and the time of dipping, substrate B was dipped successively into Solution A1 for 60 s dried in Nitrogen and then dipped again in solution B1 for 60s. This cycle was

repeated 6 times. In order to see the effect of drying the substrate C was dipping in the same conditions as substrate B but without drying.

Figure 4- 25 a,b, and c reveals the top view of the ZnO NWs sensitized by PbS NPs. The PbS NPs were randomly distributed on top of the ZnO NWs. Figure 4- 25 illustrates the TEM images of the co-sensitized ZnO NWs by PbS NPs. It is clearly shown that the PbS NPs distributed homogeneously on the lateral sides of the ZnO NWs size of 5-7 nm. On the other hand the concentration was increase and substrate D was dipped successively into Solution A2 for 60 s dried in Nitrogen and then dipped again in solution B2 for 60s. This cycle was repeated 10 times. Figure 4- 25 d reveals the ZnO Nanowall network with honeycomb structure after PbS deposition, the NPs were distributed randomly on the surface with a size of 9-12 nm.

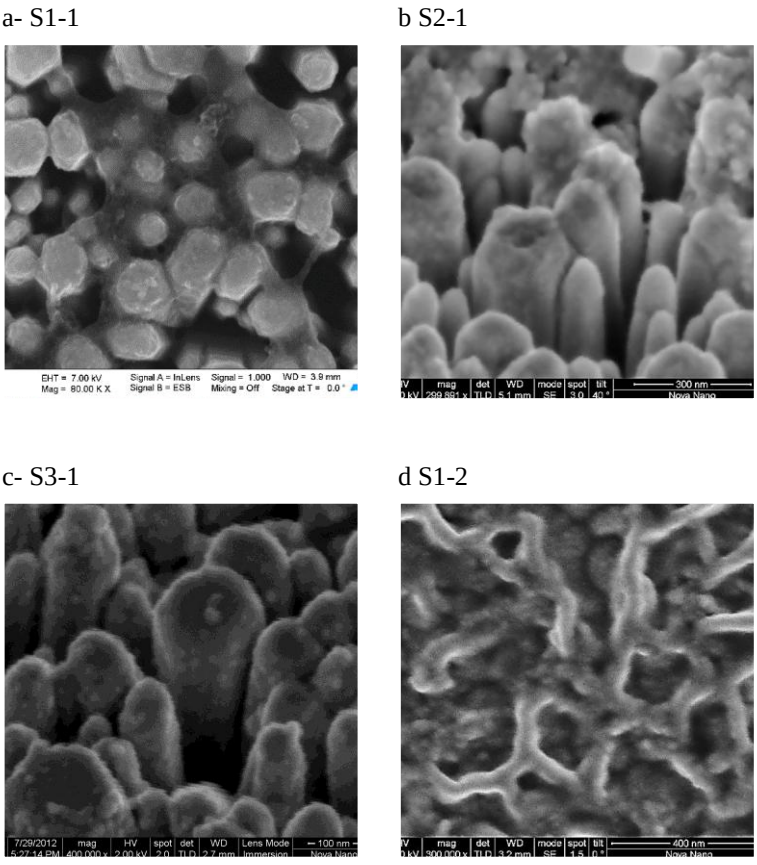

Figure 4- 25- SEM Images of PbS deposition on a,b,c) ZnO Nws grown by Hydrothermal d) ZnO nanowall

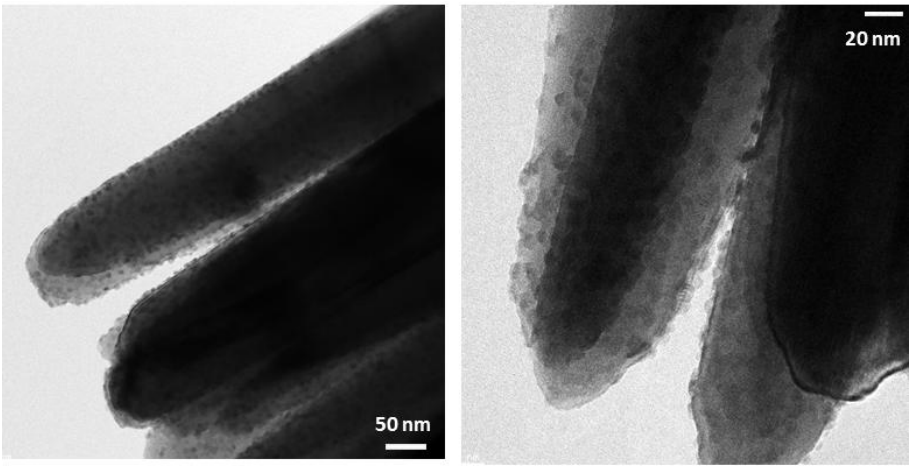

Figure 4- 26-TEM Images of PbS NPs Grown by SILAR on ZnO NWs synthesized by Hydrothermal .

Figure 4-26 is the TEM image of the as-synthesized PbS NPs. Nearly mono-disperse PbS NPs with a diameter of about 6 nm were synthesized successfully. The average size of particles was 5 ± 0.7 nm, with sizes ranging from 4-6 nm.

The TEM image of PbS NPs–ZnO NWs displays that each ZnO nanowire was decorated by PbS NPs. High density of PbS NPs attached along the surface of the ZnO nanowires (~700 nm in length and ~100 nm in diameter).

The TEM image of PbS NPs–ZnO NWs was observed after scratching the top surface of the substrate and putting it on the TEM Grid during the sample preparation. PbS NPs nanoparticles did not dissociate from ZnO nanowires, which confirmed that PbS nanoparticles were well fixed on the ZnO nanowire surface.

The study of the photoluminescence property can provide some information about defects in the nanostructure arrays and show their potential applications. The curves a, b, and in Figure 4-27 demonstrate the photoluminescence spectra of the ZnO/PbS nanostructure arrays of Samples S1-1,S3-1 and S1-2, respectively. RT PL spectra show a strong ultraviolet (UV) emission and broad visible emission. It is reported that the UV emission originates from the recombination of free excitons in the near-band-edge of the wide band gap ZnO and the broad visible luminescence has commonly been attributed to the oxygen vacancies of ZnO[54]. The appearance of the broad visible PL band indicates that there are oxygen vacancies in the synthesized ZnO nanowire arrays. Both theoretical and experimental results have proved that the oxygen vacancies can increase the electrical conductivity remarkably by inducing defect states in the band gap [55][56]. In this case, oxygen vacancies can improve the electrical transport properties of ZnO just as an n-type dopant in the nanostructures.

After the PbS growth, the ZnO/PbS basically exhibit the PL behavior of the ZnO cores with a small blue shift in the UV region and a slight decrease in luminescence intensity. The shift in the PL spectrum can be attributed to the strain caused by the lattice mismatch between ZnO and PbS. Both of the PL spectra show a broad visible band, implying that the prepared ZnO and ZnO/PbS nanostructures should have preferable electronic transport properties.

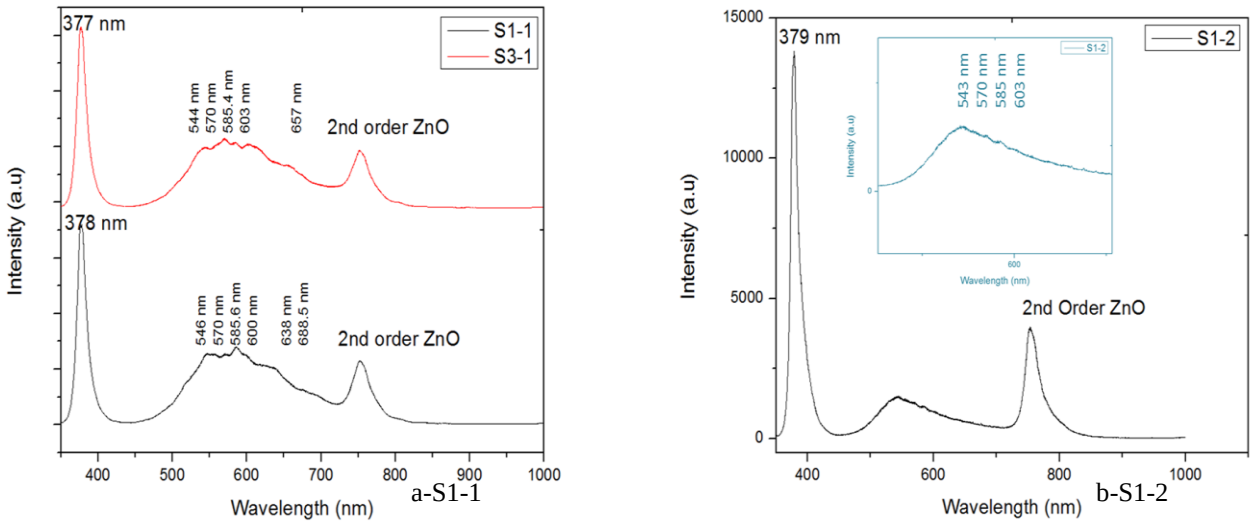

Figure 4- 27- PL Spectra of PbS deposition on a) ZnO Nws grown by Hydrothermal b) ZnO nanowall

From the optical band gap (in eV), the diameter (d in nm) of PbS QDs can be calculated following the empirical equation developed by Iwan Moreels et al[57].

$$E_g = 0.41 + (0.0252d^2 + 0.283d)^{-1}$$

$$0.0252d^2 + 0.283d - \frac{1}{E_g - 0.41} = 0$$

Table 4- 3- The optical band gaps and the diameters of PbS quantum dots

Wavelength (nm)	Eg (eV)	D (nm)
653	1.89868	2
749	1.65533	2.347
761	1.629227	2.3896
820	1.512	2.603
822	1.5083	2.610

Scenario 2: Mixing cationic and anionic solutions

In this set of experiments 1.5 ml of cationic (Pb^{2+}) solution and 1.5 ml of anionic (S^{2-}) were mixed together. The substrates were submersed and left in the mixed solution for around 18 hours. Process is illustrated in Figure 4- 28a. The different mixed solutions are presented in Figure 4- 28b. Parameters of the concentration of the 2 solutions and solvent used are presented in Table 4- 5.

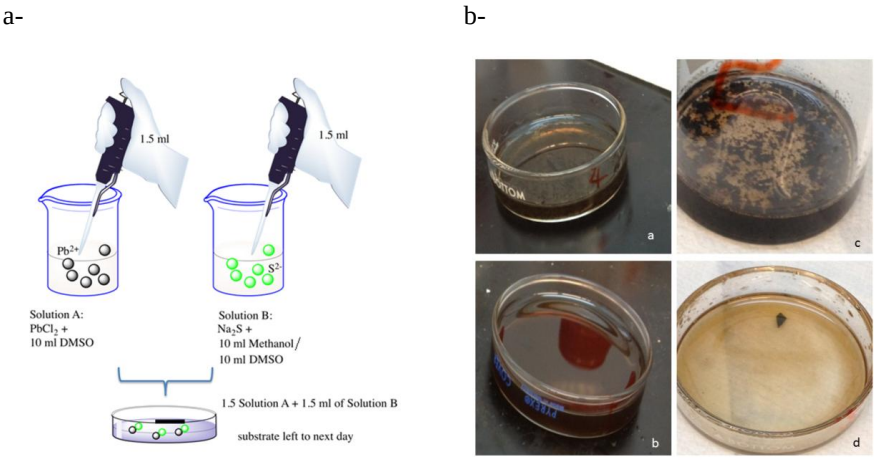

Figure 4- 28- a- Illustration of PbS synthesis process, and b- ZnO substrates immersed and left in the different mixed solutions

16.8 mg of $PbCl_2$ dissolved in 10 ml of DMSO , was mixed with 4.8 mg of Na_2S dissolved in Methanol were mixed the Substrate A was left dipped in the mixed solution for 18 hours . On the other hand substrate B was left dipped for 18 hours in a mixed solution of 16.8 mg $PbCl_2$ dissolved in 10 ml DMSO with 4.8 mg of Na_2S dissolved in DMSO. By increasing the concentration of cationic and anionic precursors, two mixed solutions were prepared. 1.5 ml of solution A (18.4 mg of $PbCl_2$ with 10 ml DMSO) was mixed with 1.5 ml of solution B (5.21 mg of Na_2S dissolved in 10 ml Methanol). 1.5 ml of solution A (18.4 mg of $PbCl_2$ with 10 ml DMSO) was mixed with 1.5 ml of solution B' (5.21 mg of Na_2S dissolved in 10 ml DMSO). Substrate C and D were left dipped in the two mixed solution respectively for 18 hours. Summary of the concentrations summarized in Table 4- 3.

Table 4- 4- Parameters of the PbCl2 and Na2S concentration and the different solvents used

	$PbCl_2$ (mg)	Na_2S (mg)	Solvent
S4-1	16.8	4.8	Methanol
S5-1	16.8	4.8	DMSO
S2-2	18.4	5.21	Methanol
S3-2	18.4	5.21	DMSO

Obviously, aggregated particles are deposited on the top of the ZnO nanorods arrays. The formation of the aggregated particles is due to inconsistent nucleation and growth rate at this sol concentration, and the diameter of these clusters is too large to enter into the narrow gap of the ZnO nanorods, so most of PbS particles are accumulated on the top of ZnO nanorods. Figure 4- 29 illustrates the SEM images of the PbS nanoparticles on top of the Nanorods. Figure 4- 29a shows the hexagonal shape of the PbS particles which size varies between 600 and 1300 nm covering some areas of the substrate. For Substrate B Figure 4- 29b, aggregated nanoparticles of different sizes aggregated on the top of the Nanorods sizes vary between 30- 75 nm.

On the hand , Figure 4- 29 c reveals the SEM images of substrate C , PbS particles of 550 nm diameter distributed on the top of the Nanorods. Figure 4- 29 d , shows the deposition of PbS particles (100-140 nm) on the top of the Nanorods and we can see small PbS NPS (20-50 nm) distributed on top of the ZnO NWs.

TEM images (Figure 4- 30) confirm the circular shape of the PbS NPs of the substrate B ranging from 30nm to 75 nm with an average size of 63 nm. The aggregated PbS particles on the top of the ZnO nanorods , implies that the growth rate of the PbS particles is too fast .

a- S4-1

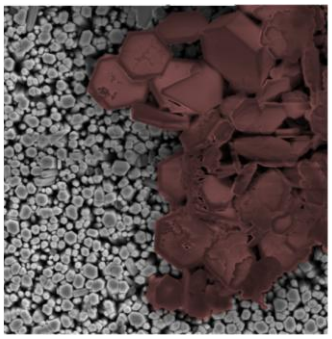

b- S5-1

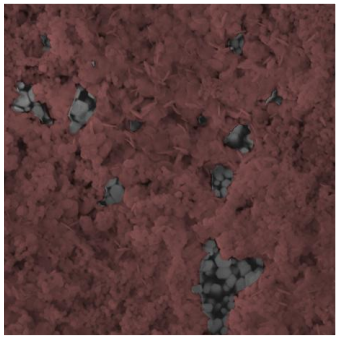

c- S2-2

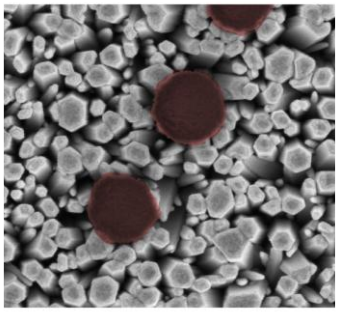

d S3-2

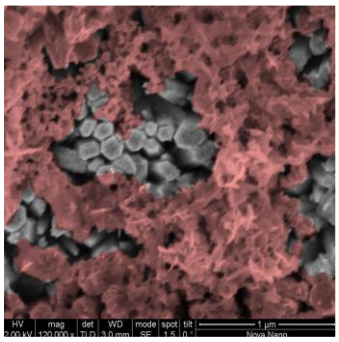

Figure 4- 29- SEM images of PbS NPS synthesized by mixed 2 solutions with differnet concentrations of cationic Pb2+ and anionic S2- on ZnO NWs grown by hydrothermal.

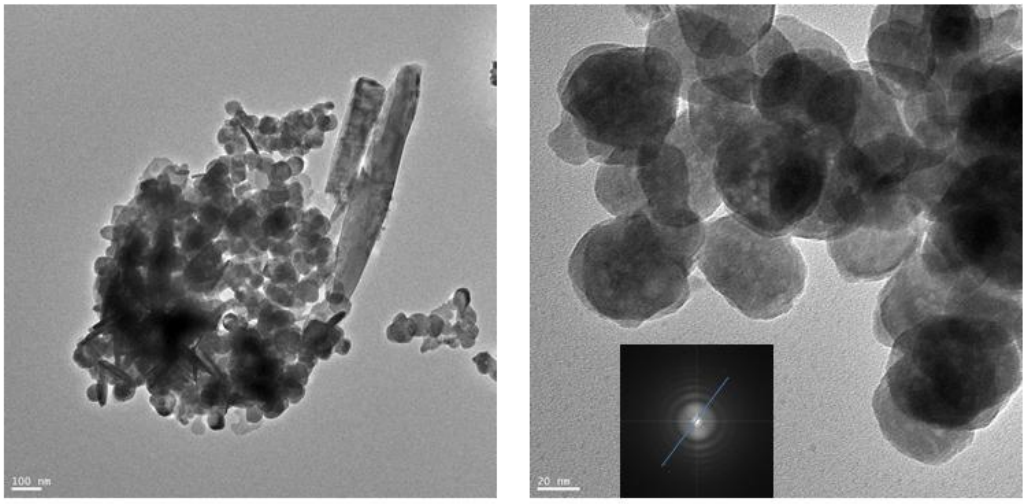

Figure 4- 30- TEM Images of PbS NPs synthesized by mixing 1.5 ml of $PbCl_2$ dissolved in 10 ml of DMSO and 1.5 ml of N_2S dissolved in 10 ml of DMSO.

PL results similar to the one we got previously. Figure 4-31 depicts the PL spectra of the 3 samples. It shows an intense peak at 378 nm for sample S4-1 and S2-2 while S5-

1 the UV shift had a blue shift to 376 nm. On the other hand more peaks can be identified in the visible range. Sample S5-1 reveals very intense in the visible zone higher than the UV peak at 376 nm.

a- S4-1

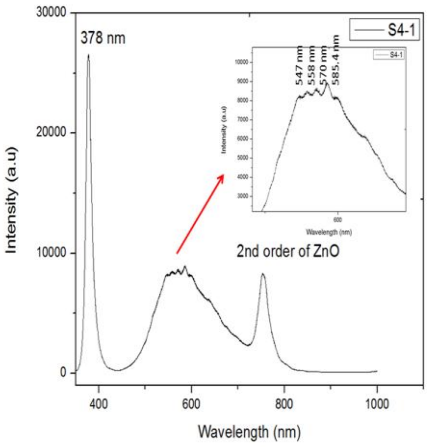

b- S5-1

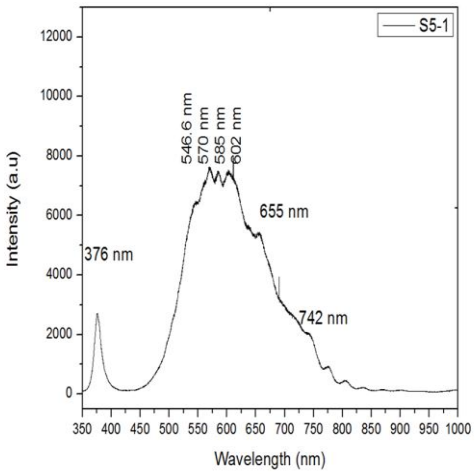

c- S2-2

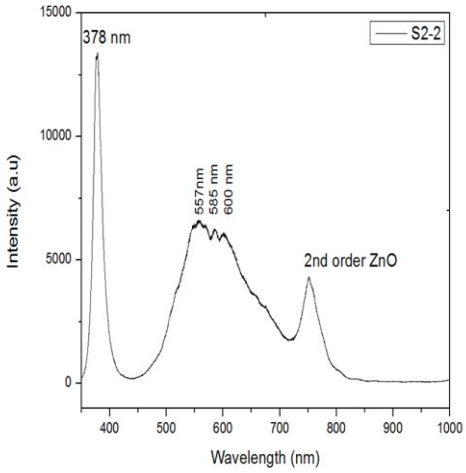

Figure 4- 31- PL Spectra of the PbS NPs syntehsized by Mixed cationic Pb^{2+} and anionic S^{2-} solutions

Scenario 3: SILAR with rinsing

ZnO NWs were dipped successively into $PbCl_2$ dissolved in 10 ml of Dimethyl sulfoxide (DMSO) solution for different period of times(60s / 70s) rinsed and dried in Nitrogen and then dipped again for (60s / 70s) into Na_2S dissolved in Methanol. The rinsing was done in same solvent or in distilled water. Illustration of Process presented in Figure 4- 32.

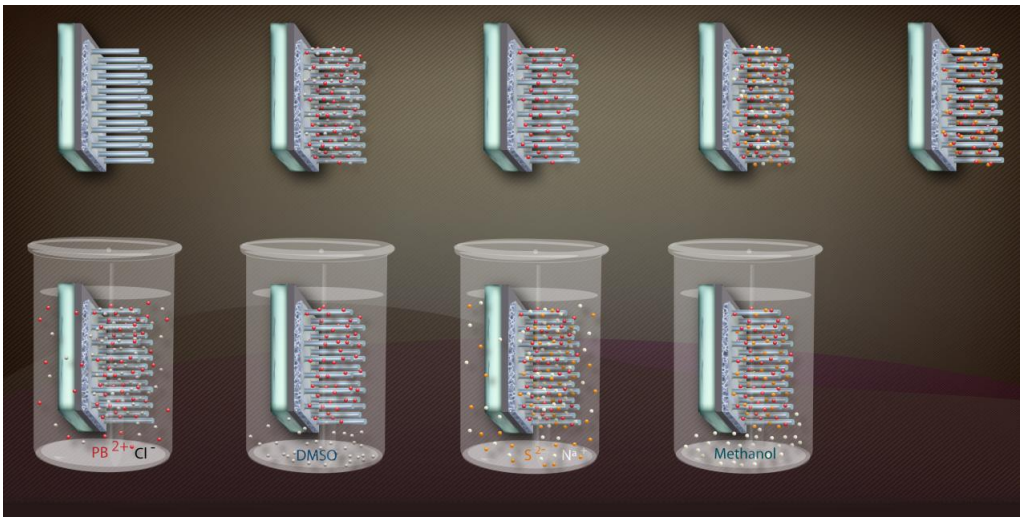

Figure 4- 32- Illustration of the SILAR Process

Table 4- 5- Parameters of PbS synthesized used in the SILAR method in different conditions and on different types of ZnO nanostructures.

	Rinsing	Dipping time	# of cycles	Comments
S 5-2	DMSO/Methanol	60s	10 cycles	Hydro- NWs
S2-4	DMSO/Methanol	60s	10 cycles	Short NWs

Sample A and B composed of ZnO Nanorods synthesized by hydrothermal method and ZnO NWs grown by PLD respectively. The 2 samples were dipped successively, into $PbCl_2$ Dimethyl sulfoxide (DMSO) solution for 60 seconds, rinsed with DMSO for 10 s and dried with Nitrogen (N_2). Than they were dipped into Na_2S Methanol solution for another 60s, rinsed with Methanol for 10 s and dried with N_2. This whole process is referred to as one full coating cycle that has been repeated 10 times. . It clearly shows that PbS NPs have been deposited on ZnO NWs with different sizes and that it has been successfully distributed on the lateral of the ZnO NWs instead of only on the top, which will play the important role in improving the conversion

efficiency. It is noticed that the deposited PbS NPs has spherical shape, the size of PbS NPs for Sample A (Figure 4- 33a), ranges from 6 nm- 13.5 nm which was confirmed by TEM (Figure 4- 34). While for sample B Figure 4- 33b the size of the NPS was around 8 nm. The TEM image of PbS NPs–ZnO NWs displays that each ZnO nanowire was decorated by PbS NPs. The density of Pt particles was estimated to be 24-30 attached along one face of ZnO nanowires (~110 nm in length and ~70 nm in diameter), The TEM image of PbS NPs–ZnO NWs was observed after scratching the top surface of the substrate and putting it on the TEM Grid during the sample preparation. PbS NPs nanoparticles did not dissociate from ZnO nanowires, which confirmed that PbS nanoparticles were well fixed on the ZnO nanowire surface.

a- Tilted view of co-sensitized ZnO Nanorods by Hydrothermal with PbS NPs

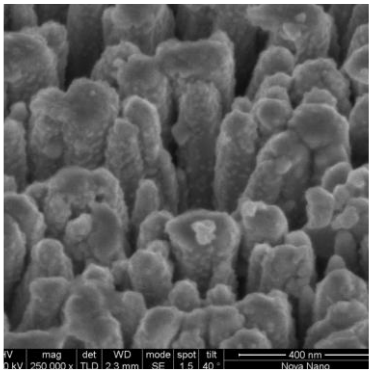

b- Tilted view of co-sensitized ZnO NWs by PLD with PbS NPs

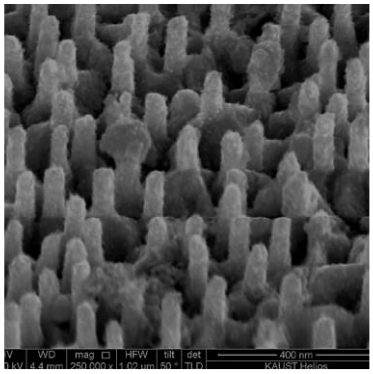

c- PL Spectrum of co-sensitized ZnO Nanorods by Hydrothermal with PbS NPs

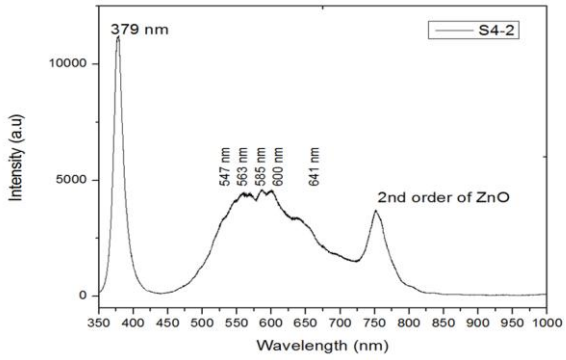

Figure 4- 33- SEM images tilted view of PbS NPs grown by SILAR method on a- PbS NPS on ZnO NWs by Hydrothermal rinsing with DMSO/ Methanol , b- PbS NPs on ZnO NWs grown by PLD rinsing with water c- PL Spectrum of sample S5-2

Figure 4-33 reveals the RT PL spectra of the S4-2 showing a sharp peal in at 379 nm which correspond to ZnO (as previously mentioned) and broad weal peaks in the visible zone between 540 nm and 641 nm).

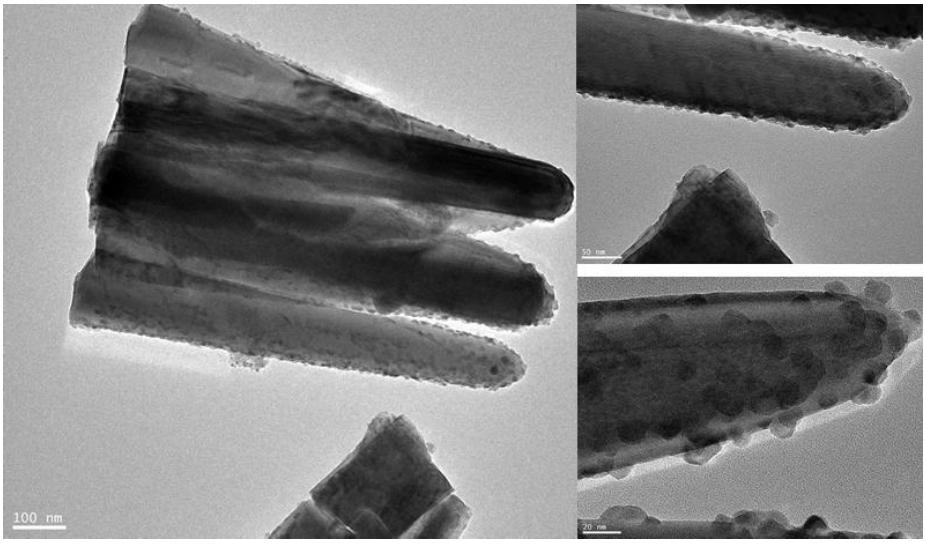

Figure 4- 34- TEM images of PbS NPs synthesized by SILAR method on ZnO NWs grown by Hydrothermal technique rinsing with DMSO/ Methanol Sample A

The sample C , ZnO NWs synthesized by PLD at 5 Torr, were dipped successively, into $PbCl_2$ Dimethyl sulfoxide (DMSO) solution for 70 seconds, rinsed with deionized water for 10 s and dried with Nitrogen(N_2). Than they were dipped into Na_2S Methanol solution for another 70s, rinsed with deionized water for 10 s and dried with N_2. This whole process is referred to as one full coating cycle that has been repeated 10 times. Figure 4- 30 a reveals the co- sensitized ZnO NWs with PbS NPS of 5-7 nm of size .The NPS were uniformly distributed on the lateral side of the ZnO NWs.

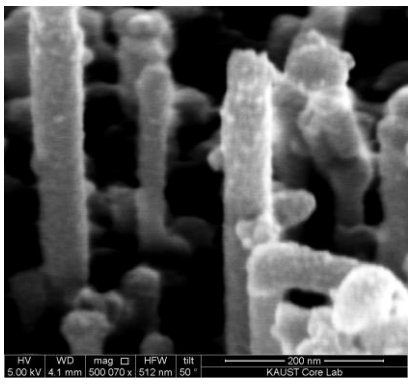

Figure 4- 35-Sem Tilted view of co-sensitized ZnO NWs by PLD with PbS Synthesized by SILAR by

Scenario 3a: Effect of number of cycles:

ZnO NWs Grown by PLD at 5 Torr of 1.3 µm lengths and diameter of 50 nm were used in this experiment. Parameters are summarized in table 4-6.

Table 4- 6- Parameters used for SILAR

	Rinsing	Dipping time	# of cycles
S1-4	DMSO/Methanol	70s	16 cycles
S1-3	DMSO/Methanol	70s	10 cycles
S1-5	DMSO/Methanol	70s	5 cycles

Sample A, B and C were dipped successively, into $PbCl_2$ Dimethyl sulfoxide (DMSO) solution for 60 seconds, rinsed with DMSO for 10 s and dried with Nitrogen (N_2). Than they were dipped into Na_2S Methanol solution for another 60s, rinsed with Methanol for 10 s and dried with N_2. This whole process is referred to as one full coating cycle that has been repeated 16, 10 and 5 times respectively. It was noticed that the substrate became dark after several cycles because of the deposition of small PbS NPs. Figure 4- 36 a,b show the top view and tilted view of the ZnO NWs without PbS NPS while Figure 4- 36 (c,d),(e,f), (g,h) illustrates the ZnO NWs sample A, B, C top view and tilted view of co-sensitized with PbS Nps at different cycles 16,10 and 5 respectively. It clearly shows that PbS NPs have been deposited on ZnO Nws with different sizes and that it has been successfully distributed on the lateral of the ZnO NWs instead of only on the top, which will play the important role in improving the conversion efficiency. It is noticed that the size of the deposited PbS NPs for 16 cycles ranges from 7 to 11 nm, while for 10 cycles it is ~ 8 nm and 3.6 nm for 5 cycles.

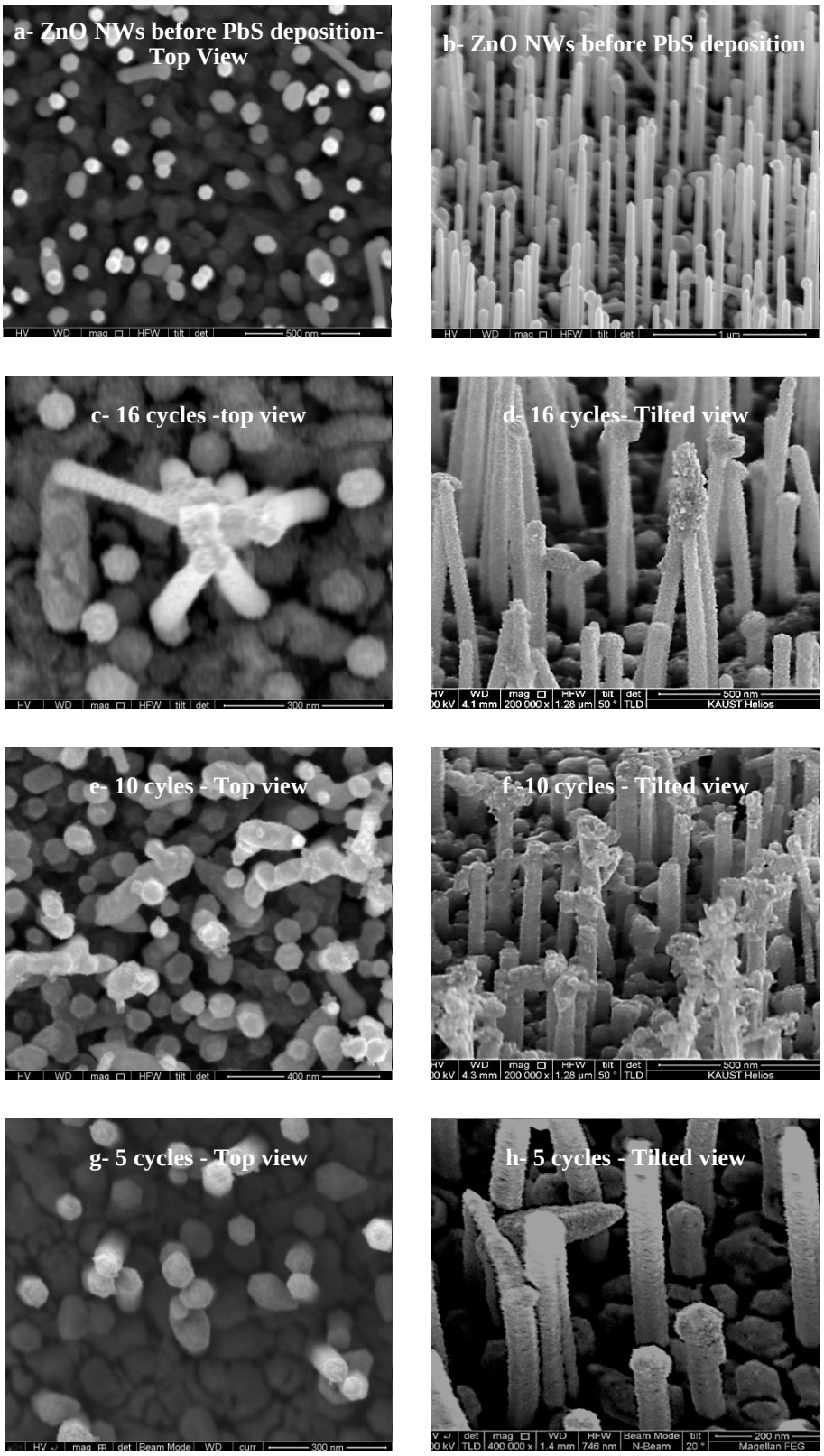

Figure 4- 36- SEM images of ZnO NWs grown by PLD Top (a,c,e,g) and tilted (b,d,f,h) view , before PbS growth (a,b) and after PbS deposition for different cycles c,d – 16 cycles , e,f -10 cycles and g,h- 5 cycles.

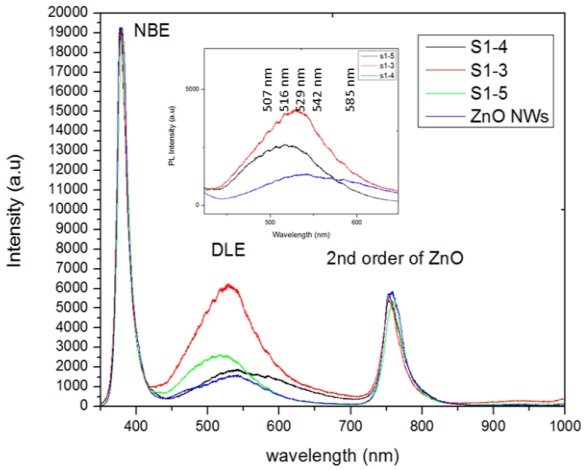

a-PL Spectra of ZnO Nanowires decorated with PbS Nanoparticles at different number of SILAR cycles

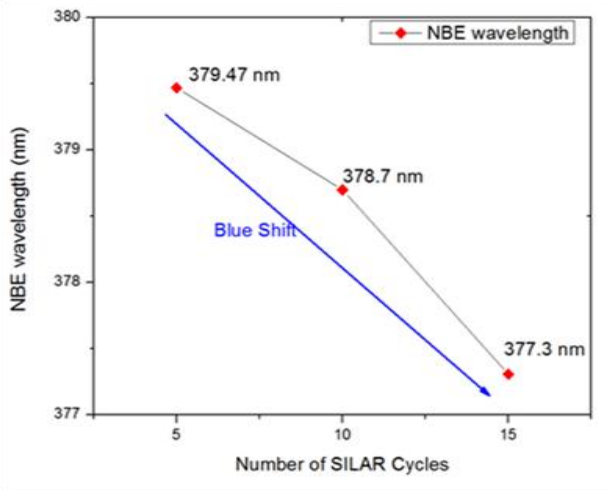

b-NBE wavelength in function of different number of SILAR cycles

Figure 4- 37- PL Spectra of the ZnO NWs grown by PLD a) at different SILAR Cycles and b) NBE wavelength of the ZnO NWs decorated by PbS NPs in function of number of cycles

Figure 4-37a depicts the PL measurements at Room Temperature using HeCd laser (325 nm, 8 mW) for all the 3 samples. It is clear the deposition of PbS nanoparticles at different number of cycles (5 , 10 and 15 cycles) on ZnO nanowires showed very similar PL spectra, dominated by a strong narrow ultraviolet (UV) emission centered at 379.47 nm (3.26 eV) , 378.7 nm (3.274 eV) and 377.3 nm (3.289 eV) respectively . By increasing the number of the cycles the corresponding NBE shows a blue shift (figure 4-37b). The shift in the PL spectrum can be attributed to the strain caused by the lattice mismatch between ZnO and PbS. Both of the PL spectra show a broad visible band, implying that the prepared ZnO and ZnO/PbS nanostructures should have preferable electronic transport properties. The DLE band is broad and intense. It is composed of an emission peak centered in the green and yellow band. The peak in the green zone is assigned to shallow donor effects (oxygen vacancies) at 517.47 nm, 529 nm and 543 nm corresponding the 5, 10 and 15 SILAR cycles respectively. The peak in the yellow zone is assigned to deep effects (oxygen interstitials) at 584 nm. The intensity ratio NBE to DLE for the green emission is respectively 7.2,3 and 10.1 which shows that the intensity of the green emission is lower at higher concentration. On the other hand the intensity ratio NBE to DLE for the yellow emission is 20, 6.86 and 12 respectively to the number of SILAR cycles. It is noticed that the intensity of

the DLE is the lowest before depositing the PbS Nanoparticles which implies surface modifications caused by the attachment of PbS on the surface.

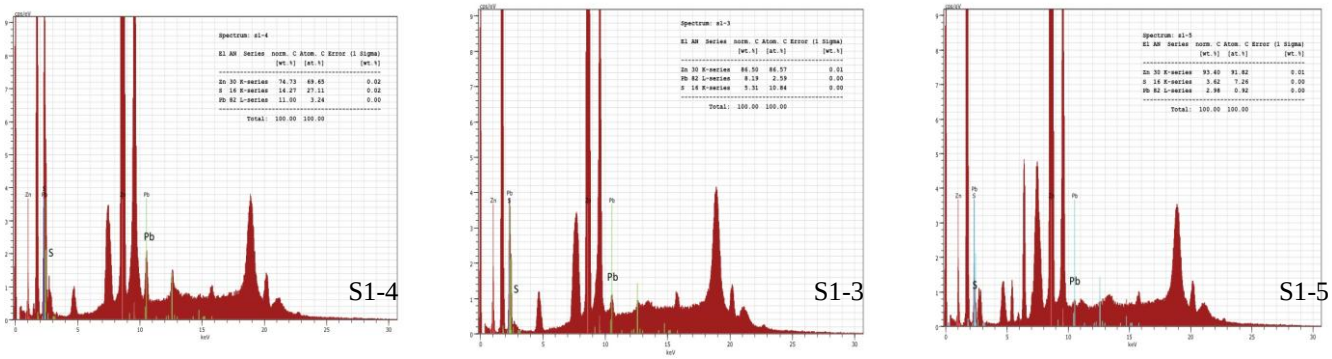

Figure 4- 38- XRF Spectra of the ZnO/PbS hetero-structure at different concentration.

Figure 4- 38 Shows the X-Ray fluorescence (XRF) data on the relative intensity of lead (Pb), Sulfur (S) and Zinc (Zn) in 3 different samples where ZnO NWs were grown by PLD and PbS deposited by SILAR with different number of cycles. The difference in intensity is due to the different concentration of PbS grown directly on the ZnO NWs. Higher intensity is identified in S1-4 which corresponds to the higher number of cycles.

PbS Nanoparticles synthesized by in-situ growth using SILAR method are polycrystalline. Figure 4- 39 illustrates the XRD spectra of the ZnO/PbS hetero-junction. The Plane (220) of PbS can be identified on the spectrum in addition to the plane of ZnO identified at 34.4° that corresponds to the plane (002). The (220) Plane of the PbS was also confirmed by TEM , that also reveals 2 other plane (111) and (200) based on the d spacing of the PbS NPs.

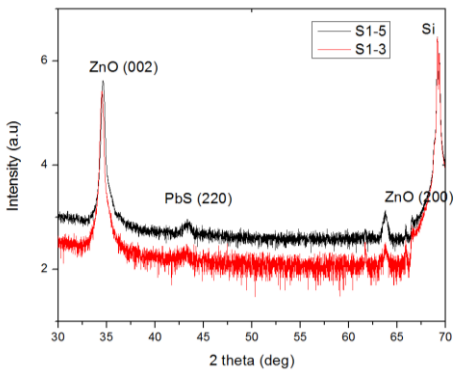

Figure 4- 39-XRD Spectra of ZnO/PbS hetero-Junction S1-5 and S1-3.

PbS NPs were grown on ZnO NWs by SILAR process at different number of cycles (16, 10, 5 cycles).

From the HR-TEM images shown in Figure [4-40], some important aspects, on how SILAR processed PbS QDs are deposited on the ZnO nanowires, are pointed:

1) After repeating the PbS SILAR process for 5, 10 and 16 times, PbS QDs were deposited homogeneously on the ZnO NWs surface.
2) The size of most PbS QDs deposited 5, 10 and 16 times are presented in table 4-7. The size of the PbS NPS is in the range of 3.1 to 4.3 nm , 4.7 to 6 nm and 7 to 9 nm diameter for 5 , 1- and 16 cycles respectively .the shape is hemispherical, facing towards the ZnO surface.
3) Much of the ZnO Nanowire surface is still plain, that is, not covered with PbS QDs. The density increases with the increasing number of cycles.
4) FFT images reveals the d spacing of the deposited PbS NPs. The different planes identified are summarized in table 4-8.

It is expected that we still have many possibilities to improve the photovoltaic performance by finding a way of depositing a higher density of PbS QDs.

Table 4- 7- Summary of PbS NPs sizes deposited at different number of Cycles

Sample	Number of Cycles	**PbS NPs Size** spherical Shape
S1-4	**16**	**~ 7nm-9 nm**
S1-3	**10**	**~ 4.7 nm- 6 nm**
S1-5	**5**	**~ 3.1 nm- 4.3 nm**

Three different d spacing were identified summarized in Table 4-11.

Table 4- 8- d spacing identified by TEM and its corresponding Plane

D (A°)	**Plane**
3.5	(111)
2.53	(200)
2.12	(220)

a- S1-4 (16 cylces)

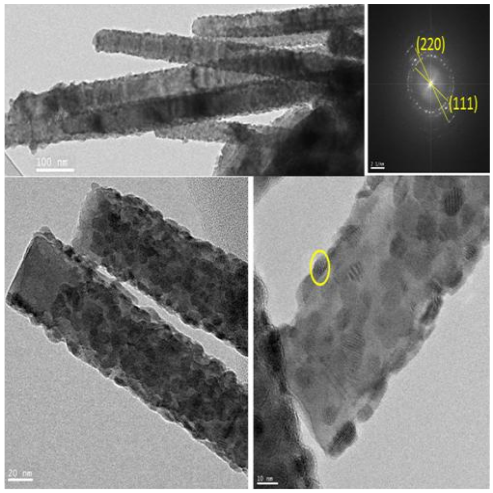

b- S1-3 (10 cycleS)

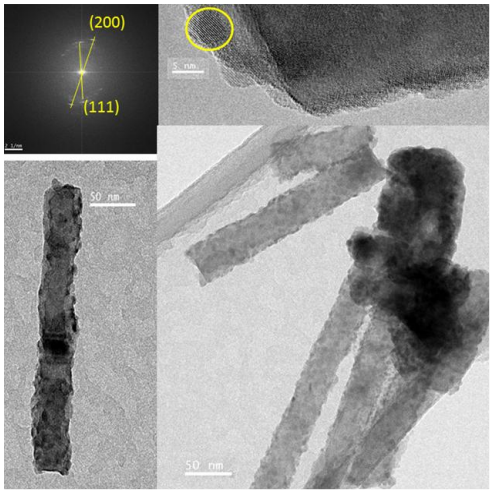

c- S1-5 (5 cycles)

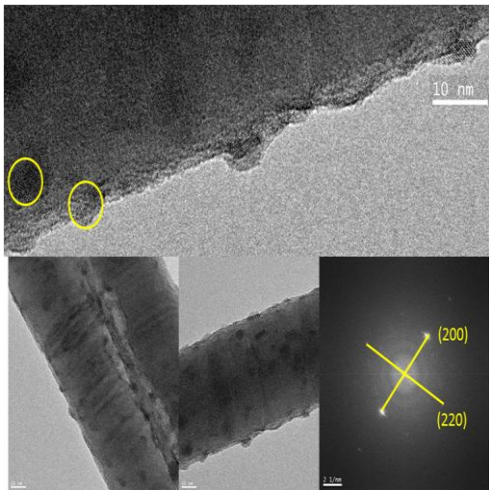

Figure 4- 40- Low & high-resolution TEM images demonstrate the configuration of the PbS-QD/ZnO –NWs, Corresponding FFT patterns revealing the ordering of the super lattices of a)PbS deposition at 16 SILAR Cycles b) PbS deposition at 10 SILAR cycles c)PbS deposition at 5 SILAR cycles.

Conclusion:

In principle, SILAR is a deposition method in which thickness of the layer has determined by the number of deposition cycles.

PbS NPs are successfully attached on the ZnO NWs by SILAR technique. No organic materials were used. The number of cycles affected the density and the sizes of the NPs. The grown NPs are crystalline confirmed by XRD and TEM.

Scenario 3b: Effect of Rinsing:

Sample A and B composed of ZnO Nanowall Network with honeycomb structure deposited by PLD discussed in chapter 3. Sample A was dipped successively, into $PbCl_2$ (DMSO) solution for 70 seconds, rinsed with DMSO for 10 s and dried with Nitrogen (N_2). Then it was dipped into Na_2S Methanol solution for another 70s, rinsed with Methanol for 10 s and dried with N_2. This whole process was repeated 10 times. On the other hand, Sample B was dipped in the same conditions but it was rinsed with deionized distilled water. Parameters are summarized in table 4-9.

Table 4- 9 – Parameters used

	Rinsing	Dipping time	# of cycles
S3-3	Water	70s	10 cycles
S2-5	DMSO/Methanol	70 s	10 cycles

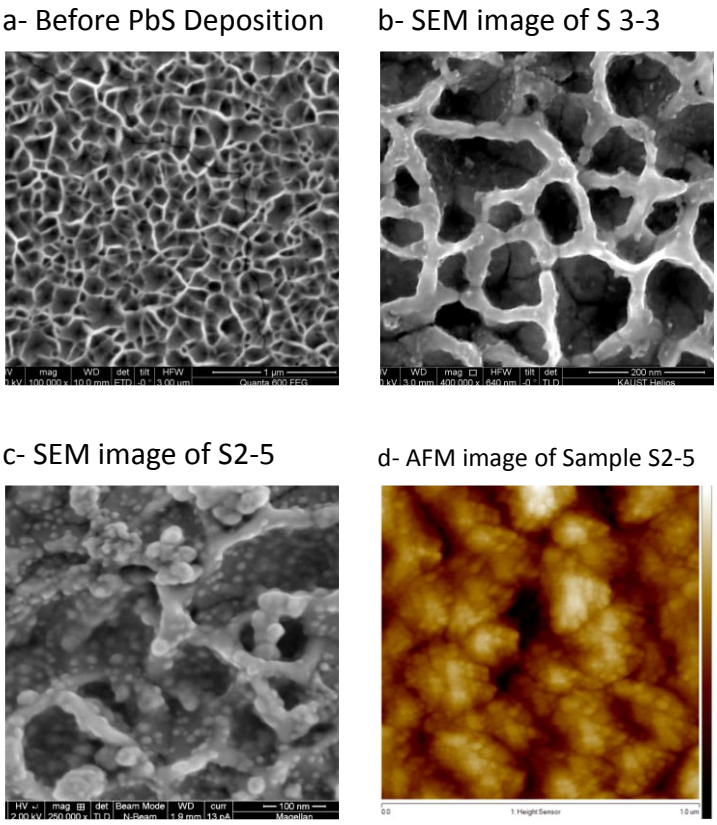

Figure 4- 41- SEM images of ZnO Nanowall Network with honeycomb structure deposited by PLD a- before PbS deposition , b) after PbS deposition with Water rinsing and c) after PbS deposition with DMSO/Methanol rinsing

Figure 4- 41 a reveals the top view SEM image of the ZnO Nanowall network before deposition. Figure 4- 41 b and c show the Co-sensitized ZnO Nanowall network with PbS NPs rinsing with Water and solvent respectively. It is clearly shown that rinsing with the same solvent gave more homogenous NPs distributed randomly on both the inside and outside of the Nanowalls . The size of the PbS NPs was around 8-13 nm for sample A rinsed with water , and 9-11 nm for the sample B rinsed with the solvent confirmed with the AFM topography images Figure 4- 41d.

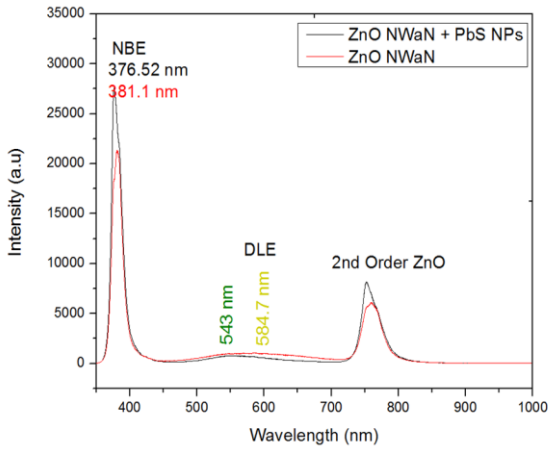

Figure 4- 42- PL Spectra of ZnO Nanowall Network with honeycomb structure deposited by PLD before and after PbS deposition DMSO/Methanol rinsing

PL spectra in figure 4-42 a shows the PL spectra of ZnONanowall Network with honeycomb structure before and after PbS deposition. It is noticed that the intensity of the NBE in the UV (376.52 nm- 3.293 eV) of the ZnO NWaN with PbS NPS is lower and blue shifted of 39 meV for the NBE of the ZnO NWaN (381.1 nm-3.253 eV) before PbS deposition.

Conclusion:

SILAR method is based on the successive dipping of substrate in cationic precursor solution and anionic precursor solution. Film formation in the SILAR method is occurred by successive adsorption of cations followed by reaction with anions. The process is summarized in figure 4-43. It required a time consuming rinsing step between the sequential adsorption process of Pb^{2+} cations and S^{2-} anions to remove the excess ions from the surface.

The rinsing can be done with deionized water or DMSO, or methanol to avoid homogeneous precipitation in the solution, so that only the tightly adsorbed layer stays on the substrate. The adsorption is a surface phenomenon occurring due to

attractive force between ions and surface of substrate. This attractive force is of van der Waals type that basically originates due to the residual or unbalanced force present in the substrate. Thus, ad-atoms can be holding on the surface of the substrate by that residual force.

Number of cycles and the concentration of the solution play an important role in the growth of the PbS NPs on the surface of the ZnO NWs.

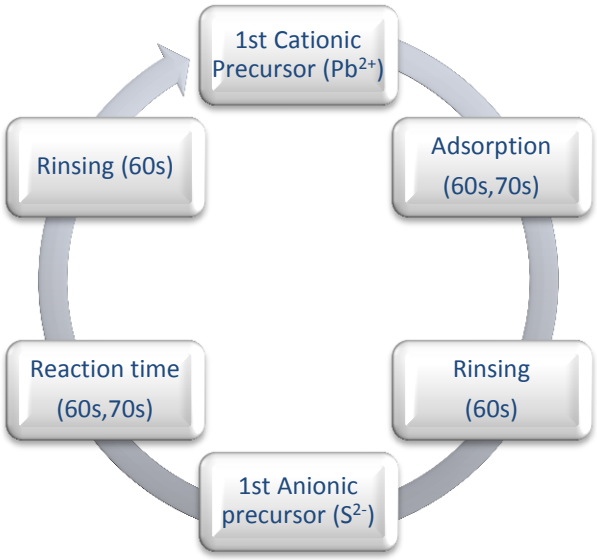

Figure 4- 43- SILAR Process illustration

4-6-4 Surface photo-voltage spectroscopy

Surface photovoltage spectroscopy (SPS) measurements were performed by Prof.Iain Baikie from KP Technology [2]England. The samples were mounted on an Aluminium sample holder using Al tape with conductive glue. The sample holder was then introduced to a darkened enclosure (LE450). In some cases the small sample dimension meant that, after mounting, the sample surface exposed was of a similar dimension as the Kelvin probe vibrating tip.The samples were given an opportunity to come into equilibrium with dark conditions. A measurement of the dark Contact Potential Difference was recorded. The samples were illuminated by dc light of wavelength 400-1000 nm (3.1 – 1.24 eV), i.e., the light intensity was not chopped; it remains constant at each wavelength. The wavelength was scanned from 400 to 1000 nm.

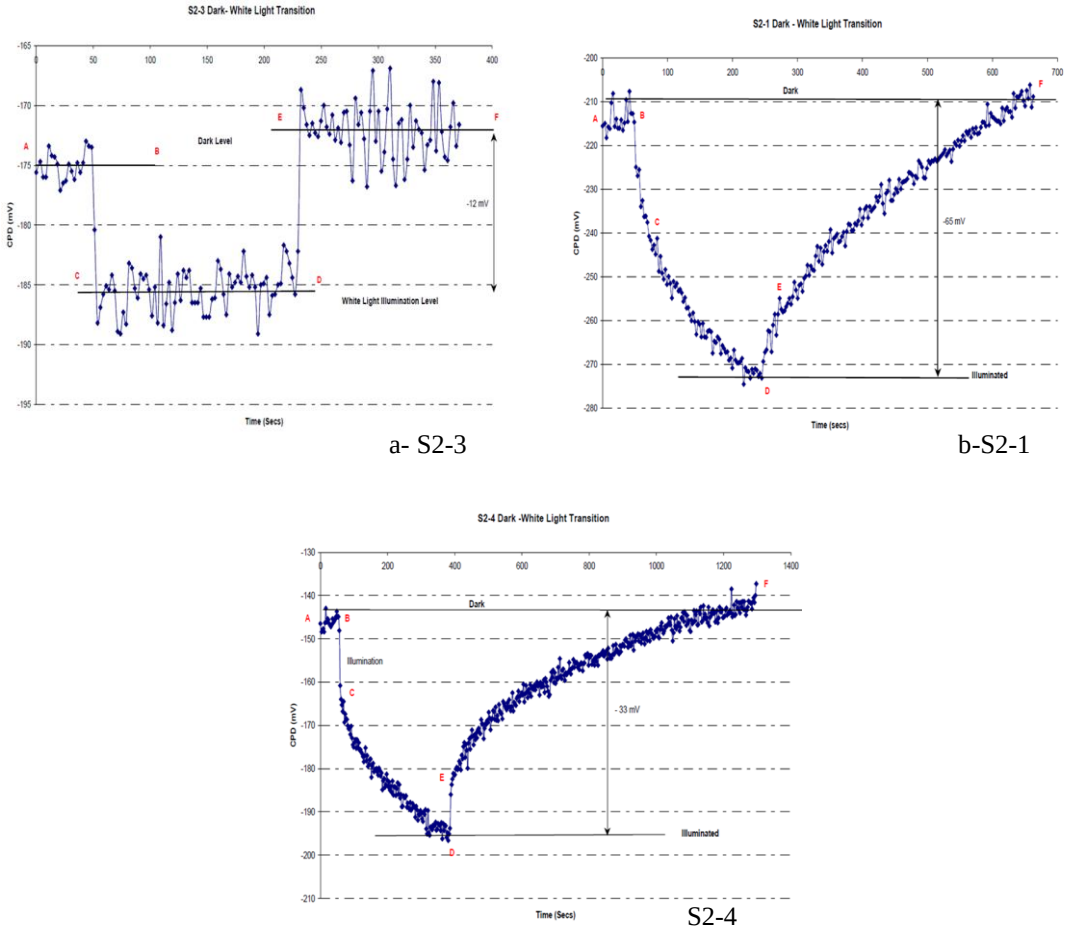

a- S2-3 b-S2-1

S2-4

Figure 4- 44- Contact potential difference (CPD) in function of time under Dark (AB), Illumination (CD) and Dark (EF) for the 3 samples S2-3, S2-1 and S2-4.

[2] http://www.kelvinprobe.com

Figure 4-44b shows the Dark-White Light-Dark transition for S2-1. AB represents the original dark level; it may not be constant due to the prior illumination (SPS scan). There is an initial fast response taking say 30 seconds followed by a slow charging. After about 250 seconds, the light source was switched off and the sample CPD initially changed reasonably quickly (point E) and then a slow delay to F. The magnitude of the change observed was 65 mV and clearly there are at least two light adsorption mechanisms. Figure 4-44 c shows the data for S2-4, the data are broadly similar to S2-1 above, however this initial change in CPD with illumination is much faster, as is the change immediately after the light source is switched off. The reason the dark level appears to change is that the sample surface was not completely discharged from the initial SPS scan which the light source was originally switched on. In this case the magnitude of the change was 33 mV.

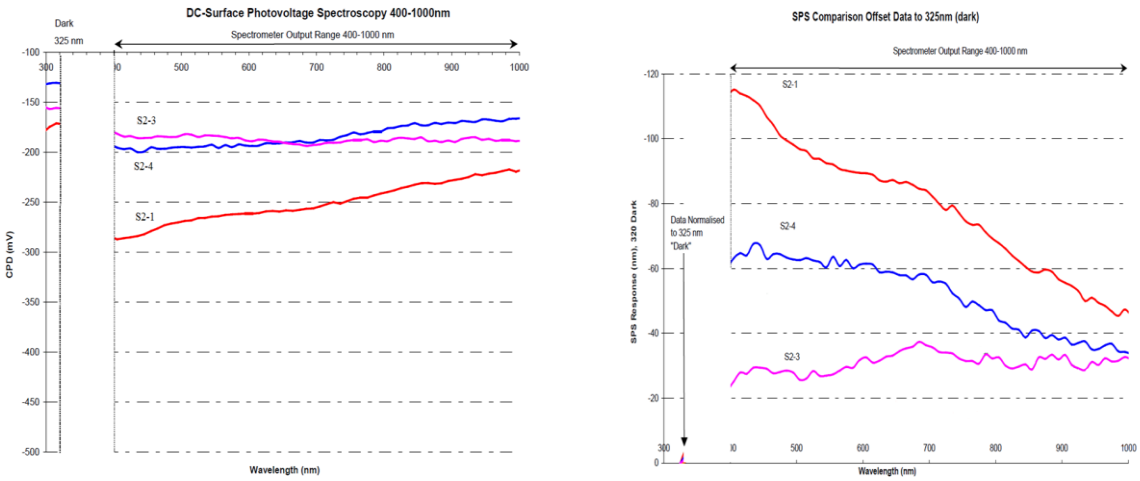

a b

Figure4- 45- a) Dark CPD difference of Samples 1-5 (at an indicated wavelength of 325 nm), followed by the DC-SPS response as a function of wavelength between 400 and 1000 nm. b) Relative SPS data between 400 –1000 nm, normalized at the dark level (325 indicated).

It is noted that in figure 4-45a the valid output range of 400 – 1000 nm is indicated. The transition from 325 to 400 nm is not indented to represent actual wavelength data, rather the indicated 325 nm represents darkness (no illumination) and 400 nm is the first valid data point. Thus the transition between 325 and 400 nm is an equipment artifact and does not represent the sample response. We observe that the dark values

for (S2-1 ,S2-4 and S2-3) are lower than the kelvin probe tip . The 3 samples have dark work function approximately –150 mV lower than the Kelvin probe tip. In all cases the effect of illumination was to decrease the work function of the sample. The magnitude of work function change ranges from about 18 mV to approximately 117 mV, (S2-1). The maximum achieved photovoltage, see figure4-45 b, and was –117 mV @400 nm for S2-1, - 69 mV @440 nm for S2-4, and -38 mV @700 nm for S2-3.

4-7 ZnO Nanostructures Based Hetero-junctions:

A key issue governing efficient electron transfer between two semiconductors (and, consequently, photocurrent generation) is interfacial energy alignment. In a quantum dot-sensitized solar cell, the energy level of the transient electron within the exciton must lie above the conduction band minimum (CBM) of the wide band gap semiconductor ZnO while that of the hole must lie below the valence state of the hole conductor. An optimal alignment of electronic energy levels at the interface is a balance between multiple factors. The excited donor levels must lie sufficiently above the CBM where the density of states is high enough to make electron injection into the semiconductor competitive with other relaxation processes. Excess energy of the photo-injected electron can be rapidly thermalized by electron-phonon scattering and not recovered as electrical energy. So, the ability to tune electronic energy alignment at the quantum dot semiconductor interface allows one to optimize solar-to-electric power conversion efficiencies in semiconductor quantum dot-based excitonic solar cells.

4-7-1 PN Junction

Different ZnO based hetero-junctions were demonstrated in this research such as: p-Si/n-ZnO Nanowall Network, p-Si/n-ZnO Nanowires, n-ZnO Nanowall/p-PbS NPs and n-ZnO Nanowire/p-PbS NPs(Figure 4- 46,47)

An energy band diagram is drawn in Fig44 based on individual band structures to explain the behavior of *n*-ZnO/ *p*-Si and n-ZnO/p-PbS hetero-junction. It is known that the energy gaps (*Eg*) for ZnO and Si are 3.27 and 1.12 eV, respectively. While the energy gaps (Eg) for PbS NPs is tuned from 0.41 eV to ~ 2 eV by varying the NPs Size. The valence band offset is much larger than the conduction band offset. The higher barrier in the valence band prevents the holes' movement. Therefore, the conductive property of this hetero-junction is determined by the electrons in the

conduction band. However, these arguments are for the ideal case, and direct measurements are required to determine the exact band structure of the hetero-junction.

a- p-Si/n-ZnO Nanowall

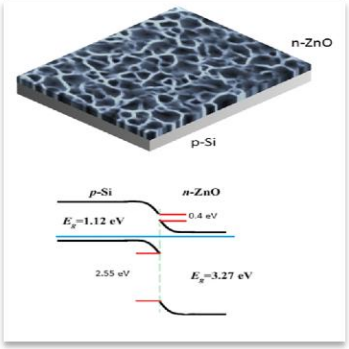

b- p-Si/n-ZnO Nanowires

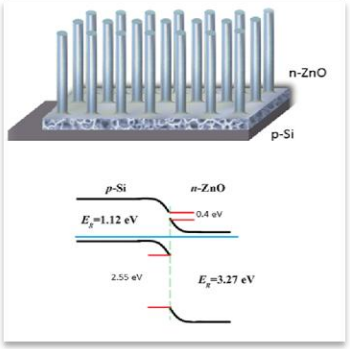

c- p-PbS/n-ZnO Nanowall

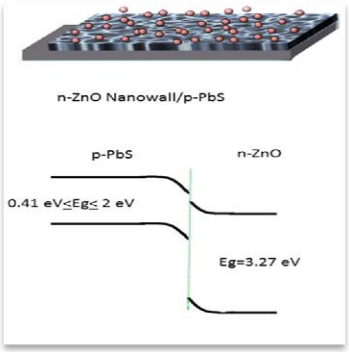

d- p-PbS/ n-ZnO Nanowires

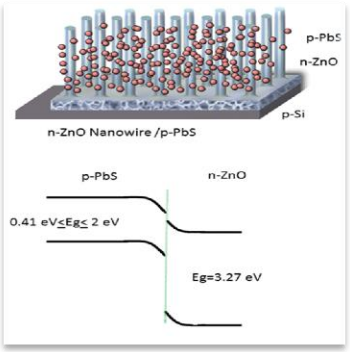

4-7-2 Electrode Selection

Selection of electrodes has to be selected in respect with the energetic alignment: many electrodes can be used. Work functions of different electrodes presented in Table 4- 10.

Table 4- 10: Work function of different electrodes

Electrode	Work function
Al	4.08 eV
C	4.81 eV
Au	5.1 eV
Ag	4.73 eV
Pt	6.53 eV
ITO	4.8 eV

The fundamental requirement for a working solar cell is that it must be able to absorb light and move electrons and holes in an ordered and repeatable fashion, generating usable long term current. Note that the position of ZnO and PbS conduction and valence bands are arranged in a way that promotes cell operation. The energy levels of the valence and conduction bands must be aligned such that electrons can be collected at one electrode and holes at the other one (Figure 4- 47b). Electrons are energetically drawn to transfer to states as low in energy as possible (electrons sink) and holes transfer to states as high as possible (holes float). In our case Silver (Ag) or Gold (Au) can be used. The performance of a QDSC dramatically depends on the relation among the rates of electron injection (PbS to ZnO), electron transport to electrode (anode) (ZnO to ITO) , hole transport to electrode (cathode) (PbS to Ag or Au) and the different rate of recombination (PbS internal recombination), and recombination via ZnO/PbS. The hole transfer from PbS to electrode would produce photocurrent in the opposite direction of the forward bias dark current and generate power. However electrons can transfer to the electrode contact since this process is energetically favorable. The electron transfer would produce a shunt current that opposes the photocurrent and limit the solar cell efficiency. To block the parasitic flow of electrons and inhibit the formation of a schotky junction, hole transporting materials (HTM) have to be incorporated between the PbS NPs and the electrode (Cathode).

Kurtis et al (2007) and Gardner et al (2006) [58][59] and others used electrolyte containing the triiodide/iodide (I^{3-}/I^{-}) redox couple to neutralize the positively charged QDs. Quantum dots are also known to corrode in this electrolyte and, therefore, QDSSC performance is expected to degrade over time [60]. Zaban et al.[61] reported that n-type InP quantum-dot-sensitized TiO_2 solar cells were unstable in this electrolyte.

Improvements in power conversion efficiency may be attained for ZnO/PbS hetero-junction QD PVs through the incorporation of a MoO3 interlayer between the PbS colloidal quantum dot film and the top-contact anode [62]. Gao and Luther[63] have shown that Fermi-level pinning can lead to the formation of a Schottky barrier even between PbS and gold, despite the close alignment between the Fermi level of gold and the valence band edge of PbS. It is demonstrated that the insertion of a thin film

of molybdenum oxide (MoO_3) between the PbS photoactive layer and the anode contact inhibits the formation of a Schottky junction. Molybdenum oxide has previously been utilized as a hole-injection layer for organic thin films, [64] as both an electron-blocking layer and a physical buffer layer in photovoltaic [65][66]. In the architecture designed by Brown et al (2011) [67], the high work function of MoO3 is found to pin the Fermi level of the top electrode, enabling the formation of an ohmic contact to PbS and allowing even low-work function metals to be used as the anode without forming a voltage-limiting Schottky contact.

On the other hand, Kurtis et al (2009) [68] used 15-30 nm In α-NPD [*N*,*N*'-bis(1-naphthalenyl)-*N*,*N*'-bis(phenylbenzidine)] layer as interface between PbSe and Au electrode. The thin layer of α-NPD is expected to block the parasitic flow of electrons between the PbSe NCs and gold film. α-NPD is commonly used in organic light-emitting devices[69] and solar cells[70]as a hole injection and hole transport layer. Moreover, α-NPD protects the NPs from physical damage during metal evaporation. When a α-NPD layer is present between the PbSe NPs and gold film, the electrons would have to increase their energy markedly in order to transfer to the gold contact from the PbSe NCs.

Based on the above, we do recommend the sputtering of MoO_3 of (10nm thickness) on the surface of the substrates.

4-7-3 Demonstrated Solar Cell

The behavior of PV cells where the ZnO Nws are in contact with PbS NPs is examined. Illustration is presented in Figure 4- 47a,b along with its energy diagram. The first trial was the following: Silver Electrode was deposited by sputtering for 15 minutes in Argon environment, for a thickness of around 290 nm, forming a square of 9 mm^2 area (Figure 4- 48a).

a- Illustration of p-PbS/n-ZnO Solar Cell

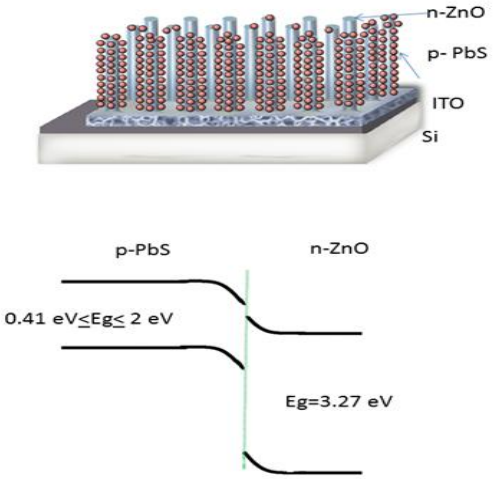

b- Energy Level diagram for a p-PbS/n-ZnO (Energy With respect to the vacuum level)

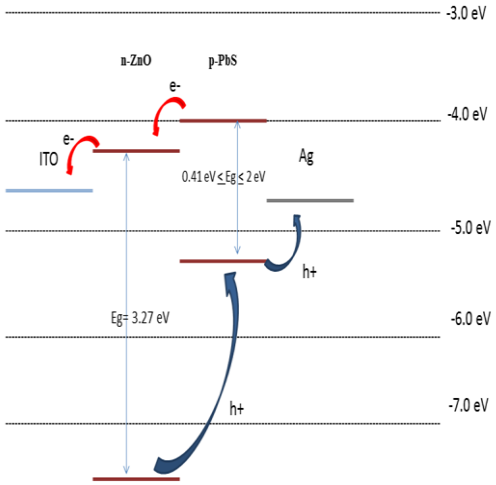

Figure 4- 46- a) Illustration of ZnO based Hetero Junction by Hydrothermal b) Energy diagram of p-PbS/n-ZnO

a- Sample: Solar Cell Prototype

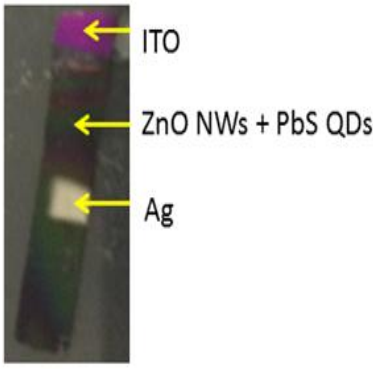

b- External Quantum Efficiciency spectrum

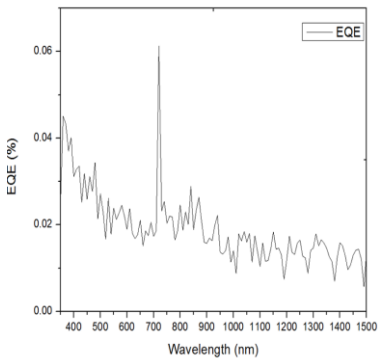

Figure 4- 47: EQE spectra of the n-ZnO/p-PbS with ITO and Ag electrode .

External Quantum efficiency (EQE) spectrum is presented in Figure 4- 48b. (Needs to be identified and improved)

4-8- Conclusion

ZnO/PbS QD heterojunction for photovoltaic device was successfully demonstrated. PbS NPs were successfully attached to ZnO NWs by different techniques. PbS NPs at different sizes and different concentration were decorating the lateral sides of the ZnO Nanowires. A simple and cheap sunthetic route to high qulity PbS NPS without any ligand or olive oil was described and studied by varying different parameters such as concentration, rinsing solutions and number of cycles (Figure 4- 47) . SEM and TEM images confirm the different-sized PbS-QD formation on the ZnO NWs. XRD and FFT of HRTEM confirms the crystallization of the synthesized PbS NPs. Basic SPS measurement were performed checking the CPD of the 3 samples in function of time. XRF measurements confirm the Pb and S elements identified on the sample. PbS is transparent to UV radiation, and ZnO is opaque to NIR; therefore, the top region must be sensitive to NIR radiation.

A demo solar cell was fabricated by depositing a silver electrode on top of the ZnO Nws decorated with PbS NPs. EQE was very weak, that needs to be improved and increased which can be done in our future work.

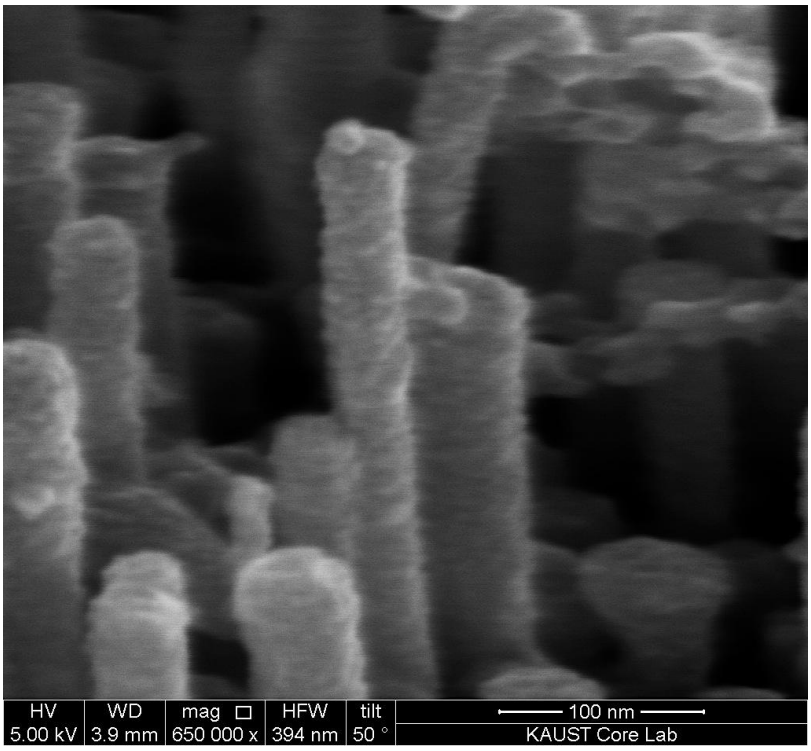

Figure 4- 48-Demosntrated n-ZnO/p-PbS heterojunction for Solar cell

References

[1] A. Kudo, MRS Bull., 2011, 36, 32–38.
[2] A. Franceschetti, MRS Bull., 2011, 36, 192– 197.
[3] A. I. Hochbaum and P. Yang, Chem. Rev., 2010, 110, 527–546.
[4] K. Q. Peng and S. T. Lee, Adv. Mater., 2011, 23, 198–215
[5] E. H. Sargent, Nat. Photonics, 2009, 3, 325– 331.
[6] P. Yang, R. Yan and M. Fardy, Nano Lett., 2010, 10, 1529–1536.
[7] Minsu Seol, Easwaramoorthi Ramasamy, Jinwoo Lee, and Kijung Yong J. Phys. Chem. C 2011, 115, 22018–22024
[8] P. Yang, R. Yan and M. Fardy, Nano Lett., 2010, 10, 1529–1536.
[9] L. Spanhel, H. Weller, A. Henglein, J. Am. Chem. Soc. 109 (1987) 6632.
[10] Prashant V. Kamat Acc. Chem. Res., (2012) 10.1021/ar200315d
[11] S.C. Lin, Y.L. Lee, C.H. Chang, Y.J. Shen, Y.M. Yang, Appl. Phys. Lett. 90 (2007) 143517
[12] I. Robel, V. Subramanian, M. Kuno, P.V. Kamat, J. Am. Chem. Soc. 128 (2006) 2385.
[13] R. Plass, P. Serge, J. Kruger, M. Gratzel, J. Phys. Chem. B 106 (2002) 7578.
[14] A. Zaban, O.I. Micici, B.A. Gregg, A. Nozik, J. Langmuir 14 (1998) 3153.
[15] P. Yu, K. Zhu, A.G. Norman, S. Ferrere, A.J. Frank, A.J. Nozik, J. Phys. Chem. B 110 (2006) 25451.
[16] G.M. Wang, X.Y. Yang, F. Qian, J.Z. Zhang, Y. Li., Nano Lett.,doi:10.1021/nl100250z.
[17] H.J. Lee, P. Chen, S.J. Moon, F. Sauvage, K. Sivula, T. Bessho, D.R. Gamelin, P. Comte, S.M. Zakeeruddin, S.I. Seok, M. Gratzel, Md. K. Nazeeruddin, Langmuir 25 (2009) 7602.
[18] Moreels, I.; Fritzinger, B.; Martins, J. C.; Hens, Z. J. Am. Chem. Soc. 2008, 130, 15081–15086.
[19] Dai, Q. Q.; Wang, Y. N.; Zhang, Y.; Li, X. B.; Li, R. W.; Zou, B.; Seo, J.; Wang, Y. D.; Liu, M. H.; Yu, W. W. Langmuir 2009, 25, 12320–12324
[20] Sykora,M.;Koposov,A. Y.;McGuire, J.A.; Schulze,R.K.;Tretiak, O.; Pietryga, J. M.; Klimov, V. I. ACS Nano 2010, 4, 2021–2034.
[21] Hines, M. A. and G. D. Scholes , Advanced Materials 15 (21): 1844-1849 (2003).
[22] Chen, S. W., L. A. Truax, et al. Chemistry of Materials 12 (12): 3864-3870 (2000).
[23] Kane, R. S., R. E. Cohen, et al. " Chemistry of Materials 8 (8): 1919-1924 (1996).
[24] W. Lee, S. K.Min, V. Dhas, S. B. Ogale' S.-H. Han , electrochemistry communication (2009) ,Vol11 ,issue 1 , P.103-106
[25] Sun W T, Yu Y, Pan H Y, Gao X F, Chen Q and Peng L M 2008 J. Am. Chem. Soc. 130 1124
[26] M. Shalom, S. Dor, S. Ruhle, L. Grinis and A. Zaban, J. Phys. Chem. C, 2009, 113, 3895.
[27] H. Choi, R. Nicolaescu, S. Paek, J. Ko and P. V. Kamat, ACS Nano, 2011, 5, 9238.
[28] V. Chakrapani, D. Baker and P. V. Kamat, J. Am. Chem. Soc., 2011, 133, 9607.
[29] S. Gim_enez, I. Mora-Ser_o, L. Macor, N. Guijarro, T. Lana-Villarreal, R. G_omez, L. J. Diguna, Q. Shen, T. Toyoda and J. Bisquert, Nanotechnology, 2009, 20, 295204.
[30] S.Chen, W.Liu Materials Chemistry and Physics 98 (2006) 183–189
[31] M. A. Hines , G. D. Scholes , Adv. Mater. 2003 , 15 , 1844 .
[32] Jiang Tang and Edward H. Sargent Adv. Mater. 2011, 23, 12–29
[33] Talapin, D. V.; Lee, J.-S.; Kovalenko, M. V.; Shevchenko, E. V. Chem. Rev. 2010, 110, 389–458.
[34] Pattantyus-Abraham, A. G. et al.. ACS Nano 4, 3374_3380 (2010).
[35] Luther, J. M. et al.. Nano Lett. 8, 3488_3492 (2008).
[36] Koleilat, G. I. et al.. ACS Nano 2, 833_840 (2008).
[37] Talapin, D. V. & Murray, C. B.. Science 310, 86_89 (2005).
[38] D.V.Talapin , and C.B. Murray , Science 310 , 86 (2005)
[39] E.J.D.Klem, D.D.MacNeil, P.W.Cyr,L.Levina and E.H.Sargent , App.Phys Lett 90, 183113 (2007)
[40] J.M.Luther , M.Law , Q.Song , C.Perkins, M.C.Beard, A.J.Nozik, ACS Nano , 2, 271 (2008)
[41] Konstantatos, G.; Levina, L.; Fischer, A.; Sargent, E. H.. Nano Lett. 2008, 8, 1446–1450.
[42] Hinds, S.; Levina, L.; Klem, E. J. D.; Konstantatos, G.; Sukhovatkin, V.; Sargent, E. H. Adv. Mater., 2008, 10.1002/adma.200800452.

[43] D. Aaron R. Barkhouse, Andras G. Pattantyus-Abraham, Larissa Levina, and Edward H. Sargent (2008) ACSNano VOL. 2 ▪ NO. 11 ▪ 2356–2362 ▪ 2008
[44] Jeong KS, Tang J, Liu H, Kim J, Schaefer AW, Kemp K, Levina L, Wang X, Hoogland S, Debnath R, Brzozowski L, Sargent EH, Asbury JB. ACS Nano. 2012 Jan 24;6(1):89-99
[45] R. Rhodes, P. OBrien, B.R. Saunders, J. Colloids Interface Sci. 358 (2011) 151.
[46] Brian R. Saunders Journal of Colloid and Interface Science 369 (2012) 1–15
[47] J. Peet, J.Y. Kim, N.E. Coates, W.L. Ma, D. Moses, A.J. Heeger, G.C. Bazan, Nature Mater. 6 (2007) 497.
[48] Z. Tang, N.A. Kotov, M. Glersig, Science 297 (2002) 237.
[49] Shuang Chena, Weimin Liu , Materials Chemistry and Physics 98 (2006) 183–189
[50] Ristov M, Sinadinovski G J and Grozdanov I 1985 Thin Solid Films 123 63
[51] Nicolau Y F 1985 Appl. Surf. Sci. 22/23 1061
[52] Nicolau Y F and Minnard J C 1988 J. Cryst. Growth 92 128
[53] Nicolau Y F, Dupuy M and Brunel M 1988 J. Electrochem. Soc. 128 1347
[54] S.H. Choi, E.G. Kim, J. Park, K. An, N. Lee, S.C. Kim, T. Hyeon, , J. Phys. Chem. B 109 (2005) 14792–14794.
[55] D.C. Look, G.C. Farlow, R. Reunchan, S. Limpijumnong, S.B. Zhang, K. Nordlund, , Phys. Rev. Lett. 95 (2005) 225502-1–225502-4.
[56] X.B. He, T.Z. Yang, J.M. Cai, C.D. Zhang, H.M. Guo, D.X. Shi, C.M. Shen, H.J. Gao, , Chin. Phys. B 17 (2008) 3444–3447.
[57] I. Moreels, K. Lambert, D. Smeets, D. De Muynk, T. Nollet, J. Martins, F. Vanhaecke, A. Vantomme,C. Delerue, G. Allan, and Z. Hens. .ACS NANO.2009, 3, 3023-3030.
[58] Kurtis S. Leschkies, Ramachandran Divakar, Joysurya Basu, Emil Enache-Pommer, Janice E. Boercker, C. Barry Carter, Uwe R. Kortshagen, David J. Norris, and Eray S. Aydil, Nano Lett., Vol. 7, No. 6, 2007
[59] Gardner, J. M.; Abrahamsson, M.; Farnum, B. H.; Meyer, G. J. J. Am. Chem. Soc. 2009, 131, 16206
[60] Gratzel, M. J. Photochem. Photobiol., C 2003, 4, 145.
[61] Zaban, A.; Micic, O. I.; Gregg, B. A.; Nozik, A. J. Langmuir 1998, 14, 3153.
[62] Patrick R. Brown, Richard R. Lunt, Ni Zhao, Timothy P. Osedach, Darcy D. Wanger, Liang-Yi Chang, Moungi G. Bawendi, and Vladimir BuloviNano Lett. 2011, 11, 2955–2961
[63] Gao, J.; Luther, J. M.; Semonin, O. E.; Ellingson, R. J.; Nozik, A. J.; Beard, M. C. Nano Lett. 2011, 11, 1002–1008.
[64] Kr€oger, M.; Hamwi, S.; Meyer, J.; Riedl, T.; Kowalsky, W.; Kahn, A. Appl. Phys. Lett. 2009, 95, 123301.
[65] Hancox, I.; Chauhan, K. V.; Sullivan, P.; Hatton, R. A.; Moshar, A.; Mulcahy, C. P. A.; Jones, T. S. Energy Environ. Sci. 2010, 3, 107.
[66] Sun, Y.; Takacs, C. J.; Cowan, S. R.; Seo, J. H.; Gong, X.; Roy, A.; Heeger, A. J. Adv. Mater. 2011, 23, 2226–2230.
[67] P. R. Brown, R. R. Lunt, N. Zhao, T. P. Osedach, D. D. Wanger, L.-Y. Chang, M. G. Bawendi, and V. Bulovic, Nano Lett. 2011, 11, 2955–2961
[68] Kurtis S. Leschkies, Timothy J. Beatty, Moon Sung Kang, David J. Norris, and Eray S. Aydil, ACS Nano VOL. 3 ▪ NO. 11 ▪ 3638–3648 ▪ 2009
[69] Meng, H.; Herron, N. Li, Z., Meng, H., Eds.; CRC Press: Boca Raton, FL, 2007; p 295.
[70] Kushto, G. P.; Kim, W.; Kafafi, Z. H. Appl. Phys. Lett. 2005, 86, 093502.

Findings and Future Work

Contents

1- Thesis Findings

During the past decade, the development of nanoscience and nanotechnology has launched new ways to design efficient solar cells. Strategies have been developed to design nanostructure architectures of semiconductors, metals, and polymers for solar cells. Having large surface area, and providing long electron diffusion length, ZnO Nws were used to introduce 1 D structure simple to prepare and to sensitize by the mean of 0D semiconductors, PbS QDs, to significantly impact power conversion efficiency of QDSSCs. Third generation Solar Cell based on 1 D and 0 D nanostructures may hold the key of solving the world's increasing demand for clean and low cost energy.

To the end of improving device design and performance, two aspects of the QDSSCs were examined in this thesis: the synthesis of vertically oriented ZnO NWs on different substrates without metal catalyst and the attachment of p-type PbS NPs of different sizes and different densities on the as-synthesized ZnO NWs.

The device structure consists of 0D semiconductor NPs as light harvester for light absorption and charge generation, decorating 1D semiconductor NWs as light trapper, for charge separation and transportation.

Growth of vertically Oriented ZnO NWs:

A variety of ZnO nanostructures were grown by Physical Vapor deposition (PVD) on various substrates like Silicon and Glass. (.

High quality ZnO Nanowall Network with Honeycomb structure was grown by Pulsed Laser Deposition (PLD) without chemical etching or catalyst / template usage, and used as seed layer These novel nanostructures have unique two dimensionality properties that hold promise for applications requiring high surface area such as Solar cell and gas sensors.

High quality self-catalyzed ZnO Nanowires were grown by PLD at relatively low temperature in different Argon pressures environment and on different substrates. The length and the spacing of the Nanowires vary in function of the growth parameters.

It is been identified that the growth parameters (temperature, pressure and substrate-target distance) are vital to control the crystallinity, morphology and the defect levels in the synthesized nanostructures. The issue of controlling the orientation of the nanostructures was addressed. SEM, XRD, TEM, HRTEM analysis show that the nanostructures are highly crystalline and are vertically oriented.

Growth of PbS NPS on the lateral sides of the ZnO NWs:

The synthesized ZnO Nanowires were sensitized by PbS Nanoparticles for Quantum Dots sensitized Solar Cells. Ex-situ growth and In-situ growth of PbS Nanoparticles were employed in this research on different ZnO nanostructures. Commercial Oleic Acid (OA) capped PbS NPs by ex-situ growth with different sizes (2.4, 3.2 and 5.4 nm) were bought from MK Nano. Different trials and techniques were addressed to attach the PbS NPs on the ZnO Nanowires. It was noticed that the OA capped PbS NPS were randomly deposited with very small density on the lateral side of the ZnO NWs. Ligand exchange was tested for the OA capped PbS NPs with EDT and MPA. The Ligand Exchange with EDT leads to the aggregation of the PbS NPs in form of nanobelts that might improve the efficiency of the ZnO Nws based Quantum Dots Solar cells.

The in-situ growth by SILAR method was used for growing PbS NPs on the ZnO NWs. Different sizes of PbS NPs with different densities were grown, covering the lateral side of the ZnO NWs. SEM, TEM, XRD, XRF, HRTEM, FFT, absorption and PL were studied to identify the structural, optical and morphological properties of the deposited PbS NPs on ZnO NWs and ZnO Nanowalls.

The comparative study of the attachement of PbS Nps on ZnONWs , highlight the potential use of the in-situ growth technique as it does not incorporate the use of organic material and eliminate the problem arised by the use of long chain ligand.

In short n-ZnO/p-PbS junction was demonstrated with polycrystalline PbS NPs laterally attached on highly oriented ZnO Nws /Nanowall

Results are summarized in figure 5-1 showing the 2 structures nZnO Nanowires/p-PbS NPS and n-ZnO Nanowall / p-PbS NPs

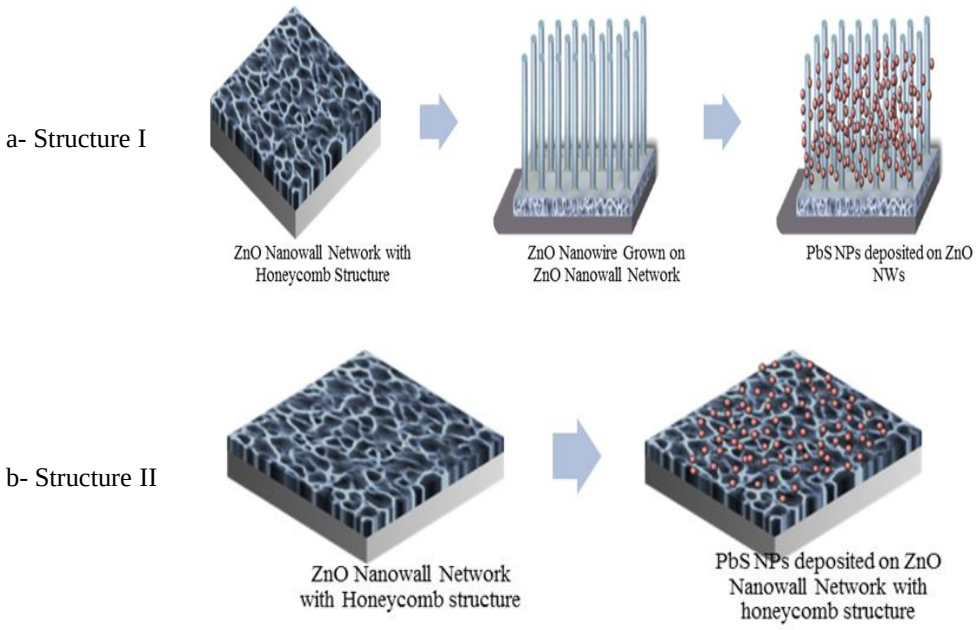

Figure 5- 1 – One Dimensional – Zero Dimensional Nanostructures Combined to form a p-n junction for solar cell applications

In conclusion, the following thesis goals have been achieved:

1) Investigation of the ZnO NWs /PbS NPs for Solar cell structure to Design the NWs based QDSSCs
2) Optimized Synthesis of c-axis oriented ZnO Nanowall network with honeycomb structure on a Glass_ITO and Silicon substrates as textured seed layer without catalyst, and without chemical etching;
3) Optimized Synthesis `of self-catalyzed vertically oriented ZnO nanowires array on a Glass_ITO and Silicon substrates;
4) Morphological, structural and optical characterization of the textured Seed layer and the Nanowires;
5) Attachment of the PbS NPs on the ZnO NWs and Nanowall Network
6) Morphological, structural and optical characterization of PbS NPs/ZnO NWs
7) Demonstration of the n-ZnO/p-PbS Heterojunction
8) Surface photo-votlage characterization.
9) Investigation of the top contact configuration

2- Future Work

In future research, Quantum Dots Sensitized Solar cell (QDSSC) has to be developed, presented in figure 5-2, based on the n-ZnO/p-PbS junction demonstrated in this thesis.

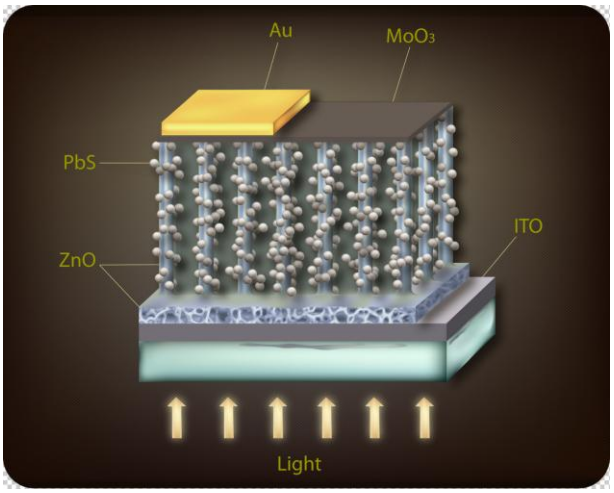

Figure 5- 2- Illustration of the proposed Nanowire Based Quantum Dots Sensitized Solar Cells

To optimize the solar efficiency the following strategies can be followed:

N-type Layer:

- Study the Solar Cell Properties in function of ZnO Nws length , diameter and spacing
- Treatment of ZnO Nws (

P-type Layer:

- Study the solar cell properties in function of the size and density of the PbS NPS
- Change the PbS by another semiconductor having a small band gap energy and respecting the energetic alignment of the structure.

Electrode:

- Improve conductivity of ITO sputtered on thin glass substrates for increasing electron extraction
- Select the best top electrode metal in respect with the energetic alignment (figure 3a,b)

- Deposition of MoO3 by sputtering will be incorporated between PbS NPS and Gold electrode.
- Select the design the top electrode geometry (figure 5-3c)
- Optimize the thickness of the deposited metal top electrode (100 nm of thickness)

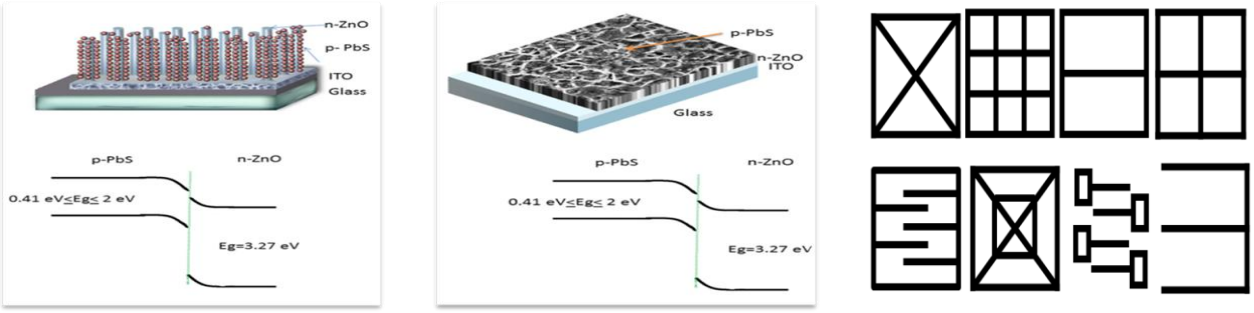

a- n-ZnO Nanowire/p-PbS QDs

b- n-ZnO Nanowall/PbS QDs

c- Proposed electrode Mask

Figure 5- 3: Illustration of ZnO based Heterojunction by PLD on Glass and Proposed electrode Mask

Device Characterization:

- Characterize the solar cell prototype :
  - a- I-V in the dark and under 1 sun illumination
  - b- Incident photon to current conversion efficiency IPCE
  - c- Photocurrent – voltage (J_{sc} (mA/cm^2), V_{0c} (mV), FF, and efficiency)

Résumé

Le développement des nanotechnologies offre de nouvelles perspectives pour la conception des cellules solaire à fort rendement de conversion. Jusqu'à présent les efforts se sont portés principalement sur des structures à base de semi-conducteurs, de métaux et de polymères. Dans nos travaux, nous avons considéré des nanoparticules de Sulfure de Plomb (PbS) pour lesquelles l'énergie de bande interdite et les propriétés optiques sont fonction de la taille de la particule afin de tirer parti de l'ensemble du spectre optique couvert par l'énergie solaire. Nous avons également considéré des nanofils d'oxyde de zinc (ZnO) pour la séparation et le transport des charges photo-crées. Nous pensons que l'association des nanoparticules de PbS avec des nanofils de ZnO devrait pouvoir augmenter considérablement le rendement des cellules solaires. Dans ce but, nous avons démontré la croissance auto-ordonné des nanofils de ZnO sur substrats silicium et verre par dépôt laser pulsé (pulsed laser deposition) utilisant le réseau de nanoparois de ZnO en forme de nid d'abeille comme couche germe. Nous avons démontré que les conditions de croissance sont essentielles pour contrôler la cristallinité, la morphologie des nanofils de ZnO , ainsi que la densité de défauts de croissance. Les analyses MEB, DRX, TEM, et HR-TEM montrent que nous avons obtenu des nanostructures très cristallines et orientées verticalement. Nous avons également démontré la croissance in-situ de nanoparticules de PbS sans ligand sur la surface des nanofils de ZnO verticaux à l'aide de la technique SILAR (Successive Ionic Layer Adsoprtion and Reaction). Nous avons constaté que les nanoparticules de PbS sont fortement accrochées à la surface des nanofils de ZnO avec différentes dimensions et des densités variables .Ces résultats ont été obtenus sans introduire de matière organique (Ligand) qui pourrait perturber à la fois la structure électronique à l'interface ZnO/PbS et le transfert des électrons du PbS au ZnO. Les analyses MEB, TEM et HR-TEM confirment le bon accrochage des nanoparticules de PbS sur les nanofils de ZnO. Leur forme est sphérique et elles sont poly-cristallines. A la fin de ce travail de thèse nous proposons une hétérojonction p-PbS/n-ZnO constituée de nanoparticules de PbS dopées P et de nanofils de ZnO dopés n pour de futures applications en photovoltaïque.

Abstract

To date, the development of nanotechnology has launched new ways to design efficient solar cells. Strategies have been employed to develop nanostructure architectures of semiconductors, metals, and polymers for solar cells. In this research we have considered the Lead sulfide (PbS) nanoparticles with their tunable band gap and optical properties to harvest the entire solar spectrum which can improve the optical absorption, and charge generation. On the other hand, Zinc oxide (ZnO) nanowires will provide the charge separation and transportation. The ZnO Nanowires sensitized with PbS nanoparticles might significantly impact power conversion efficiency of the solar cells Driven by these unique properties, we demonstrate the successful growth of self-catalyzed ZnO nanowires on silicon and glass substrates, by pulsed laser deposition (PLD) using ZnO nanowall network with honeycomb structure as seed layer. We identified that the growth parameters are vital to control the crystallinity, morphology and the defect levels in the synthesized ZnO nanowires. SEM, XRD, TEM, HRTEM analysis show that the nanostructures are highly crystalline and are vertically oriented. We also report the in-situ growth of PbS nanoparticles without linker on the surface of well –oriented ZnO NWs by (SILAR) technique. The PbS Nanoparticles are packed tightly on the surface of the ZnO Nanowires with different sizes and densities, without insulating nature organic ligands, which might affect both the electronic structure at the interface and the electron - transfer rate. The SEM, TEM, HRTEM, PL and XRD analysis, confirm the attachment of the spherical shape polycrystalline PbS nanoparticles.
We propose at the end of the thesis the p-PbS /n-ZnO hetero-junction with its future applications in solar cells.